Arabidopsis NOT4 E3 Ligases: Key Regulators of TOR Signalling and Co-Translational Protein Quality Control

By

Maximillian Andreas Schwarze

A thesis submitted to
The University of Birmingham
for the degree of

DOCTOR OF PHILOSOPHY

School of Biosciences
College of Life and Environmental Sciences
University of Birmingham

October 2024

Abstract

Protein synthesis and degradation are both essential for regulating proteome homeostasis and cellular function. In eukaryotes the predominant mechanism for regulated protein degradation is via the ubiquitin proteasome system (UPS), where substrates are marked for degradation through the addition of a polyubiquitin chain by enzymes called E3 ubiquitin ligases. The UPS is important for degrading proteins when they are no longer needed, but also plays a key role in clearing misfolded proteins that arise during stress or in response to translational errors as proteins are synthesised. In yeast and metazoans, the NOT4 E3 ligase has been shown to play a role in co-translational mRNA and protein quality control to limit translational errors, but the presence and functions of NOT4-like proteins in plants has not been investigated.

Three putative NOT4 E3 ligases (*At*NOT4A, B and C) were identified in *Arabidopsis* and shown to contain the unique and characteristic combination of a RING domain and RNA recognition motif (RRM), which places their function at the interface of proteolysis and RNA biology. Phenotypic and RNA-seq analyses of single and combination *Atnot4* mutants revealed redundant functions for these proteins in controlling plant growth – likely due to energy deficiencies – and regulating the expression of genes linked protein translation. Further analyses showed that plants lacking functional *AtNOT4s* have increased global translation rates, accumulate polyubiquitinated proteins, and are sensitive to protein-folding elicitors, which is indicative of increased error rates during protein biogenesis.

*At*NOT4s had previously been identified as targets of the *At*TOR kinase, a master regulator in energy- and nutrient-responsive translation. Given the growth and translational phenotypes observed in *Atnot4* mutants, an assessment of their relationship to *At*TOR signalling was undertaken. *Atnot4* mutants were found to have increased basal rates of *At*TOR activity, which may explain the increased rates of translation in these mutants. Moreover, biochemical, plant growth, and RNA-seq analyses showed that *Atnot4* mutants are sensitive to chemical inhibitors of the *At*TOR signalling cascade, suggesting that they are required for normal *At*TOR functions.

In summary, the data presented in this thesis describe for the first time a role for plant NOT4-like proteins in regulating protein translation linked to *At*TOR signalling, suggesting they function as part of a conserved co-translational surveillance mechanism that coordinates and safeguards protein production. This has important implications for our understanding of proteostatic quality control mechanisms across kingdoms, whilst also identifying new potential targets for enhancing plant performance through improving translational fidelity under normal and stress conditions.

Acknowledgements

I would like to first thank my supervisor, Professor Daniel Gibbs, for supporting me over the past 4 years. I am very grateful for the continuous help, guidance, and freedom to explore, which helped me develop both as a researcher and as an individual.

Thank you to the current and former Gibbs Lab members (Tumie, Mark, Gunjan, Anne-Marie, Jo, Lina, Natassa, Alex) and members of the W203/4 for all the favours and expertise. Thank you, Ross, for showing me the ropes and making me feel comfortable in the lab when I first joined. A huge thank you to Rory for acting as a role model who encouraged, mentored, and taught me all the lab skills I needed to conduct my experiments. I would also like to thank Sjon for all the input and memories we made during my first year.

I would like to extend my thank you to Syngenta for funding my PhD. Particularly, I would also like to thank Dr Christian Noble and the Herbicide Biochemistry team at Syngenta for hosting me to conduct the experiments that opened up new research leads. I am grateful to all the technical staff at the University of Birmingham for their services, which made conducting research in the lab safer and easier. Additional thanks go to Dr Juliet Coates for acting as my secondary supervisor and providing fresh perspectives during our meetings. Thank you to Dr Andy Plackett for all the scientific contributions during lab meetings.

To my closest friends, Charles and David, thank you for all the conversations, memories, and fun we had in Birmingham. You made challenging times much easier. I could have never been in the position I am in without my family. Thank you for believing in me and showing endless support for me. Finally, to Ilaria, for always being there and making me a better person every day. I could not imagine doing my PhD without you.

Authors Declaration

I certify that this thesis is presented in accordance with University of Birmingham regulations for the degree of Doctor of Philosophy. A third-party editor (Professor Daniel Gibbs) was used for advice on language (spelling and grammar), and formatting (improving tables and illustrations for clarity) in accordance with the Code of Practice on Plagiarism section 3.7.

Funding

This work was supported by the Biotechnology and Biological Sciences Research Council (BBSRC) and University of Birmingham funded Midlands Integrative Biosciences Training Partnership (MIBTP) [grant number BB/T00746X/1], and by Syngenta Limited.

Table of Contents

List of Figures

List of Tables

List of Abbreviations

aa	Amino acids
ABA	abscisic acid
AZD	AZD8055 (TOR inhibitor)
CHX	Cycloheximide
CMA	Chaperone-mediated autophagy
DEG	Differentially Expressed Gene
DMSO	Dimethyl sulfoxide
ERAD	Endoplasmic reticulum associated degradation
GO	Gene ontology
GUS	β-glucuronidase
JA	Jasmonic acid
LD	Long day
P-RPS6	Phosphorylated RPS6
PCR	Polymerase chain reaction
PTM	Posttranslational modification
qRT-PCR	Quantitative RT-PCR
RAP	rapamycin
ROS	Reactive oxygen species
RPS6A	Ribosomal protein subunit 6 A
RRM	RNA recognition motif
SGA	Synthetic genetic array
Tm	Tunicamycin
TOP	Tract of oligopyrimidines
TOR	Target of rapamycin
TORC	Target of rapamycin complex
UPR	Unfolded protein response
UPS	Ubiquitin proteasome system
UTR	Untranslated region
WT	Wild type

Chapter 1 – Literature Background and Research Context

1.1 Importance of proteins and implications in real world settings

Proteins are macromolecules common to all cells in all systems ranging from lower prokaryotic organisms to higher complex eukaryotes (Callis, 2014; Nelson & Millar, 2015). In fact, all biological processes have proteins implicated in them: the maintenance of cellular integrity, catalysis of enzymatic activity, modulation of gene expression, and signal transduction for cell-to-cell communication. Phenotypic traits and the ability for an organism to adapt to its surrounding environment highly depends on the proper function of proteins (Nelson & Millar, 2015). The dynamic balance of protein production, folding, co- and post-translational modification, and destruction all collectively coordinate protein homeostasis (proteostasis). Expanding our current knowledge of the mechanisms governing protein synthesis and degradation (i.e., turnover) is critical for addressing global challenges like food security, as it offers new opportunities to manipulate plant traits that enhance growth efficiency, stress resilience, and yield (Kim et al., 2014).

The regulation of protein synthesis and degradation during periods of biotic and abiotic stress is closely monitored. Otherwise, the coordination of growth, development and resistance to these stresses can lead to disruption in plant productivity and overall survival. Improving our understanding of this regulation has the potential to identify and develop novel targets for manipulating traits of agronomic importance and could facilitate the development of improved crop varieties with enhanced performance. Breeding strategies can be aimed to optimise crop adaptation to environmental stressors that optimise energy allocation and storage during protein translation or by minimising errors that occur during translation when nutrients are scarce. Fluctuating environmental conditions are inevitable, given the current threat we are facing due to climate change. Therefore by enhancing our understanding of how proteins are regulated, innovative solutions can be fostered to develop a more sustainable agricultural system that enhances food security for a growing population (Mbow et al., 2020; Wheeler & Von Braun, 2013).

1.2 Protein turnover and protein homeostasis

Protein turnover involves the continuous synthesis and degradation of proteins within cells. This process is a key component in maintaining overall cellular homeostasis (Labbadia & Morimoto, 2015). The constant production, modification and destruction of proteins is highly maintained to ensure adequate cellular function, especially when cells are needed to respond timely to changing environment conditions.

Amino acids (aa) are the fundamental building blocks that make up new polypeptides during protein synthesis (Houlihan et al., 1995). Briefly, protein synthesis starts with a specific gene segment that is transcribed from DNA into messenger RNA (mRNA) (Carter & Houlihan, 2001). The mRNA molecule holds the genetic code in the form of nucleotide sequences. A series of three-nucleotides is known as a codon, and encodes a specific aa or a start/stop signal (Carter & Houlihan, 2001; Zoghbi, 2013). Crucial components of protein synthesis are the ribosomes; complex macromolecular machines composed of ribosomal RNA (rRNA) and proteins (Baldwin, 1999). They represent the site where mRNA and aa are brought together to produce polypeptide chains, a process known as translation. The ribosomes move along the mRNA molecule, reading the codons in a sequential manner. Briefly, initiation factors, elongation factors, and termination factors control the three different stages of protein synthesis (*to be further discussed in Section 1.7.1 and 1.7.2*) (Carter & Houlihan, 2001; Duttler et al., 2013).

Ribosomal activity is influenced by various regulatory proteins and signalling cascades to help align translation with cellular priorities during development and in response to environmental change. For example, modulation of Target of rapamycin (TOR), an essential and conserved kinase (Dobrenel, Caldana, et al., 2016; van Dam et al., 2011), and it's signalling pathways in response to nutrient availability and environmental cues significantly influence translation (Iadevaia et al., 2014; Jiang et al., 2016; B. Menand et al., 2002). Global translation can be influenced by TOR signalling especially in the context of nutrient availability, hormonal cues, and energy supply. TOR can increase the synthesis of key proteins necessary for cellular growth and overall development by promoting ribosome biogenesis and polysome loading (Busche et al., 2021; Iadevaia et al., 2014; Tcherkezian et al., 2014).

The subsequent sections will expand on TOR with a specific emphasis on the dynamic signalling pathways it controls in the model plant *Arabidopsis thaliana* (*Arabidopsis*), highlighting its importance for plant growth and development through modulation of protein synthesis.

1.3 Origin and evolution of TOR

TOR is part of a dynamic signalling network (**Figure 1**) where many of its target substrates are also protein kinases. This includes the ribosomal protein S6 serine/threonine kinases (S6Ks) (Chen et al., 2018; Magnuson et al., 2012) and the dual-specificity tyrosine/serine/threonine kinase YET ANOTHER KINASE 1 (YAK1) (Barrada et al., 2019; Zurita-Martinez & Cardenas, 2005). Both kinases transduce signals to modulate transcriptional and translational activity. Moreover, through substantial evidence indicating important roles in many signalling and metabolic networks, TOR has emerged as a 'master regulator' in all eukaryotes. Following its initial discovery in budding yeast (*Saccharomyces cerevisiae*) in the early 1990s (Heitman et al., 1991), TOR was subsequently identified in non-photosynthetic complex multicellular organisms like mammals (Brown et al., 1994; Chiu et al., 1994; Sabatini et al., 1994), fungi (Cruz et al., 1999), and *Drosophila* (Oldham et al., 2000) marking the beginning of TOR signalling research (**Figure 2**).

The TOR inhibitor rapamycin (RAP) – which gave TOR its name (Target of Rapamycin) - was first isolated from the soil bacterium *Streptomyces hygroscopicus* (Boutilier, 1992; Vézina et al., 1975) and contributed significantly to the discovery and subsequent understanding of TOR signalling mechanisms and function in mammals (Brown et al., 1994; Busche et al., 2021; Chiu et al., 1994; Cruz et al., 1999; Magnuson et al., 2012; McCready et al., 2020; Nishizawa et al., 1998; Sormani et al., 2007; Wolfson & Sabatini, 2017). RAP interacts with and inhibits TOR by forming a complex with FKBP12, a member of the FK506-binding protein family. This FKBP12-RAP complex binds to the FKBP12-RAP-binding (FRB) domain of TOR (*see Section 1.4*), adjacent to its catalytic kinase domain, thereby inhibiting TOR's kinase activity. While RAP susceptibility is widespread among eukaryotes, affecting the growth of most fungi and animal cells, most land plants are resistant to its action (Liu et al., 2012; B. Menand et al., 2002; Montane & Menand, 2013; Xiong & Sheen, 2012; Xu et al., 1998). The difference in aa sequence in plant FKBP12 hinders the ability to bind to RAP, thus preventing the formation of the FKBP12-RAP-TOR inhibitor complex. (Crespo et al., 2005; Xu et al., 1998). Supporting this, FKBP12 from *Vicia faba* was unable to restore RAP sensitivity in yeast FKBP12 mutants (Xu et al., 1998). Yeast two-hybrid experiments also demonstrated that the FRB domain of *Arabidopsis* TOR (*At*TOR) can still bind FKBP12 from yeast (*Sc*FKBP12) in a RAP-dependent manner but fails to interact with *At*FKBP12, further confirming that the structural differences in FKBP12 are responsible for the resistance (B. Menand et al., 2002; Sormani et al., 2007).

The study of plant TOR has largely focussed on the model plant *Arabidopsis,* with a select few other plant species confirming the evolutionary conservation (McCready et al., 2020). Similarly to most animals and humans, a single large TOR gene exists in *Arabidopsis* (B. Menand et al., 2002) (**Figure 1**). This singular TOR gene conservation is further seen in *Chlamydomonas* (Crespo et al., 2005), *Gossypium hirsutum (F. Li et al., 2015; Song et al., 2019)*, and *Oryza sativa* (De Vleesschauwer et al., 2018) whereas two TOR genes have been identified for *Glycine max* (Um et al., 2013), *Populus trichocarpa* (Fu et al., 2020; Tuskan et al., 2006), and *Brassica rapa* (Lu et al., 2019).

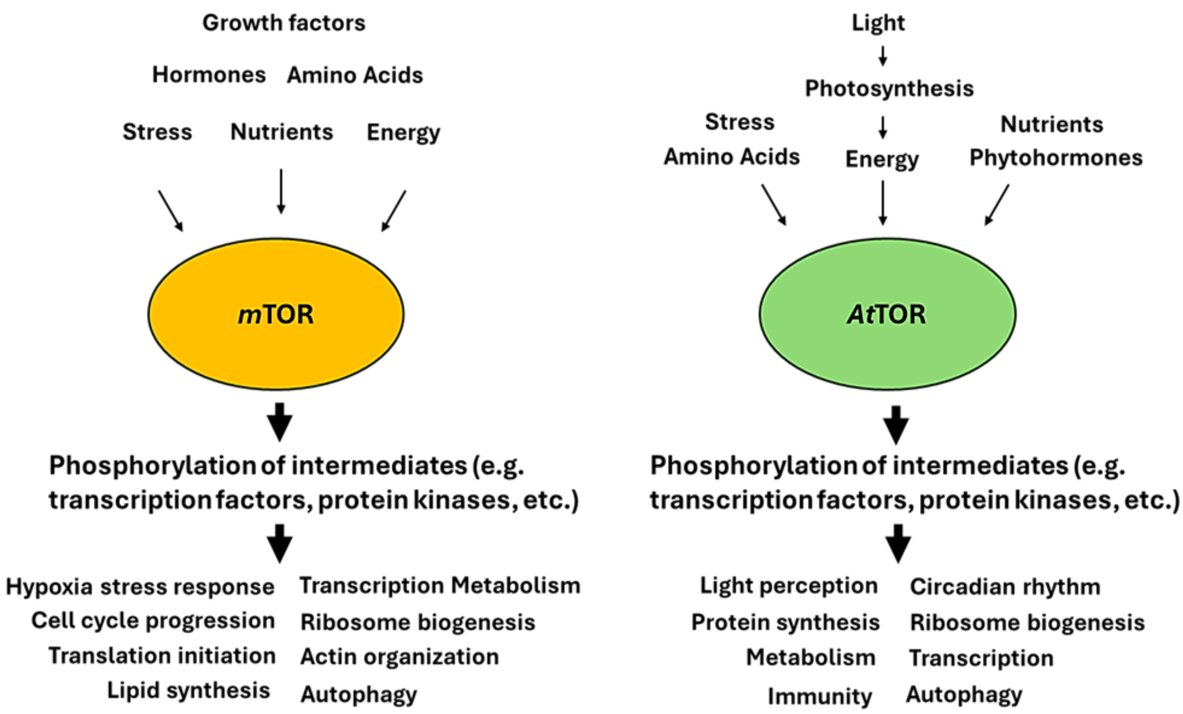

Figure 1 - Overview of the dynamic signalling pathway of mammalian *m*TOR and *Arabidopsis At*TOR. Growth factors, hormones, amino acids, stress, nutrients, and energy are all upstream signal perceived my *m*TOR (yellow). The upstream signals of *At*TOR (green) include light, energy, stress, amino acids, nutrients, and phytohormones. Downstream responses in *m*TOR signalling that are induced include hypoxia adaptation, cell cycle, initiation of translation, lipid synthesis, transcription regulation, metabolism, ribosome biogenesis, actin organization, and autophagy. Other downstream effects of the *At*TOR signalling include a response to light perception, protein synthesis, metabolic processes, immune response, regulation of circadian rhythm, ribosome biogenesis, transcription, and autophagy.

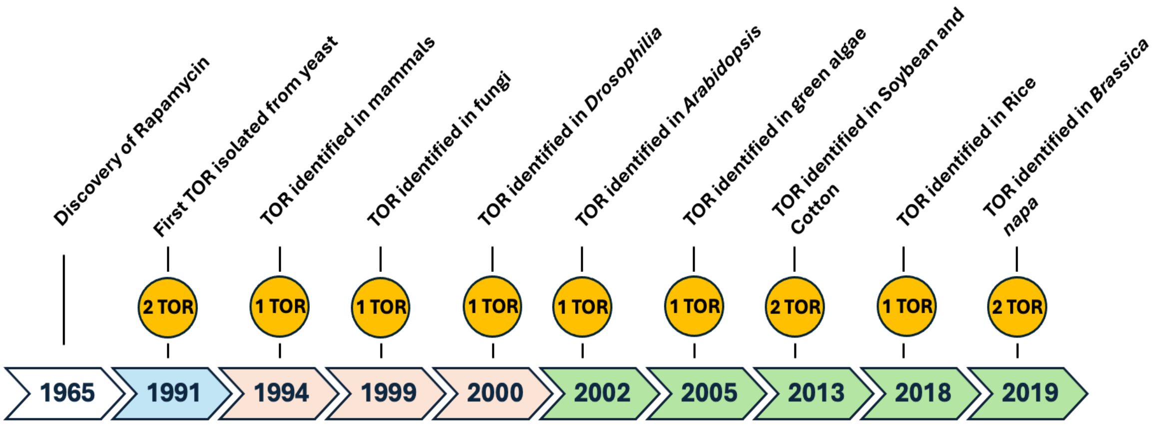

Figure 2 - Timeline of Significant Publications in TOR Research Spanning Unicellular and Multicellular Organisms. *Based on Rabeh et al., 2024*

1.4 TOR protein structure

TOR is large kinase with a molecular weight of 280kDA (Engelman et al., 2006; Heitman et al., 1991). Besides its kinase domain, TOR consists of four additional domains: an N-terminal HEAT (Huntington, Elongation Factor 3 regulatory, subunit A of PP2A) repeat, FAT (focal adhesion target), FRB (FKBP12-RAP-binding), and C-terminal FAT (FATC) domain (**Figure 3**) (Alarcon et al., 1999; Heitman et al., 1991; Rexin et al., 2015; Schmelzle et al., 2002; Wullschleger et al., 2005). The HEAT repeat is responsible for protein-protein interactions and membrane associations whereas the FAT and FATC domains are involved in kinase activation (Wullschleger et al., 2005). As outlined earlier, the FRB domain is a target binding site for the inhibitor FKBP12-RAP complex (Heitman et al., 1991; Sormani et al., 2007).

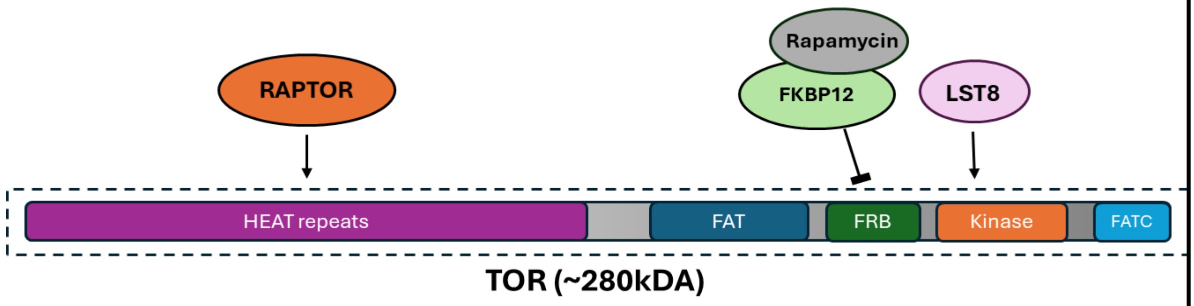

Figure 3: Molecular structure of the TOR protein highlighting the 5 domains. HEAT repeats (purple), FAT (dark blue), FRB (green), Kinase (light orange), and FATC (light blue). RAPTOR (orange), an associate protein that forms the TOR complex (TORC) (*see Section 1.5*) binds to the HEAT repeat domain whereas LST8 (light purple), another TORC subunit, interacts with the Kinase domain. The FKBP12-RAP (light green and grey, respectively) complex interacts with the FRB domain. *Based on Heitman et al., 1996; Wullschlegler et al., 2005.*

1.5 TOR complex (TORC) - components and function

TOR is well conserved, while main differences between plant TOR and mammalian TOR are formed through the complexes. Precisely, in mammals, TOR forms two well-characterized complexes: *m*TORC1 and *m*TORC2 (Frias et al., 2006; Kim et al., 2017). *m*TORC1 includes *m*TOR, REGULATORY-ASSOCIATED PROTEIN OF TOR (RAPTOR), LETHAL WITH SEC THIRTEEN 8 (LST8), Proline-Rich Akt Substrate of 40 kDa (PRAS40), and DEP Domain Containing *m*TOR Interacting Protein (DEPTOR), and is primarily involved in regulating cell growth (Düvel et al., 2010), protein synthesis (Beretta et al., 1996), and autophagy (Jung et al., 2009), responding sensitively to nutrients, growth factors, and cellular energy status (Frias et al., 2006; Kim & Guan, 2019). *m*TORC2, on the other hand, includes *m*TOR, rapamycin-insensitive companion of TOR (RICTOR), LST8, mammalian Stress-Activated Map Kinase-Interacting Protein 1 (*m*SIN1), and Proline-rich Protein 5 (PRR5, also known as PROTOR1/2) (**Figure 4**). *m*TORC2 regulates the cytoskeleton (Jacinto et al., 2004), and cell survival (Sarbassov et al., 2005), being less sensitive to nutrients but more so to growth factors (Kim & Guan, 2019).

In contrast, *Arabidopsis* has only one TOR complex (*At*TORC1), similar to *m*TORC1, which includes TOR kinase (*At*TOR), RAPTOR1, LST8-1, and a unique plant-specific protein called TAP46 (**Figure 4**) (Tatebe & Shiozaki, 2017). Two homologs of the mammalian RAPTOR gene exist in *Arabidopsis*, RAPTOR 1 and RAPTOR 2 (Anderson et al., 2005; Deprost et al., 2005). An *in-silico* analysis by Diaz-Troya *et al*. revealed that RAPTOR1 is highly expressed throughout development, whereas RAPTOR2 is present at relatively low levels. Furthermore, as there is only one RAPTOR gene in algae (Díaz-Troya et al., 2008), it has been suggested that RAPTOR2 may be the result of a duplication event of the ancestral RAPTOR gene in the land plant lineage, and may therefore be a functionally redundant copy (Deprost et al., 2005). Similar to RAPTOR, two LST8 genes (LST8-1 and LST8-2) also exist in *Arabidopsis,* and has again been suggested to be the result of another duplication event in their common ancestor (Moreau et al., 2012).

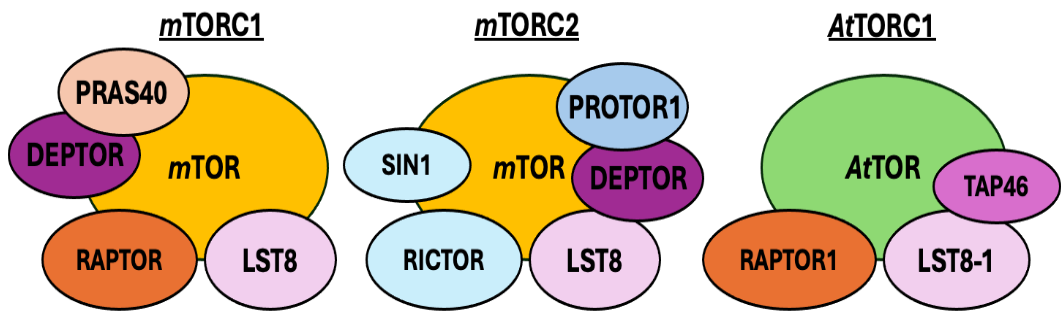

Figure 4 - Composition of mammalian TOR complexes *m*TORC1 and *m*TORC2, and *Arabidopsis* TOR complex (*At*TORC) with their respected subunits. *Adapted from Frias et al., 2006; Kim et al., 2017.*

1.6 Functions of TOR in plant development

As sessile organisms, plants have evolved key processes that allow them to adapt to changing environments in accordance with their growth and development. TOR is well known for its regulation of growth-related processes (Caldana et al., 2013; Wullschleger et al., 2005; Xiong & Sheen, 2015). As mentioned earlier, TOR integrates a variety of signals; these functions are highlighted in **Figure 5** and discussed in further detail in the following sections (*Sections 1.6.1 – 1.6.10*).

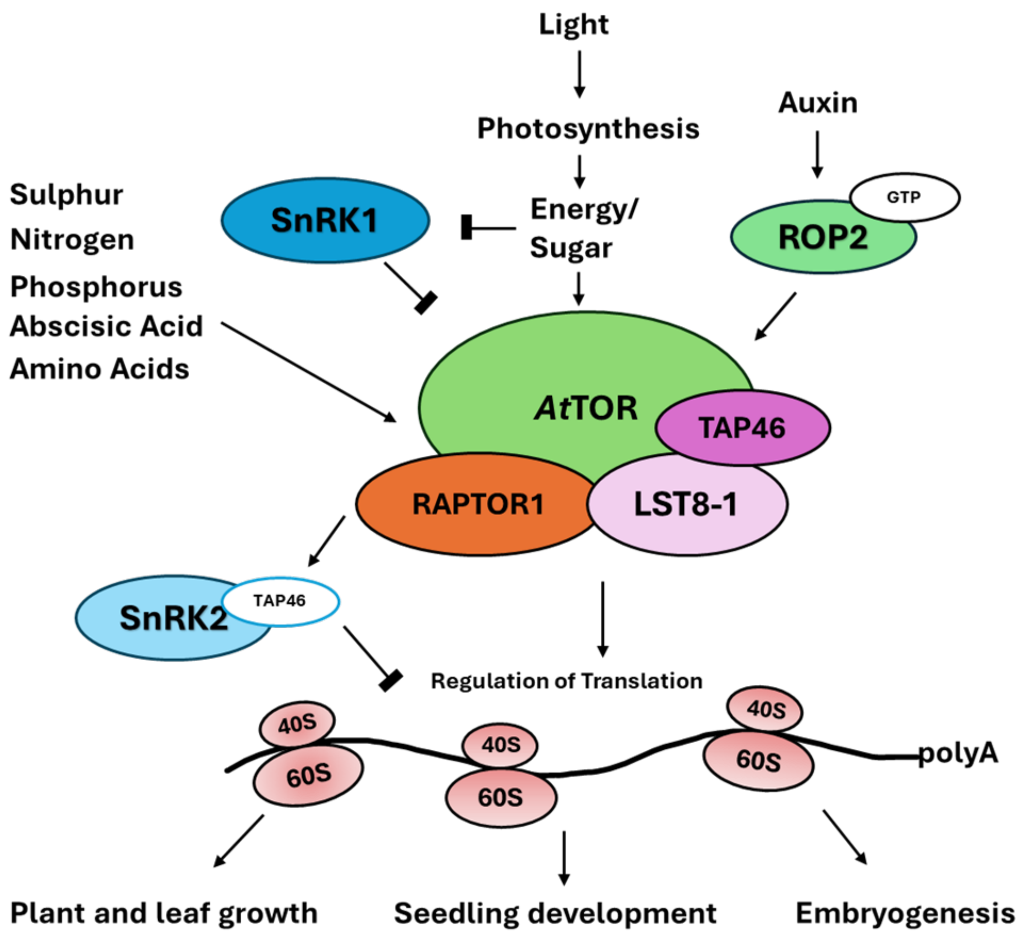

Figure 5 - *At*TOR forms a central complex with RAPTOR and LST8 to regulate various downstream processes through integration and transduction of upstream signals. Several upstream signals can differentially regulate translation and ultimately lead to plant and leaf growth, seedling development and embryogenesis. Notable proteins involved in these pathways are ROP2, SnRK1, SnRK2, and TAP46 which have distinct upstream signals in their activation/repression. *Adapted from Schepetilnikov & Ryabova 2018*

1.6.1 Embryogenesis

In 1995, Meinke discovered an essential role for *At*TOR during the early stages of embryo formation (Meinke, 1995). It was later discovered that the embryos of *tor* mutants in *Arabidopsis* arrested early during the dermatogen stage while having cells still present in the metaphase (Benoît Menand et al., 2002). Though cell division itself is not directly inhibited by the disruption of *At*TOR in the embryo, overall cell growth is supressed (Benoît Menand et al., 2002). Translational machinery and cell wall modifying enzymes such as CELLULASE SYNTHASE 6 (CESA6) and EXPANSIN B1 (EXPB1) are also downregulated in the absence of *At*TOR (Rabeh et al., 2024; Xiong & Sheen, 2015). Interestingly, it still remains unclear whether RAPTOR1 plays a role in embryogenesis as *raptor1* displayed viable embryos suggesting that *At*TOR's function in embryogenesis is independent of RAPTOR1 (Anderson et al., 2005). Conflicting observations by Deprost et al. (2005) showed embryo lethality when working with the same *raptor1* line. Thus, different environmental cues such as temperature and light may be affecting the severity of the phenotype observed (Deprost et al., 2005; McCready et al., 2020; Xiong & Sheen, 2012).

1.6.2 Seedling development

*At*TOR is known to be involved in the transition from skotomorphogenesis (growth in darkness) to photomorphogenesis (light-driven development) during seedling development. The opening of the apical hook, cessation of hypocotyl cell elongation, and chloroplast maturation causing vegetative growth in the true leaves are influenced during this transition (Dong et al., 2022; McCready et al., 2020; Xiong et al., 2013). Upon *At*TOR inhibition (*to be discussed further in Chapter 5, Section 5.3*), it was found that seedlings experienced chlorosis in cotyledons which hindered overall growth (Chen et al., 2018; McCready et al., 2020; Rabeh et al., 2024). The auxin-*At*TOR-ribosome protein S6A (*At*RPS6A) was shown to be activated through light which enhanced translation in photomorphogenic *Arabidopsis* seedlings. (Chen et al., 2018). *At*RPS6 is a phospho-target of *At*TOR and known to regulate BR INSENSTIVE 2 (BIN2) to promote chloroplast development and seedling growth (McCready et al., 2020; Shi et al., 2018). Other studies have demonstrated that auxin can activate *At*TOR through Rho-like small GTPase 2 (ROP2) (*see Section 1.6.3.1*). This highlights a light-triggered signalling pathway for translational regulation in which *At*TOR may coordinate light and auxin levels to facilitate the timely development of de-etiolating seedlings.

1.6.3 Plant growth

Nutrients (*see Section 1.6.3.1*), hormones (*see Section 1.6.3.2*), energy supply (*see Section 1.6.3.3*), and amino acids (*see Section 1.6.3.4*) are all important cues that can enhance *At*TOR activity to stimulate plant growth. In short, when nutrients are abundant, *At*TOR can promote protein synthesis, utilising the availability to actively contribute to growth related processes. Under nutrient limiting conditions, the activity of *At*TOR decreases and then acts as a cue for plants to limit their growth and induce the recycling of cellular components through an adaptive response called autophagy.

The following sections will go into detail of how specific nutirients and phytohormones are integrated to activate or repress *At*TOR activity in relation to growth. The modulation of *At*TOR activity through energy availability as well as amino acids will also be discussed.

1.6.3.1 Nutrients

Macronutrients such as sulphur, nitrogen and phosphorus can induce plant growth and development through *At*TOR signalling. Allocation of resources between stress response pathway and growth-promoting pathways have identified sulphur signalling as a driving factor (McCready et al., 2020). Use of suflite reductase deficient mutants (*sir1*), underlined the complex interplay between sulfur signalling and *At*TOR function which infulences sulfide production. Significant growth inhibition, lower rRNA levels, decreased global translation and induced autophagy - events all downstream of AtTOR - were impacted upon starvation for sulfur and in the *sir1-1* mutant. (Speiser et al., 2018). By manipulating sulfur flux from cysteine to glutathione, it was discovered that reducing the synthesis of glutathione can restore plant growth and meristematic activity, ultimately increasing *At*TOR activity (Speiser et al., 2018; Xiong & Sheen, 2015). This may suggest that *At*TOR has an important function in reallocating cysteine from glutathione synthesis to protein synthesis (Speiser et al., 2018). Moreover, sulfur availability was also shown to be involved in glucose signalling to activate *At*TOR (Caldana et al., 2013; Dong et al., 2022). Genome-wide transcript profiling reveals that glucose-*At*TOR signaling activates genes involved in sulfur assimilation and glucosinolate biosynthesis (Xiong et al., 2013).

Besides sulfur, nitrate and ammonium are inorganic nitrogen compounds that act as a nutrient signals to promote shoot and root growth in *Arabidopsis* (Dobrenel et al., 2016; Liu et al., 2012) through *At*TOR's positive regulation of root development (Deprost et al., 2005; Rabeh et al., 2024). Nitrogen assimilation, the process in which inorganic nitrogen compounds undergo a conversion process to become glutamine and other amino acids, are known to take place in both the roots and shoots (Ingargiola et al., 2020; Miflin & Lea, 1976). It has been suggested that nitrate and ammonium act as primary nitrogen signals, capable of activating *At*TOR independently of nitrogen assimilation pathways. Even when key nitrogen assimilation enzymes such as nitrate reductase or glutamine synthesase are chemically inhibited, *At*TOR is still activated (Liu et al., 2021). Thus, the presence of nitrate and ammonium alone is sufficient to trigger *At*TOR activity. Furthermore, glutamine, nitrate, and ammonium together can stimulate Rho-related protein from plants 2 (ROP2), which in turn activates *At*TOR, promoting true leaf development (Liu et al., 2021). *At*TOR activity is decreased when glutamine and other amino acids build up as a result of processes that depend on glutamine synthesase (Ingargiola et al., 2023). Thus, *At*TOR pathway's influence over protein synthesis and degradation (*to be described in Section 1.9.1*) has important ramifications for nitrogen dynamics (Ingargiola et al., 2023; Scarpin et al., 2022).

In addition to nitrogen, phosphorus can influence plant growth and development through *At*TOR signalling pathways. Photosynthesis, nucleic acid synthesis and energy allocation are linked to growth and are governed by *At*TOR activity (Cho et al., 2023; Dobrenel, Caldana, et al., 2016). The activity of *At*TOR kinase is highly linked to phosphorus sensing, affecting primary metabolism as well as directing cell cycle progression, and ultimately leading to growth (Dobrenel et al., 2021). As a key component of nucleotides, phosphorus may directly lead to nucleotide biosynthesis by enhancing *At*TOR activity. When nucleotides are abundant, *At*TOR becomes more active leading to the phosphorylation of several transcription factors involved in nucleotide biosynthesis (Busche et al., 2021). In turn, the increase in nucleotide availability encourages ribosome biogenesis through *At*TOR signalling pathways, thus ensuring an appropriate integration of phosphorus to promote growth and cellular functions (Haq et al., 2022; Scarpin et al., 2022).

Apart from its function in nucleotide production, the availability of phosphorus has a direct influence on *At*TOR signaling via other regulatory mechanisms. For example, in *Chlamydomonas*, phosphorus stimulates *ch*TOR, but a shortage in phosphorus destabilizes the *ch*LST8 protein, which lowers *ch*TOR activity (Couso et al., 2020). Inositol phosphates (InsPs) are known to decrease in the presence of TOR inhibitors implying that InsPs functions downstream of *ch*TOR. A key component necessary for phosphorus sensing in *Arabidopsis* is Inositol pentakisphosphate 2-kinase 1 (IPK1) as it converts inositol pentakisphosphate (InsP5) to inositol hexakisphosphate (InsP6) (Dobrenel et al., 2021). According to Dong et al. (2015), mutants with decreased inositol phosphates have higher sensitivity to TOR inhibitors. IPK1-produced inositol polyphosphates function downstream of *At*TOR (Dong et al., 2015) . While partial loss-of-function mutants show shoot and root abnormalities, complete loss of IPK1 is fatal suggesting that that InsP6 is required for proper *At*TOR signaling (Dobrenel et al., 2021).

1.6.3.2 Phytohormones

Auxin and abscisic acid (ABA) are two examples of phytohormones that have a fundamental role in promoting growth via *At*TOR signalling. Auxin has the ability to activate *At*TOR, which causes mRNAs with upstream open reading frames (uORFs) in their 5' untranslated regions (UTRs) to reinitiate, promoting selective protein translation (Schepetilnikov et al., 2013). This process guarantees that auxin signalling, especially in the presence of fluctuating nutritional circumstances, can control the expression of important growth-regulating genes in plants. ROP2-GTPase is a crucial component of the auxin-*At*TOR relationship (**Figure 5**) which is activated by auxin and has been shown to promote *At*TOR signalling (Schepetilnikov et al., 2017). The interaction of ROP2 with *At*TOR results in increased translation of a number of auxin-responsive genes that leads to leaf and root development. The ability of auxin to control the *At*TOR-dependent protein synthesis with ROP2-GTPase unravels an elaborate system that accomplishes the fine-tuning of plant growth responses to external nutrient availability with internal hormonal signals.

ABA is another example of a phytohormone that interacts with *At*TOR to modulate growth and development (Wang et al., 2018). In unfavourable conditions, ABA will bind to PYR1/PYL/RCAR (PYL) receptors which activates SUC NON-FERMENTING 1-RELATED KINASE 2 (SnRK2s) (**Figure 5**). SnRK2s, once activated, target RAPTOR for phosphorylation to inhibit the *At*TORC signalling. In contrast, under favourable conditions, *At*TOR targets PYL receptors for phosphorylation by blocking ABA binding and inhibiting ABA-independent PYLs activity. The multilayered interaction of the ABA signalling components with *At*TORC represents a conserved way of controlling and optimizing plant fitness under stress conditions to support recovery of growth when the stressful environment is relieved (Haq et al., 2022; Rabeh et al., 2024).

1.6.3.3 Sugar and Energy

Besides nutrients and hormones, sugars provide the energy for plant growth and development via *At*TOR signalling. Biological processes that are influenced through sugar availability and thus via the *At*TOR signalling pathway are protein translation and cell cycle. Research has demonstrated that glucose stimulates *At*TOR to control important developmental processes such as root meristem activation and root hair formation through its metabolic intermediates in glycolysis and the Krebs cycle (Xiong et al., 2013; Xiong & Sheen, 2012). Brassinosteroid (BR) pathways are also involved in this complex interaction between sugar and *At*TOR signalling where glucose signalling regulates the aggregation of the BR-signalling transcription factor BZR1; an essential transcription factors for growth promotion (Zhang et al., 2016). Apart from growth regulation, glucose-induced activation of *At*TOR impacts transcriptional reprogramming. The glucose-*At*TOR signalling pathway achieves metabolic and environmental input by controlling gene expression responsible for the maintenance of health and adaptation of plants in regard to metabolism, the cell cycle, and stress response (Xiong et al., 2013). Besides glucose, the regulation of *At*TOR activity is also closely linked to the SnRK1 protein kinase, an energy sensor acting antagonistically to *At*TOR. Under low-energy conditions, SnRK1 becomes activated and inhibits energy-consuming processes such as cell growth and division, while stimulating energy-producing processes related to stress, including autophagy and starch mobilization (Baena-González & Sheen, 2008). In the presence of glucose, SnRK1 becomes inactive and indirectly activates *At*TOR to promote growth-related processes. This negative regulation in which the two kinases function antagonistically to each other has evolved as a key mechanism for the plant to rapidly switch between growth and stress response in accordance with energy availability.

1.6.3.4 Amino acids

Amino acids represent basic constituents of proteins. Besides their structural function, they act as signaling and regulatory molecules (Häusler et al., 2014). Essential upstream signals regulate the activity of *At*TORC, and aa represent a central component of these signals. Inhibition of the leucine biosynthesis in *Arabidopsis* resulted in the induction of *At*TORC activity and higher total branched valine chains (Cao et al., 2019). Furthermore, glutamine and Isoleucine can activate *At*TOR in mature leaves to stimulate further growth of plants by increasing protein synthesis (O'Leary et al., 2020). Lastly, O-acetylserine, the precursor of cysteine (Cys) can also activate *At*TOR signalling, showing a strong link with glucose availability to promote growth (Mallén-Ponce et al., 2022).

Conversely, changes in amino acid accumulation and cellular metablism can result from the inhibiton of *At*TOR signalling (Busche et al., 2021; Scarpin et al., 2022). Amino acids such as glycine and asparagine, which are involved in processes such as nitrogen transport and storage were shown to accumulate when *At*TOR activity is hindered (Ingargiola et al., 2023; Moreau et al., 2012). It was shown in *Chlamydomonas* under carbon starvation conditions that amino acids accumulate (Lee & Fiehn, 2013). Thus, it has been speculated that AAs accumulation following *ch*TOR inhibiton could be due to either attenuated mRNA translation (Rabeh et al., 2024; Sormani et al., 2007) or increased autophagy (Soto-Burgos & Bassham, 2017). In addition, such an increase in AAs appears to be linked, at least partly, to enhanced assimilation of exogenous nitrogen in *Chlamydomonas*. Under conditions of nutrient starvation, AAs accumulation is lowered, irrespective of the presence of translational or proteolytic inhibitor (Mubeen et al., 2018).

1.7 The role of TOR signalling in translation

Several upstream cues of TOR signalling can modulate translation, though the way in which TOR interacts with translational components for this to occur remains to be discussed. Thus, the following section goes into the details of the regulatory networks in which TOR regulates ribosomal biogenesis and translation, further placing it at the centre of protein synthesis and cellular metabolism.

1.7.1 TOR and mRNA translation: an overview

The three main stages involved in mRNA translation are initiation, elongation and termination. Evolutionary conserved proteins such as the initiation factors (eIFs), eukaryotic elongation factors (eEFs), and eukaryotic release factors (eRFs) make up the translation machinery (Kapp & Lorsch, 2004). Initiation begins with messenger Ribonucleoprotein (mRNP) formation facilitated by the interaction of mRNA with the cap-binding complex eIF4F, consisting of eIF4G, eIF4E, and eIF4A, at the mRNA's 5' end, and a poly(A)-binding protein (PABP) at the 3' end (**Figure 6**). Next, additional initiation factors, eIF4A and eIF4B bind to subsequently recruit the 43S pre-initiation complex, which consists of the small ribosomal subunit (40S) bound by initiation factors: eIF1, eIF1A, eIF3, and eIF5. Collectively, these entities form the open conformation 48S complex, which scans the mRNA until recognition of the start codon (AUG). Transitioning to a closed conformation, the 48S complex dissociates some initiation factors, recruits the eIF6-bound 60S ribosomal subunit, and assembles the 80S ribosome with the aid of eIF5B GTPase, initiating translational elongation (Hinnebusch, 2014; Jackson et al., 2010).

Elongation involves ribosomes scanning transfer ribonucleic acids (tRNAs) with eEF1A, transferring peptides upon recognition of mRNA codons, and moving along the mRNA with eEF2 GTPase. This continues until a stop codon, such as UAG, UAA, or UGA, is reached; this then provides the signal for translational termination. eRF1 identifies the stop codon to initiate peptide release and ribosome dissociation, respectively aided by eRF3 GTPase and ATP-binding protein ABCE1. Quality control mechanisms monitor translation steps for the maintenance of fidelity and efficiency in protein synthesis throughout.(Browning & Bailey-Serres, 2015; Kapp & Lorsch, 2004; Schuller & Green, 2018). La-related protein 1 (LARP1) modulates the translation of mRNAs containing the 5' terminal oligopyrimidine tract (5'TOP) in reaction to TOR activation (Smith et al., 2021). Many of the eukaryotic factors involved in mRNA translation are transcriptionally induced by TOR, translationally regulated by TOR-LARP1 signalling (5’TOP), or TOR-induced/repressed through phosphorylation upon TOR activation (**Figure 6**), (Scarpin et al., 2022; Schepetilnikov & Ryabova, 2018).

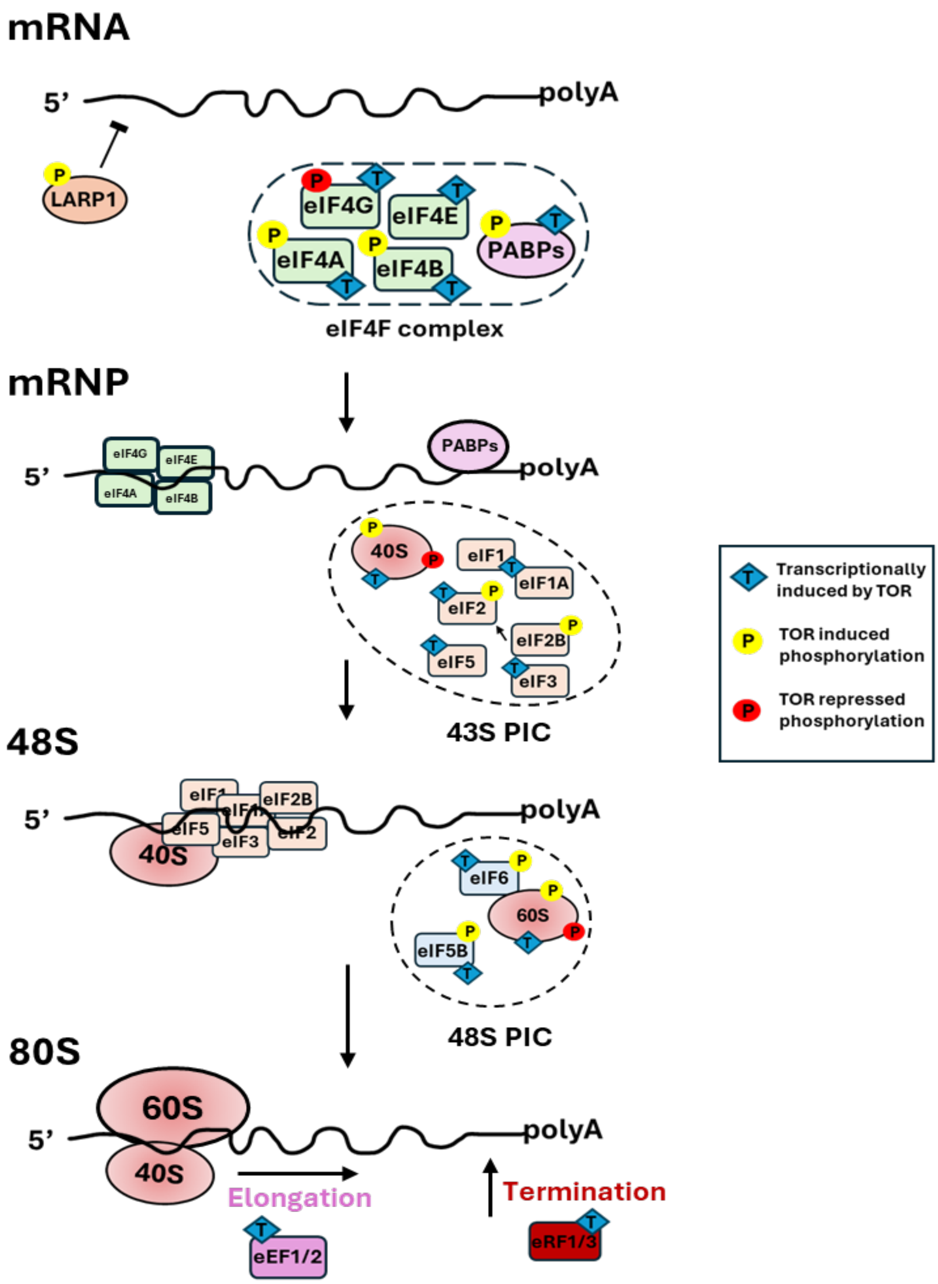

Figure 6 - mRNA translation initiated by loading mRNAs with eukaryotic initiation factors eIF4A, eIF4B, eIF4E, eIF4G and PABPs to form eIF4F complex and mRNPs. Subsequently, formation of the 43S PIC, consisting of eIF1/1A, eIF2/2B, eIF3, eIF5, and the 40S small ribosomal subunit, is recruited by the eIF4F complex and scans the mRNPs to form 48S complex. When start codon is located, 60S, eIF6 and eIF5B forms the 48S PIC and is recruited to the 43S PIC. Combining the 40S and 60S ribosomal subunits form a functional 80S ribosome in which translation elongation can commence with assistance from eEF1/2 eukaryotic elongation factor. mRNA translation is terminated when eRF1 and eRF3 recognize the stop codon causing the growing polypeptide to be released. Note: each protein is labelled to indicate TOR's influence: transcriptionally induced by TOR (blue diamond with 'T'), phosphorylated upon TOR activation (yellow circle with 'P' indicates TOR-induced phosphorylation, red circle with 'P' indicates TOR-repressed phosphorylation. *Adapted from Scarpin, Simmons & Brunkard, 2022.*

1.7.2 *m*TOR & Translation Initiation Factors

*m*TOR regulates protein synthesis at many steps. *m*TOR has a greater impact at the initiation step where mRNAs are transcriptionally induced by *m*TOR to elevate the protein synthesis. In addition to acting transcriptionally, *m*TOR also directly and indirectly phosphorylates the following regulatory proteins participating in translation initiation: the initiation factors eIF4B, eIF4G, and eIF4E-binding proteins (4E-BPs) and LARP1 (**Figure 6**) (Hinnebusch, 2014; Holz et al., 2005; Pause et al., 1994; Raught et al., 2000; Smith et al., 2021). Phosphorylation of eIF4B leads to increased translation of eIF4A/B transcripts which are known to be long mRNAs with highly structured 5' UTR regions (Shahbazian, 2008). eIF4G phosphorylation leads to eIF4F assembly, encouraging its association with eIF4E and further phosphorylation of 4E-BPs which prevents them from binding to and inhibiting eIF4E (Dong et al., 2023). Phosphorylated eIF4G targets short, highly expressed and unstructured transcripts (Rajyaguru et al., 2012). Thus, each phosphorylation event can influence translational initiation of various mRNA transcripts based on the sequence and structure of the 5'UTR region, where eIF4G and eIF4A/4B regulate translation initiation of specific mRNA populations (Leppek et al., 2018; Sen et al., 2016). Additionally, LARP1 can repress translation of mRNAs with a 'tract of oligopyrimidines' (5'TOP) motif at the 5'cap (Lahr et al., 2017). The release from the 5'cap occurs when LARP1 is phosphorylated (**Figure 6**), allowing translation of 5'TOP mRNAs (Jia et al., 2021; Lahr et al., 2017; Philippe et al., 2020).

1.7.3 *m*TOR and Protein S6 kinase (S6K)

*m*TOR has been demonstrated to directly phosphorylate S6Ks at the conserved threonine residue that results in activation and subsequent phosphorylation of a number of protein substrates, including eIF4B and LARP1. A target of phosphorylation by the S6Ks is the ribosomal protein S6 (RPS6), a component of the 40S ribosomal subunit and influences global translation(Chen et al., 2018; Creff et al., 2010; Ruvinsky et al., 2005). Though the functional significance of RPS6 remains under investigation (Meyuhas, 2008), the analysis of RPS6 phosphorylation has been established as a measure of *m*TOR activity (Dong et al., 2022; McCready et al., 2020). Many TOR-dependent kinase signalling pathways also incorporate signals from upstream regulators. For instance, full activation of S6K in both humans and plants necessitates further post-translational modifications, such as the phosphorylation by PHOSPHOINOSITIDE-DEPENDENT PROTEIN KINASE 1 (PDK1) (Pullen et al., 1998). Several ribosomal proteins undergo differential phosphorylation in response to TOR activity; however, the specific molecular consequences remain relatively unexplored (Jiang et al., 2016). *m*TOR–S6K signalling additionally regulates translation elongation by activating eEF2 through phosphorylation of its own kinase (eEF2K) (Horman et al., 2002), ultimately enhancing the rate of protein synthesis. In contrast to translation initiation, it remains unclear whether specific mRNAs are affected by eEF2 phosphorylation. However, it is suggested that transcripts susceptible to inefficient translation and ribosome collisions, partly due to suboptimal codon usage or complex mRNA secondary structures, may be particularly sensitive to the TOR-S6K-eEF2K-eEF2 signalling pathway.

S6Ks form part of the *m*TOR-S6K-RPS6 signalling cascade (**Figure 7**); a pathway known to promote ribosome biogenesis, polysome loading and ultimately translation. RPS6 is part of the 40S small ribosomal unit and is directly phosphorylated by S6K at several conserved serine residues (Ser235, Ser236, Ser240, and Ser244). However, the exact role of RPS6 in global translation is still an ongoing discussion. Research has shown a primary function in regulating ribosome biogenesis (RiBi) through transcriptional regulation of nucleolar proteins Nop56, Gar1 and Rrp12; all of which are vital for ribosomal RNA (rRNA) synthesis, assembly and processing. In turn, translation capacity is significantly influence by regulating the production of ribosomes (Chauvin et al., 2014). Therefore, it was concluded that the S6K-mediated RPS6 phosphorylation indirectly influences translation.

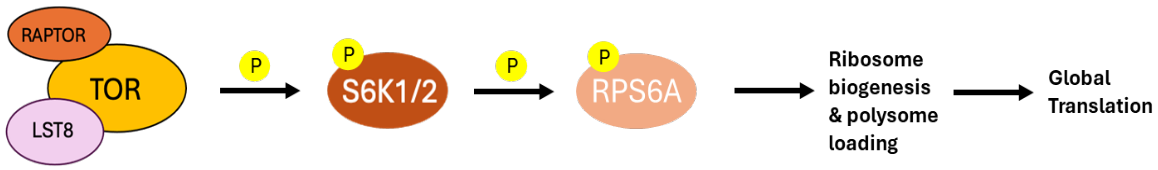

Figure 7 - mTOR-S6K-RPS6 signalling pathway. *m*TORC1, composed of TOR, RAPTOR, and LST8, phosphorylates S6K1/2, which in turn phosphorylates RPS6A (a component of the 40S ribosomal subunit). This phosphorylation cascade promotes ribosome biogenesis and indirectly enhances global translation.

1.7.4 *m*TOR and ribosome biogenesis

*m*TOR activity enhances protein synthesis by promoting ribosome biogenesis. Typically, ribosomal proteins are encoded by mRNAs containing a 5′TOP within their 5′ UTRs. Such a sequence motif serves as a regulatory region which could be activated by the *m*TOR-LARP1 signalling pathway. LARP1 has the ability to 5′TOP mRNAs and represses their translation initiation when *m*TOR is inactive. A proteomic screen identified LARP1 as an *m*TOR-sensitive 5′cap-binding protein, indicating its responsiveness to TOR activity (Tcherkezian et al., 2014). Early studies were divided on whether LARP1 enhances or inhibits 5′TOP mRNA translation, sparking extensive research into *m*TOR–LARP1 signalling. These investigations have demonstrated that LARP1 has additional roles in translation efficiency and mRNA stability (Jia et al., 2021; Smith et al., 2021). However, the prevailing view supports that LARP1 primarily binds to 5′TOP mRNAs and suppresses their translation initiation when *m*TOR is inactive, thereby ensuring that *m*TOR activity can increase the expression of ribosomal protein mRNAs, which in turn enhances the overall translation efficiency of various transcripts (Philippe et al., 2020; Scarpin et al., 2020).

1.7.5 Translation Regulation by *At*TOR

In plant systems, specifically *Arabidopsis*, *At*TOR is also known to promote translation (Chen et al., 2018; Scarpin et al., 2022; Schepetilnikov & Ryabova, 2018). eIF4G, S6K, and LARP1 are all conserved downstream translation-related proteins from *At*TOR (Scarpin et al., 2022). Other proteins, have significantly diverged across eukaryotic lineages, evolving a plant-specific isoform encoded by a paralogous gene (Gallie & Browning, 2001); an example being eIF4B, known in plants as the isoform eIFiso4G. Plant orthologs of 4E-BPs are not conserved (Brunkard, 2020), although several other proteins have been identified that interact with eIF4E via a 4E-BPs-like eIF4E-binding motif, such as CONSERVED BINDING OF eIF4E 1 (CBE1) and CERES (Patrick et al., 2018; Toribio et al., 2019). S6K and LARP1 have been functionally reported to regulate translation downstream of *At*TOR in plants (Chen et al., 2018; Schepetilnikov & Ryabova, 2018). Recognition of specific mRNAs via *At*TOR-S6K signalling promotes translation reinitiation through the specificity of short upstream ORFs (uORFs) located within the 5'UTR region (Schepetilnikov et al., 2013). Additionally, regulation of 5'TOP mRNAs translation known to be involved in ribosome biogenesis have also been reported and thus the TOR-LARP1-5'TOP signalling pathway is conserved across the plant kingdom (Scarpin et al., 2020).

Large-scale phosphoproteomics analyses have been conducted over the years to capture the landscape of the *At*TOR kinase (Scarpin et al., 2020; Van Leene et al., 2019). Briefly, a total of 160 *AtT*OR-responsive phosphoproteins were identified in which translation factors and cytosolic ribosome proteins were significantly enriched. Among these, E3 ligases known as *At*NOT4s (*described later in this Chapter*) have been identified (though not yet characterised), suggesting a direct link between *At*NOT4s and *At*TOR signalling pathways (*further discussed in Chapter 5).* When *At*TOR is active, regulatory proteins involved in the mRNP loading phase of translation initiation are phosphorylated. This includes LARP1, eIF4E-binding protein CBE1, eIF4A, eIFiso4g (eIF4B), and PABP. In the absence of *At*TOR activity, eIF4G is phosphorylated indicating that another kinase signalling pathway opposes *At*TOR in regulating translation initiation. Within the 43S and 48S pre-initiation complexes (PICs), *At*TOR facilitates the phosphorylation of components of the GTPase eIF2 and its guanine exchange factor, eIF2B, which are crucial for accurate selection of start codons during mRNA scanning. Similarly to mammals, several ribosomal proteins within the 40S and 60S subunits exhibit differential phosphorylation in response to *At*TOR activity, notably the C-terminal phosphosites of RPS6, a direct substrate of *At*TOR-activated S6K.

Beyond its roles in regulating translation, *At*TOR promotes the transcription and stability of many mRNAs associated with translation. These include mRNAs encoding ribosomal protein subunits, initiation and elongation factors, and several accessory proteins. Studies have identified *At*TOR dependent expression of eIF3, eEF1B, and ribosomal proteins (Scarpin et al., 2020). This is likely achieved by modulating both synthesis and degradation rates by inhibiting ribosomal autophagy (Hillwig et al., 2011; Wyant et al., 2018). Thus, *At*TOR not only directly influences translation but also enhances translation efficiency by regulating RNA and protein metabolism. Thus, *At*TOR modulates various aspects of translation in plants, representing one of several mechanism in which global protein synthesis is modulated.

The *At*TOR-S6K-RPS6 signalling pathway plays a role in regulating translation, especially in response to light signals during early development. This mainly occurs during the developmental changes that occur during etiolation and de-etiolation, where light influences the growth of several photosynthetic organs transcriptionally and translationally (Chen et al., 2018). It was shown that *At*TOR activity is essential for light-dependant translation, with RPS6 phosphorylation being a key step in enhancing protein synthesis in de-etiolating *Arabidopsis* seedlings. Upon light perception by phytochrome A (phyA) and cryptochromes (CRYs), COP1 becomes inactive. The inactivity of COP1 permits Auxin to further activate the *A*tTOR-S6K-RPS6 signalling cascade, and therefore leading to an increase of protein synthesis to drive overall growth and development. In support of this, mutants with defects in *At*TOR, S6K or RPS6 had reduced translation efficiency. Phosphorylation of RPS6 can also be stimulated from far-red (FR) and blue (B) light, confirming that the *At*TOR-S6K-RPS6 pathway is responsive to light even before seedlings fully establish photosynthetic activity. Thus, light alone can greatly influence translation through its activation of *At*TOR, highlighting a diverged mechanism evolved solely in plants.

1.8 Regulated Protein Degradation

Previous sections highlighted several biological processes, molecular functions and cellular components that impact protein translation. However, maintenance of proteostasis also includes the removal of proteins that are no longer necessary or have become dysfunctional or misfolded (Callis, 1995). Therefore, protein degradation is just as important as synthesis. As such, conserved mechanisms have evolved to ensure protein quality control, that in turn regulate overall cellular functions (Duttler et al., 2013). In eukaryotes, the two predominant mechanisms for regulated protein degradation are autophagy and targeted proteolysis via the UPS, discussed below.

1.8.1 Autophagy

Autophagy is the major intracellular degradation system whereby cytoplasmic materials are delivered to and degraded in the lysosome in animals and to vacuoles in plants (Bassham et al., 2006; Mizushima & Komatsu, 2011). This system also allows the recycling of cellular components essential in maintaining homeostasis (Tanida, 2011). There are three main forms of autophagy, namely: macroautophagy, microautophagy, and chaperone-mediated autophagy (CMA) (Mizushima & Komatsu, 2011; Tanida, 2011). Briefly, macroautophagy forms 'autophagosomes' in order to degrade target proteins whereas microautophagy directly engulfs target substrate through invagination of lysosomal membranes (Feng et al., 2014; Li et al., 2012). CMA is where chaperone proteins and lysosomal receptors combine to target substrates for degradation (Dice, 2007). Among these, macroautophagy is the most studied type, predominating and often merely called "autophagy." It is highly inducible, especially by nutrient deprivation (e.g., nitrogen or aa starvation), whereby increased formation of autophagosomes is induced (Feng et al., 2014). Interestingly, this process is been primarily modulated through the *m*TORC1 pathway, which initiates a negative feedback loop that can restore amino acid levels by suppressing autophagy upon nutrient replenishment (Jung et al., 2009; Mizushima & Komatsu, 2011).

The endoplasmic reticulum (ER), golgi complex, mitochondria, and plasma membrane all play a part in the formation of autophagosomes. Since it is still a subject of investigation to define an exact role of each contributing membrane in autophagosome biogenesis, their involvement reinforces the multi-faceted nature of autophagy regulation (Mizushima & Komatsu, 2011; Tanida, 2011). Heat shock proteins (HSPs), an example of molecular chaperones, can recognize and transport aberrant proteins that were either incorrectly folded or damaged to lysosomes (Liebl & Hoppe, 2016). CMA depends on the specific recognition of a pentapeptide motif-containing proteins (KFERQ), through the chaperone protein HSP70, which guides the substrates to the lysosome for degradation (Tsai et al., 2003). Cathepsins are proteolytic enzymes that are located within lysosomes and degrade proteins into smaller fragments (Figura & Hasilik, 1986). In conclusion, bulk degradation allows autophagy to be an important process in which the cell is capable of recycling large portions of cytoplasmic contents, mainly organelles and proteins, for cellular renewal and metabolic balance.

1.8.2 Ubiquitin proteasome system (UPS)

Another major pathway for regulated protein degradation in eukaryotes is the ubiquitin proteasome system. This system, in a highly regulated and coordinated fashion (see Section 1.9.2.1) targets a myriad of proteins within the proteome. The three main enzyme-types that make up the UPS pathway are E1 (ubiquitin activating enzymes), E2 (ubiquitin-conjugating enzymes), E3 (ubiquitin ligases, *further discussed in Section 1.9.2.2*). E3's make-up the final step in targeting proteins for degradation through acting as substrate-specificity components. The recognition and interaction between E3 ligases and substrates are mainly mediated by structural motifs and sequences that allow the transfer of ubiquitin molecule(s) from the E2 to the substrate, in a process called ubiquitination (*see Section 1.9.2.3*). Ubiquitination can occur in several different ways and therefore influence the protein's fate (*see Section 1.9.2.4*). In many cases, upon substrate polyubiquitination, the protein is targeted for degradation by the conserved 26S proteasome.

The next section describes the ubiquitination cascade, the function of E3 ligases in substrate recognition, the structural motifs that target proteins for ubiquitination, and the several types of ubiquitination that regulate various cellular activities.

1.8.2.1 Ubiquitination cascade

Ubiquitin is a small proteinaceous molecule consisting only of 76 aa which corresponds to a size of about 8.6 kDa. As mentioned briefly before, transfer of ubiquitination occurs in a three-step enzymatic cascade involving E1, E2, and E3 enzymes (**Figure 8**). First, the free ubiquitin monomer is activated by the covalent attachment of AMP to the C-terminus by an E1 enzyme. It is then able to transfer the activated ubiquitin to an E2 enzyme where it interacts with an E3 (ubiquitin-ligase) enzyme to form an E2-E3 complex. The target protein is then bound by the E2-E3 complex primarily via E3's recognition capabilities (*explained in the section that follows*). Thus, the E3 enzyme catalyses the transfer of ubiquitin from the E2 enzyme to the substrate, allowing specific ubiquitination to take place (Callis, 2014; Ciechanover, 1994; Scheffner et al., 1995). Specificity in protein ubiquitination is provided mainly by the E3 enzyme, which recognizes specific protein degrons to facilitate selective protein ubiquitination. (Callis, 2014; Hershko & Ciechanover, 1998).

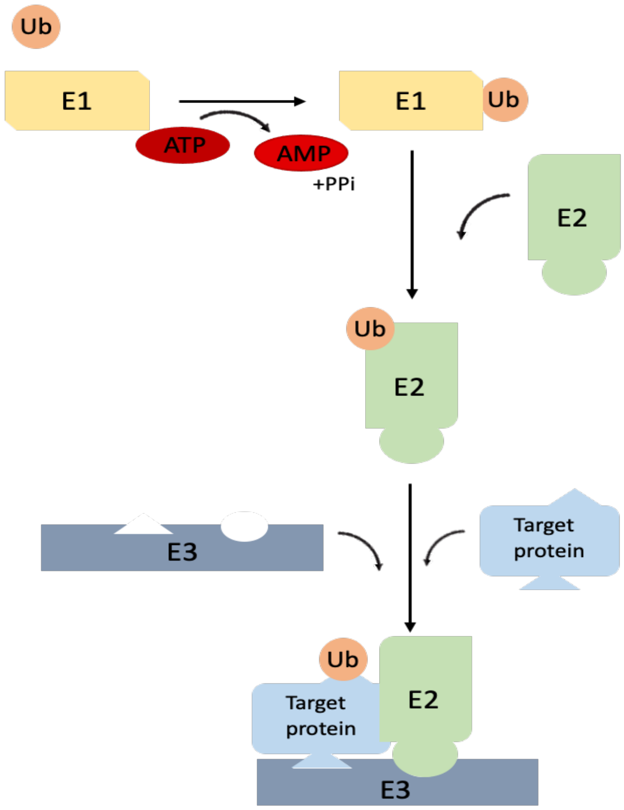

Figure 8 – Enzymatic cascade involved in protein ubiquitination. Ubiquitin (Ub, orange) is first activated by the E1 enzyme (yellow) and transferred to the E2 enzyme (green). The E3 enzyme (dark blue) then recognizes the target protein (blue) and facilitates the transfer of ubiquitin from E2 to the substrate, marking it for degradation. *Adapted from Ciechanover, 1994; Scheffner et al., 1995; Callis, 2014)*

1.8.2.4 Ubiquitination of proteins

Lysine residues determine the various ubiquitination patters that may occur. This becomes more complex in the case of multiple Lys residues present in both substrate and ubiquitin. The ubiquitination pattern in such a case may lead to multiple ubiquitin monomers covalently bonding to these sites causing multi-monoubiquitination (**Figure 9).** In addition to monoubiquitination of substrate lysine residues, internal lysine residues found within ubiquitin, along with its N-terminus, all provide multiple additional sites for polyubiquitination, leading to the development of ubiquitin chains (Akutsu et al., 2016). In *Arabidopsis*, six internal ubiquitin lysine residues have been observed as ubiquitination sites, allowing the formation of diverse branching ubiquitin chain topologies (Callis, 2014). While lysine-48 linked polyubiquitin chains were historically believed to be required for degradation, the 26S proteasome targets a range of polyubiquitin chains including lysine-11 and lysine-63 linked chains (Clague & Urbé, 2010). Polyubiquitin chains linked to Lysine-11 are important for cell cycle regulation, especially during mitosis as substrates are marked via anaphase-promoting complex (APC/C) for degradation. Chains linked at Lysine-63 are mainly important for functions that are non-proteolytic such as DNA repair and signalling (Clague & Urbé, 2010; Song & Rape, 2010). These non-proteolytic signals occur in the *Arabidopsis* transcription factor HY5, an essential regulator in light signalling pathways, for example. The attachment of polyubiquitin chains allows HY5 to aggregate and activate several genes responsive to light which modulates growth and development according to light conditions (Komander & Rape, 2012). Alongside lysine residues, other structural motifs have been described as potential sites for ubiquitination (Ciechanover, 1998; Dikic & Schulman, 2023).

Ubiquitination can also occur on non-lysine residues such as threonine, cysteine and arginine as well as lipids and sugars (**Figure 9**). (Cadwell & Coscoy, 2005; Dikic & Schulman, 2023). Arginine ubiquitination is very uncommon and has only been reported in pathogen-host interactions, such as with *Legionella pneumophila's* effector SdeA, which attaches ubiquitin to arginine via a phosphoribosyl linkage (Qiu et al., 2016). This bypasses the traditional pathway of the ubiquitination cascade, which allows the pathogen to infiltrate host functions and therefore evade the immune response. Threonine ubiquitination has been studied in neural development and injury responses. The E3 ligase MYCBP2 catalyses threonine ubiquitination via a special RING-Cys-relay (RCR) mechanism (Pao et al., 2018). E3 ligase HOIL1 is part of the Linear ubiquitin chain assembly complex (LUBAC) and can attach ubiquitin to serine hydroxyl groups. Target substrates that are subjected to this kind of ubiquitination are proteins associated to the Myddosome inflammatory complex. Interestingly, sugar can also be ubiquitinated in a similar fashion but instead occurs on hydroxyl groups (Kelsall et al., 2019). RNF213 is an E3 ligase that has the ability to attach ubiquitin to lipids, specifically reported in the lipid A moiety of bacterial lipopolysaccharides triggering antibacterial responses (Otten et al., 2021).

The signalling properties of ubiquitin are further expanded by modifications to the protein itself, such as acetylation on lysine residues and phosphorylation on serine or threonine residues (Swatek & Komander, 2016). For example, phosphorylation of ubiquitin at serine-65 may change its structure and interaction with ubiquitin-binding domains, thus affecting the stability of polyubiquitin chains and resistance against deubiquitinating enzymes (Wauer et al., 2015). When ubiquitin is acetylated it interferes with the formation of polyubiquitin chains, shifting the balance toward mono- or oligoubiquitination and affecting the functional outcomes of the modification (Ohtake et al., 2015). Various changes in ubiquitin structure and attachment sites greatly extend the regulatory possibilities of the ubiquitin system, but many aspects of these modifications remain underexplored (Dikic & Schulman, 2023).

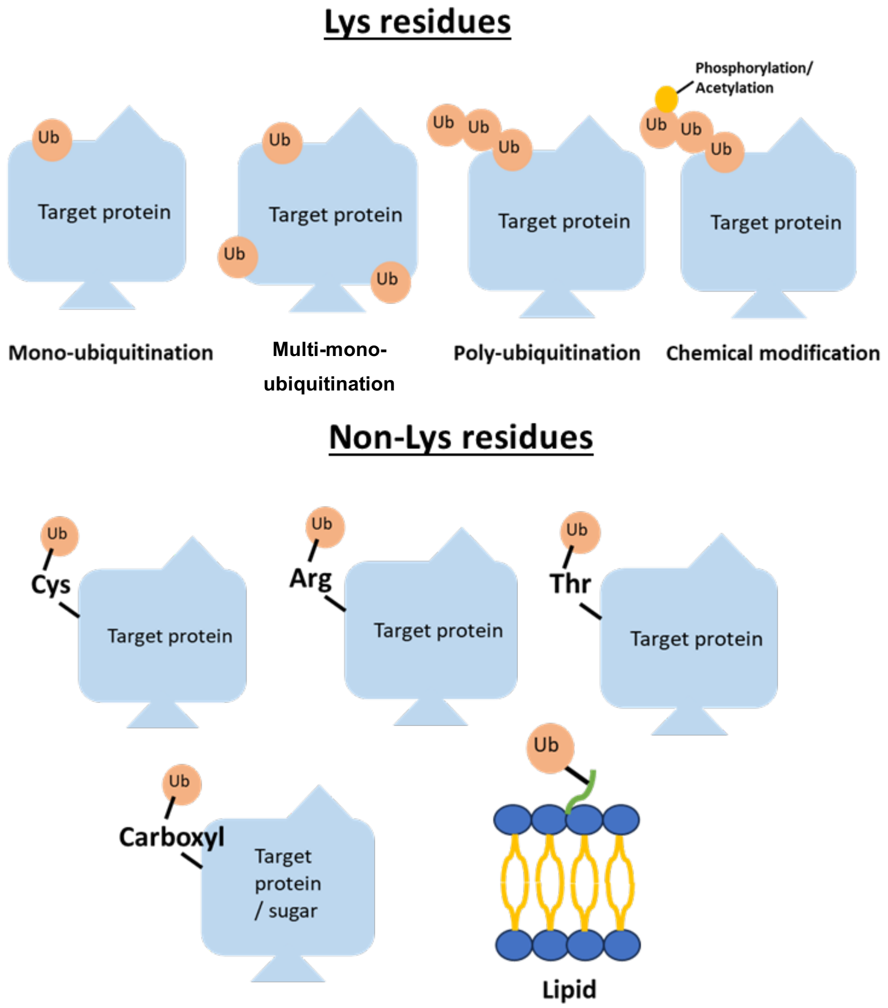

Figure 9 – Ubiquitination patterns and its modifications. Lys residue based: Proteins can be either mono-ubiquitinated (single site and single Ub attachment), multi-mono-ubiquitination (multiple sites, multiple single Ub attachments) or poly-ubiquitinated (single site, multiple Ub to form a chain). On the ubiquitin molecule itself, a further chemical modification can be made such as phosphorylation or acetylation. Non-Lys residue based: ubiquitin is attached to residues other than Lys, such as cysteine (Cys), arginine (Arg), Threonine (Thr) as well as non-protein targets like lipids and carbohydrates. *Adapted from Dikic and Schulman 2023.*

1.8.2.3 Structural motifs targeting proteins for ubiquitination

Ubiquitin ligases recognize, bind and ubiquitinate their substrate(s) depending on particular structural motifs – often referred to as degrons. Degrons can be intrinsic sequences or structural features within the protein or in certain cases only become accessible under specific conditions (Ciechanover, 1998; Randles & Walters, 2012). Degrons play an important feature in determining the rate of protein degradation since they serve as key signals for ubiquitination and proteasomal degradation. A well-studied degradation pathway involves identification of N-degrons (N-end rule) in which single N-terminal amino acids regulate the half-lives of proteins (Varshavsky, 2019). Their type and abundance have a substantial impact on the stability of the protein, and they can be found at different positions within a polypeptide. Thus, the half-life can hugely vary between some minutes to years depending on the availability and accessibility of such degron motifs present in the proteins. (Glickman & Ciechanover, 2002; Ravid & Hochstrasser, 2008).

Post-translational modifications can create secondary motifs that facilitate ubiquitination (**Figure 10**). Evidence indicates that many proteins are targeted for ubiquitination through phosphorylation. For example, degradation of the yeast G1 cyclin CLN3 (Schneider et al., 1998; Yaglom et al., 1995) and the GCN4 transcriptional activator (Hope & Struhl, 1987; Kornitzer et al., 1994) through phosphorylation at a PEST sequence. In contrast, mammalian G1 cyclin D1 undergoes degradation through phosphorylation at a threonine residue located outside a PEST sequence (Diehl et al., 1997). IκBα is targeted for degradation by phosphorylation at serine residues Ser32 and Ser36, with these phosphorylation sites serving as the ligase-binding site (Heyninck et al., 2003). Ultimately, phosphorylation acts as a signal for ubiquitination, which is necessary for processes such as the internalization of ligand-receptor complexes (Hicke et al., 1998).

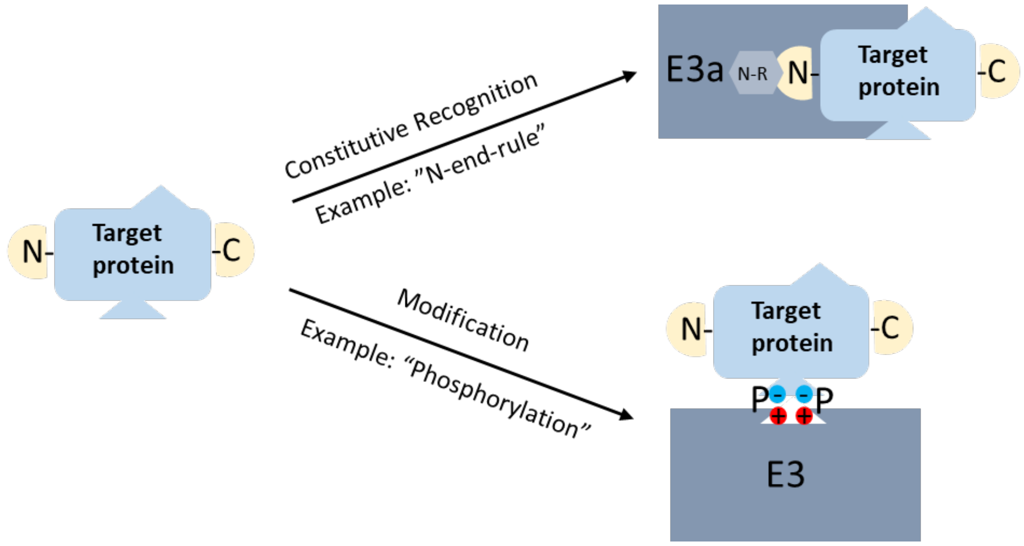

Figure 10 – Two modes of recognition of target proteins by E3 ligases. 1) Constitutive Recognition via "N-end rule", 2) Posttranslational modifications such as "Phosphorylation", *Based on Randles & Walters, 2012.*

1.8.2.2 E3 ligases

In contrast to other eukaryotes, plants have a higher abundance of E3 ligases, which highlights the significance of the UPS in this kingdom (Yee & Goring, 2009; Zhang et al., 2021). Over 1500 E3s have been identified in *Arabidopsis*, which possesses only two E1 and 37 E2 enzymes (Kraft et al., 2005). This not only indicates the ability of E2s to interact with multiple E3s but also highlights E3s as the most diverse class of enzymes within the ubiquitin cascade. The enhanced diversity of E3 ligases in plants, relative to other eukaryotes, stems primarily from the expanded abundance of RING-type E3s (Chen & Hellmann, 2013; Kraft et al., 2005).

E3 ligases operate through one of two primary mechanisms. They either act as catalytic intermediates in the process of ubiquitination, like E1 and E2 enzymes, or they facilitate the direct transfer of ubiquitin from E2~Ub to the substrate (**Figure 11**) (Callis, 2014; Ciechanover, 1994). The basis for high specificity in this system lies in the binding of target proteins to ligases before their conjugation, and this aspect is also brought to focus when considering the mode of action for E3s. Even though research carried out has greatly extended our knowledge on E3 ligases in plants, mechanisms are still complex in view of their immense diversity, often context-specific actions, and the fact that many E3 ligases control distinct signalling pathways by use of a variety of multi-subunit complexes.

E3 enzymes are typically grouped into three main classes, namely RING (Really Interesting New Gene), U-box, and HECT-type E3s. This all depends on the structure of the specific E2-binding domain found within the E3 which in turn varies the way in which ubiquitin is transferred (**Figure 11**). Interestingly, RING and U-box domains have a high degree of structural similarity and only differ in the mechanisms by which their structures are formed (Aravind & Koonin, 2000; Pruneda et al., 2012). U-box domains produce their structure through non-covalent interactions between nearby amino acids, whilst RING domains acquire their structure by binding two zinc ions (Morreale & Walden, 2016; Pruneda et al., 2012). When a RING or U-box E3 ligase binds concurrently to both the E2 enzyme and the substrate protein, it facilitates the direct transfer of ubiquitin from the E2 to the substrate (Berndsen & Wolberger, 2014; Pruneda et al., 2012). *At*PRT6 is an example member of the family of E3 ubiquitin ligases, and plays a crucial role in recognizing and targeting proteins with destabilizing N-terminal residues including Met-Cys- (MC)-proteins marking them for proteasomal degradation via the Arg/N-end rule pathway (Garzón et al., 2007; Gibbs et al., 2014).

HECT domains, on the other hand, have a catalytic cysteine residue that forms a thioester bond with ubiquitin in addition to having an E2 binding site (Scheffner et al., 1993). Consequently, ubiquitination by HECT-type E3 ligases involves the transfer of ubiquitin from the E2 to the E3 and subsequently to the substrate (Rotin & Kumar, 2009; Scheffner et al., 1993). The evolution of the HECT ligase family is marked by the extensive diversification of N-terminal protein–protein interaction domains (Grau-Bove et al., 2013). The architecture of these N-terminal regions varies widely, with some HECT ligases containing a single protein–protein interaction domain, while others have multiple domains. These N-terminal domains facilitate interactions with both substrates and the proteasome. Through physical interaction, HECT ligases impart ubiquitin ligase activity to the proteasome (Wang & Spoel, 2022). Similar to extrinsic proteasome receptors, some HECT ligases interact with the proteasome via N-terminal UBA, Ubl, and ubiquitin-interacting motif (UIM) domains. However, UPL3 (Ubiquitin Protein Ligase 3) utilizes an armadillo repeat domain-containing N-terminus to engage with the proteasome (Furniss et al., 2018). It has also been demonstrated that other members of the UPL family interact with the proteasome, including *Arabidopsis* UPL1, which also has armadillo-type folds and a UBA domain, and UPL5, which has a Ubl domain.

UPL3 has been linked to a number of cellular functions, such as hormone signalling and plant immunity (Downes et al., 2003; Kraft et al., 2005). In particular, UPL3 is an important modulator ubiquitination and degradation of the transcriptional regulator NPR1, which is critical for salicylic acid-induced transcriptional reprogramming. Impaired UPL3 function leads to poor turnover of NPR as well as dampened immune gene expression and reduced resistance against pathogens. Furthermore, UPL3 functions in coordination with the proteasome to further increase global polyubiquitination levels, reinforcing the importance of its role in proteasome-mediated transcriptional regulation (Furniss et al., 2018; Wang & Spoel, 2022). Besides immunity, UPL3 plays a role in other hormone signalling pathways in which it acts in a feedback mechanism controlling other transcriptional activators such EIN3 (Wang et al., 2022).

Another class of E3 ligases is formed by so-called RBR-type (RING-Between-RING) E3 ligases, which contain two RING domains, one of which adopts the typical RING domain structure. Although there are two RING domains, the substrate protein undergoes attachment of ubiquitin similar to the HECT-type mechanism, with an E2 bound to the canonical RING domain and ubiquitin being transferred to the substrate by a thioester bond with a cysteine residue in the non-canonical RING domain. Thus, RBR E3 ligases are considered as a hybrid class of E3 ligase (Eisenhaber et al., 2007; Morreale & Walden, 2016).

The best-studied roles of E3 ligases include those involved in phytohormone signalling and abiotic stress response, whereby they become key modulators in both hormone signal perception and adaptation of plants to an ever-changing environment (Al-Saharin et al., 2022; Kelley, 2018). As an example, SCFTIR1 is essential for auxin signalling because it facilitates the auxin/indol-3-acetic-acid transcriptional repressors' degradation, which allows auxin-induced gene expression (Dezfulian et al., 2016). In a similar aspect, SCFCOI1 is involved in the sensing and signalling of Jasmonic acid (JA) and targets JAZ proteins for degradation, hence promoting transcription that responds to Jasmonic acid (Xu et al., 2002). Moreover, E3 ligases regulate phytohormone interactions by mediating signalling pathways. For example, the MAX2 E3 ligase, involved in strigolactone (SL) signalling (Wang et al., 2013), also influences other pathways such as gibberellin and Brassinosteroids (BR) signalling, thus integrating developmental and environmental cues to modulate plant growth. Several E3 ligases are reported in ABA signalling which include the class of RING-type ligases (*to be discussed later on in this section*) that modulate stress responses through targeting negative regulators of ABA signalling and can increase drought tolerance (Cheng et al., 2017; Zhao et al., 2014). RGLG1 E3 RING ligase in *Arabidopsis* enhances drought tolerance through the degradation of several signalling proteins. (Cheng et al., 2012). Other E3 ligases such as *At*PQT3 are associated to oxidative stress, regulating the expression of antioxidant enzymes in protection against reactive oxygen species (ROS) damage (Luo et al., 2016). *At*PUB48 is an E3 ligase that targets HSPs under heat stress to promote thermotolerance. (Peng et al., 2019).

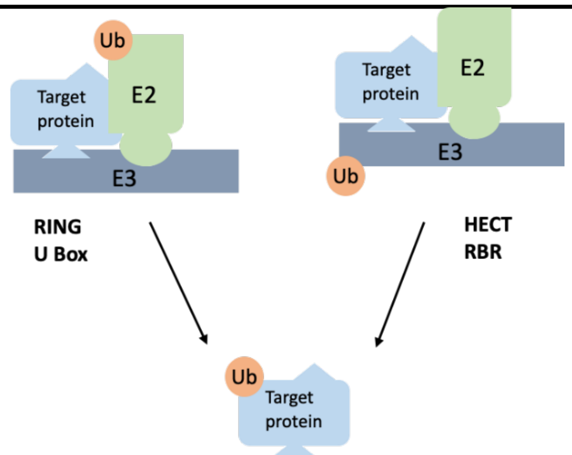

Figure 11 – Mode of action of different E3 ligases classes. Ubiquitin ligases are categorised based on the structure of the specific E2-binding domain which also determines how ubiquitin is transferred. RING and U-box domain-containing E3s mediate transfer of ubiquitin (U) directly from the E2-Ub intermediate to the substrate protein. HECT domain-containing E3s form an E3-Ub intermediate prior to the transfer of ubiquitin to the substrate protein. *Based on Ciechanover, 1994.*

1.9 NOT4 E3 ligases

The NOT4 E3 ligase was identified and first characterized in yeast. It was initially described to be a general negative regulator that acts upon tetracycline-dependent transcription (Collart & Struhl, 1994). Subsequently, it was revealed that NOT4 forms part of the CCR4-NOT complex (**Figure 12)**; a complex comprised of 8 other proteins (Collart & Panasenko, 2012). In addition to ubiquitination activity carried out by NOT4, the CCR4-NOT complex also possesses deadenylase activity, which is carried out by the CCR4 and CAF1 subunits (Tucker et al., 2002; Tucker et al., 2001). NOT4, along with NOT2 and NOT5, binds to the C-terminal region of the complex's scaffold protein, NOT1 (Basquin et al., 2012). Meanwhile, the deadenylase module associates with a central domain of NOT1 (Maillet et al., 2000). These two enzymatic functions, ubiquitination and deadenylation, are positioned at opposite ends of the scaffold (Collart & Panasenko, 2012). While these activities coexist within the same complex, it remains unclear whether they are directly linked or operate independently.These processes likely function in parallel to regulate mRNA fate, but their mechanistic connection is still an open question (Azzouz, Panasenko, Deluen, et al., 2009; Halter et al., 2014).

NOT4 was further identified as having a role in transcriptional regulation and mRNA decay indicating an importance in proper mRNA deadenylation and the negative regulation of transcription elongation by RNA polymerase II (Liu et al., 1998). Remarkably, studies of NOT4 have also revealed its association with ribosomes, its role in co-translational quality control of mRNA and protein, its role in proteasome assembly, and finally it has been proposed to function as an N-recognin E3 ligase of the acetylation-dependent N-end rule pathway in yeast (Albert et al., 2002; Collart & Struhl, 1994; Liu et al., 1998; Preissler et al., 2015).

The following section will focus on the mechanistic and biological functions of *Sc*NOT4, specifically highlighting its localisation, structure, and functional conservation across homologs such as Human NOT4 (CNOT4) and *Arabidopsis* NOT4s (*At*NOT4A, *At*NOT4B and *At*NOT4C).

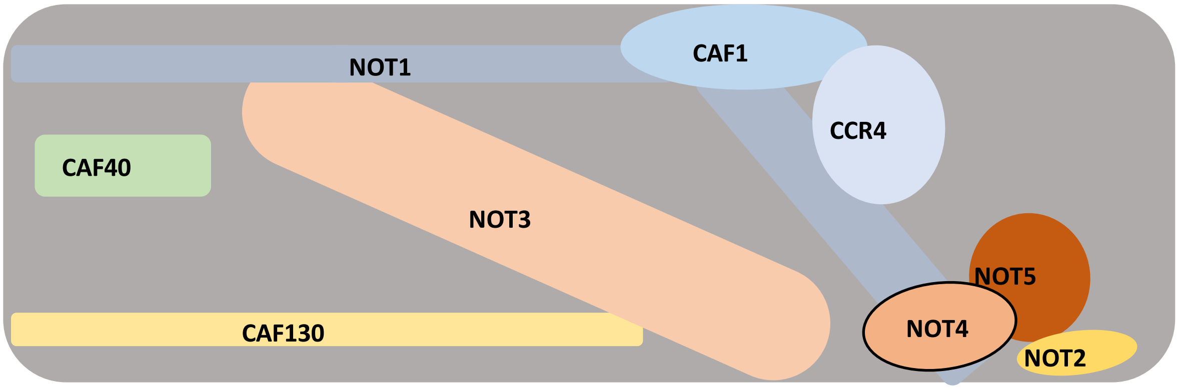

Figure 12 – The CCR4-NOT complex consists of 9 proteins. NOT1 acts as a central scaffold organizing the assembly and function of the complex. NOT2 stabilizes the complex because of its interaction with NOT1. NOT4, together with NOT5, modifies the two major activities, namely, transcription and the deadenylation of mRNA. NOT4 is an E3 ubiquitin ligase that tags the target proteins for degradation. CCR4 and CAF1 are the deadenylases that finally shorten the poly(A) tails to commit the mRNA for degradation. CAF40 helps in binding RNA and maintaining mRNA stability, while CAF130 helps in the assembly and structural integrity of the complex.

1.9.1 Subcellular localisation and structure of *Sc*NOT4

Localised to the nucleus and the cytoplasm (Panasenko & Collart, 2011). *Sc*NOT4 contains 587 aa with an approximate size of 65kDa. Notably, the structure of *Sc*NOT4 contains two conserved domains: the RING finger domain, and an RNA recognition motif (RRM) (*See Chapter 3.1,* **Figure 14**). These structural features, particularly the RING finger domain for proteolytic functions , and the RRM for RNA binding, contribute to its multifaceted roles in co-translation quality control, transcriptional regulation, and protein degradation to ensure efficient and correct translation of polypeptides (Collart, 2013a; Halter et al., 2014; Panasenko & Collart, 2011; Preissler et al., 2015).

1.9.2 The diverse biological functions of *Sc*NOT4

*Sc*NOT4 was first known as SIG1, MOT2 and eventually NOT4. Early genetic screens performed in yeast were carried out to characterise the function of *Sc*NOT4 as its specific roles were unknown. Based on this, *Sc*NOT4 was concluded to be involved in G-protein signalling, thus providing a clear role in gene expression regulation (Cade & Errede, 1994; Collart & Struhl, 1994; Leberer et al., 1994). Application of a synthetic genetic array analysis further provided clarity by employing a high-throughput approach of mapping genetic interactions between *Sc*NOT4 and other yeast genes (Mulder et al., 2007). Using both the not4Δ (complete knock out) and not4L35A (with an abolished RING domain) mutants, this SGA screen revealed important genetic interactors related to transcription, protein degradation, and stress responses. Importantly, the study confirmed the E3 ligase activity of ScNOT4 through its interactions with ubiquitin-conjugating enzymes Ubc4p and Ubc5p (Mulder et al., 2007).

A total of 49 genetic connections were found by the SGA analysis, several of which suggested that *Sc*NOT4 is involved in DNA damage responses, the ubiquitin-proteasome system (UPS), and transcriptional control. Further evidence of *Sc*NOT4's role in preserving cellular homeostasis was provided by the phenotypes seen in not4Δ mutants, such as sensitivity to translation inhibitors (e.g., cycloheximide and hygromycin B) (Panasenko & Collart, 2011), growth defects at high temperatures (Mulder et al., 2007), and defects in proteasome function (Panasenko & Collart, 2011). ScNOT4's specific ubiquitination targets and roles in transcriptional regulation, the ubiquitin-proteasome system, mRNA degradation, ribosome interactions, and co-translational quality control are highlighted in **Figure 13** and will be discussed in the sections that follow.

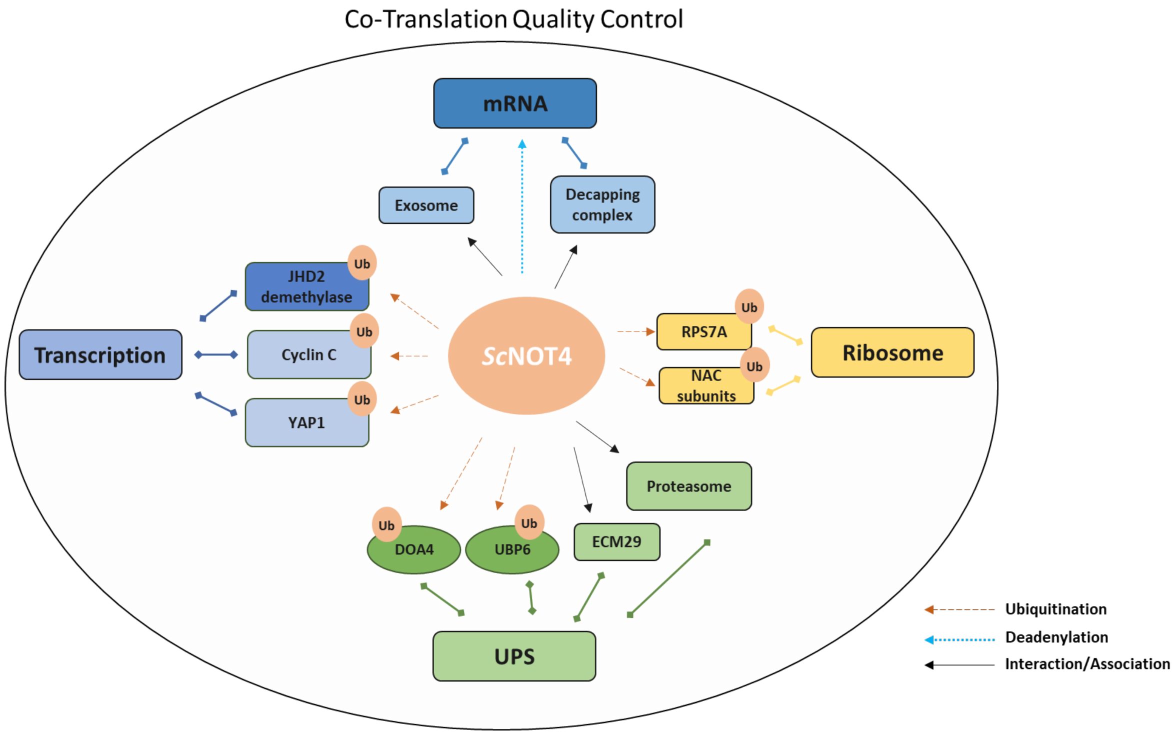

Figure 13 – Diverse biological functions of *Sc*NOT4. *Sc*NOT4 contributes to mRNA degradation through deadenylation, interaction with the decapping complex, and the exosome. It also regulates ribosome function by ubiquitinating RPS7A and NAC subunits. Additionally, *Sc*NOT4 is involved in the ubiquitin-proteasome system (UPS) by ubiquitination components like DOA4 and UBP6, as well as interacting directly with the proteasome and interactors like ECM29. It also contributes to the regulation of transcription by ubiquitinating transcription factors (Cyclin C and YAP1), and JHD2 demethylase. Overall highlighting its role in co-translation quality control. *Adapted from Mulder et al., 2007.*

1.9.2.1. *Sc*NOT4 and Transcription

Many genes identified in the *Sc*NOT4 synthetic genetic array (SGA) screen encode proteins linked to transcription (Mulder et al., 2007). Recent research has shown that the CCR4-NOT complex interacts with RNA polymerase II, playing a role in transcription elongation (Kruk et al., 2011). *Sc*NOT4 targets several proteins directly involved in transcription for polyubiquitination and subsequent proteasomal degradation (Collart, 2013b). For instance, the JHD2 demethylase, which removes methyl groups from histone H3 lysine 4, is ubiquitinated and degraded by *Sc*NOT4. In *Sc*NOT4 -deficient cells, JHD2 accumulates, leading to reduced trimethylation of histone H3 lysine 4, which is associated with transcription regulation (Laribee et al., 2007; Mersman et al., 2009). Thus, *Sc*NOT4 impact on transcription could be partially mediated through its regulation of JHD2. *Sc*NOT4 can act both in the cytoplasm and nucleus as evidenced through its degradation of cyclin C and YAP1, respectively. As part of the cyclin-CDK8 complex which is associated with RNA polymerase II and the mediator complex, Cyclin C is a nuclear protein that is translocated to the cytoplasm where *Sc*NOT4 targets it for degradation. In contrast, the YAP1 transcription factor is degraded in the nucleus by *Sc*NOT4 under oxidative stress (Gulshan et al., 2012). These examples highlight the versatility of *Sc*NOT4 abilities to degrade transcription-associated proteins in different cellular compartments.

1.9.2.2 *Sc*NOT4 and the Ubiquitin-Proteasome System (UPS)

Among the proteins identified in the SGA screen are the deubiquitinating enzymes DOA4 and UBP6. Cells deleted for ScNOT4 have impaired proteasome function and therefore less free ubiquitin accumulating polyubiquitinated proteins (Panasenko & Collart, 2011; Park et al., 1997; Swaminathan et al., 1999). *Sc*NOT4's interaction with proteasome subunits and its role in maintaining proteasome integrity suggest that it contributes to proteasome assembly and stability (Laribee et al., 2007). In *Sc*NOT4-deficient cells, proteasomes are either unstable or incorrectly assembled, highlighting *Sc*NOT4's role in ensuring proper proteasome function (Panasenko & Collart, 2011). In particular, *Sc*NOT4 appears to promote the assembly of the regulatory particle of the proteasome in conjunction with Extracellular Mutant 29

(ECM29). ECM29 is a proteasome-associated protein that maintains the structural integrity and stability of the proteasome (Lehmann et al., 2010). In the absence of *Sc*NOT4, the regulatory particle becomes unstable, and some proteasomes exhibit aberrant salt-resistant assembly, a phenotype shared with *ecm29* mutants (Lehmann et al., 2010). These interactions of ScNOT4 with ECM29 and proteasome subunits may promote proper proteasome assembly to function properly (Collart, 2013b; Panasenko & Collart, 2011).

1.9.2.3 *Sc*NOT4 and mRNA Degradation

As part of the CCR4-NOT complex, which includes major eukaryotic deadenylases, *Sc*NOT4's role in mRNA deadenylation linked to the CCR4 and CAF1 components is not well understood (Tucker et al., 2002). The rate of poly(A) tail shortening in certain mRNAs is only slightly. Beyond deadenylation, *Sc*NOT4 may influence mRNA degradation through its association with components of the decapping complex and the exosome (Azzouz, Panasenko, Colau, et al., 2009; Maillet & Collart, 2002). *Sc*NOT4 has also been implicated in nuclear exosome functions, such as snoRNA processing and quality control of nuclear export (Assenholt et al., 2011).

1.9.2.4 *Sc*NOT4 and the Ribosome

RPS7A and NAC subunits were identified as ubiquitination targets of *Sc*NOT4, thus highlighting a relationship between *Sc*NOT4 and ribosomes (Panasenko et al., 2006; Panasenko & Collart, 2011; Panasenko et al., 2009). Interestingly, RPS7A seems to be ubiquitinated by *Sc*NOT4 independent of the CCR4-NOT complex. Similar to most ribosomal proteins in yeast, RPS7A has a paralog known as RPS7B. Among both paralogs, the lysine residues are conserved and are highly similar in protein sequence, though RPS7B is not ubiquitinated by *Sc*NOT4. The key difference between RPS7 paralogs is the N-terminal domains which suggests that this may be the region that *Sc*NOT4 recognises (Panasenko & Collart, 2012). With regards to NAC subunits and *Sc*NOT4, it was shown that ribosome subunit Rpl25 does not co-immunoprecipitated with NAC in the absence of ScNOT4. The ubiquitination of NAC facilitates its co-immunoprecipitation with Rpl25 and therefore shows the importance of *Sc*NOT4s connecting NACs with the ribosome (Panasenko et al., 2009). Another finding showed that the absence of *Sc*NOT4 leads to alterations in polysome profiles and accumulation of protein aggregates. Though the exact role in which *Sc*NOT4 plays in ribosome function and protein aggregation is not fully understood, the ubiquitination activity of *Sc*NOT4 has highlighted an important aspect in regulating protein homeostasis and proper ribosome function (Collart, 2013b; Halter et al., 2014; Preissler et al., 2015).

1.9.2.5 *Sc*NOT4 and Quality Control

*Sc*NOT4s association with polysomes and its function in targeting ribosome-associated and ribosomal proteins for ubiquitination have proposed *Sc*NOT4 as an important factor in co-translational quality control (Assenholt et al., 2011; Collart, 2013a). Though, the underlying mechanism in which *Sc*NOT4 contributes to co-translational quality control remains under investigation. One hypothesis is that *Sc*NOT4 acts as a surveillance unit by ubiquitinating arrested nascent chain proteins, provoking translational arrest and triggering their degradation via the proteasome in a process. However, this became more complicated when it was concluded later that the RING E3 ligase LTN1 is primarily responsible , challenging *Sc*NOT4's involvement in the process (Bengtson & Joazeiro, 2010). The deletion of *Sc*NOT4 seemed to increase levels of truncated nascent polypeptides when LTN1 E3 ligase was also deleted (Ralser et al., 2012). Thus, ScNOT4 may function as an ancillary surveillance complex in collaboration with LTN1 (Collart, 2013a).

1.9.3 Homologues of *Sc*NOT4

1.9.3.1 The human homologue of *Sc*NOT4 –CNOT4

NOT4 in humans, named CNOT4, was first identified in 2001 through the identification of its RING domain structure (Hanzawa et al., 2001). In contrast to *Sc*NOT4, CNOT4 appears to more loosely associate with the CCR4-NOT complex (Albert et al., 2002; Chapat & Corbo, 2014). Like *Sc*NOT4, CNOT4 possesses a RING domain, which facilitates its interaction with various ubiquitin-conjugating E2 enzymes (Panasenko et al., 2006). In both yeast and human cell lines, CNOT4 has been shown to target multiple proteins for ubiquitination, including the master regulator of meiosis MEI2 (Simonetti et al., 2017), the co-translational quality control factor ABCE1 (Wu et al., 2018), the histone H3 lysine-9 demethylase JHD2 (Mersman et al., 2009), the transcriptional coactivator YAP1 (Gulshan et al., 2012) , and the ribosomal protein RPS7A (Panasenko & Collart, 2012).

Beyond its E3 ligase activity, the CNOT4 RRM domain has been characterised to having a role in embryo development, specifically in the progression of meiosis during spermatogenesis (Chapat & Corbo, 2014; Dai et al., 2021). Male germ cells that have impaired CNOT4 function leads to dysfunctional DNA damage repair as well as improper homologous crossover between allosomes (Dai et al., 2021). When analysing its role when bound to the CCR4-NOT complex, it was found that CNOT4 plays an import role in mRNA deadenylation in conjunction with CNOT7. CNOT4 is responsible for targeting specific mRNAs to CNOT7 which leads to the degradation of their poly(A) tails. This process ensure the removal of mRNAs particularly important when the cell is transitioning from the zygotene stage to the pachytene stage during meiosis (Morgan et al., 2019). This has a vital impact in later stages of spermatogenesis as the mRNA degradation ensures the correct expression of genes needed for the transition of stages. Overall, the proper crossover between allosomes, DNA damage repair and overall male fertility is all regulated by CNOT4 (Dai et al., 2021).

1.9.3.2. The *Arabidopsis* homologues of *Sc*NOT4 – *At*NOT4A, *At*NOT4B and *At*NOT4C

Despite the diversity of established roles for NOT4 in yeast and mammals, the presence and functions of NOT4-like E3 ubiquitin ligases in plants has not been studied. In contrast, several homologs of other CCR4-NOT components have been investigated in plants (Arae et al., 2019; Motomura et al., 2020; Schwenk et al., 2021; Suzuki et al., 2015; Walley et al., 2010), but there is a lack of information regarding how this complex might connect to protein degradation or interact with the translational machinery to monitor protein synthesis. Indeed, knowledge of co-translational protein degradation mechanism in plants is lacking more broadly. The *Arabidopsis* genome encodes for three NOT4-like E3 ligases: *At*NOT4A (AT5G60170), *At*NOT4B (AT3G45630), *At*NOT4C (AT2G28540) (*see Chapter 3.1*). Like the single copy in yeast and mammals, *At*NOT4s also consist of sequential RING and RRM domains, indicating likely proteolytic and RNA-binding function. Downstream of this, *At*NOT4 paralogs diverge and show significant differences suggesting that they may have different targets and biological processes. Perhaps, the expanded number of NOT4 proteins in plants grants them greater flexibility in monitoring and precisely controlling translation. Additionally, each paralog may have evolved distinct functions to regulate specific aspects of both basal and stress-responsive translation or other functions. Given this background, the next section will focus on the specific objectives and hypotheses of this study, which broadly aims to uncover the unique roles and regulatory mechanisms of NOT4-like E3 ligases in plant co-translational quality control.

1.10 Focus of this Study

Among the E3 ubiquitin ligases involved in the UPS, the NOT4 proteins have been implicated in co-translational quality control and the regulation of protein synthesis in yeast and metazoans. However, the presence and functional roles of NOT4-like proteins in plants remain unexplored. This study focuses on understanding the roles of three putative NOT4 paralogues (*At*NOT4A, *At*NOT4B, and *At*NOT4C) in *Arabidopsis thaliana*, with a view to advancing our knowledge of proteostatic mechanisms and their connection to plant growth and stress responses.

Specifically, this study aims to:

1. **Define the roles of *Arabidopsis* NOT4-like proteins** by characterizing single and combination mutants to reveal their functional contributions to plant growth and development. This involves investigating whether these proteins have overlapping or specialized functions and whether their redundancy compensates for the absence of one another.
2. **Elucidate the links between *Arabidopsis* NOT4s and protein homeostasis mechanisms** such as co-translational quality control, ubiquitination, and translational fidelity. By analysing translational dynamics and proteome integrity in mutant plants, this work investigates how *At*NOT4s contribute to preventing translational errors and managing protein misfolding under normal and stress conditions.
3. **Investigate the functional relationship between AtNOT4s and the TOR kinase** pathway, a master regulator of energy- and nutrient-dependent translation. This includes examining TOR activity in *Atnot4abc* mutants and exploring how *At*NOT4s contribute to TOR-mediated growth and translation regulation.

The study aims to advance the state-of-the-art by uncovering the roles of plant-specific NOT4-like proteins in maintaining proteostasis and their unique interplay with TOR signalling. By identifying the impact of *At*NOT4s on growth, translation, and stress responses, this research not only provides fundamental insights into conserved quality control mechanisms across kingdoms but also highlights potential targets for enhancing plant resilience and productivity through improved protein homeostasis. This is directly linked to the overarching objective of understanding how plants balance protein synthesis and degradation to support growth and stress adaptation.

Chapter 2 - Materials and Methods

2.1 Organisms and Strains

2.1.1 *Arabidopsis thaliana*

2.1.1.1. Wildtype

The *Arabidopsis thaliana* Columbia-0 (Col-0) ecotype was used as the wild-type background for all experiments. All plants were grown under controlled environmental conditions (*see 2.5*.).

2.1.1.2 T-DNA insertion lines

T-DNA insertion mutants were acquired from the GABI-KAT (*not4a*; GABI_134E03), SAIL (*not4b*; SAIL_274_D03) and SALK (*not4c*; SALK_099755), collections from the Nottingham *Arabidopsis* Stock Centre (NASC). The *pgr3-4* line (FLAG 086D06) was acquired from the Versailles *Arabidopsis thaliana* Stock Centre.

2.2.2.Bacterial strains

2.2.2.1 *Escherichia coli (*NEB® 5-alpha)

For bacterial transformation and plasmid propagation, NEB® 5-alpha Competent *E. coli* (High Efficiency) was used.

2.2.3 *Agrobacterium tumefaciens* (GV3101)

Arabidopsis thaliana was stably transformed by *Agrobacterium tumefaciens* strain GV3101. GV3101 contains the disarmed Ti plasmid pMP90 providing gentamycin resistance, and this strain also carries rifampicin resistance.

2.2 List of Vectors

Table 1 – List of Gateway compatible Vectors used for cloning

Gateway Entry Vectors for *E.coli*			
Vector	*Selection Marker*	*Size (bp)*	*Description*
pDONR™221 (Invitrogen)	Kanamycin	4,762	Directionally clone a blunt-end PCR product into a vector for entry into the Gateway™ System.
pENTRY/D-TOPO® (Invitrogen)	Kanamycin	2,820	To generate an entry clone, and subsequently recombine gene of interest into a variety of expression vectors adapted for use in Gateway™ Technology.

Gateway Destination Vectors				
	Selection Marker			
Vector	*E.coli*	*A.thaliana*	*Size (bp)*	*Description*
pGWB533 (Nakagawa et al., 2007)	Spectinomycin and Chloramphenicol	Hygromycin	12,977	Gateway cloning compatible binary vector for C-terminal fusion with GUS
pEarleyGate103 (Earley et al., 2006)	Kanamycin	Basta	12,411	Gateway cloning compatible binary vector with C-terminal fusion with mGFP5

2.3 List of Antibodies

Table 2 – List of primary and secondary antibodies used for Western blotting

Primary Antibodies		
Antibody	**Protein Target**	**Host Species**
α-RPS6 (AS19 4292)	40S ribosomal protein S6-1	Rabbit
α-RPS6-P (Ser237) (AS19 4291)	Phosphorylated (Ser237) 40S ribosomal protein S6-1	Rabbit
α-TOR (AS12 2608)	Target of Rapamycin	Rabbit
α-S6K1/2 (AS12 1855)	Ribosomal S6 kinase 1/2	Rabbit
α-RAPTOR1/2 (AS23 4912)	Regulatory-associated protein of TOR 1/2	Rabbit
α-UBCJ2 (BML-PW8810-0500)	Mono and polyubiquinated conjugates	Mouse
α-PURO (Merk- MABE343)	Puromycin	Mouse
α-GUS (Sigma-Aldrich G5420)	β-glucuronidase	Rabbit
α-GFP (ROCHE 11814460001)	Green Fluorescent Protein	Mouse
α-ACT (Abcam ab184220)	Actin	Mouse
Secondary Antibodies		
Antibody	**Protein Target**	**Host Species**
α-MOUSE (Sigma-Aldrich A5278)	40S ribosomal protein S6-1	Goat
α-RABBIT (Cell Signalling Technology 7074)	Phosphorylated (Ser237) 40S ribosomal protein S6-1	Goat

2.4 List of selective agents

Table 3 – List of antibiotics and herbicides used as selection markers for transformants

List of Antibiotics and Herbicides	
Selection Marker	**Working Concentration (µg/ml)**
Kanamycin	50
Spectinomycin	80
Chloramphenicol	100
Rifampicin	50
Hygromycin	30
BASTA	20

2.5 Growth conditions, propagation, and treatment

2.5.1 *Arabidopsis thaliana*

2.5.1.1 Growth on Soil

Arabidopsis seeds were sown in pots composed of Levington M3 compost, vermiculite, and perlite (4:2:1 ratio, respectively). Depending on the experiment, plants were either grown in a controlled glass house or growth chamber (Weiss Technik Fitotron SGC 120 biological chamber) under long day conditions (16-hour light/8-hour dark cycles) , with white, fluorescent light at an intensity of 90–100 µmol m^{-2} s^{-1}, and regulated temperatures between 20-22 °C.

2.5.1.2 Sterile Growth

Table 4 – Composition of growth media for *Arabidopsis* cultivation

½ Murashige and Skoog (MS) Media
2.15 g/l Murashige and Skoog Basal Salt Mixture (Sigma-Aldrich)
1% Agar
KOH to adjust pH to 5.8

Seeds were sterilized by agitating them in a 10% bleach solution for 10 minutes, followed by five rinses in sterile deionized water. They were then plated onto half-strength Murashige and Skoog (½ MS) media (**Table 4**) with appropriate selective agents (**Table 3**), or supplements (**Table 5**) added as necessary. The ½ MS medium was prepared with 1% agar and was autoclaved at 121°C for 15 minutes. The plated seeds were stratified at 4 °C for 48 hours. After stratification, the plates were transferred to a constant temperature growth room set to 20-22 °C under LD conditions with 90–100 μmol m^{-2} s^{-1} fluorescent white light.

2.5.1.3 Cross fertilisation of *Arabidopsis*

Closed buds (petals not visible) were selected on female parent plants and isolated by removing neighbouring buds with scissors. Using fine sharp forceps, sepals, petals, and stamens were carefully removed, leaving only the pistil intact. Mature flowers with fully splayed petals were selected from male donor plants and the base of each bud was gently squeezed with sterile forceps to expose stamens containing pollen. Pollination was achieved by rubbing pollen-containing anthers against the exposed pistils of the isolated female flowers. Subsequently, pollinated pistils were isolated to prevent additional pollen contact and allowed to develop into mature seed-bearing siliques. Seed were then harvested for propagation on soil.

2.5.1.4 Histochemical staining

1% 100 mM potassium ferricyanide and 100 mM potassium ferrocyanide to pre-made GUS stain solution (0.1M PBS (pH 7.0), 2mM X-gluc, and 0.1% Triton-X-100 (v/v)). n 1ml of the GUS stain solution was added to seedlings and placed in darkness at 37 °C for 24 hrs. Subsequently, the GUS stain solution was replaced with 1ml of fixative (3:1- ethanol:acetic acid, with 1% Tween v/v). Samples were gently shaken at room temperature, refreshing the fixative until tissues became transparent. Cleared and fixed samples were briefly rinsed with SDW and mounted on microscope slides using 50% glycerol. Images were captured using a bifocal light microscope and the software Touplite.

2.5.1.5 Chemical treatments

10-day-old *Arabidopsis thaliana* seedlings were exposed to various chemical treatments, targeting a range of biological pathways (**Appendix 2**) as a part of a high-throughput chemical screening assay conducted in conjunction with Syngenta Crop Protection AG. From this, chemicals that exhibited unique responses, whether that be sensitivity or resistance, were further explored as part of the chemical characterisation of NOT4s (**Table 5**). These treatments were administered either by incorporating the chemical directly into the ½ MS growth medium (before plate preparation) or through transient treatments (solid and liquid form). For the transient treatment assays, seedlings first grew on solid ½ MS medium for 6 days, then transferred aseptically to plates containing the desired chemical at different concentrations for an additional 6 days. For transient liquid treatments, seedlings were placed in wells with liquid ½ MS media containing the appropriate concentration of the chemical. After the indicated incubation time, the seedlings were taken from the liquid treatments for further analyses such as western blotting.

Table 5 – Inhibitors and elicitors used for *Arabidopsis* treatment

Chemical	Target	Concentrations used
Rapamycin	TOR	10μM,12μM,15μM
AZD-8055	TOR	1μM, 2μM, 5μM, 10μM
TORIN1	TOR	10μM,15μM, 20μM
PF-4708671	S6K1/2	1μM, 2μM, 5μM, 10μM, 15μM
Tunicamycin	Protein glycosylation (ER stress)	50ng/ml, 75ng/ml, 100ng/ml
Dithiothreitol (DTT)	Disulfide bonds in proteins (ER stress)	0.5mM, 1mM
Puromycin dihydrochloride	Protein Translation	50μM
Cycloheximide	Protein Translation	50μM

2.5.2 *Escherichia coli*

Lysogeny broth (LB) with appropriate antibiotics was used to cultivate *E. coli* colonies on agar plates and in liquid cultures. Colonies and cultures were incubated at 37 °C, with liquid cultures shaken at 200 rpm.

2.5.3 *Agrobacterium tumefaciens*

A. tumefaciens was cultured on LB agar plates and in liquid LB containing rifampicin, and vector specific antibiotics. Colonies were incubated at 28 °C, with liquid cultures shaken at 200rpm.

2.6 Molecular biology related techniques

2.6.1 *Arabidopsis thaliana*

2.6.1.1 Genomic DNA extractions

DNA was isolated from *Arabidopsis thaliana*, (single rosette leaf or 5-day old seedlings) by adding 40 µl of extraction buffer (**Table 6**) and grinding the leaf tissue with a 200 µl pipette tip. The samples were then heated at 95 °C for 10 minutes using a heat block, cooled on ice for 5 minutes, and diluted with 40 µl of dilution buffer (**Table 6**). After centrifugation at maximum rpm for 30 seconds in a benchtop centrifuge, 1-3µl of the supernatant was used for subsequent analysis.

Table 6 – DNA extraction buffers for *Arabidopsis*

Extraction Buffer	Dilution Buffer
0.25M KCL	3% BSA in SDW (w/v)
10mM EDTA	
100mM Tris-HCL (pH 9.5)	

For the genetic analysis of the relationship between *PGR3* and *NOT4A* (*see* **Appendix Chapter**), DNA was extracted using GenElute™ Plant Genomic DNA Miniprep Kit (SIGMA) following the manufacturer's protocol.

2.6.1.2 Total RNA extraction

Arabidopsis tissue, (~10 5-day-old seedlings), were harvested in 1.5 ml Eppendorf tubes and snap-frozen in liquid nitrogen. Following grinding, total RNA was extracted using the RNeasy Plant Mini Kit (QIAGEN) following the manufacturer's protocol. On column DNAse I treatment was performed using the Qiagen DNAse I Set (50) kit according to manufactures protocol. High-quality RNA was subsequently eluted in RNase-free water or Elution Buffer (EB). The quantity and quality of the extracted RNA was analysed using a NanoDrop™ 1000 spectrophotometer (ThermoFisher Scientific).

2.6.1.3 RNA sequencing (RNAseq)

RNA was extracted from 12-day-old *Arabidopsis thaliana* seedlings (*as described in 2.6.1.2*). The quality and quantity of RNA samples obtained was analysed using a NanoDrop™ 1000 spectrophotometer (ThermoFisher Scientific).

Library construction, quality control and sequencing

Samples were then shipped to Novogene UK Company Ltd where quality control was first performed using a 1% Agarose gel electrophoresis presence of clear bands corresponding to 28S and 18S ribosomal RNAs, NanoDrop™ 1000 spectrophotometer reading to check for RNA amount and purity, and Agilent 2100 bioanalyzer to check for RNA Integrating Number (RIN). mRNA was purified from total RNA using poly-T oligo attached magnetic beads. After fragmentation, the first cDNA strand was synthesized using random hexamer primers, followed by the second cDNA strand synthesis using either dUTP for direction library or dTTP for non-directional library (Parkhomchuk et al., 2009). The library was analysed with Qubit Fluorometer™ (Invitrogen), followed by qPCR for quantification and Agilent 2100 bioanalyzer for size distribution detection. Quantified libraries were pooled and sequenced on Illumina NovaSeq 6000 platform.

Data processing, mapping and quantification of gene expression level

The resulting paired-end sequencing data (raw reads) were first processed through in-house perl scripts. In short, low quality and poly-N reads were filtered and adapter sequences were trimmed from each read pair (trimmed reads). Trimmed reads were then aligned to the indexed *A.thaliana* genome (TAIR10) using Hisat2 v2.0.5 (Mortazavi et al., 2008). The mapped reads were assembled by StringTie v1.3.3b in a reference-based approach to assemble and quantitate full length transcripts representing multiple splice variants for each gene locus (Pertea et al., 2015).

Mapped read counts to each locus were quantified using FeatureCounts v1.5.0-p3. Gene expression levels were then estimated by calculating the FPKM (Fragments Per Kilobase of transcript per Million mapped reads) for each gene (Liao et al., 2014).

Differential expression analysis

Differential expression analysis between two conditions (with three biological replicates per condition) was conducted using the DESeq2 R package (v1.20.0) (Love et al., 2014). P-values obtained from the analysis were adjusted for multiple testing using the Benjamini-Hochberg method to control the false discovery rate (Benjamini & Hochberg, 1995). Genes with a p-value of ≤ 0.05 were classified as differentially expressed and a fold change of $\log_2(2)$ except for the for comparison between Atnot4abc and Col-0 in which a fold change of $\log_2(1.5)$ was used.

GO and KEGG enrichment analysis of differently expressed genes

Gene Ontology (GO) enrichment analysis (Young et al., 2010) of differentially expressed genes was implemented using the topGO R package (Alexa & Rahnenfuhrer, 2010). GO terms with p-value less than 0.05 were considered significantly enriched. The Kyoto Encyclopaedia of Genes and Genomes (KEGG) is a 4-database resource for understanding high-level functions and utilities of the biological system, such as the cell, the organism and the ecosystem, from molecular-level information, especially large-scale molecular data sets generated by genome sequencing and other high-through put experimental technologies (http://www.genome.jp/kegg/). The R package clusterProfiler was used to test the statistical enrichment of differential expression genes in KEGG pathways (Kanehisa & Goto, 2012).

2.6.1.5 cDNA synthesis

cDNA was synthesized from 1 µg of DNase-treated total RNA extracts using oligo(dT) primers and SuperScript™ II Reverse Transcriptase (ThermoFisher

Scientific) per manufacturer's instructions. The resulting cDNA samples were then diluted to a final of 5 ng/μl with elution buffer (EB).

2.6.2 *Escherichia coli*

2.6.2.1 Plasmid DNA extractions

Cultivated for at least 16 hr at 37 °C, *E.coli* cells were centrifuged at 3000 rpm for 10 min at 4 °C on a large benchtop centrifuge. The supernatant was then removed, and plasmid DNA was purified from the pellet via the QIAprep Spin Miniprep Kit according to the manufacturer's protocol. The purity and concentration of the extracted plasmid DNA were determined by a NanoDrop™ 1000 spectrophotometer (ThermoFisher Scientific); clones were considered positive and further confirmed by PCR or restriction digest.

2.6.2.2 Restriction digests

Restriction enzymes were acquired from New England Biolabs. 0.2-0.5 μg of plasmid DNA was mixed with 0.5 μl of restriction enzyme(s), and 2 μl of reaction buffer, brought to a total volume of 20 μl. The mixtures were incubated at 37 °C for periods ranging from 30 min to 2 hrs. The reactions were terminated by heat inactivation. When multiple endonucleases with different buffer requirements were used, sequential digests were performed according to enzyme-specific protocols generated with NEBcloner® (New England Biolabs).

2.6.4 Sequencing

2.6.4.1 Sanger DNA sequencing

The Functional Genomics Laboratory at the University of Birmingham conducted sequencing service. 100-400 ng of DNA, and 3.2 pmol of the corresponding primer were mixed in 10 μl SDW and sent for sequencing. Sanger sequencing was performed using an ABI 3730 capillary sequencer (Applied Biosystems).

2.7 Polymerase chain reaction

2.7.1 General

DNA fragments were amplified using either MyTaq™ Red Mix (Meridian Bioscience) or NEB Phusion® High-Fidelity DNA Polymerase (New England Biolabs), following manufacturer's specifications. Annealing temperatures were computed from the melting temperature of primers or determined through gradient PCR in case of need. *List of used primers can be found in **Appendix 3**.*

2.7.1.1 Primer design

The primers were designed using a range of online tools that predicted their specificity and efficiency. Primer-BLAST (NCBI) was used for the design of primers showing optimized binding characteristics and verification against non-specific binding to off-target sequences. In addition, primer design for T-DNA insertion sites was performed using the T-DNA Primer Design Tool, now running at Genome Express Browser Server.

2.7.2 Genotyping PCR

PCR-based genotyping was performed in SureCycler 8800 (Agilent Technologies) with MyTaq™ Red Mix or NEB Phusion® High-Fidelity DNA Polymerase following the manufacturer's guidelines. Reactions were set up using either two primers flanking the T-DNA insertion site (forward and reverse primers positioned on either side) or a combination of a T-DNA-specific border primer with a corresponding flanking primer.

2.7.3 Colony PCR

Colonies of *E. coli* or *A. tumefaciens* were screened via PCR to confirm the presence of transformed vectors containing the DNA sequence of interest. Selected single colonies were directly suspended in 11µl PCR Mix (consisting of 6µl MyTaq™

Red Mix, 2µl of primers, 3µl of SDW). Primer pairs consisted of one gene-specific primer and one vector-specific primer, facilitating the identification of colonies containing recombinant plasmids.

2.7.4 RT-qPCR

qPCR reactions were prepared using Brilliant III Ultra-Fast SYBR® Green qPCR Master Mix with Low ROX (Agilent). qPCR reaction mix contained 10 ng of template cDNA. AriaMx Real-time PCR System (Agilent) was used for 96-well plates reactions and QuantStudio5 applied biosystem (Thermo Fisher Scientifc) was used 384-well plates. qPCR primers were designed to span on exon-exon junctions. To ensure no contamination of gDNA was present, a negative control was always included. Primer specificity was verified through melt-curve analysis. The ΔCt method was used to calculate relative gene expression (Livak and Schmittgen, 2001).

2.7.5 Gel electrophoresis

Agarose gels were made by dissolving agarose in Tris-Borate-EDTA (TBE) buffer (0.66% to 2.00% w/v) then heating the mixture gently in the microwave until agarose was dissolved. Ethidium bromide at 0.05 µl/ml was then added. Mixture was poured into gel molds with combs. The gels were first-soaked in TBE running buffer in electrophoresis tanks. The DNA samples, after being mixed with loading buffer, were loaded into the wells prior to electrophoresis. DNA migration through the gel matrix was performed at an applied voltage of 90 to 120V. Finally, the gels were taken out from the buffer, and the DNA bands were documented using the Gel Doc™ XR+ Gel Documentation System (BioRad).

2.8 Biochemistry

2.8.1 Total protein extraction from *Arabidopsis thaliana*

Total protein extracts were generated from 7-day-old seedlings that had been homogenized into a fine powder using TissueLyser II (QIAGEN) in liquid nitrogen. The frozen plant powder was combined with buffer B (**Table 7**) at a ratio of 1:4 (w/v). The mixture was centrifuged at maximum rpm for 30 minutes at 4 °C to pellet cell debris and the supernatant obtained was used as the crude protein extract.

Table 7 – Protein extraction and sample buffers for *Arabidopsis thaliana*

Protein Extraction Buffer A	
Component	**Concentration**
Tris-HCl pH 7	150mM
NaCl	150mM
EDTA	5mM
EGTA	2mM
Glycerol	5% (v/v)

Protein Extraction Buffer B	
Component	**Concentration**
Buffer A	-
Triton 100x	1% (v/v)
SDS	0.5% (v/v)
cOmplete™, Mini, EDTA-free Protease Inhibitor Cocktail (Roche)	1 per 10ml
DTT	10mM

4x SDS Sample Loading Buffer	
Component	**Concentration**
Tris-HCl pH 6.8	120mM
Glycerol	20%
β-mercaptoethanol	10%
SDS	4%
Bromophenol blue	0.02%

2.8.2 Bradford assay (Quantification of protein concentration)

Protein extract concentrations were determined using the Bradford Assay (Bradford 1976). Prior to adding sample buffer, 1 µl samples of protein extract were added to 19 µl of SDW. 200 µl of Bradford Reagent (AppliChem) was then added to the diluted protein samples and the absorbance at 595 nm was then measured using Infinite M Nano (TECAN) 96-well plate reader er. Measured absorbances were compared to a standard curve (bovine serum albumin (BSA)) from to provide an estimation of protein concentration and used for equal loading in SDS-PAGE.

2.8.3 SDS-page

Dependent on the volume of the sample, a suitable quantity of 4x sample buffer was added and boiled at 98 °C for 5 minutes. The samples cooled to room temperature, after which they were used for SDS-PAGE or frozen in a freezer at -80 °C for long-term storage. Proteins were separated by size using 8-10% polyacrylamide gels (**Table 8**) that were cast manually. The gels were submerged in running buffer (**Table 8**) and initially subjected to a voltage of 90V until samples entered resolving phase, at which point the voltage was increased to 120V.

2.8.4 Western blotting

Separated protein samples were transferred from polyacrylamide gels to PVDF membranes at 4 °C overnight at 24 V or using the Trans-Blot Turbo Transfer System (BIO-RAD) according to manufacturer's instruction. Following the transfer, the membranes were blocked with 5% milk powder in TBS containing 0.1% Tween® 20 (Merck); TBST) (**Table 8**). Primary antibody incubation time was dependent on the specific experiment and the antibody itself whereas secondary antibody incubation time was 1 hr. All antibodies were diluted in 5% Milk TBST. Membranes were rinsed three times, washed once for 15min, then three times for 5min with TBST in between primary and secondary antibody incubation. After washing, membranes were then incubated with Pierce^{TM} ECL Western Blotting Substrate (Thermo Scientifc-32106) for one minute. Chemifluorescence was captured using X-ray film (FujiFilm Super Rx) in a HI-SPEED-X intensifying screen binder in a dark room. Development of exposed film was done using Xograph Compact X4 Automated Processor and the results were imaged on a light box with a Nikon D40 SLR camera.

Table 8 – Reagents for SDS-PAGE and Western Blotting

SDS-PAGE and Western Blotting related recipes				
Stacking Polyacrylamide Gel (5%)	**Resolving Polyacrylamide Gel (10%)**	**Running Buffer**	**Transfer Buffer**	**TBST**
Acrylamide/bis-acrylamide (30%)	Acrylamide/bis-acrylamide (30%)	SDS 0.1 %	Methanol 10 %	NaCl 150 mM
125 mM Tris-HCl (pH 6.8)	375 mM Tris-HCl (pH 8.8)	Tris 25 mM	Tris 25 mM	Tris 50 mM Tris (pH adjusted to 7.5 with HCl)
SDS 0.1 % (w/v)	SDS 0.1 % (w/v)	Glycine 192 mM	Glycine 192 mM	Tween-20 0.1 %
Ammonium persulfate 0.1 % (w/v)	Ammonium persulfate 0.1 % (w/v)			
TEMED 0.01 % (v/v)	TEMED 0.004 % (v/v)			

2.8.5 Coomassie brilliant blue (CBB) staining

CBB staining was performed as a loading control for Western blot analysis. PVDF membranes were immersed in Coomassie stain (**Table 9**) with gentle agitation. After 15 minutes, the stain was discarded and replaced with destaining solution (**Table 9**) for an additional 10 minutes. The destaining solution was then removed, and the membrane was gently pat-dried with a paper towel and left to air-dry before imaging with a Nikon D40 SLR camera.

Table 9 – Coomassie brilliant blue related solutions

CBB Staining solution	CBB Destain solution
50% Acetic Acid (v/v)	10% Acetic Acid (v/v)
20% Methanol (v/v)	45% Methanol (v/v)
0.5g Coomassie Brilliant Blue R250 (Thermo Fisher Scientific)	

2.8.6 Puromycin incorporation assay

A puromycin incorporation assay was performed to assess global translation rates. 7-day-old seedlings were added to wells that contained 3ml of ½ MS supplemented with 50 µM of puromycin dihydrochloride (Sigma – P8833) having 10-15 seedlings removed at 0-, 30-, and 60-minute time points. After 60mins, samples were then treated with the translational inhibitor cycloheximide (CHX) at a concentration of 50 µM or DMSO (equivalent volume) for a further 60 mins. Samples were blotted dry with paper towels, flash frozen and stored at -80 °C or directly used for total protein extraction (*see 2.8.1*) and subsequently western blotting (*see 2.8.5*).

2.9 Molecular cloning

2.9.1 Gateway recombination cloning

Primers were designed specific to the ORFs of genes of interest with an addition of 31bp (forward) or 30bp (reverse) overhang including the Gateway® attB sites (**Table 10**). Amplified genes of interest via PCR were incorporated into Gateway® compatible entry vectors by BP recombination reaction.

Table 10 – Primer sequences used for BP recombination reaction

Primers	Sequence
Forward	GGGGACAAGTTTGTACAAAAAAGCAGGCTNN(5'end - gene of interest)
Reverse	GGGGACCACTTTGTACAAGAAAGCTGGGTN(3'end - gene of interest)

Phusion® High-Fidelity DNA Polymerase (NEB) was used to perform PCR that produced a blunt-end double-stranded product with attB forward and reverse sequences. These PCR products were subsequently cloned into donor vectors to create entry clones utilizing the Gateway® BP Clonase® II enzyme mix (Thermo Fisher Scientific). The BP reaction was made with 50 fmol of attB-flanked DNA, 150 ng of donor vector (pDONR™221), and 1 µl of Gateway® BP Clonase® II enzyme mix. Incubation was carried out at room temperature for one hour. Later, 0.5 µl of Proteinase K solution (Invitrogen) was added to the mixture, and further incubation was done at 37 °C for 10 min.

Entry clones were then transformed into NEB® 5-alpha competent *E. coli* cells (see 2.10.2). Positive colonies that showed antibiotic resistant were then screened by colony PCR (see 2.7.3), with confirmed colonies then being cultured overnight in LB broth (with addition of appropriate antibiotic). Plasmid preparation was performed from the overnight cultures by miniprep (see 2.6.2.1) and sent for sequencing (see 2.6.4.1).

Confirmed entry clones were transferred to a destination vector by LR ligation reactions using 25 ng of entry and 40 ng of destination plasmids with 0.5 µl LR Clonase™ enzyme mix (Invitrogen) in a reaction volume of 2.5 µl and incubated at 25 °C for 1 hr. The entire LR reaction mixture was then used to transform competent NEB® 5-alpha competent *E. coli* cells (see 2.10.2). Positive colonies that were resistant to the relative antibiotic were screened by colony PCR, with confirmed colonies grown in 10ml of LB broth (plus appropriate antibiotic) overnight. Expression clones were then extracted by miniprep (see 2.6.2.1) and sequenced (see 2.6.4.1). Sanger sequenced verified the gene was error-free and correctly orientated, making it suitable for further transformations.

2.10 Transformation methods

2.10.1 Transformation and growth of *Escherichia coli*

Full reaction volumes of either BP or LR mixture was added to NEB® 5-alpha competent *E. coli* cells. The mixture was gently agitated and incubated on ice for 30 mins. Cells were heat shocked for 30 s at 42 °C in a water bath and immediately returned to ice for 5 minutes. 950 µl of Super Optimal Broth (SOB; New England Biolabs) media was added to the cooled heat shocked cells and placed in a 37 °C growth room at 200 rpm shaking. After 1 hr, the cells were centrifuged at 2000 x g to form a pellet. Approximately half of the supernatant was carefully removed, and the cells were resuspended in the remaining volume by gently pipetting. The bacterial suspension was spread across LBA plates containing appropriate antibiotics (see 2.4) and incubated at 37°C overnight.

Positive colonies that were resistant to the appropriate antibiotic were subjected to colony PCR (see 2.7.3) to screen for the presence of the gene of interest. Once confirmed, the remaining half of the positive colony was suspended in 10ml of LB broth (LBB) with appropriate antibiotic and left to incubate at 37°C overnight with 200rpm shaking.

2.10.2 Transformation and growth of *Agrobacterium tumefaciens*

Transformation of *A. tumefaciens* was performed using the free-thaw method (Jyothishwaran et al., 2007) in order to integrate plant transformation vectors suitable for *Arabidopsis* transformation. 200 µl of competent *A. tumefaciens* cells were thawed on ice and combined with 1 µg of expression clone. The mixture was gently agitated and further incubated on ice for 5min, and subsequently placed in liquid nitrogen for 5minutes. Immediately after, the mixture was placed for 5 min in a 37°C water bath. 800µl of LBB was added and left to incubate at 28 °C with 120 rpm shaking. After 2hrs, cells were centrifuged at 2000 x g for 1 min to form a pellet. 750 µl of supernatant was discarded and the pellet was resuspended in the remaining volume by gently pipetting. The entire content was spread across LBA plates with appropriate antibiotics and left to incubate at 28°C for 72 hours. Lastly, resulting colonies were screened by colony PCR (see 2.8.3)

Successfully transformed *A. tumefaciens* colonies were inoculated into 10 ml of LBB supplemented with rifampicin, and vector-specific antibiotics. The cultures were incubated at 28°C with shaking at 200 rpm until significant growth was observed typically within 24 to 48 hrs. Samples were spun at 4000 x g for 10 min at room temperature. The pellet was resuspended in 3 ml of 5% Sucrose + 0.02% Silwett L77(v/v).

2.10.3 Transformation and selection of *Arabidopsis thaliana*

Transformation and growth of transformed *Arabidopsis* was based on the floral dip method (Clough & Bent, 1998) with a few alterations. Once *Arabidopsis* plants began bolting, the primary bolts were clipped to encourage the formation of multiple secondary bolts. Plants with multiple secondary bolts that were no larger than 1 cm in height were subjected for transformation. A paint brush was used to gently cover meristematic tissue on secondary bolts, allowing any subsequent growth to contain the expression clone (assuming successful integration). The painted plants were left for 2 days before covering with a flowering sleeve.

T1 seeds were screened on ½ MS media with appropriate antibiotics using the rapid and method of identifying transformants by Harrison et al. (2006). Antibiotic-resistant individuals were transplanted and grown in standard growth conditions (see 2.5.1). The T2 generation was screened on ½ MS plates to identify a 3:1 resistance to susceptibility ratio, which would indicate single insertion in transformants. The resistant transformant was then transplanted to soil. T3 seed were screened to confirm homozygous lines by analysing resistance pattern to appropriate antibiotic.

Chapter 3 - Functional Characterisation and Genetic Analysis of *A*tNOT4s

3.1 Introduction

NOT4 is an E3 ubiquitin ligase that was first identified as a core CCR4-NOT component in yeast and regulates a range of processes linked to genome control, translational repression, and mRNA and protein degradation (Collart, 2013a; Preissler et al., 2015). Basic Local Alignment Search Tool (BLAST) analysis was conducted in which three putative *Arabidopsis* orthologues of *Sc*NOT4 were identified: *At*NOT4A (AT5G60170), *At*NOT4B (AT3G45630), and *At*NOT4C (AT2G28540). Interestingly, only one copy exists in humans and yeast (Collart, 2013a; Dai et al., 2021) These homologues exhibit a high degree of conservation within key functional domains such as the RING domain and the RNA recognition motif (RRM), but also contain regions of increased divergence suggesting potential specialization in their biological roles (**Figure 14a**). An AlphaFold model was considered to further investigate the structural differences between the NOT4 proteins. However, the prevalence of unstructured regions in these proteins limits the model's ability to generate reliable and informative predictions.

In *Arabidopsis*, *AtNOT4A* spans 6659 base pairs (bp) of genomic DNA and encodes a protein of 987 aa, whereas *AtNOT4B* is 6952 bp in length and produces a protein consisting of 989 aa. In comparison, *AtNOT4C* is slightly shorter, covering 5855 bp and results in a protein of 960 aa. All three are substantially larger than *ScNOT4*, which is 1764 bp in length comprising 587 aa (**Figure 14c**) which may reflect potential differences in regulatory complexity and function between species. *AtNOT4A* is found on Chromosome 5, where *AtNOT4B* is situated on Chromosome 3, and *AtNOT4C* is located on Chromosome 2 (**Figure 14b**). *At*NOT4A, *At*NOT4B, and *At*NOT4C are postulated to have roles in co-translational quality control, mRNA degradation, and ubiquitin-mediated proteolysis, similar to their yeast counterpart (Collart, 2013b; Halter et al., 2014). However, the expanded number of NOT4 homologues in *Arabidopsis* suggests potential evolved mechanisms and an expanded diversity of functions that could allow for greater specificity and adaptability in normal cellular function and stress responses.

The work described in this chapter analysed *At*NOT4A, *At*NOT4B, and *At*NOT4C for their resemblance to *Sc*NOT4 and their respective functions in *Arabidopsis* by using physiological, molecular, and transcriptomic approaches.

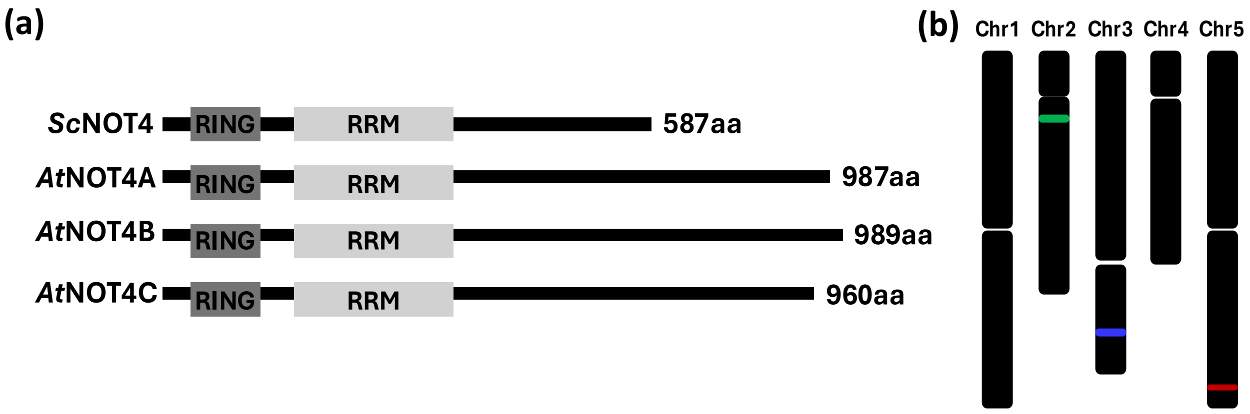

(c)

	Size (aa)	Full length gDNA (bp)
*Sc*NOT4	587	1764
*At*NOT4A	987	6659
*At*NOT4B	989	6952
*At*NOT4C	960	5855

Figure 14 – Genetic comparison of ScNOT4 and AtNOT4. (**a**) The domain structures of the yeast RING E3 ligase *Sc*NOT4 and its three *Arabidopsis* homologues: *At*NOT4A, *At*NOT4B, and *At*NOT4C. Each protein contains a conserved RING domain (depicted in dark grey) and an RNA recognition motif (RRM, depicted in light grey). Sequences were obtained from UniProt and aligned using the Clustal Omega program Multiple Sequence Alignment Tool. (**b**) Schematic genomic positions of the putative *Arabidopsis* homologues of the yeast *Sc*NOT4 gene: *At*NOT4A on Chromosome 5 (in red), *At*NOT4B on Chromosome 3 (in blue), and *At*NOT4C on Chromosome 2 (in green). (**c**) comparison of protein size in amino acids (aa) and genomic DNA (gDNA) length of yeast and *Arabidopsis* NOT4s.

3.2. *At*NOT4s share protein sequence homology and conserved domains with *ScNOT4*

The difference in genomic and protein size prompted a further investigation into the protein sequence to identify conserved regions and domains. Conserved domains may be indicative of shared functions which highlights commonalities across kingdoms. Thus, EMBL-EBI Clustal Omega (www.ebi.ac.uk/jdispatcher/msa/clustalo) was used to study the protein sequence alignments. *At*NOT4 full protein sequences were aligned to each other and to *Sc*NOT4 (**Figure 15**). Highest degree in similarity was observed between *At*NOT4A and *At*NOT4B with a total of 68.54% shared. *At*NOT4A and *At*NOT4C had less than half the identity, 44.32%, shared. This was also reflected when comparing *At*NOT4B and *At*NOT4C as only 44.51% identity shared. When comparing the sequence homology to *Sc*NOT4, only 27.45%, 29.32% and 29.22% is identical for *At*NOT4A, *At*NOT4B and *At*NOT4C respectively. If the conserved RING and RRM domains were excluded, the similarity scores between the AtNOT4 paralogues and between AtNOT4s and ScNOT4 would likely be much lower. This suggests that these domains contribute significantly to the observed homology and further reflect conserved functional roles across these proteins.

	***At*NOT4A**	***At*NOT4B**	***At*NOT4C**	***Sc*NOT4**
***At*NOT4A**	100%	68.54%	44.32%	27.45%
***At*NOT4B**	68.54%	100%	44.51%	29.32%
***At*NOT4C**	44.32%	44.51%	100%	29.22%
***Sc*NOT4**	27.45%	29.32%	29.22%	100%

Figure 15 – Full-length amino acid sequence comparison of *At*NOT4s and *Sc*NOT4. Sequences were obtained from UniProt and aligned using the Clustal Omega program (Multiple Sequence Alignment Tool). Percent Identity Matrix function was used to calculate a numeric score for each pair of aligned sequences, reflecting the number of identical residues in relation to the alignment length to generate the heatmap. The darker the blue colour, the higher the percentage identity between the compared proteins. The full sequence alignment can be found in the **Appendix 1**.

3.2.1. Conserved RING Domain

A RING domain is one of many (*see Chapter 1, Section 1.9.2.2*) domains that carries out the ubiquitin ligase activity of E3s, including *Sc*NOT4 (Collart, 2013a; Gulshan et al., 2012; Preissler et al., 2015). Amino acid sequences of *At*NOT4A, *At*NOT4B, and *At*NOT4C were analysed for the presence of this domain using the SMART protein domain annotation resource (http://smart.embl-heidelberg.de/) (Letunic & Bork, 2018). RING domains of *At*NOT4A, *At*NOT4B, and *At*NOT4C were shown to be highly conserved with 95.92% identity between *At*NOT4A and *At*NOT4B, 87.76% identity between *At*NOT4A and *At*NOT4C, and 87.76% identity between *At*NOT4B and *At*NOT4C (**Figure 16**). The RING domain of *Sc*NOT4 shares 56.52% identity with each of the *Arabidopsis* homologues. Crucially, critical cysteines that make up the consensus RING domain sequence are highly conserved across all four proteins.

(a)

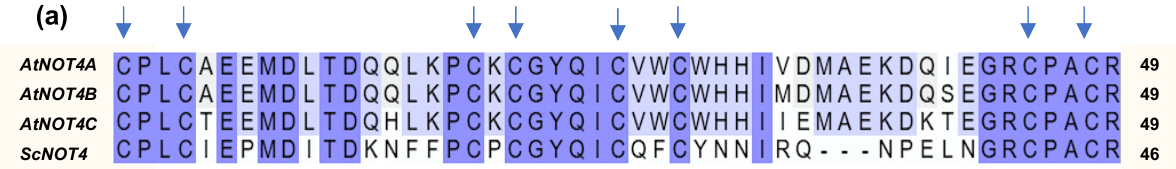

(b)

	*At*NOT4A	*At*NOT4B	*At*NOT4C	*Sc*NOT4
***At*NOT4A**	100%	95.92%	87.76%	56.52%
***At*NOT4B**	95.92%	100%	87.76%	56.52%
***At*NOT4C**	87.76%	87.76%	100%	56.52%
***Sc*NOT4**	56.52%	56.52%	56.52%	100%

Figure 16 – Full-length amino acid sequence of the RING domain from *At*NOT4s and *Sc*NOT4. (a) Aligned Sequences that were obtained from UniProt and aligned using the Clustal Omega program (Multiple Sequence Alignment Tool). **(b)** Percent Identity Matrix function was used to calculate a numeric score for each pair of aligned sequences, reflecting the number of identical residues in relation to the alignment length to generate the heatmap. The darker the blue colour, the higher the percentage identity between the compared proteins. Blue arrows above sequence indicate conserved pattern of cysteine and histidine residues.

Complete conservation of the zinc-coordinating cysteine and histidine residues within these domains underlines their functional importance in ubiquitin-mediated proteolysis. The RING domain represents a higher-order class of a zinc finger domain that binds two zinc ions through a conserved cysteine and histidine pattern, generally in the arrangement **C-X2-C-X(9-39)-C-X(1-3)-H-X2-3-C-X2-C-X(4-48)-C-X2-C** (Borden & Freemont, 1996). This configuration is essential for the integrity of the domain, providing it with the ability to facilitate the transfer of ubiquitin from an E2 ubiquitin-conjugating enzyme onto a substrate protein. These key residues are conserved in *At*NOT4A, *At*NOT4B, and *At*NOT4C, indicating that these proteins retain the basic mechanism of ubiquitin transfer, pointing to their probable role in similar proteolytic functions as *Sc*NOT4 in *Arabidopsis*.

3.2.2. Conserved RRM Domain

The RRM domain is critical for RNA binding, the function central to the role of NOT4 proteins in the degradation and regulation of mRNA. The RRM domains of *At*NOT4A, *At*NOT4B and *At*NOT4C were also well conserved. *At*NOT4A shares 93.10% identity with *At*NOT4B, 75.86% identity with *At*NOT4C and 38.55% identity with *Sc*NOT4 in the RRM domain. *At*NOT4B has 79.31% identity with *At*NOT4C and 38.55% identity with *Sc*NOT4 in this domain (**Figure 17**). *At*NOT4C and *Sc*NOT4 exhibit 36.14% identity. The sequence conservation within this domain further supports the functional similarities among the *Arabidopsis* homologues and their yeast counterpart.

Although *At*NOT4s contain an RRM domain, it does not fully conform to the recognised RRM consensus sequence. RRM domains typically consist of two highly conserved sequences necessary for RNA binding which are known as RNP1 and RNP2. Located near the N-terminal end of the domain, RNP2 typically displays the pattern [I/L]-[F/Y]-[V/I]-[G/A]-[N/L]. The consensus sequence for RNP1is located closer to the C-terminal and commonly comprised of [K/R]-G-[F/Y]-[G/A]-[F/Y]-[I/L/V]-X-[F/Y] (Maris et al., 2005; Soni et al., 2023). There are certain aromatic residues within RNP1 and RNP2 that are important for RNA-binding such as phenylalanine (F) and tyrosine (Y). Lysine (K) and arginine (R) are also important for the stability of protein-RNA interactions. Upon closer examination, the four aromatic residues are conserved in the RRM domain of *At*NOT4s, thus it is likely that they retained their of RNA-binding functions.

(a)

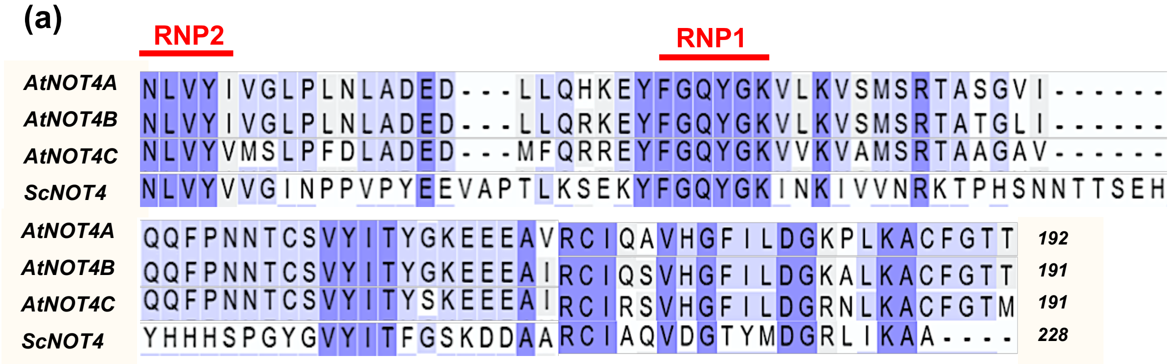

(b)

	*At*NOT4A	*At*NOT4B	*At*NOT4C	*Sc*NOT4
*At*NOT4A	100%	93.10%	75.86%	38.55%
*At*NOT4B	93.10%	100%	79.31%	38.55%
*At*NOT4C	75.86%	79.31%	100%	36.14%
*Sc*NOT4	38.55%	38.55%	36.14%	100%

Figure 17 – Full-length amino acid sequence of the RRM domain from *At*NOT4s and *Sc*NOT4. **(a)** Aligned sequences that were obtained from UniProt and aligned using the Clustal Omega program (Multiple Sequence Alignment Tool). **(b)** Percent Identity Matrix function was used to calculate a numeric score for each pair of aligned sequences, reflecting the number of identical residues in relation to the alignment length to generate the heatmap. Consensus sequences of RNP1 and RNP2 are indicated in red.

3.3 Generating genetic tools for characterising *At*NOT4 function

A set of T-DNA insertional mutants were identified for *in-planta* functional studies of *At*NOT4s and evaluating their importance during growth and development. Seeds were obtained from Nottingham *Arabidopsis* Stock Centre (NASC) for *AtNOT4A* (GABI_134E03), *AtNOT4B* (SAIL_274_D03), and *AtNOT4C* (SALK_099755). The genetic disruption of their transcription would prevent the synthesis of the protein, therefore allowing the molecular consequences and phenotypic assessment to be characterised.

3.3.1. Generation of single, double and triple mutants

The initial step involved confirming the presence of the respective T-DNA insertions via PCR (**Figure 18**) and ensuring homozygosity. To distinguish between wild-type and T-DNA insertion alleles for each *AtNOT4* gene, specific primer combinations were used for genotyping (*see* **Appendix 3**). To further validate the exact location of the T-DNA insertions within specific exons and ensure the disruption of these genes, we analysed mapped read data from RNA-seq experiments (**Figure 19)**. This was done through the Integrative Genomics Viewer IGV which gave an overview of the expression levels for each *AtNOT4* in the T-DNA insertion lines relative to wild-type. The underlying RNA-seq data analysis will be further discussed later in this chapter (*see 3.4*). T-DNA insertions were inserted in the 7th, 9th and 3rd exon in *Atnot4a*, *Atnot4b* and *Atnot4c* respectively. All three *AtNOT4* genes showed reduced mRNA signal downstream of their respective T-DNA insertion sites. Confirmed homozygous single mutants were then used to generate double and triple mutants through several cross-fertilisations, and identification of desired genotypes in the progenies was done via PCR (**Figure 18**)

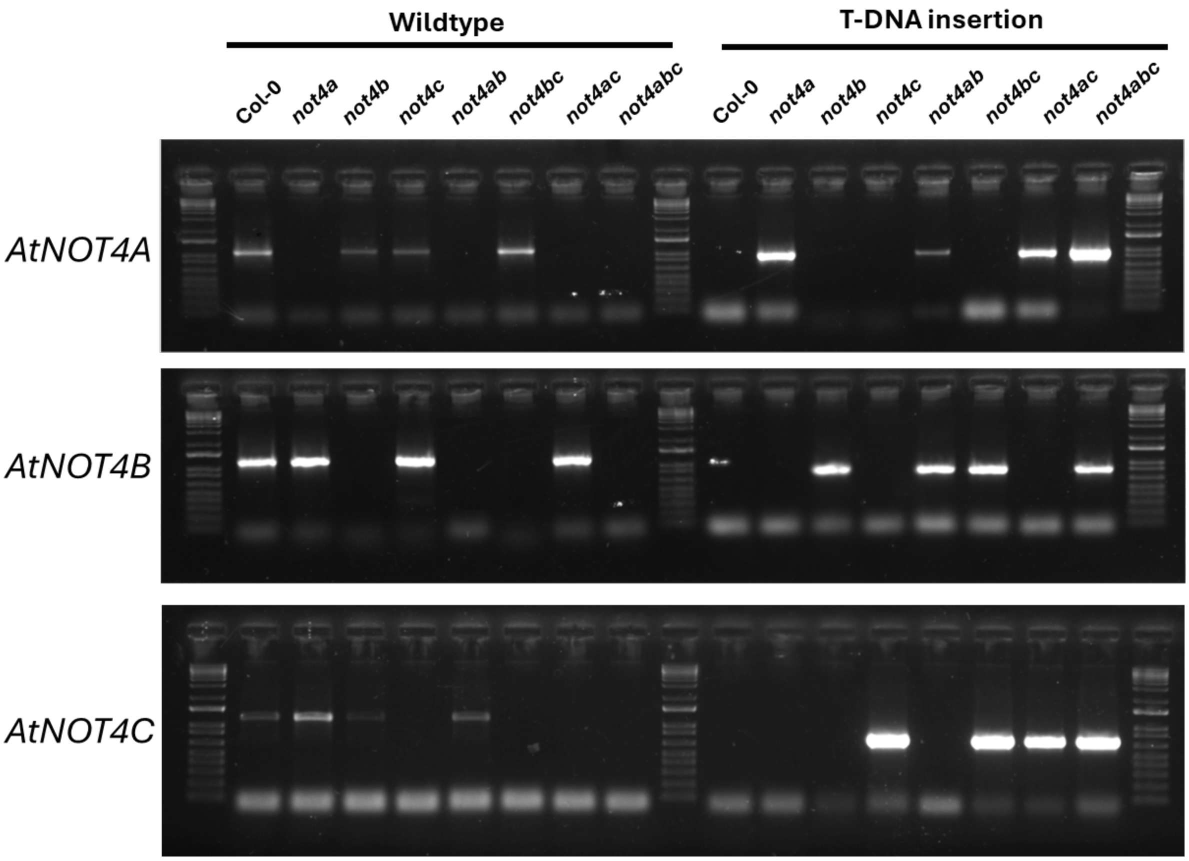

Figure 18 – Genotyping PCR results confirming homozygosity of single, double and triple *At*NOT4 mutants. Gel electrophoresis was performed to analyse PCR amplification products for each mutant and the Col-0 (wild-type). For the wild-type *AtNOT4A*, an amplicon of 1105 bp was expected, whereas the T-DNA insertion line produced an amplicon of approximately 900 bp. The expected amplicon size for a wild-type *At*NOT4B was 1207 bp, and in the T-DNA insertion line was approximately 850 bp. Amplification for *At*NOT4C wild type yielded an amplicon of 1222 bp, while the T-DNA insertion line had an amplicon of around 700 bp.

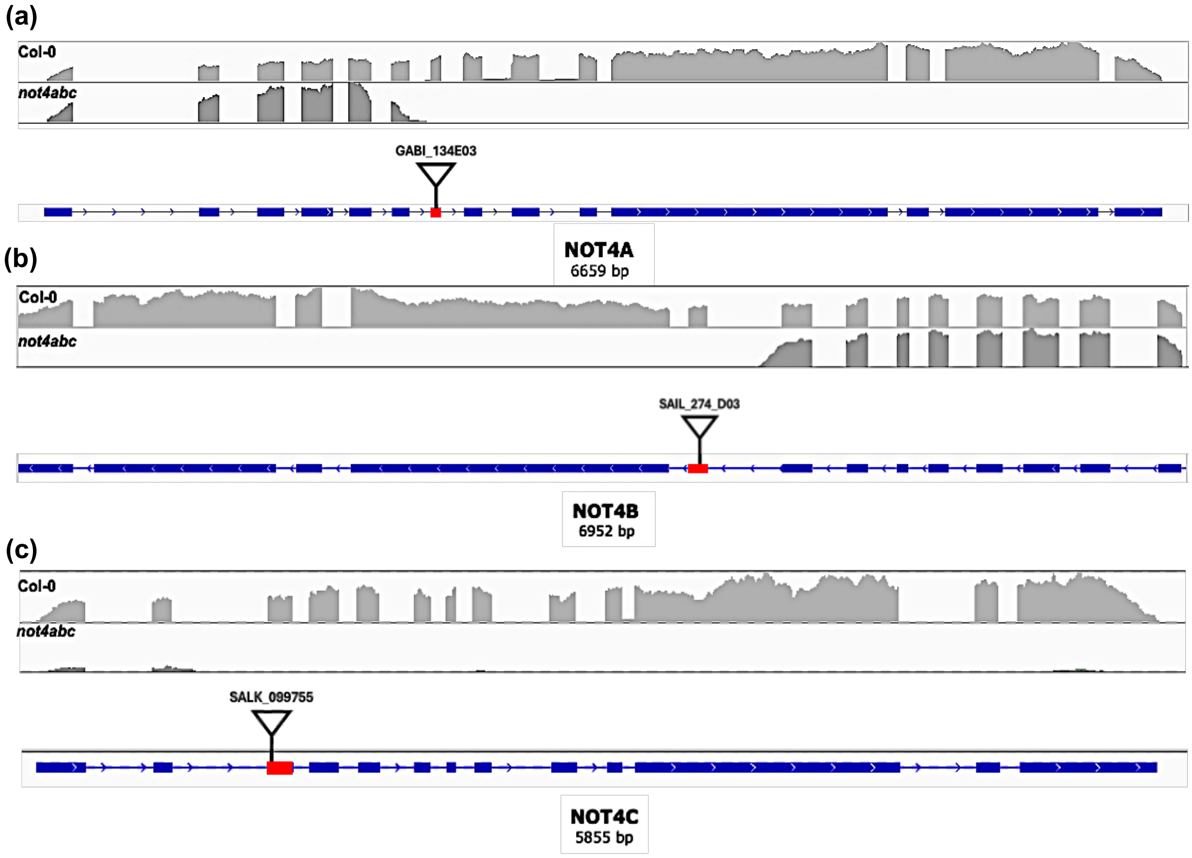

Figure 19 - T-DNA insertion sites within the (a) *AtNOT4A*, (b) *AtNOT4B*, and (c) *AtNOT4C* genes confirming the disruption of these genes in specific exons. The mapped reads from the RNA-seq data are shown in grey and illustrates the lack of transcript abundance downstream of the insertion site in *Atnot4abc* vs Col-0, providing evidence that the T-DNA effectively disrupt each gene. The specific exons in which the T-DNA insertions are located are highlighted in red.

3.4 Phenotypic analysis of single, double and triple mutants

Single, double, and triple mutants were grown and compared to each other as well as wild type (Col-0) to determine if there were any obvious developmental phenotypes arising from disrupting NOT4 function in *Arabidopsis*. At the seedling stage, the *Atnot4a* line exhibited a distinct growth phenotype characterized by reduced total seedling length (p-value < 0.0001, one-way ANOVA; **Figures 20a and b**), with an average length of 3.948 cm compared to 4.533 cm in wild-type of 12-days-old seedlings. When grown to maturity, *Atnot4a* also produced noticeably smaller rosettes (**Figure 21a**) and flowered significantly later than the wild type under normal growth conditions (p-value < 0.0001, one-way ANOVA), with an average of 34 days compared to 27 days in wild type (**Figure 21b and c**). However, despite flowering temporally later, the *Atnot4a* mutants did not show a significant difference in the number of leaves (not significant, one-way ANOVA) present at the time of bolting compared to the wild type, with the average across all lines being approximately 9 (**Figure 21d**). This suggests a growth or energy-related defect rather than a floral development phenotype. The growth retardation, smaller rosettes, and delay in the number of days to flowering (but not number of leaves) was consistently observed in higher-order mutants containing the *Atnot4a* T-DNA insertion (**Figure 21a-d**), and this phenotype was not amplified in higher order mutants.

Interestingly, supplementation of ½ MS growth media with 1 % sucrose abolished the delayed growth phenotype of *Atnot4a* and its associated higher order mutants (*Atnot4ab*, *Atnot4ac* and *Atnot4abc*). The total seedling length was restored to that of wild-type and other *Atnot4* mutants, with an overall mean of 4.65 cm (not significant, one-way ANOVA; **Figure 20b**). The restoration of growth observed in *Atnot4a* may therefore be related to energy utilisation or storage, suggesting a likely role for *At*NOT4A in growth-related pathways that have a high demand in energy supply. Furthermore, the lack of a clear growth phenotype in *Atnot4b* and *Atnot4c* (**Figure 20-21**) highlights that each *At*NOT4 has evolved specialised functions. Perhaps, *At*NOT4A may be responsible for ensuring adequate energy during specific growth periods. Even when analysing *Atnot4bc* - where both *At*NOT4B and *At*NOT4C are absent - no obvious growth phenotype was observed which further emphasises the unique role that *At*NOT4A has in growth and development.

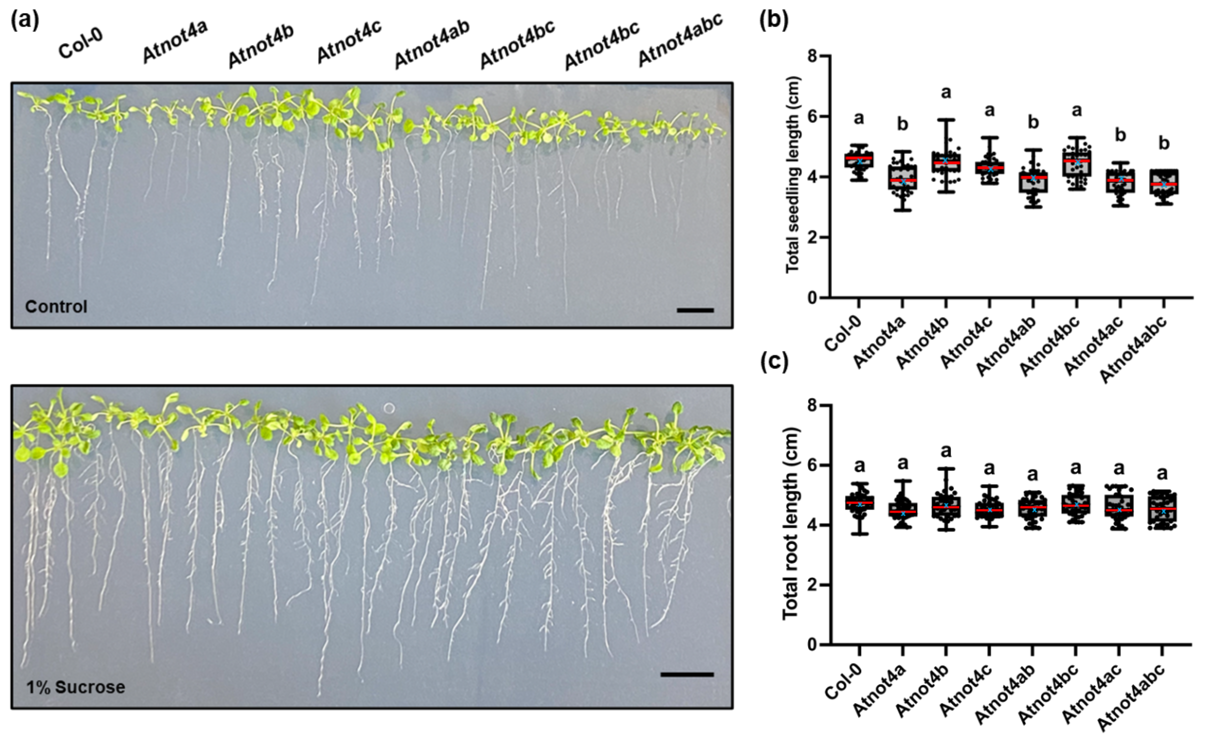

Figure 20 – Sucrose treatment analysis of *At*NOT4 single, double and triple mutants.

(a) Representative images of 12-day-old wild-type and *AtNOT4* mutant seedlings grown on ½ MS medium +/- 1% sucrose supplementation. Scale bar = 1 cm. **(b)** Quantification of total seedling length in Col-0 and *AtNOT4* mutants grown on ½ MS medium **(c)** Quantification of total seedling length in Col-0 and *AtNOT4* mutants grown on ½ MS medium with 1% sucrose. Box and whiskers plots show max and min, 25–75th percentiles (box), median (red line) and mean (blue 'x') Different letters (a , b) indicate statistically significant differences ($p < 0.05$) as determined by one-way ANOVA, Tukey's test. Data represents two biological replicates, each consisting of ~20 seedlings.

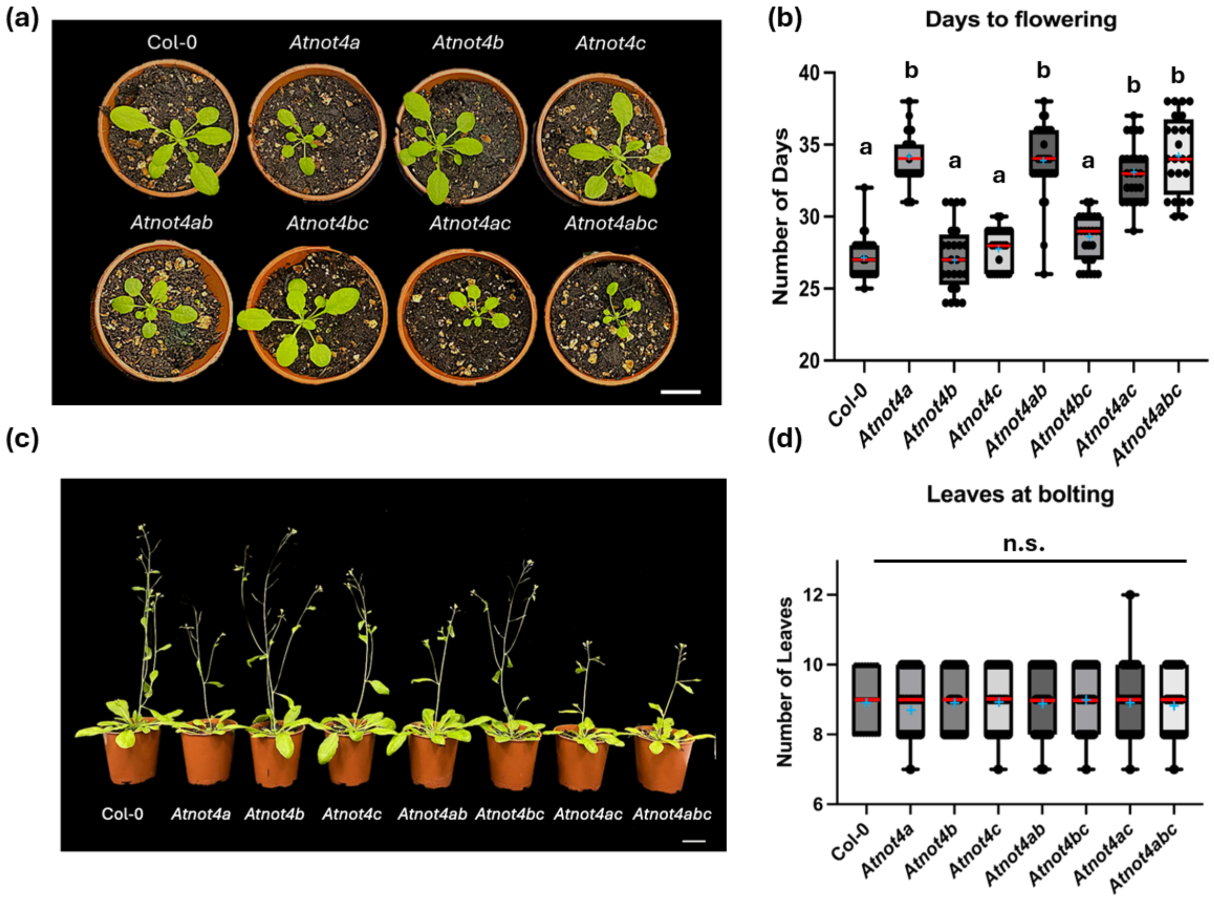

Figure 21 – Phenotypic analyses of *At*NOT4 single, double and triple mutants growing on soil. (a) Representative rosette images of 21-days-old wild-type and various *AtNOT4* single, double, and triple mutants. The *Atnot4a*, *Atnot4ab*, *Atnot4ac*, and *Atnot4abc* mutants exhibit smaller rosettes and delayed growth compared to wild-type and other mutants. Scale bar = 1cm. **(b)** Box plot displays the number of days to flowering for wild-type and *At*NOT4 mutants. Box and whiskers plots show max and min, 25–75th percentiles (box), median (red line) and mean (blue '+'). Different letters indicate statistically significant differences ($p < 0.05$) as determined by one-way ANOVA **(c)** Representative images of wild-type and various *At*NOT4 mutants at the bolting stage. The *Atnot4a*, *Atnot4ab*, *Atnot4ac*, and *Atnot4abc* mutants show delayed bolting and reduced growth compared to wild-type and other mutants. Scale bar = 1cm **(d)** Box plot showing the number of leaves at bolting for wild-type and *At*NOT4 mutants. No significant differences (n.s.) as determined by one-way ANOVA were observed among the genotypes. Box and whiskers plots show max and min, 25–75th percentiles (box), median (red line) and mean (blue '+'). This represents two biological replicates, each consisting of 12-14 plants.

3.4.1 Expression profile of *At*NOT4s in *Arabidopsis*

3.1.1.1. *At*NOT4s are widely expressed in *Arabidopsis* tissues

To investigate *At*NOT4 protein expression and localisation, transgenics expressing *AtNOT4-GUS* translational fusions driven by their native *At*NOT4 promoters were developed. Here, full length gDNA sequences including a 2 kb of upstream promoter sequence were cloned in frame with a C-terminal GUS fusion, and the resulting *AtNOT4A-GUS, AtNOT4B-GUS* and *AtNOT4C-GUS* constructs were transformed into the corresponding *Atnot4a*, *Atnot4b,* and *Atnot4c* mutant backgrounds. To visualise the expression and localisation of GUS-tagged *At*NOT4s in whole and organ specific *Arabidopsis* seedlings of different developmental stages (**Figure 22-24**), histochemical staining was performed (*see Chapter 2, section 2.5.1.4*). 24-hour incubation with X-gluc solution produced widespread staining, specifically in regions of rapid growth and high protein turnover.

In 7-day-old seedlings, *At*NOT4A-GUS was expressed and localised mainly in the vascular tissue, apical meristem, and emerging leaf primordia (**Figure 22a**). In contrast, *At*NOT4B-GUS and AtNOT4C-GUS lines showed a wider pattern of staining. These lines showed, besides staining in the vascular tissue and apical meristem, also strong signals throughout the cotyledons (**Figure 23-24a/f**). All three *At*NOT4-GUS proteins were highly expressed and localized in the root meristem and lateral root primordia in 7-day-old seedlings (**Figure 22-24b-d**). Notably, staining of *At*NOT4B-GUS appeared stronger in 14-day-old seedlings (**Figure 23f**) compared to *At*NOT4A-GUS and *At*NOT4C-GUS (**Figure 22f, 24f**). GUS signals were also visible in rosette leaves, regardless of their age (**Figure 22-24g/i)** as well as in the cauline leaves (**Figure 22-24h**). While there were some differences in the intensity and distribution of the staining, the patterns appeared overall quite similar across all three paralogues. Furthermore, all *At*NOT4-GUS proteins were observed in the inflorescences and individual flowers (**Figure 22-24e/j**), indicating their expression and localization in these reproductive structures. *At*NOT4 proteins appear to be in meristemic regions such as primordia and dividing or expanding tissues of younger plants. There are visible differences in expression, particularly in 7-day-old seedlings between *At*NOT4A and *At*NOT4B/C, which highlights divergence in paralogue functions.

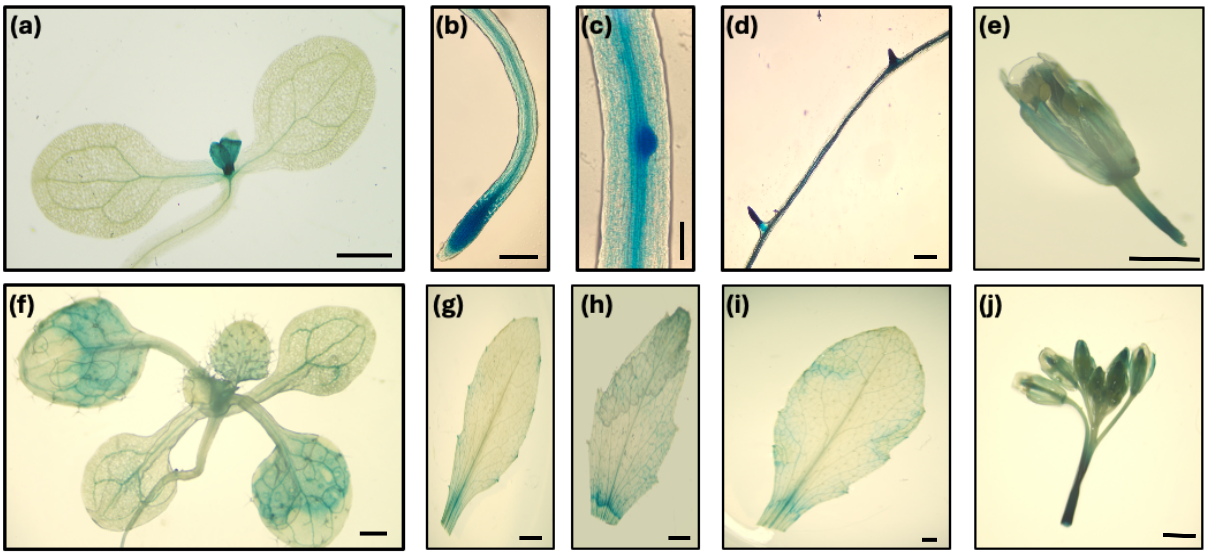

Figure 22 – Histochemical staining pattern of transgenic lines expressing *pAtNOT4A::AtNOT4A-GUS* following 24hrs incubation in X-gluc. **(a)** cotyledons of 7-day old seedling. **(b and c**) roots of 7-day-old seedlings. **(d)** roots of 14-day old seedlings. **(f)** Rosette of 14-day old seedling. **(g)** leaf of a 14-day old plant **(h)** cauline leaf. **(i)** rosette leaf of a 21-day old plant **(e and j)** inflorescence. All images are representative of the staining patterns observed in two independent transgenic lines. Scale bar = 1 mm.

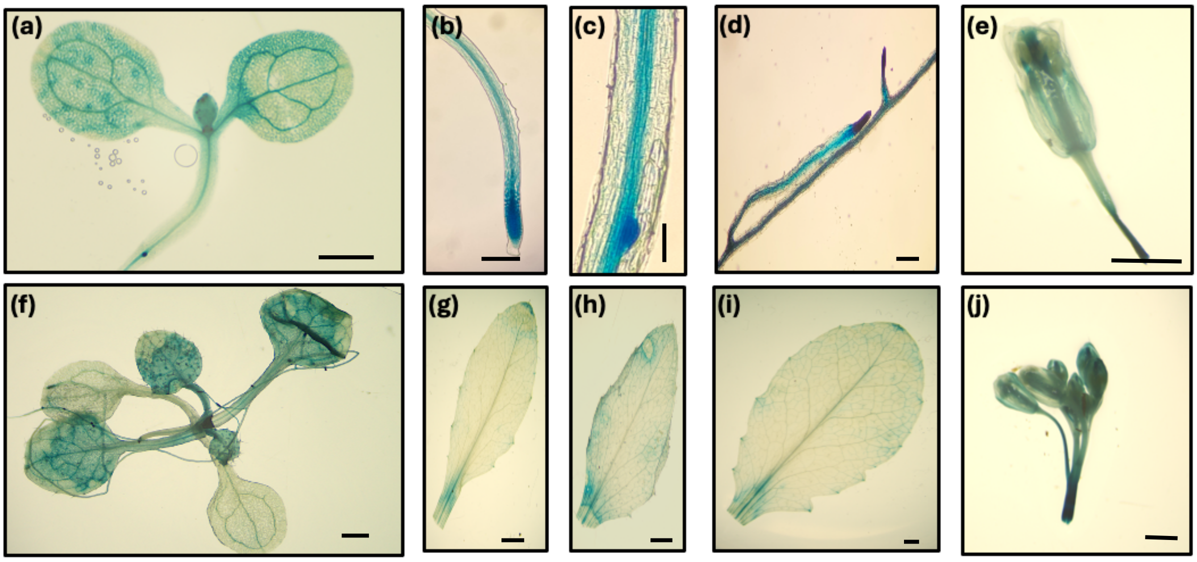

Figure 23 – Histochemical staining pattern of transgenic lines expressing *pAtNOT4B::AtNOT4B-GUS* following 24hrs incubation in X-gluc. **(a)** cotyledons of 7-day old seedling. **(b and c**) roots of 7-day-old seedlings. **(d)** roots of 14-day old seedlings. **(f)** Rosette of 14-day old seedling. **(g)** leaf of a 14-day old plant **(h)** cauline leaf. **(i)** rosette leaf of a 21-day old plant **(e and j)** inflorescence. All images are representative of the staining patterns observed in two independent transgenic lines. Scale bar = 1 mm.

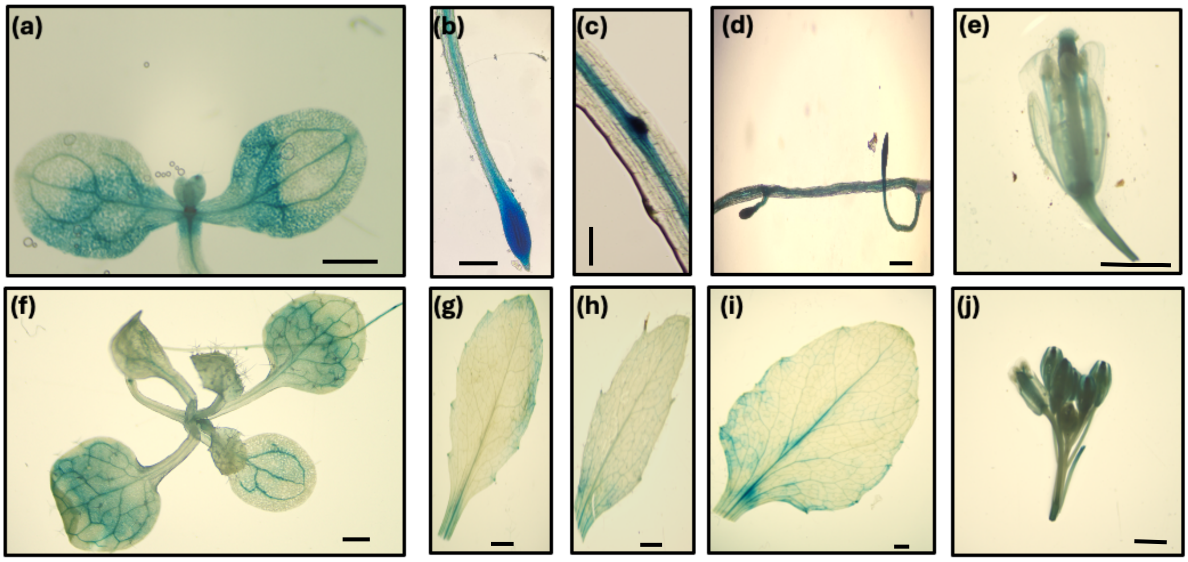

Figure 24 – Histochemical staining pattern of transgenic lines expressing *pAtNOT4C::AtNOT4C-GUS* following 24hrs incubation in X-gluc. **(a)** cotyledons of 7-day old seedling. **(b and c**) roots of 7-day-old seedlings. **(d)** roots of 14-day old seedlings. **(f)** Rosette of 14-day old seedling. **(g)** leaf of a 14-day old plant **(h)** cauline leaf. **(i)** rosette leaf of a 21-day old plant **(e and j)** inflorescence. All images are representative of the staining patterns observed in two independent transgenic lines. Scale bar = 1 mm.

3.4.1.2. qPCR Results Indicate Potential Genetic Redundancy Among *AtNOT4* Paralogs

It is possible that *At*NOT4 proteins share functions related to proteolysis and RNA regulation as indicated by the high sequence homology in the RING and RRM domains. The observed growth phenotype only observed in *Atnot4a* further emphasis that each paralog may have evolved discrete and process-specific roles. The opposite may also be true in which *At*NOT4s may complement each other in its absence through shared functional roles. Such compensation can usually be seen in the form of transcriptional feedback (i.e. knocking out one leads to the increase in the expression of another). To investigate whether genetic redundancy across *At*NOT4 paralogs exists, qPCR was performed to measure the expression of the single, double and triple mutants. The method involved designing primers that would anneal upstream and downstream of each T-DNA insertion (**Figure 25-27**). Thus, the expression prior to and after the insertion can be assessed.

In the *Atnot4a* single mutant, *AtNOT4A* expression is still detectable at the 5' end, upstream of the T-DNA insertion (**Figure 25 and Figure 19**). Interestingly, expression of this region is approximately 40x higher in *Atnot4a* compared to WT, suggesting the presence of a compensatory feedback mechanism for increasing transcription of *NOT4A* in the absence of full length *At*NOT4A protein (**Figure 25**). An even stronger apparent autofeedback was observed for the 5' region of *AtNOT4B* in *Atnot4b,* which was expressed at levels 400 x higher than in WT (**Figure 26)**. Since the T-DNA insertion in *AtNOT4C* is located much closer to the 5' end of the gene, primers that effectively detected *AtNOT4C* expression upstream of the insertion could not be found despite multiple attempts, and so feedback onto *AtNOT4C* expression in *Atnot4c* lines could not be detected. *AtNOT4A* expression was also significantly increased in the *Atnot4b* and *Atnot4c* single mutants compared to wild type, with an approximate 4-fold upregulation, indicating that the absence of *AtNOT4B* and *AtNOT4C* forces an upregulation of *AtNOT4A* transcription (**Figure 25**). This pattern is similarly observed with *AtNOT4B* expression in *Atnot4a* and *Atnot4c*, where an approximately 3-fold increase is detected (**Figure 26**). In contrast, *At*NOT4C expression is not induced in *Atnot4a* or *Atnot4b* mutant lines, displaying comparable levels in expression to wild-type (**Figure 27**). This lack of upregulation suggests that *AtNOT4C* does not exhibit the same compensatory transcriptional response as *AtNOT4A/B*. As expected, no expression was detected downstream of the T-DNA insertion in any of the lines (**Figure 26-27**).

An intriguing observation is seen in the analysis of the double mutants. The hypothesis of genetic redundancy is significantly emphasised in *Atnot4bc* as a substantial increase in *AtNOT4A* expression (**Figure 25**) is detected. To be specific, *AtNOT4As* expression was 40 times greater compared to any single *Atnot4* mutants or wild-type (**Figure 25**). While an increase in *AtNOT4A* expression is already observed in the single *Atnot4b* mutant, the effect becomes markedly amplified when two *AtNOT4* genes are knocked out, indicating a clear additive response (**Figure 25-27**). This is further seen in *Atnot4ac* where *AtNOT4B* is hyperactive as it is 500-fold more expressed than any single *Atnot4* mutant or wild-type (**Figure 26**). Similarly, in *Atnot4ab* but not to the same extent, *AtNOT4C* expression increases by 35-fold (Figure 26) which is a notable observation considering no substantial increase was observed in the single mutants. This heightened expression is further pronounced in *Atnot4abc*, with the highest level of transcriptional feedback in *AtNOT4A* was observed with a 100-fold increase. *AtNOT4B* had an approximate 200-fold increase in expression in *Atnot4abc* further showing it is additive. Thus, these results emphasise the dynamic regulatory network that govern *AtNOT4* gene expression, highlighting that *At*NOT4s likely share regulatory roles.

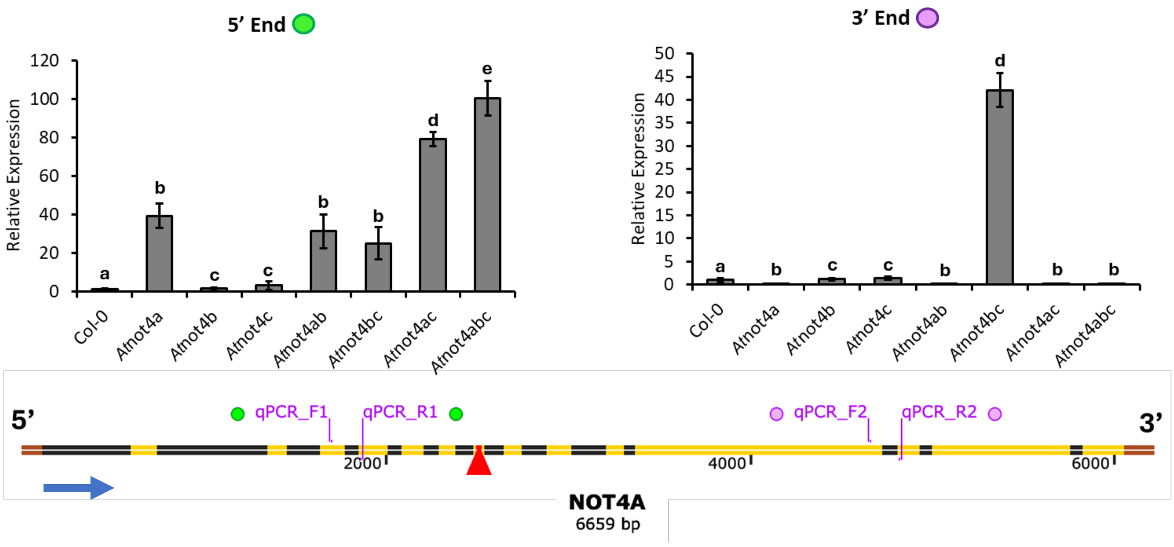

Figure 25 - Relative Expression Levels of *AtNOT4A* in Various *Arabidopsis* Mutant Backgrounds. **Top Panel:** Bar charts visualising relative expression of *AtNOT4A* determined by RT-qPCR and normalised against Col-0 across different mutant backgrounds at the 5' end (left graph) and 3' end (right graph) of the gene. Letters above the bars indicate statistical significance ($p < 0.05$) determined by ANOVA among the groups. **Bottom Panel**: Schematic representation of the *AtNOT4A* gene with the T-DNA insertion site (red triangle) and the positions of the qPCR primers (qPCR_F1 (Primer 7) qPCR_R1 (Primer 8) , qPCR_F2 (Primer 9), qPCR_R2 (Primer 10) created using SnapGene Viewer. Sequences obtained from Tair (https://www.arabidopsis.org/). The data represents the mean of 4 technical replicates of 3 biological replicates. Blue arrow indicates the gene's transcriptional orientation.

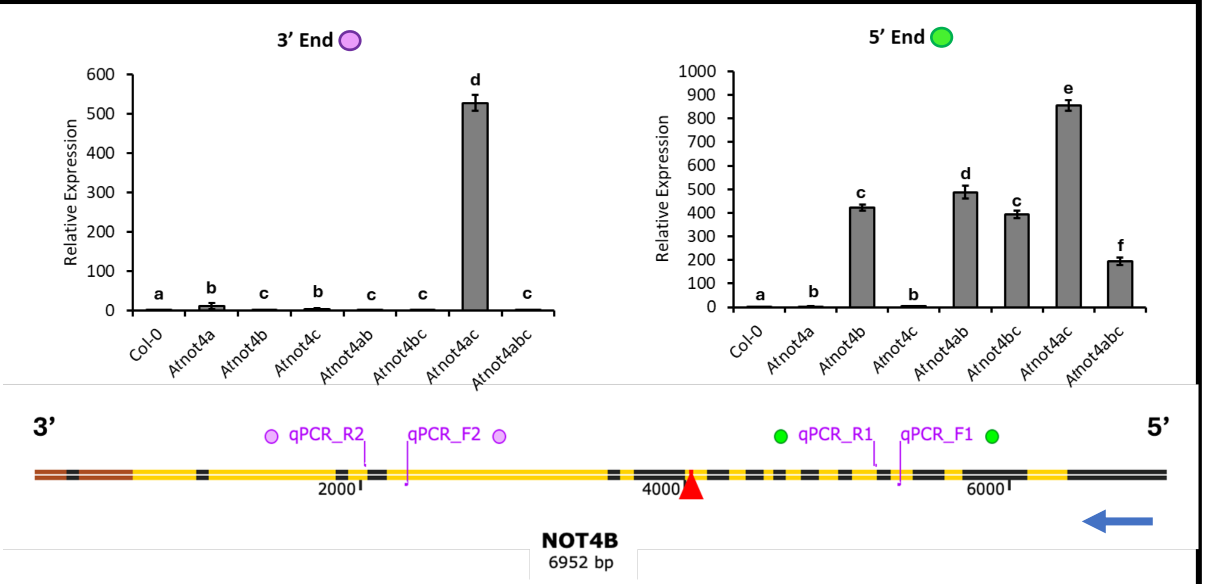

Figure 26 - Relative Expression Levels of *AtNOT4B* in Various *Arabidopsis* Mutant Backgrounds. **Top Panel:** Bar charts visualising relative expression of *AtNOT4B* determined by RT-qPCR and normalised against Col-0 across different mutant backgrounds at the 5' end (left graph) and 3' end (right graph) of the gene. Letters above the bars indicate statistical significance ($p < 0.05$) determined by ANOVA among the groups. **Bottom Panel:** Schematic representation of the *AtNOT4B* gene with the T-DNA insertion site (red triangle) and the positions of the qPCR primers (qPCR_F1 (Primer 11) qPCR_R1 (Primer 12) , qPCR_F2 (Primer 13), qPCR_R2 (Primer 14) created using SnapGene Viewer. Sequences obtained from Tair (https://www.arabidopsis.org/). The data represents the mean 4 technical replicates of 3 biological replicates. Blue arrow indicates the gene's transcriptional orientation

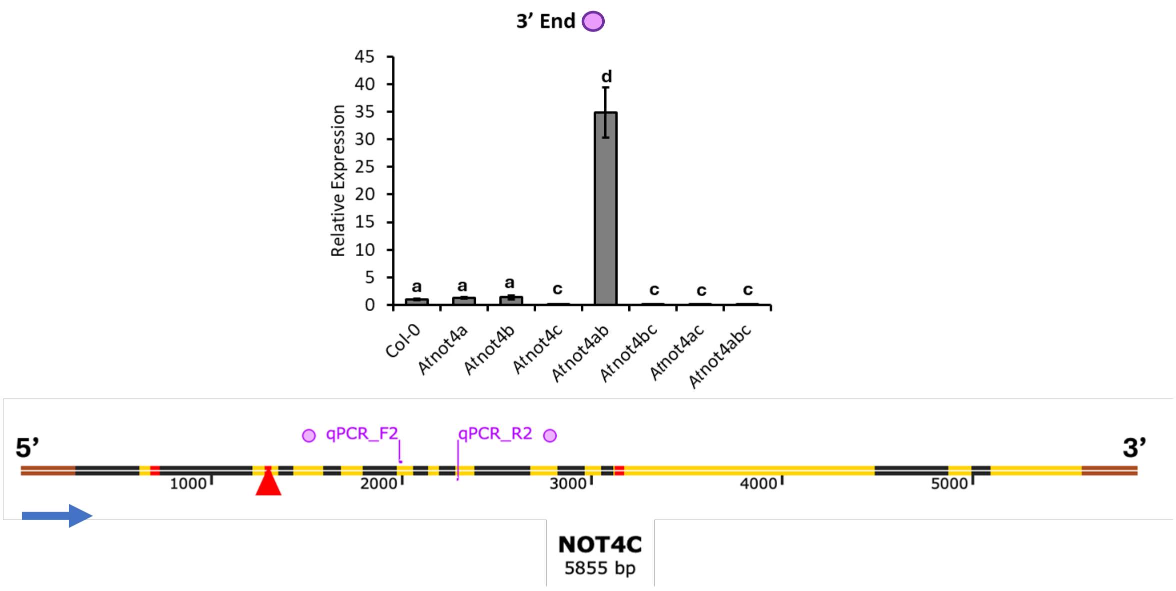

Figure 27 - Relative Expression Levels of AtNOT4C in Various Arabidopsis Mutant Backgrounds. Top Panel: Bar charts visualising relative expression of *AtNOT4C* determined by RT-qPCR and normalised against Col-0 across different mutant backgrounds at the 5' end (left graph) and 3' end (right graph) of the gene. Letters above the bars show statistical significance as tested among groups using ANOVA at $p < 0.05$. **Bottom Panel:** Schematic of the *AtNOT4C* gene showing the site of the T-DNA insertion (red triangle) and location of q-PCR primers qPCR_F2 (Primer 15), qPCR_R2 (Primer 16) designed using SnapGene Viewer. Sequences were obtained from TAIR (https://www.arabidopsis.org/) Data represent the mean 4 technical replicates of 3 biological replicates. Blue arrow indicates gene transcriptional orientation.

3.5 Transcriptome analysis of *Atnot4abc*

The genetic redundancy among *At*NOT4 paralogs likely means that each *At*NOT4 may share yet also possess diverged functional roles. Therefore, *Atnot4abc* was selected for further analysis to fully understand the functional importance of *At*NOT4 in *Arabidopsis*, specifically in context of growth and development. A broad overview on the processes that *At*NOT4s regulate or take part in can be deduced from transcriptomic analysis. Total mRNA was extracted (*see Chapter 2, Section 2.6.1.2*) from 12-day-old Col-0 and *Atnot4abc* seedlings that were grown on vertical ½ MS plates and sent for RNA-sequencing performed by Novogene (UK) Company Limited (Cambridge) (*see Chapter 2, Section 2.6.1.4*).

3.5.1 Differentially Expressed Genes (DEGs) analysis of *Atnot4abc*

A volcano plot (**Figure 28**) was used to visually summarise the resulting differentially expressed genes (DEGs) between *Atnot4abc* and Col-0. Each data point confers to a specific gene that had a fold change > 0.58 for upregulation (red) or < 0.58 for downregulation (blue), and a statistical significance with a p-value < 0.05 (as -Log10(p-value) > 1.3), which are plotted in the x- and y-axis respectively. The horizontal dashed lines are the thresholds set. Overall, a total of 3747 genes were identified to be differentially expressed in *Atnot4abc*. Among these, 2348 genes were significantly downregulated, while 1399 genes were upregulated. As expected, *AtNOT4A*, *AtNOT4B* and *AtNOT4C* were all significantly downregulated.

Furthermore, the substantial amount of DEGs is reflective of the various biological processes, molecular functions and cellular components that are affected in the absence of *At*NOT4s under normal growth conditions. The broad impact *At*NOT4s have on the transcriptome can provide valuable insights of the specific functions, specifically in the context of maintaining cellular homeostasis. Therefore, Gene Ontology (GO) term enrichment analysis was conducted to identify key processes that are dysregulated when *At*NOT4s are disrupted in hope to identify the regulatory networks that *At*NOT4s operate in.

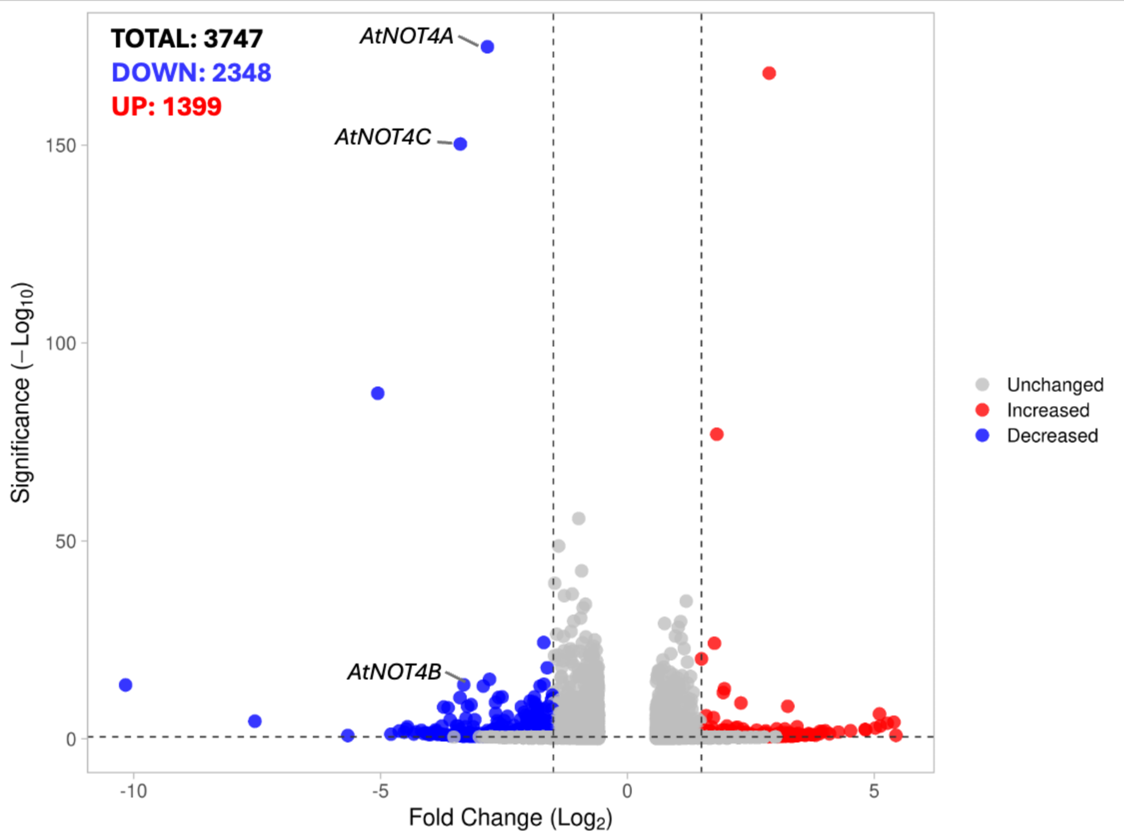

Figure 28 - Differential Expression Analysis of Genes in *Arabidopsis*. Volcano plot displays the differential expression of genes. the fold change ($Log_2(1.5)$) on the x-axis and the significance ($-Log_{10}$(p-value) on the y-axis.

3.5.2 GO Term Enrichment Analysis for Upregulated Genes in *Atnot4abc*

The 1399 significantly upregulated genes in *Atnot4abc* vs Col-0 underwent GO term enrichment analysis. The results were visualised in a dot plot which summarised the enriched GO terms associated to specific biological processes (**Figure 29a**). Each dot represents a significantly enriched GO term. The size of the dots represents the number of genes in the significant upregulated DEGs associated with the GO term and the colour of the dots represent the p-values

Significantly enriched GO terms were 'translation' (25 DEGs, p-value = 3.4×10^{-7}, Fischer's exact test) and 'ribosome biogenesis' (8 DEGs, p-value = $3.81\times10^{-3,}$ Fischer's exact test) (**Figure 29b, d**). This indicates increased expression of genes linked to the protein synthesis machinery and mRNA translation in *Atnot4abc* compared to wild type. Such upregulation may reflect a compensatory mechanism to counterbalance the disruption of *At*NOT4s function, which may be essential for maintaining proper protein translation and homeostasis, or it may point to *At*NOT4s being negative regulators of these processes. This is certainly of interest, given the fact that NOT4s have an RRM domain, suggesting links to RNA biology, and previous work in yeast has connected *Sc*NOT4 function to the regulation of translation (Collart, 2013a; Dimitrova et al., 2009; Preissler et al., 2015; Wu et al., 2018). Genes linked to the formation of ribonucleoprotein complexes, essential for various cellular processes including ribosome assembly and function, are also notably upregulated ('ribonucleoprotein complex biogenesis', 18 DEGs, p-value = 1.08×10^{-6}, Fischer's exact test; **Figure 29a**). This also highlights the cellular emphasis on maintaining efficient protein synthesis in the absence of *AtNOT4s*.

A closer look at the 25 and 8 DEGs linked to the 'translation; and 'ribosome biogenesis' GO terms, respectively, reveals that several classes of core translation associated genes are upregulated (**Figure 30-31**). This includes seven subunits of eukaryotic translation initiation complex, and two translation elongation factors. In addition, four 40S ribosomal subunits and five 60S ribosomal subunits are significantly upregulated, alongside three tRNA ligases (Asparagine, Proline and Threonine), two aminoacyl tRNA synthetases and a poly(A) binding protein. As such, multiple factors linked to protein translation are upregulated in *Atnot4abc*, suggesting that the mutant might have altered protein synthesis rates or regulation (*see next chapter*).

In addition to multiple genes and GO terms linked to translation and ribosomes, the enrichment of the ‘peptide metabolic process’ term (37 genes, p-value = 4.16×10^{-6}, Fischer’s Exact Test) indicates enhanced metabolic activities related to peptide and protein processing (**Figure 29a**). This further suggests that the *Atnot4abc* experiences increased protein turnover and processing, possibly as a response to the altered proteostasis resulting from *AtNOT4* disruption. Furthermore, several enriched GO terms are associated with the regulation of ‘regulation of transcription’ (149 DEGs, p-value = 1.6×10^{-5}, Fischer’s Exact Test) (**Figure 29c**) and ‘RNA biosynthetic processes’ (156 DEGS, p-value = 1.9×10^{-5}, Fischer’s Exact Test), pointing to a broader impact on the transcription. Perhaps, this indicates a cellular effort to modulate transcriptional activities in response to the loss of *At*NOT4s function. Enriched genes generally associated to RNA metabolic process like GO terms ‘regulation of RNA metabolic process’, ‘RNA biosynthetic process’, and ‘regulation of RNA biosynthetic process’ suggests an import function of *At*NOT4s in RNA processing and turnover. This in turn may also be highlighting the value of the RRM domain in *At*NOT4s even though they are primarily classed as RING E3 ubiquitin ligases. This also may be indicative of a role for *At*NOT4s in mRNA quality control which draws several parallels to their yeast counterpart (Collart, 2013a; Dai et al., 2021).

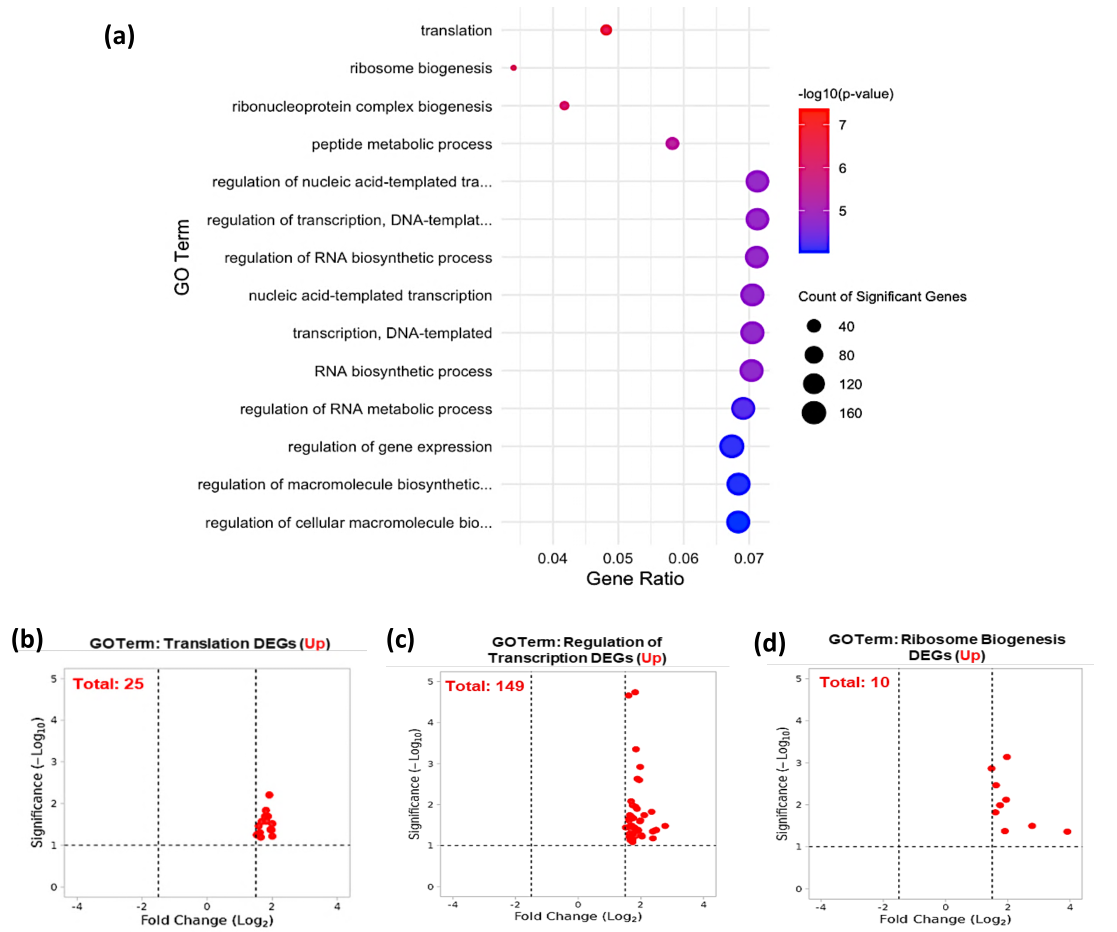

Figure 29 – Gene Ontology (GO) Enrichment Analysis of Upregulated DEGs. **(a)** dot plot illustrates top GO terms enriched in *Atnot4abc* . The x-axis represents the gene ratio, while the y-axis lists the GO terms associated with biological processes. Dot size indicates the count of significant genes, and colour intensity reflects the significance level (–$\log_{10}$ (p-value)). Key enriched GO terms include **(b)** translation, **(c)** regulation of transcription, and **(d)** ribosome biogenesis are highlighted in the volcano plots.

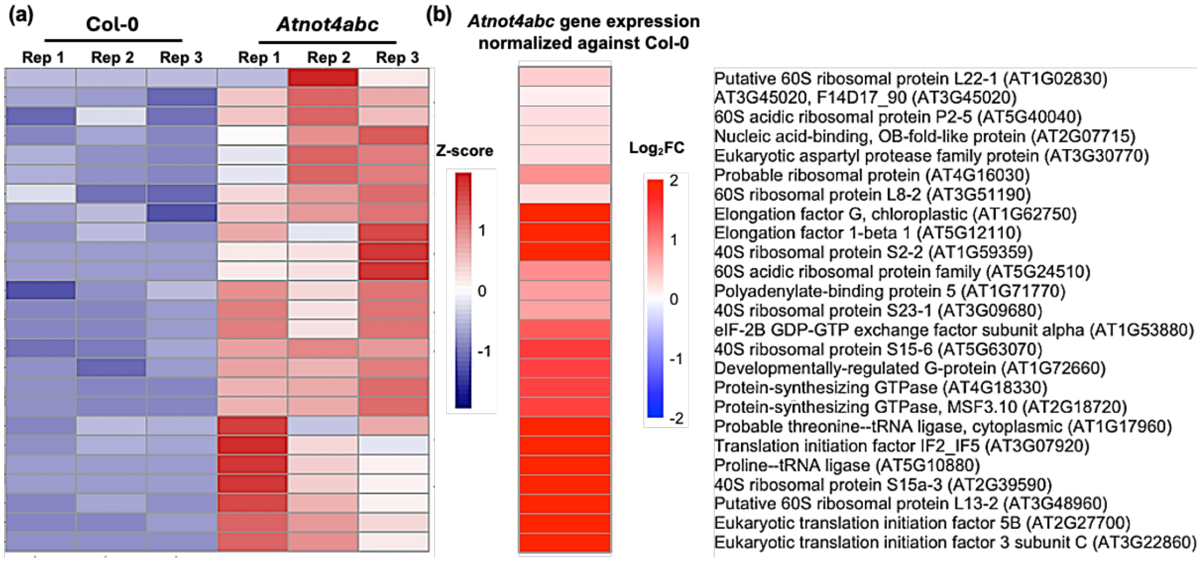

Figure 30 : Heatmap displaying the individual genes associated with the GO Term 'Translation' in Col-0 and *Atnot4abc*. (a) Relative expression of individual genes across three biological replicates. The heatmap depicts scaled expression of each biological replicates. This was done by comparing the expression value for a specific gene in each sample to the mean expression across both genotypes in all biological replicates. This method highlights deviation of each gene's expression from the overall average of that specific gene in this sample set by calculating a Z-score. A Z-score value of 0 indicates no deviation from the mean. The Z-score decreases with darker shades of blue which is not implying that the gene is downregulated in an absolute sense but rather has a lower-expression relative to the combined mean expression across both genotypes. Thus, this heatmap emphasises the relative differences in the context of the overall dataset as opposed to an absolute reference baseline expression. (**b)** Heatmap displaying log_2foldchange (Log_2FC) values normalised against Col-0 highlighting differentially expressed genes upregulated in GO term 'Translation'.

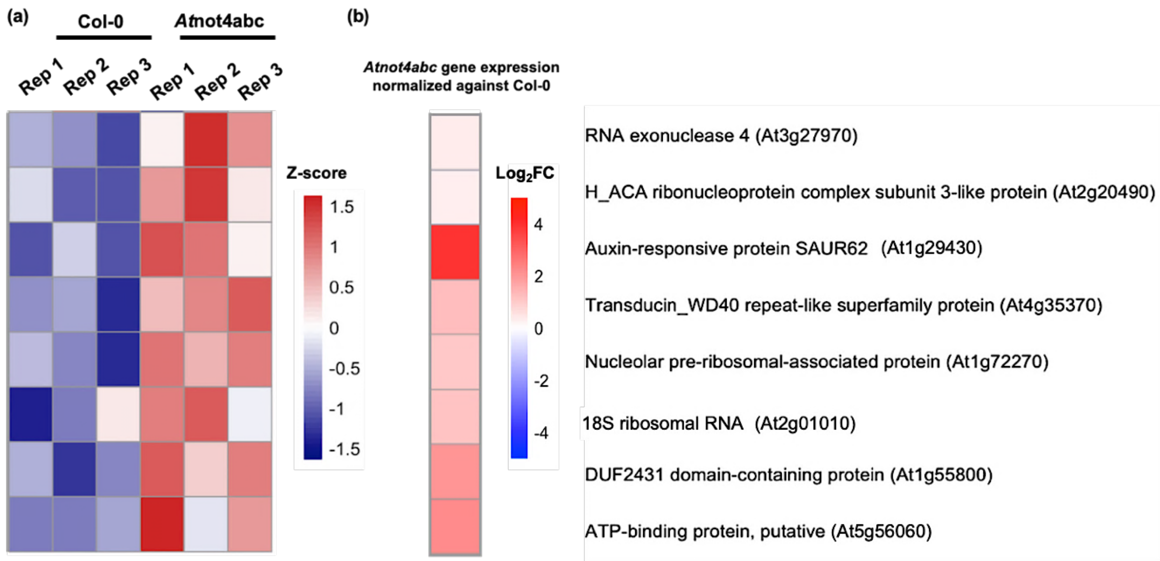

Figure 31: Heatmap highlighting individual genes associated with the GO Term 'Ribosome biogenesis' in Col-0 and *Atnot4abc*. (a) Relative expression of individual genes across three biological replicates. The heatmap depicts scaled expression of each biological replicates. This was done by comparing the expression value for a specific gene in each sample to the mean expression across both genotypes in all biological replicates. This method highlights deviation of each gene's expression from the overall average of that specific gene in this sample set by calculating a Z-score. A Z-score value of 0 indicates no deviation from the mean. The Z-score decreases with darker shades of blue which is not implying that the gene is downregulated in an absolute sense but rather has a lower-expression relative to the combined mean expression across both genotypes. The same applies to positive Z-scores which are depicted in shades of red and indicate a higher-expression compared to the average. Thus, this heatmap emphasises the relative differences in the context of the overall dataset as opposed to an absolute reference baseline expression **(b)** Heatmap displaying log_2foldchange(Log_2FC) values normalised against Col-0 highlighting differentially expressed genes upregulated in GO term 'Ribosome biogenesis'.

3.5.3 GO Term Enrichment Analysis for Downregulated Genes in *Atnot4abc*

GO term enrichment analysis was also performed on the 2348 identified downregulated genes in *Atnot4abc* and depicted in the dot plot (**Figure 32a**).

The most enriched GO term is "cell wall organization or biogenesis" with a total of 106 DEGS (p-value=6.4x10-17, Fischer's Exact Test). This points to an important role of *At*NOT4s in the regulation of cell wall structure and formation (**Figure 32b).** Cell walls are essential because they give plants the stiffness and support, they need to maintain their shape and withstand mechanical stress. They also govern the flow of substances like nutrients and dictate the direction and rate of cell growth; all of which are essential to the plant's overall development. The “Secondary Metabolite Biosynthetic Process” term (47 DEGs, p-value = $1.7x10^{-13}$) points to the significant reduction in the biosynthesis of secondary metabolites (**Figure 32c**). These compounds, although not directly involved in growth and development, play key roles in plant signalling, and interactions with the environment. The downregulation of carbohydrate metabolic processes (132 DEGs, p-value = $4.3x10^{-9}$, Fischer’s Exact Test) indicates that *At*NOT4s are needed for managing the plant’s energy and carbon storage necessary for growth and development. This impact on metabolism could explain the observed growth defects in the *Atnot4abc* mutant.

It seems that *At*NOT4s also have an important role in redox homeostasis with a total of 105 DEGs being enriched to the GO term “Oxidation-Reduction Process” (p-value = 1.6x10-8, Fischer’s Exact Test). This implies that the plant may be more sensitive to reactive oxygen species (ROS) which can have severe consequences as ROS build-up may occur due to suppressed redox processes and ultimately cause cellular damage. Plant signalling may also be compromised as GO terms related to biosynthetic pathways, such as isoprenoid, polysaccharide, terpenoid, and phenylpropanoid metabolic processes, are also significantly downregulated (**Figure 32a/d**).

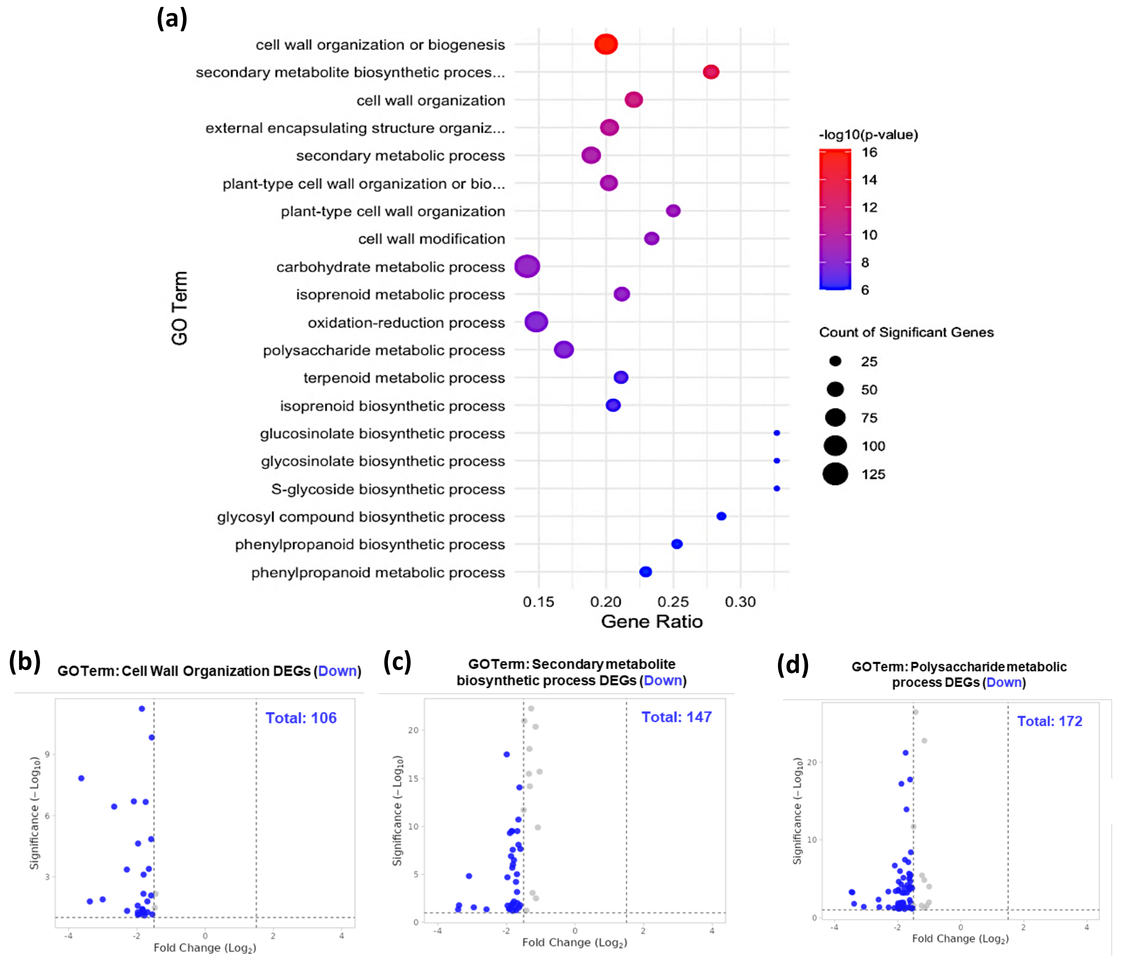

Figure 32 – Gene Ontology (GO) Enrichment Analysis of Downregulated DEGs. (a) dot plot illustrates top GO terms enriched in *Atnot4abc*. The x-axis represents the gene ratio, while the y-axis lists the GO terms associated with biological processes. Dot size indicates the count of significant genes, and colour intensity reflects the significance level ($-\log_{10}$ (p-value)). Key enriched GO terms include **(b)** Cell wall Organisation, **(c)** Secondary metabolite biosynthetic process, and **(d)** Polysaccharide metabolic process are highlighted in the volcano plots.

3.6 Discussion

This chapter presents the findings of the phenotypic and genetic analysis of *Atnot4* single, double and triple mutants, alongside a broader analysis of their expression and localization using translational GUS fusions. Functional characterization of genetic mutants in all three *AtNOT4* genes points towards their possible relevance for growth regulation, stress response, and general transcriptional and translational fidelity. The distinct growth phenotype of the *Atnot4a* mutant hypothesises *At*NOT4As importance in modulating energy allocation and utilisation.

Following up on *At*NOT4As proposed role in energy metabolism, the rescue in growth phenotype in *Atnot4a* upon sucrose supplementation certainly supports this hypothesis further. The observed phenotype is more likely to be linked to energy rather than intrinsic developmental delays. Restoration of growth defects upon additional energy supply has been well-documented in *Arabidopsis*, for example in HEXOKINASE1 (HXK1) and their role in leaf growth. The addition of sucrose managed to restore some metabolic responses in *hxk1* mutants by highlighting HXK1 role in sucrose-induced cell proliferation and chloroplast differentiation (Van Dingenen et al., 2019). The role of sucrose in restoring growth phenotypes through signalling functions as opposed to direct metabolic energy supply has been also reported (Laloum et al., 2022). Perhaps, certain signalling networks upstream of growth-related pathways are compromised in *Atnot4a* which results in the observed phenotype. Therefore, it could be a combination of sucrose signalling and energy metabolism that causes this phenotypic delay in *Atnot4a*. Though the underlying mechanism remains to be understood, and further investigation is needed.

The distinct expression and localisation of *At*NOT4s was analysed through GUS reporter lines. *AtNOT4A* was primarily expressed in the vascular tissues and emerging leaves in 7-day old seedlings whereas *AtNOT4B* and *AtNOT4C* had a widespread expression with GUS stains appearing in the cotyledons. The roots also displayed GUS staining in meristemic regions such as the root tip and lateral root primordia. This must be analysed cautiously as the intensity of GUS signal may not be indicating more expression of E3 ligase, rather the dividing cells in these regions are far more concentrated than elongated cells per se, and therefore lead to a more intense signal of GUS staining. However, the localisation and expression of *AtNOT4s* as E3 ligases is consistent with other known E3 ligases that display similar GUS staining pattern (Etherington et al., 2023; Zhang et al., 2017).

Genetic redundancy was inferred from the qPCR analysis of *Atnot4* single, double, and triple mutants. Specifically, the qPCR results suggested transcriptional feedback in which the upregulation of one *AtNOT4* was induced in the absence of either paralog. An additive effect was also observed in double mutants, where the expression was substantially increased in the remaining *AtNOT4* to compensate for the loss of the other two paralogs. Genetic redundancy has been reported in other E3 ligases across kingdoms. For example, mammalian Mouse double minute 2 (MDM2) and its homolog MDMX display functional redundancy in regulating the tumour suppressor p53, ensuring critical regulation is sustained despite the loss of one gene (Klein et al., 2021; Shadfan et al., 2012). In plants, *Arabidopsis* Tóxicos en Levadura 31 (ATL31) and *Arabidopsis* Tóxicos en Levadura 6 (ATL6) exemplifies this concept (Maekawa et al., 2012). Both ATL31 and ATL6 are ubiquitin ligases associated to membranes and play an important role in carbon/nitrogen (C/N) response. It was shown that the disruption or complete knockout of ATL31 leads to the transcriptional induction of ATL6 and vice versa, particularly under C/N stress. The resulting genetic redundancy through transcriptional feedback may have evolved to confer resistance against genetic perturbations and environmental stresses, permitting growth and development to proceed unimpeded.

Transcriptional regulation, mRNA metabolism, co-translational quality control and the targeted protein degradation via UPS are all possible conserved functions of *At*NOT4s due to the high identity in RING and RRM domains shared with *Sc*NOT4 (Collart, 2013b; Dai et al., 2021; Halter et al., 2014; Panasenko & Collart, 2011, 2012). It is likely that some or all the *At*NOT4s play a role in these fundamental processes as evident by the expression of these proteins in high metabolic regions where rapid growth occurs as well as their impact on overall gene expression. For example, functional roles in transcriptional regulation and mRNA metabolism was suggested by the RNAseq data, as the upregulated genes associated to GO terms such as ‘regulation of RNA metabolic process’, ‘RNA biosynthetic process’, and ‘regulation of

RNA biosynthetic process' were enriched. *Sc*NOT4 is known to play a role in deadenylating-dependent mRNA decay (Panasenko & Collart, 2012). Thus, *At*NOT4s may be involved in similar processes analogous to the role of *Sc*NOT4 in mRNA regulation. There is likely reduced mRNA fidelity and the cell is attempting to counterbalance the loss of *At*NOT4s by upregulating these genes in response.

Another hypothesized function of *At*NOT4s are their role in ubiquitin-mediated protein degradation as part of the UPS to regulate protein quality control; similar to the reported role of *Sc*NOT4 (Dimitrova et al., 2009; Panasenko & Collart, 2011). The regions of rapid growth and high protein turnover where *At*NOT4s are localised and expressed suggests that *At*NOT4s may be present to monitor and regulate mRNA translation during development. The growth phenotype in *Atnot4a* could also be a consequence of an impaired UPS, leading to the aggregation of erroneous proteins and ultimately causing growth delays. However, unlike yeast, where *Sc*NOT4 has a well-established role in regulating proteasome activity, proteasome-related genes were not notably upregulated in *Atnot4a* mutants. If the growth phenotype of *Atnot4a* were primarily due to an impaired UPS, as hypothesized, one would expect to see an upregulation of proteasome-related genes in the transcriptome. The absence of such an upregulation may suggest that the observed phenotypes stem more directly from translational dysregulation rather than proteasome impairment.

Drawing further parallels to *Sc*NOT4, *At*NOT4s could be critical in co-translation quality control by ubiquitinating stalled nascent peptides and ensuring proper protein synthesis. The phenotypic rescue of *Atnot4a* with 1% sucrose supplementation and the induction of genes involved in translation in *Atnot4abc* points towards the possibility that *At*NOT4 proteins monitor and maintain translation efficiency and fidelity in conformity with energy availability. In yeast, *Sc*NOT4 is critical for repressing the expression of genes encoding ribosome-related proteins and translation initiation factors (Azzouz, Panasenko, Deluen, et al., 2009). This repression conserves energy and resources under nutrient-scarce conditions, downregulating translation and slowing growth to adapt efficiently to environmental stresses by modulating translational capacity and resource allocation (Azzouz, Panasenko, Deluen, et al., 2009; Collart, 2013a).

*At*NOT4A appears to function similarly to *Sc*NOT4 in this regard as the restoration of growth upon sucrose addition supports a comparable role. It is possible that *At*NOT4A may adjust the growth and development through regulating translation machinery in accordance with resource availability, specifically energy. Further supporting this proposed role of *At*NOT4s is the upregulation of genes associated to biological processes such as translation and ribosome biogenesis in *Atnot4abc*. The repression of translation initiation and ribosome genes by *Sc*NOT4 is similarly observed in *Atnot4abc* as the loss of *At*NOT4s leads to an increase of these processes. So, the absence of this repression in the *Atnot4abc* mutant likely results in dysregulated translational capacity whereby the addition of sucrose bypasses the requirement for such high translation activity, and normalizing growth rates in the *Atnot4a* mutants. *Sc*NOT4 in yeast has also been identified as a key player in the modulation of translational machinery in response to various environmental and metabolic cues (Collart, 2013a; Halter et al., 2014; Panasenko & Collart, 2011).

Further insights into the roles of *At*NOT4s can be made by analysing the phenotypes associated with *Sc*NOT4 mutants and drawing potential similarities (Collart, 2013a). Upon high temperatures and treatment with Cycloheximide (CHX), a translational inhibitor, *Sc*NOT4-deficient mutants display hindered growth and development (Panasenko & Collart, 2011). Given the conservation of key functional domains between *Sc*NOT4 and *At*NOT4s, it is possible that *At*NOT4s function similarly in modulating translation during stress in *Arabidopsis*. If *At*NOT4s function analogously to *Sc*NOT4 in repressing translation-related genes, a reasonable prediction would be that *Atnot4* mutants would become more sensitive to high temperatures, like the reported yeast phenotype. Under such conditions, dysregulated translation machineries would lead to the accumulation of aberrant proteins that saturate cellular quality control systems. Moreover, CHX and/or other translation-related stressors may further increase the load on the translation machinery in *Atnot4* mutants and thus provoke more severe growth defects compared to wildtype plants. However, this remains all speculative and therefore future experiments may include treating *Atnot4* mutants to elevated temperatures and translational inhibitors such as CHX. Observing whether these mutants display impaired growth under such conditions would provide further evidence supporting the role of *At*NOT4s in managing translational homeostasis under stress, complimenting the roles of *Sc*NOT4 and highlighting a broader significance of NOT4 proteins in managing stress response mechanisms across kingdoms.

The RNA-seq analysis also revealed several GO terms associated with defence-related pathways such as isoprenoids, terpenoids, glucosinolates, and phenylpropanoids metabolic/biosynthetic pathways being downregulated in *Atnot4abc*. This could suggest a trade-off between growth and defence, a phenomenon commonly observed in plants when energy resources are limited. The downregulation of these pathways may reflect a reallocation of resources towards growth and translational processes under the conditions studied, consistent with the proposed role of *At*NOT4s in energy homeostasis. Exploring whether these changes occur due to direct regulatory functions of *At*NOT4s or as a secondary consequence of impaired translational fidelity could be an interesting area for future studies.

The findings in this chapter provided novel insights into the putative roles and possible regulatory mechanisms of NOT4s in *Arabidopsis*. A clear emphasis on their importance in regulating growth and development through modulation of transcription and translation in response to energy availability was presented. Notable observations include that these E3 ligases have evolved shared and paralog specific functions as evident by the distinct expression and localisation patterns, the genetic redundancy through transcriptional feedback and *Atnot4a* mutants obvious growth phenotype. Key features indicated from the RNA-seq analysis showed many genes upregulated in translation and ribosome biogenesis which demonstrate *At*NOT4s importance in cellular homeostasis. Thus, the next chapter builds on these findings, with the specific aim of understanding the role of *At*NOT4s in regulating translation and co-translational protein quality control.

Chapter 4 – Evaluating roles for *At*NOT4 proteins in translation and co-translational quality control.

4.1 Introduction

GO term enrichment linked to protein translation and ribosome biogenesis is further analysed in this chapter with the aim to expand our understanding of *At*NOT4s function in regulating protein synthesis and co-translational quality control. A critical step to proteome function is protein synthesis, a process where mRNAs are decoded into polypeptide chains (*see Chapter 1, Section 1.2*). Nascent polypeptides emerging from the ribosome are gradually folded to form more complex structures. However, misfolding can occur creating aberrant proteins. This is a critical step in which the co-translation quality control plays an important part as it ensures the fidelity of protein synthesis by monitoring nascent polypeptides as well as facilitating the degradation of defective ones (i.e. when they are incorrectly folded).

In yeast, *Sc*NOT4 is known to participate in ribosome-associated quality control (RQC), where knockout mutants accumulate polyubiquitinated translation arrest products and protein aggregates (Panasenko & Collart, 2011), likely due to reduced translational fidelity. Additionally, *Sc*NOT4 targets diverse substrates for ubiquitination, linking its activity to proteasomal degradation (Gulshan et al., 2012; Panasenko & Collart, 2012; Wu et al., 2018). *Sc*NOT4 also promotes efficient proteasome assembly and maturation, underscoring its central role in coordinating a broad range of biological processes related to translation, transcriptional regulation, and proteasomal function (Collart, 2013a; Preissler et al., 2015). Given the evolutionary conservation of NOT4 proteins as well as highly enriched GO terms linked to ‘translation’ and ‘ribosome biogenesis’ (*see Chapter 3*), it is plausible that *At*NOT4s perform similar functions in *Arabidopsis*. It is hypothesised that the increased number of NOT4 paralogues in *Arabidopsis* provides an enhanced flexibility in their capacity to monitor and precisely control translation, and that each paralog may have shared as well as discrete or process-specific roles. Thus, the experiments presented here aimed to evaluate how *At*NOT4 proteins contribute to co-translational quality control, ensuring efficient and accurate protein synthesis and maintaining cellular homeostasis.

4.2 Faster global translation rates relative to WT

Knockout mutants in yeast (*ΔScnot4)* showed increased global translation rates even under conditions that typically restrain protein synthesis, highlighting *Sc*NOT4s repressive role in translation (Preissler et al., 2015). To further investigate the increased upregulated ribosome biogenesis and translation-associated DEGs observed in *Atnot4abc* (*see Chapter 3, Section 3.4.2*), we aimed to analyse the role of *At*NOT4s in protein synthesis, assuming that *At*NOT4s function similarly to *Sc*NOT4 by taking on a repressive role. Therefore, we hypothesise that the increase expression of these genes might directly correlate to increase global translation in *Atnot4abc* when compared to wild type.

Global translation rates were measured using a puromycin incorporation assay. Briefly, puromycin was first discovered as a protein synthesis inhibitor. This inhibition is due to the structure of puromycin as it resembles the 3' end of aminoacylated tRNA (aa-tRNA). Beyond its close resemblance, the main distinction is the type of bond it establishes as normally a labile ester bond between amino acid and ribose takes place whereas a stable peptide bond is formed with puromycin. The similarity to aa-tRNA allows puromycin to enter the A-site of the ribosome where its able to incorporate into nascent polypeptide chains at the P-site peptidyl-tRNA due to its free amino group. However, the stable peptide bond that puromycin forms cannot be cleaved by subsequent aa-tRNAs, thus incorporation at the C-terminus is no longer viable and ultimately preventing elongation. This causes premature chain termination, thereby ending the protein synthesis process with early release of an incomplete polypeptide chain. The amount of puromycin incorporated into nascent polypeptides is therefore a direct measure of translational activity (Aviner, 2020; Baliga et al., 1970; Semenkov et al., 1992).

12-day old seedlings were treated with 50 µM puromycin in liquid ½ MS for 0, 20, 60 minutes. After the 60-minute time point, samples were treated with either the translational inhibitor cycloheximide (CHX, 50 µM) or DMSO (equivalent volume) and incubated for an additional 60 minutes. Total protein was then extracted and the levels of puromycin incorporation assessed by anti-puromycin Western blotting. Our results revealed a stronger signal for puromycin in *Atnot4abc* compared to WT within 20 minutes, with continued signal intensity at 60 minutes, indicating faster global translation rates in *Atnot4abc* mutants (**Figure 33a**). CHX was added to the samples for an additional hour which revealed no difference in translation rates between *Atnot4abc* and Col-0 (**Figure 33b**). The mock treatment of DMSO shows a noticeably stronger signal in *Atnot4abc* which indicates the continuation of enhanced translational activity compared to Col-0. This was repeated twice using two independent biological replicates in which similar results were observed.

It is clear from these results that *Atnot4abc* exhibit increase global translation rates, complimenting the transcriptomic data which showed increase DEGs in translation and ribosome biogenesis. Furthermore, this also suggests that the repressive role of *Sc*NOT4 is also conserved across kingdoms.

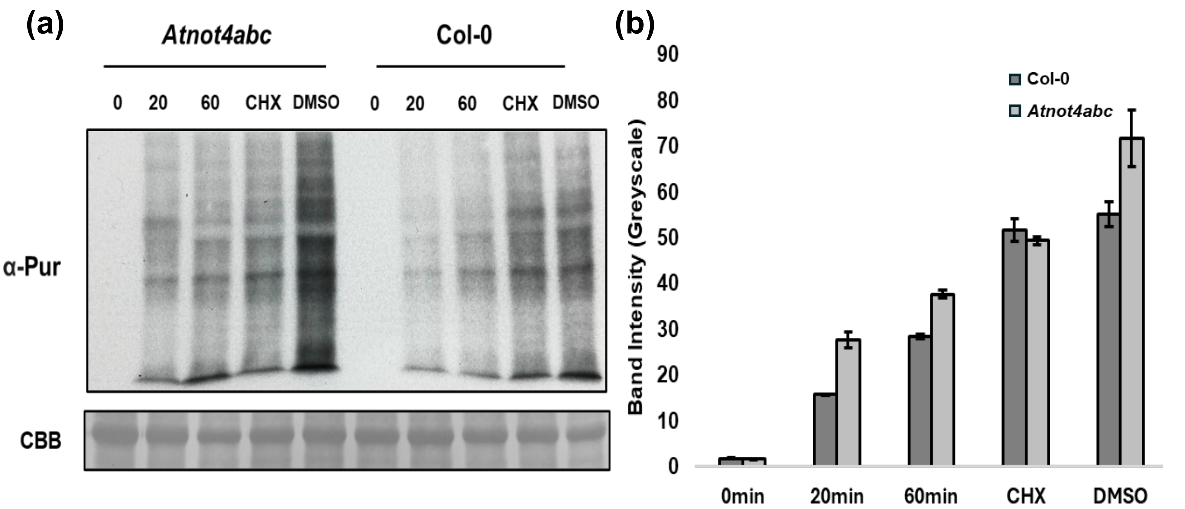

Figure 33 - Assessment of Global Translation Rates Using Puromycin Incorporation in *Atnot4* Mutants and Wild-Type. (**a**) Western blot analysis of puromycin incorporation. Seedlings were treated with puromycin for 0, 20, and 60 minutes followed cycloheximide (CHX) or mock (DMSO) treatment for an additional 60 minutes. Protein samples were then analysed by Western blot using an anti-puromycin antibody. The intensity of the puromycin signal indicates the rate of protein synthesis. The top panel shows puromycin incorporation, while the bottom panel shows the Coomassie Brilliant Blue (CBB) stained gel as a loading control. (**b**) Bar graph represents the relative puromycin incorporation levels in Col-0 (wild type) and *Atnot4abc*. Band intensities were measured by using ImageJ and processed according to protocol by Daravinejad (2015). Data represents the mean ± standard error of two biological replicates. No statistical significance could be tested as only two replicates were available.

4.3 Overaccumulation of total polyubiquitinated conjugates

Building upon the enhanced translation rates in *Atnot4abc*, we hypothesised an increase in translational errors. *Sc*NOT4 is known to play a role in co-translational quality control (Collart, 2013a). Due to the high similarity in sequence, especially the conserved RING and RRM domains, it is possible that *At*NOT4s are also involved in co-translation quality control. If co-translation quality control is compromised (due to the absent of *At*NOT4s), then the unmonitored increased translation rate may lead to the production of more defective and misfolded proteins. The accumulation of these aberrant proteins may be still targeted for degradation by other E3 ligases, therefore leading to an increase in total polyubiquitinated conjugates.

Western blotting analysis was performed to quantify the total amount of polyubiquitinated proteins in wild-type, *Atnot4* single mutants, and *Atnot4abc* using a commercially available antibody (*see Chapter 2, Section 2.3*). A stronger signal in *Atnot4abc* compared to the single mutants and wild-type was observed (p-value < 0.01, One-Way ANOVA), which suggest that there is more polyubiquitinated proteins accumulating in the absence of all three *At*NOT4s (**Figure 34a/b**). Δ*Sc*NOT4 mutants in yeast also accumulated polyubiquitinated translation arrest products (Duttler et al., 2013; Panasenko & Collart, 2011), thus correlating with the findings observed here. In yeast, the absence of *Sc*NOT4 enhances ubiquitination by other ribosome-associated E3 ligases that are known to be involved in co-translational quality control. An example of this is the E3 ligase LTN1 which in conjunction with *Sc*NOT4 regulate proteostasis through co-translation quality control (Duttler et al., 2013). In the absent of both E3 ligases, greater accumulation of polyubiquitinated proteins is observed due to nascent protein chains being translated regardless of misfolded. More evidence supporting this is the fact that *Sc*NOT4 is part of the CCR4-NOT complex which is primarily responsible for mRNA quality control and proteostasis (Chapat & Corbo, 2014; Collart & Panasenko, 2012). The impairment of this complex, such in the case of *Sc*NOT4 being absent, leads to the build-up of aberrant proteins as they can no longer be tagged for degradation. This may be also the case for *Atnot4abc* where *At*NOT4s function to prevent the accumulation of defective proteins during translation. Other well-characterised E3 ligases are also involved in protein quality control namely

DOA10 and HRD1 which further supports this hypothesis (Duttler et al., 2013; Etherington et al., 2023; Mehrtash & Hochstrasser, 2022; Schulz et al., 2017). DOA10 and HRD1 are both known to ubiquitinate defective proteins, particularly in relation to ER stress when membrane proteins are incorrectly folded. Removal of either of these E3 ligases also result in the accumulation of polyubiquitinated conjugates (Duttler et al., 2013).

It may seem rather counterintuitive that the removal of an E3 ligase, which are primarily responsible for ubiquitinating proteins, leads to an increase in polyubiquitinated proteins. Though, this paradoxical result can be explained if the broader role of *At*NOT4s in maintaining protein quality control and proteostasis is considered. Like their yeast counterpart, *At*NOT4s function more than just tagging proteins with ubiquitin for degradation. *At*NOT4s monitor the synthesis, folding and degradation of proteins closely in conjunction with ribosomes and the 26S proteasome. By coordinating with ribosome associated proteins and the CCR4-NOT complex, *At*NOT4s can ensure proper proteostasis. However, when the *At*NOT4s are non-functional, then these interactions between other important factors in maintaining proteostasis shifts. Nascent polypeptides that normally have sufficient time to fold correctly are now forced to rapidly fold due to the increase global translation rates (*see previous section)* which may lead to misfolding. The misfolded polypeptides are now in need of degradation therefore the demand of ubiquitination increases because of the cell attempt eliminate the faulty proteins to restore proteostasis. Without *At*NOT4s, this system is imperilled causing an overwhelmed and ineffective degradation system where the proteasome is unable to keep up with the excess load of defective proteins and ultimately leading to the aggregation of polyubiquitinated proteins. Besides the focus on protein quality control, the absence of *At*NOT4 could also be impairing mRNA quality control which result in the production of defective proteins in the first place as they are more prone to misfolding and subsequent ubiquitination. This mirrors the findings in yeast, where ∆*Sc*NOT4 mutants paradoxically increase in ubiquitinated nascent chains is due to impaired quality control rather than efficient degradation process.

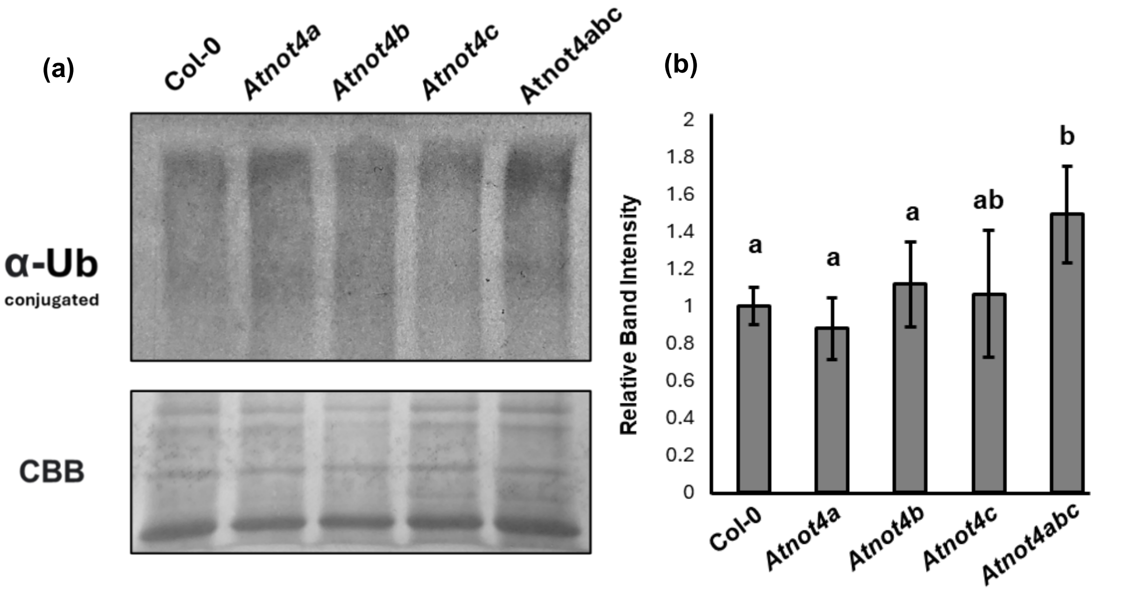

Figure 34 - Accumulation of Polyubiquitinated Conjugates in *Atnot4abc*. Western blot analysis of polyubiquitinated conjugates in wild-type and *Atnot4abc* mutant plants. **(a)** Western blot analysis of polyubiquitinated proteins using an anti-ubiquitin antibody, indicating a stronger signal in the *Atnot4abc* mutants compared to wild-type plants. **(b)** Bar chart shows quantification of bands detected by Western blot. Band intensities were measured using ImageJ, and processed following protocol by (Davarinejad, 2015). Different letters (a, b, ab) indicate statistically significant differences ($p < 0.01$) as determined by Kruskal-Wallis test. Data represents the mean ± standard error of three biological replicates.

4.4 *Atnot4abc* Reveals Altered UPR Gene Expression Under Tunicamycin-Induced Stress

There are many environmental stresses that can lead to the generation of misfolded protein within the endoplasmic reticulum (ER) (Howell, 2013; Chen et al., 2020). These factors can overwhelm the ER and increase to the point that exceeds the capacity for Endoplasmic Reticulum-associated degradation (ERAD), and thus provoking a cellular response known as the unfolded protein response (UPR). When terminally misfolded proteins are identified in the ER, they are retro translocated to the cytosol for degradation via the UPS. The overaccumulation of polyubiquitinated proteins in *Atnot4abc*, coupled with the heightened sensitivity to Tm (*to be discussed in the next section*), a potent inducer of ERAD, suggested that there might be an upregulation of the UPR in *Atnot4abc* mutants under both control and proteotoxic stress conditions. In yeast, many studies have been carried out on the ubiquitination of ERAD substrates and identified two key ER-localized E3 ligases: HMG-CoA Reductase Degradation 1 (ScHrd1) and Degradation of α2 10 (*Sc*Doa10)(Liu & Li, 2014). Mutations in components of the *Arabidopsis* HRD1 (*At*HRD1) complex, which disrupt the ERAD pathway, resulted in the enhancement of the Unfolded Protein Response (UPR) in response to protein misfolding stress. In some cases, these mutations can even lead to its constitutive activation (Hüttner et al., 2012; Lin et al., 2019; Shinjo et al., 2013). Given the fact that *Atnot4abc* display over accumulate polyubiquitinated proteins and have increased sensitivity to Tm, we therefore hypothesise that *Atnot4abc* has increased UPR.

qRT-PCR was performed to measure the expression of UPR marker genes under control and 5 µg/ml Tm-treated 12-day-old Col-0 and *Atnot4abc* seedlings (**Figure 35a-c**). The UPR marker genes that were analysed in this experiment were Binding Protein1/2 (*At*BiP1/2), Calnexin (*At*CNX1), and Basic Region/Leucine Zipper Motif 60 (*At*bZIP60); all of which are upregulated in response to ER stress (Howell, 2013; Hwang & Qi, 2018). *At*BiP1/2 are molecular chaperones known to assist in protein maturation and repair misfolded proteins (Herath et al., 2020). *At*CNX1 is a conserved ER chaperone protein that promotes folding of N-glycosylated proteins (Read &

Schröder, 2021), and AtbZIP60 is a luminal binding protein that binds to hydrophobic patches on malformed proteins (Moreno et al., 2012).

*At*BiP1/2 showed a significant increase in expression in response to Tm treatment across both wild-type (p-value < 0.01, Pair-wise Wilcoxon T-test) and *Atno4tabc* (p-value < 0.01, Pair-wise Wilcoxon T-test (**Figure 35a**). Specifically, the fold change in expression is approximately 3.9-fold in Col-0 (**Figure 35g**). In *Atnot4abc*, the expression levels are significantly higher (p-value < 0.05, Mann Whitney t-test) with a fold change increase of approximately 14-fold, indicating severe ER stress likely due to the inability to manage misfolded proteins effectively (**Figure 35g)**. Similarly, when analysing *AtbZIP60* expression, it also exhibits increased expression in response to Tm treatment (p-value < 0.05 & p-value < 0.01, Pair-wise Wilcoxon T-test; **Figure 35c**). The fold changes are approximately 2.4-fold in Col-0 compared to untreated conditions whereas in *Atnot4abc*, the expression is markedly higher, with a fold change increase of approximately 4.0-fold (p-value < 0.05, Mann-Whitney Test; **Figure 35i**). This heightened expression aligns with the increased stress response observed in *AtBiP1/2* expression. Lastly, the expression of *AtCNX1* follows a significant upregulation trend under Tm treatment (**Figure 35b**). The fold changes are approximately 2.3-fold in Col-0 compared to untreated conditions (**Figure 35h**) while in *Atnot4abc*, the expression levels are significantly elevated (p-value < 0.05, Mann-Whitney Test) , with a fold change increase of approximately 12.7-fold (**Figure 35h**). All three UPR maker genes showed a significant increase in expression (**Figure 35a-c**), confirming the treatment had worked.

When analysing the control conditions in *Atnot4abc*, the expression patterns of UPR markers show a more complex response. *At*BIP1/2 and *At*CNX1 are significantly downregulated (p-value < 0.05, Mann-Whitney Test, **Figure 35d/e**), suggesting that the absence of all three *At*NOT4 proteins might lead to an altered regulation of UPR marker expression under control conditions. In contrast, the expression of *At*bZIP60 was highly induced (p-value < 0.05, Mann-Whitney Test, **Figure 35f**) suggesting an attempt to counterbalance the applied stress although overall UPR capacity was generally low. These qRT-PCR results are in agreement with the results from our RNAseq data, under control conditions in which *At*BiP1 (log2FC = -0.45, p-value = 3.0410-9, Wald Test), *At*BiP2 (log2FC = -0.53, p-value = 3.39x10-12, Wald Test) and

*At*CNX1 (log2FC = -0.50, p-value = 4.4210-10, Wald Test) were all significantly down-regulated, whereas *At*bZIP60 was slightly upregulated (log2FC = 0.3, p-value = 0.0010135, Wald Test).

In the context of ER stress, when ERAD is triggered by protein misfolding elicitors like Tm, the absence of a functional co-translational quality control mechanism becomes more apparent. The UPS may not be able to handle the excess misfolded proteins being retro translocated from the ER in the absence of *At*NOT4s, as seen by *Atnot4abc's* increased sensitivity to Tm. The cell tries to deal with the excess of misfolded proteins by upregulating the UPR, but the response is insufficient and results in the observed hypersensitivity. The interconnectivity of these quality control systems also further supports the mixed expression profile observed for the UPR markers in *Atnot4abc*. The UPR marker genes are induced upon misfolding stress, though their expression under favourable conditions seems to be more variable with only some of these genes being downregulated. Perhaps, this indicates a predisposed state for *Atnot4abc* mutants in which they are already experiencing proteostatic stress even without additional ER stress. Therefore, when ERAD is further challenged, the lack of *At*NOT4s amplifies this stress, revealing the critical role these proteins play in maintaining cellular protein homeostasis.

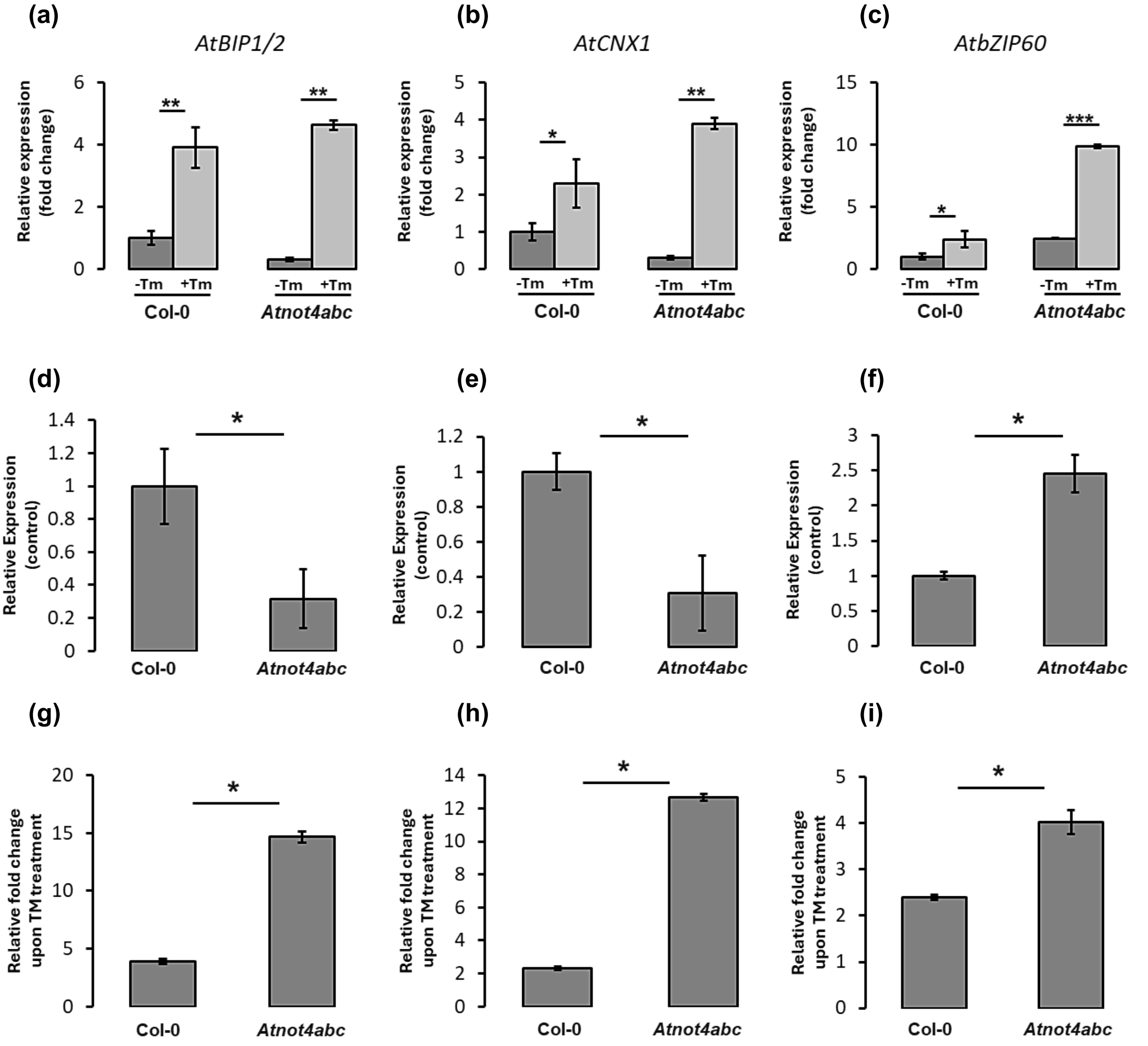

Figure 35 – Analysis of UPR genes upon Tm treatment via qPCR. (a-c) Expression levels of AtBiP1/2, AtbZIP60, and AtCNX1 in Col-0 (wild type), and triple mutant (*Atnot4abc*) under control (dark grey bars) and tunicamycin-treated conditions (light grey bars). Results are normalized to two housekeeping genes, with relative expression calculated against Col-0 in control conditions for each gene tested. Pair-wise Wilcoxon t-test was performed for statistical analyses (Asterisks indicate level of significance: *p < 0.05, **p < 0.01, ***p < 0.001). (**d-f**) Relative expression calculated against Col-0 in untreated *Atnot4abc*. Differences were determined to be statistically significant using Mann Whitney t-test (p-value < 0.05). **(g-i)** Relative fold change upon Tm treatment calculated against its own genotype. Differences were determined to be statistically significant using a Mann Whitney t-test. Error bars represent standard errors from two biological replicates, each consisting of 2-3 technical replicates.

4.5 Expression Levels of *AtNOT4* Genes Are Not Responsive to Protein Misfolding Stress

The hypersensitive response to Tm in the seedling growth assay (*see next section*) as well as the upregulation of UPR genes in response to Tm may indicate that *At*NOT4s are also activated during UPR induction. Similar approach to Section 4.5, qRT-PCT was performed to measure the expression of *AtNOT4* genes in 12-day-old wildtype seedlings treated with Tm and control conditions.

Despite the apparent critical role of *At*NOT4 proteins in co-translational quality control and the regulation of proteostasis, our data shows that the expression of *AtNOT4A*, *AtNOT4B*, and *AtNOT4C* remains largely unchanged following Tm treatment in wild-type plants (n.s., One-Way ANOVA; **Figure 36**). This lack of significant upregulation in response to Tm suggests that *AtNOT4* gene expression is not directly responsive to ER stress under the conditions tested, even though these genes are known to be involved in managing proteostasis.

In relation to our previous findings (*see Section 4.2 and 4.3*), this result demonstrates that the lack of *At*NOT4s might be hindering cellular capability to cope with misfolded proteins, which in turn renders cells more sensitive to Tm. However, no adaptive transcriptional response seems to counteract the induction of misfolded proteins in the wild-type background, where all three *AtNOT4* genes are fully functional. Therefore, it seems that *At*NOT4s may act independently of direct transcriptional regulation under ER stress to maintain co-translational quality control and proteostasis. It could be that the activity of *At*NOT4s is regulated through interaction of other components of the ERAD pathway. Nevertheless, the contrasting results of significant changes observed in UPR genes upon Tm-induced ER stress and absence of an upregulation in *AtNOT4* genes expression in Col-0 is intriguing yet requires further investigation. Perhaps the lack of *At*NOT4 induction can be partly explained by their proposed roles in co-translation quality control whereby a constitutive level of expression may be necessary to maintain baseline proteostasis, rather than an inducible stress response. This constitutive expression could be sufficient to manage routine protein synthesis and folding demands under normal conditions, while additional stress-induced pathways, such as the ERAD/UPR, are required to manage acute proteotoxic stress.

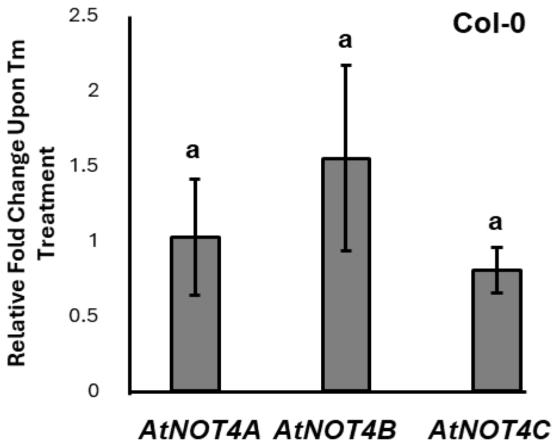

Figure 36 – Analysis of *AtNOT4* genes upon Tm treatment via qPCR. Relative fold change upon Tm treatment calculated against its own control treatment. No differences were determined to be statistically significant using a one-way ANOVA. Error bars represent standard errors from two biological replicates, each consisting of 2-3 technical replicates.

4.6 Hypersensitivity of *Atnot4abc* to protein misfolding elicitor Tunicamycin

Hypersensitivity to misfolding elicitors like azetidine-2-carboxylic acid (AZC) was observed in yeast lacking *Sc*NOT4 (Duttler et al., 2013). With paralleling functions to ∆ScNOT4 identified in *Atnot4abc* such as the increased global translation (**Figure 33**) and accumulation of polyubiquitinated proteins (**Figure 34**), it is possible that *Atnot4abc* will also experience an increase in sensitivity to protein misfolding elicitors. Therefore, it was hypothesised that *Atnot4abc* has reduced capacity to respond appropriately to proteotoxic stress due to compromised protein quality control and proteostasis.

Upon treatment with Tm at concentrations of 50, 75, and 100 ng/ml, *Atnot4abc* displayed extreme hypersensitivity compared to wild type (**Figure 37c;** $p < 0.001$, unpaired t-test). Even at the lowest Tm concentration (50 ng/ml), *Atnot4abc* seedlings showed almost complete growth inhibition, with severe whitening of the cotyledons (**Figure 37b**). Wild-type seedlings seemed to respond more in a dose-dependent manner, where the increase in Tm resulted in more severe responses. Shoot chlorosis and reduced growth was also observed in wild type, but not to the same extent as *Atnot4abc*. Even at the highest concentration (100 ng/ml), wild-type seedlings were not as severely affected as *Atno4tabc* at its lowest concentration exposure (50 ng/ml) (**Figure 37a**). Therefore, the hypersensitive response observed in *Atnot4abc* supports the proposed hypothesis and further emphasises the role that *At*NOT4 have in maintaining protein quality control and proteostasis.

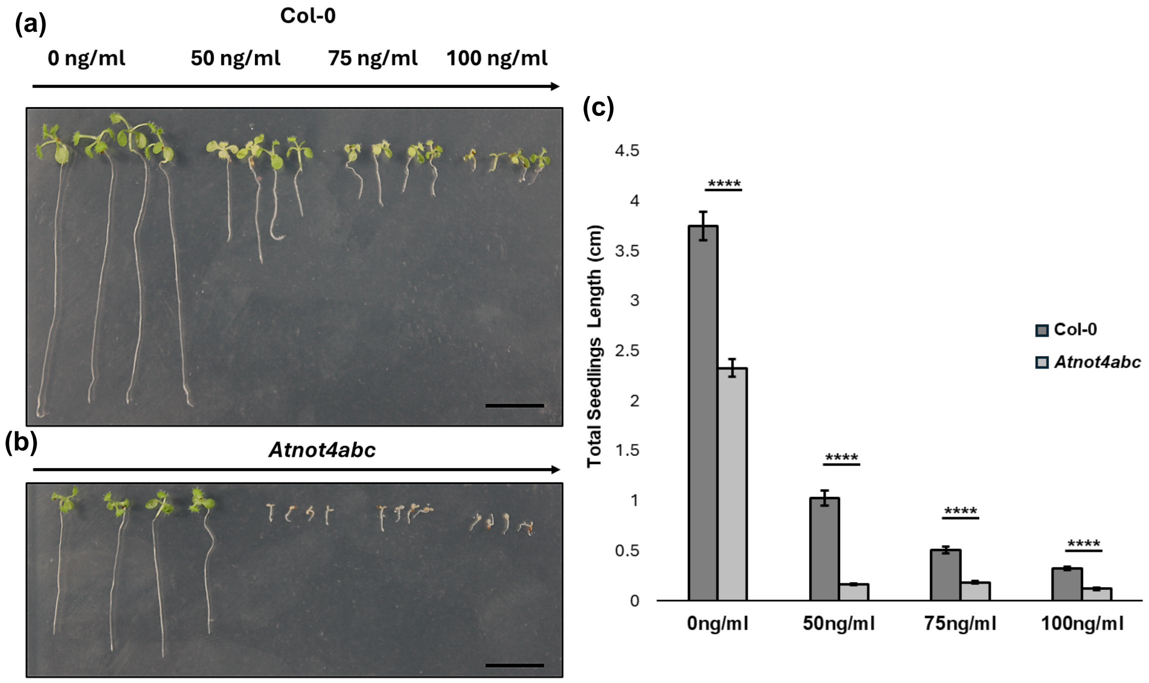

Figure 37 - Hypersensitivity of *Atnot4abc* Mutants to Tunicamycin Treatment. Representative Seedlings of the (**a**) wild-type and (**b**) *Atnot4abc* that had been grown under control conditions and in the presence of various concentrations of tunicamycin. Growth and development of both the wild-type and the mutant seedlings in control conditions are as expected (*Atnot4abc* displays growth phenotype). *Atnot4abc* shows severely impaired growth and development compared to wild-type seedlings upon tunicamycin treatment. Image is representative of 2 biological replicates of similar results. Scale bar represents 1 cm. (c) Bar chart displaying total seedling lengths with statistical significance (unpaired t-test, $p < 0.001$ of 2 biological replicates of 25)

4.7 Discussion

The objective of this chapter was set out to evaluate the role of *At*NOT4s in translation and co-translational quality control in relation to functional conservation with *Sc*NOT4 in yeast.

Global translation was measured by puromycin incorporation assay which showed increased rates in the absence of all three *At*NOT4s. These findings are in line with the RNA-seq data where a strong induction of genes involved in translation initiation and elongation, and ribosome biogenesis was detected. More precisely, we observed the upregulation of many key components of the translation machinery that included several subunits of the 40S and 60S ribosomal proteins, elongation factors, and translation initiation factors (*see Chapter 3, Section 3.4.2* ***Figure 29-31***). These findings illustrates *At*NOT4s role in the repression of genes related to translation, much like *Sc*NOT4 in yeast (Azzouz, Panasenko, Deluen, et al., 2009). The upregulated translation-related genes in *Atnot4abc* further suggests a role in modulating translation to maintain cellular homeostasis in order to prevent excessive protein synthesis that may lead to overwhelming the cell's quality control mechanisms.

The hypersensitivity of *Atnot4abc* to Tm underlines the involvement of *At*NOT4 proteins in managing protein quality control. In Col-0, the cellular machinery can effectively cope with this stress, as all quality control systems including the ones that the *At*NOT4s are involved in, are fully operational. Most importantly, hypersensitivity of *Atnot4abc* to Tm treatment proposes that cells are overloaded with aberrant proteins due to the disturbed balance between a stressed ERAD system and decreased translation fidelity. This hypersensitivity likely arises not from a direct defect in the ERAD pathway, but rather from the inability of the *Atnot4abc* mutant to manage the increased load of misfolded proteins effectively. Interestingly, single *Atnot4* mutants did not exhibit hypersensitivity to Tm (*Data not shown*), which would suggest a compensatory function among *At*NOT4 proteins. This genetic redundancy may provide resistance against protein misfolding and could thus reflect an evolutionary strategy of *Arabidopsis* toward flexibility in their surveillance and translation control.

The effect of other translational stresses should be explored for further investigation into the role of *At*NOT4s in co-translation quality control such as Dithiothreitol (DTT) and AZC. DTT would be useful moving forward as it also induces protein misfolding stress in the ER by disrupting disulfide bond formation (Konigsberg, 1972) and could complement the observations seen with Tm treatment. Additionally, AZC treatment would also be impactful in expanding insights of *At*NOT4s role in translation and co-translation quality control. AZC is a proline analogue which therefore can be incorporated into polypeptides in place of the amino acid proline. The structural difference from proline disrupts proper folding of the protein by interfering with the flexibility of the backbone, and thus induces activation of the proteostasis network (Biratsi et al., 2021). The use of AZC would also allow for a direct comparison between the results observed in *Sc*NOT4 in yeast and *At*NOT4s in *Arabidopsis*.

A Western blot analysis of *Atnot4abc* revealed a mild overaccumulation of polyubiquitinated conjugates. This is consistent with the previously described functions of *Sc*NOT4 in yeast promoting co-translational quality control and preventing the accumulation of polyubiquitinated translation arrest products in knockout mutants (Duttler et al., 2013; Halter et al., 2014). The study by Duttler et al. enriched specifically for nascent proteins (Duttler et al., 2013), thus a future experiment could involve including this enrichment step. This may lead to a more pronounced increase in polyubiquitinated conjugates in *Atnot4abc* vs Col-0. This further assessment into protein aggregation in *Atnot4* mutants will provide better understanding into how the loss of *At*NOT4 proteins impacts overall protein quality control. Furthermore, total ubiquitinated conjugates did not accumulate in the single *Atnot4* mutants which further supports the idea of genetic redundancy across the *At*NOT4 paralogs.

The observed accumulation of polyubiquitinated conjugates in *Atnot4abc* may also suggest ERAD stress. Similar to other E3 ligases involved in ERAD such as *Sc*HRD1 (Liu & Howell, 2016) and *Sc*DOA10 (Hüttner et al., 2012) in yeast, *At*NOT4 proteins might also play an important role in removing misfolded proteins that arise as a result of increased translational errors. In yeast, the *Sc*HRD1 complex represents an essential element of the ERAD pathway that mediates the ubiquitination and subsequent proteasomal degradation of misfolded proteins inside the ER. *Sc*DOA10 acts in a complementary fashion with *Sc*HRD1 to target misfolded membrane proteins for degradation in support of ER protein quality control (Mehrtash & Hochstrasser, 2022). It is therefore a possibility that *At*NOT4s may also act in relation to the activity of ERAD E3 ligases to maintain proteostasis under normal and stress conditions.

Functional redundancy across *At*DOA10s has been reported in which the turnover of *At*SQE1 is regulated by both *At*DOA10A and *At*DOA10B (Etherington et al., 2023). However, only *At*DOA10B was shown to be transcriptionally induced by AZC and Tm as well as directly interacting with ERAD-associated ubiquitin conjugase 32 (*At*UBC32). This highlights the shared yet paralog specific roles of the *At*DOA10s wherein *At*DOA10B plays a more prominent role in ERAD stress while *At*DOA10A seems to be more involved in constitutive ERAD processes (Etherington, 2022). Referring back to *At*NOT4s, several of the phenotypic observations were only possible when all three *At*NOT4s were absent. This includes the increase global translation rate, polyubiquitinated conjugates accumulation, hypersensitivity to Tm, and enhanced upregulation of UPR genes. Thus, this possible functional redundancy and specialization within the *At*NOT4 family, akin to *At*DOA10s, imply a coordinated effort ensure protein quality control and cellular homeostasis.

Despite increased sensitivity towards Tm and induction of the UPR markers in *Atnot4abc*, expression of *AtNOT4* genes themselves are not significantly changed in response to Tm treatment in wild-type plants. This suggests that *At*NOT4 proteins do not respond transcriptionally to ER stress, but rather their role in the maintenance of proteostasis might be constitutive. When the ER is further challenged by an external stressor like Tm, the absence of functional *At*NOT4 proteins likely leads to an unsustainable accumulation of misfolded proteins, triggering an exaggerated UPR that is insufficient to mitigate the proteotoxicity. These results highlight the importance of *At*NOT4s in stabilising against various forms of proteotoxic stress by maintaining a steady-state level of protein quality control, thereby preventing the cellular overload that leads to hypersensitivity under conditions that exacerbate misfolded protein accumulation.

In addition, the comparison of *Sc*NOT4s' role in co-translation quality control in yeast suggests functional conservation in *Arabidopsis*. However, the regulatory mechanisms differ as *Sc*NOT4 is more responsive at the transcriptional level, whereas

*At*NOT4s could maybe only act on protein-protein interaction and post-translational modification. Supporting this, the *AtNOT4* genes are not transcriptionally activated during tunicamycin-induced ER stress in wild-type seedlings. It could be that *At*NOT4s may function to maintain proteostasis without mechanisms that require transcriptional induction under stress conditions. Although the exact regulatory pathway of this process remains unknown, these findings certainly suggest an involvement of *At*NOT4 proteins in the plant stress response and quality control system. An area that requires further investigation is *At*NOT4s role in proteasome assembly and maturation. It was shown in yeast that *Sc*NOT4 readily associates with the components of the proteasome and contributes to its assembly and functional integrity (Panasenko & Collart, 2011). The hindered protein degradation as well as the aggregation of polyubiquitinated conjugates suggest potential impairment in proteasome activity and might reflect a broader role of *At*NOT4s.

With the putative role of *At*NOT4 proteins in co-translational quality control, potential interplay should also be considered with other major regulators of translation and cellular metabolism. Among them is the Target of Rapamycin (*At*TOR) kinase; a conserved protein orchestrating the coordination of protein synthesis with the cellular nutrient and energy status (*refer to Chapter 1, Section 1.6-1.7*). *At*TOR activity drives ribosome biogenesis, initiates translation, and modulates a series of additional cell growth and metabolic processes. The increased translation rates and ribosome biogenesis genes observed in *Atnot4abc* implies the possibility that the *At*NOT4s could modulate or be modulated by the *At*TOR signalling pathways. Given that *At*TOR represents an important node in the integration of environmental and cellular cues for the regulation of growth and metabolic pathways, changes in *At*TOR activity represents a probable explanation for the translation phenotype conferred by *Atnot4abc*. The next chapter will explore the how *At*TOR signalling is modulated by *At*NOT4s.

Chapter 5 – Functional Interplay Between *At*NOT4s and *At*TOR Signalling

5.1 Introduction

In *Arabidopsis*, *At*TOR is part of a complex network of signalling pathways that is able to perceive environmental and internal signals to regulate growth and development (**Figure 38**). Upstream signals such as nutrient abundance, hormonal presence, light conditions and energy availability can regulate plant growth and development through *At*TOR activity. A clear example of *At*TOR promoting growth is when sufficient energy and/or nutrients are available. This activates *At*TOR and in turn phosphorylates many downstream substrates, one of which being another kinase known S6 Kinase1/2 (*At*S6K1/2). Phosphorylated *At*S6K1/2 then targets ribosomal protein S6 A and B (*At*RPS6A or *At*RPS6B). This is one of many examples of a phosphorylation cascade that involves *At*TOR, however, this particular one is necessary for increasing the cell's capacity for translation and protein synthesis (*see Chapter 1, Section 1.7*). Thus, *At*TOR is able to trigger the production of several growth-related proteins. The cell cycle is also known to be modulated via *At*TOR. Specifically, e2F transcription factors are phosphor-targets of *At*TOR and are important factors known for their role in cell cycle progression. By aligning the metabolic needs to the environmental conditions, *At*TOR can drive the overall growth and development of the plant (Busche et al., 2021; Dong et al., 2022; Haq et al., 2022; Rabeh et al., 2024).

Recent publications have highlighted *At*TOR role in promoting several aspects of protein translation (Schepetilnikov & Ryabova, 2018). Specifically, *At*TOR is critical for the reinitiation of translation by promoting the production of ribosomal proteins and ensuring translation-related mRNA stability (*see Chapter 1, Section 1.7.1*). Several *At*TOR-responsive phosphoproteins involved in translation initiation and ribosome performance were identified through large-scale phosphoproteomics studies (Scarpin et al., 2020; Van Leene et al., 2019). In the same study, *At*NOT4A and *At*NOT4B were identified as a phosphotarget and direct interactor of *At*TORC, respectively (Van Leene et al., 2019). Therefore, it is possible that *At*NOT4s have a role in the dynamic signalling pathway of *At*TOR. Furthermore, this may suggest *At*NOT4s as regulators within this pathway to control translation and ribosome biogenesis due to the evidence of *At*NOT4s role in co-translational quality control. Specifically, the faster translation rates and upregulation of ribosome biogenesis and translation associated genes observed in *Atnot4abc* (*see Chapters 3.4.2 and 4.1*) certainly hints at a functional link between *At*NOT4s and *At*TOR signalling.

In this chapter, we investigate the functional interplay between *At*NOT4s and *At*TOR signalling. Firstly, *At*TOR signalling activity was analysed and considered alongside the confirmed phosphor-target and interaction of *At*NOT4s and *At*TORC (Van Leene et al., 2019). The use of TOR inhibitors and its effect on *Atnot4* mutants was also examined. This was further explored through *Atnot4abc* transcriptomic analysis upon *At*TOR inhibition. The main aim of this chapter is to provide mechanistic insights into the ways in which *At*NOT4 proteins influence protein translation by assessing their functional connection to *At*TOR.

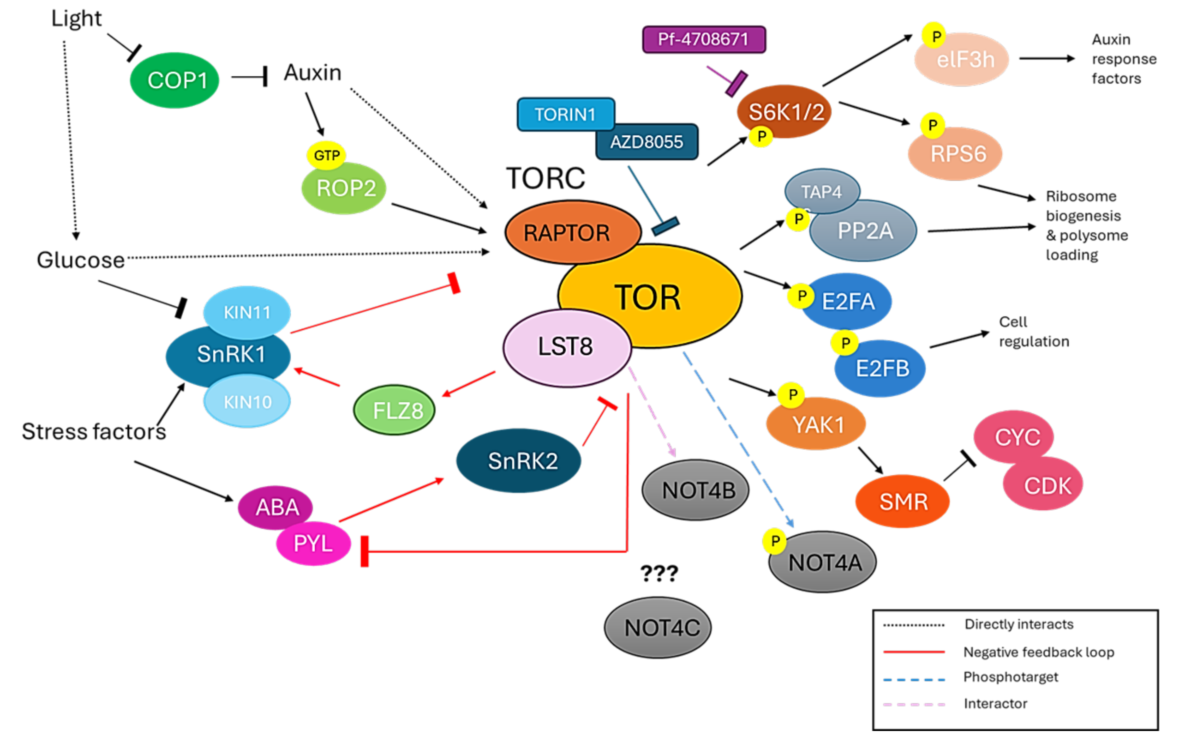

Figure 38 - Simplified adaptation of the TOR signalling pathway in plants. Simplified TOR signalling pathway in plants. Hormones, light, energy, and stress are all upstream signals perceived by TOR and affects a range of downstream processes such as auxin response factors, ribosome biogenesis and polysome loading and general cell regulation. *Adapted from McCready, Spencer, & Kim 2020*

5.2 *At*NOT4s contain multiple potential serine and threonine phosphorylation targets

PTM viewer (https://www.psb.ugent.be/webtools/ptm-viewer/) by the University of Ghent was used to analyse PTM profiles of *At*NOT4s. *At*NOT4A has a total of 15 PTM sites comprising of only 2 types of modifications, namely phosphorylation and O-fucosylation sites **(Figure 39)**. With a total of 13 phosphorylation sites, serine 888 (S888) phosphorylation is of high interest as this was confirmed to be the site phosphorylated by *At*TOR (Mergner et al., 2020; Van Leene et al., 2019; Wang et al., 2018). *At*NOT4B has less PTMs than *At*NOT4A, with a total 13 PTM sites consisting of 3 types of modifications: phosphorylation, O-fucosylation, and O-GlcNAcylation (**Figure 40**). Similar to *At*NOT4A, the phosphorylation events predominates the PTMs in *At*NOT4B. Lastly, AtNOT4C has the least PTMs present but consists of the most diverse modifications. *At*NOT4C has 4 phosphorylation sites, 1 O-fucosylation, 2 O-GlcNAcylation and notably a ubiquitination site (**Figure 41**). The fact that *At*NOT4C can be ubiquitinated is intriguing as it infers that *At*NOT4C could itself be further regulated through proteasomal pathways. The difference in PTM profiles of each *At*NOT4s may be indicative of specialised and differential roles in various cellular processes. A common feature in PTM profiles among *At*NOT4 paralogs is that none appear to be located within the RING and RRM domain. Even though they all share some common regulatory features, they have likely evolved to fulfil specialised regulatory functions in cellular processes. The *At*TOR-dependent phosphorylation of *At*NOT4A is indicative of a role perhaps in energy-dependent translation in response to nutrient availability, aligning with the well-established functions of *At*TOR signalling.

MSDHGEKTCPLCAEEMDLTDQQLKPCKCGYQICVWCWHHIVDMAEKDQIEGRCPACRTPYDKEKI
VGMTVNCDSLASEGNMERKKIQKSKSKSSEGRKQQLTSVRVIQRNLVYIVGLPLNLADEDLLQHKE
YFGQYGKVLKVSMSRTASGVIQQFPNNTCSVYITYGKEEEAVRCIQAVHGFILDGKPLKACFGTTKY
CHAWLRNVACVNPDCLYLHEVGSQDDSFTKDEIISAYTRVQQITGATNILQHHSGNMLPPPLDAYCS
DSSSAKPIIKVP**S**TNATSVPRY**S**PP**S**GSGSSSRSTALPAAASWGTHQSLAT**S**VTSNGSSDIQRSTSV
NGTLPFSAVVANAAHGPVSSNDILKRPSRKEESQIVMDKVKPSVLKPLQHNVVVSGSERITAPDRD
PTSNRL**SSS**VD**S**AYGGRDIDQPSAYSGRDIDKPSSTVSSFDAANEAVEDVPTVSNLLDGVACMRIT
MNCRDERPDITMAIGSQSDQGSIRQPGSEVSKLPDLEQCRIDSSINTDKKAISLEDRIPRTRPGWD
WISDLQSQMQGSSKLQVEDISTLDSQRPHPEEDIIHSRLLSNL**S**SS**S**LDTNHMASRSSLPCEVRGS
DRLHLPNGFGEKSM**S**SVEHSLFANEGRNKVNNAEDAILSNILSLDFDPWDESLTSPHNLAELLGEV
DQRSSTLKPSNFLKQHNNQSRFSFARYEESSNQAYDSENYSIYGQLSRDKPIQESAMSRDIYRNNL
GSVNGFASNFAGGLDNFAASPLFSSHKNPVSRPQVSAPPGFSAPNRLPPPGFSSHERVGLSSDTT
LGNRFLDSTSLRNAYQVPPPVGNSNGASDIDFVDPAILAVGRGMVNADLDMRSGFSSQLNSFENE
TGLHMLRQQ**S**LSSAQQVNGFHHDLRNL**S**PSLNDPYGFSSRLMDQTQGSSL**S**PFSQLPRQQPSAN
SILSNGHHWDKWNEGQSVNNIGMAELLRNERLGFNGSLYNNGYEEPKFRIP**S**PGDVYNRTYGI

Figure 39 - Representation of the *At*NOT4A protein sequence highlighting key post-translational modifications (PTMs). The RING-finger domain is shown in yellow, and the RRM domain in green. A total of 13 phosphorylation sites (blue) have been identified, with serine 888 (red) confirmed to be phosphorylated in a *At*TOR-dependent manner. Additionally, 2 O-fucosylation sites (pink) are annotated, contributing to the 15 total PTMs observed in *At*NOT4A. PTMs were identified using https://www.psb.ugent.be/webtools/ptm-viewer/index.php.

MSDYGEKTCPLCAEEMDLTDQQLKPCKCGYQICVWCWHHIMDMAEKDQSEGRCPACRTPYDK
EKIVGMTVDQERLASEGNMDRKKIQKSKPKSSDGRKPLTSVRVVQRNLVYIVGLPLNLADEDLLQ
RKEYFGQYGKVLKVSMSRTATGLIQQFPNNTCSVYITYGKEEEAIRCIQSVHGFILDGKALKACFG
TTKYCHAWLRNVACNNQDCLYLHEVGSQEDSFTKDEIISAHTRVQQITGATNTMQYRSGSMLPPP
LDAYTSDSSTGNPIAKVPSSTSVSAPKSSPPSGSSGKSTALPAAASWGARLTNQHSLATSALSNG
SLDNQRSTSENGTLATSTVVTKAANGPVSSSNSLQKAPLKEEIQSLAEKSKPGVLKPLQQKIVLDP
ESKRTTSPNRDPSSNQISCLVESSYNSRVIDKPSAVENSLEHTSEIAEDVFDVGKLSADVAWMGIT
TNSRDETPGVPVVIGTHCDLGSITQSDNDVQNLEQCRKQSPTNTYAEADISLNGIHGSRPEWDW
RSGLQSQIDVKEPLEVNDFSSFNNNRRGIAEAVSHSTSKFSSSISILDSNHLASRSFQNRETSCGM
DSKTGSSFEIGSDRLHLPNGFSEKAMSNMEHSLFANEGRSNIQNTEDDIISNILDFDPWDESLTSQ
HNFAKLLGQSDHRASTLESSNLLKQHNDQSRFSFARHEESNSQAYDNRSYSIYGQLSRDQPLQE
FGANRDMYQDKLGSQNGFASNYSGGYEQFATSPGLSSYKSPVARTQVSAPPGFSAPNRLPPPG
FSSHQRGDLSSDIASGTRLLDSANLLRNAYHVPPPSGNLNAAGDIEFIDPAILAVGRGRLHNGMET
ADFDLRSGFSSQLNSFDNDARLQLLAQRSLAAQQVNGFHDPRNVNNFSSSFSDPYGISSRPTDQ
TQGTGLSPFTQLPRQASANPLLSNGHWDNKWNEPQSGNNLGITQLLRNERMGFNDNVYSGFEE
PKFRRPGPGDPYNRTYGI

Figure 40 - Representation of the *At*NOT4B protein sequence highlighting key post-translational modifications (PTMs). The RING-finger domain is shown in yellow, and the RRM domain in green. A total of 10 phosphorylation sites (blue) have been identified, alongside 1 O-fucosylation site (pink) and 2 O-GlcNAcylation sites (orange). These modifications contribute to the 13 total PTMs observed in *At*NOT4B. PTMs were identified using https://www.psb.ugent.be/webtools/ptm-viewer/index.php.

MNEKGEKTCPLCTEEMDLTDQHLKPCKCGYQICVWCWHHIIEMAEKDKTEGRCPACRTRYDKEKI
VGMTVSCERLVAEFYIDRKKSQKAKPKPAEGRKDLTGVRVIQRNLVYVMSLPFDLADEDMFQRRE
YFGQYGKVVKVAMSRTAAGAVQQFPNNTCSVYITYSKEEEAIRCIRSVHGFILDGRNLKACFGTMK
YCHAWLRNMPCSNAECLYLHEIGAQEDSFSKDETISAHMRKMVQDITGWRDHYVRRSGSMLPPP
VDDYVDNESSTRIIPKVVLNNVHSAAKNSPPNDSNSHSVTLPAGAMWGMHSSVPNTPSSREPLR
DKSATVSSAVAINPTQISSRSDELRKPALEAAGGNVLKPQSLLDGKTDFPELSSSNKTQISNSRNVV
SASVDNSRAISEPSDCTDLPEHTSLSNGNKMINRRIQNGCSNVVSVDADSVVDGYHGITRSDKSHI
DHASIKPTLTEVSQDYLQRCVDEPREVQPLQKSGRTNANEVGVSREEVNRGTSLMSPLGTGHYL
EAEDDISLFYRQRLKDPEVLSCQSNGFLRPSNCMQPCSSQYKAEHDETRTVFGSSYSDSRGSNI
APISNGYTEMPLSEPNQLNGSLNHSILVPDKARDTQPIENCFVDSHESPSEIDDRIIANIMSLDLDEY
LTSPHNYANPFGESDEEARSLKLASSSKVEDNQSRFSFARQEEPKDQAFDSYNASNQMSRGNDF
YQNSSERQSPNMGMFGTYNGLSSCYRRGLDYVTESSTLPSSYKPTSVPRCPVSAPPGFSVPTPS
RPPPPGFSSNGRDHQMIDGFSGNSRFSDSIAYGNHYQQSLPIENVRDVQYMDPAILAVGQGFENA
SLDFRSNFQGNTNMYGSAAKLQQQQQAVMQNPLSMQNPLSSHQNCRFTDSLGMAPRFIDQS
QGNNLLTRNMALPNGHWNGLMSNEIQTRNRLQNERLVGSTNWIPGYNGTFRM

Figure 41 - Illustration of the *At*NOT4C protein sequence with highlighted post-translational modifications (PTMs). The RING-finger domain is indicated in yellow, and the RRM domain in green. A total of 4 phosphorylation sites (blue) have been identified, along with 1 O-fucosylation site (pink), 2 O-GlcNAcylation sites (orange), and 1 ubiquitination site (green). These modifications account for the 8 total PTMs observed in *At*NOT4C.

5.2.2 Conserved Motif Across *At*NOT4s Surrounding S888

S888 in *At*NOT4A is located within a conserved motif across all three *At*NOT4 paralogs. Upon closer examination, this is nested within a larger region containing multiple potential sites of serine and threonine phosphorylation (**Figure 42**) This may point to roles for *At*TOR phosphorylation across all three variants. Thus, this region could serve as an important 'regulatory hub' where several signalling inputs are transduced and converged. Even more interesting is how close these other phosphorylation sites are located to S888 further emphasising that this area might be related to modulation activity of *At*NOT4s in relation to *At*TOR signalling activity.

888

Conserved motif

***At*NOT4A**	**883**	DLRNLSPSLNDPYGFSSRLMDQTQGSSLSPF
***At*NOT4B**	**887**	NVNNFSSSFSDPYGISSRPTDQTQGTGLSPF
***At*NOT4C**	**886**	LSSHQNCRFTDSLGMAPRFIDQSQGNNLLTR

Figure 42 - Sequence alignment of the conserved region surrounding serine 888 (S888) in *At*NOT4A, *At*NOT4B, and *At*NOT4C. Confirmed *At*TOR-dependent phosphorylation site at S888 (indicated by the red arrow) in *At*NOT4A. The red boxes indicate potential serine (S) and threonine (T) phosphorylation sites across all three paralogs. Sequences were obtained from UniProt and aligned using Clustal Omega program (Multiple Sequence Alignment Tool). PTMs were obtained from Plant PTM Viewer 2.0 (https://psb.ugent.be/webtools/ptm-viewer/)

5.3 Chemical Inhibitors Reveal Functional Link Between *At*NOT4s and *At*TOR Signalling

As part of a collaborative project ("*Development of a high-throughput chemical screening assay to target chloroplast translation"*) with Syngenta, we observed a distinct response to the *m*TOR inhibitor rapamycin. *Atnot4a* exhibited a different level of sensitivity upon rapamycin treatment compared to wild-type. This led to a further investigation of the response of *Atnot4* mutants to inhibitors of *At*TOR signalling in more detail. Research on *Arabidopsis* has demonstrated that rapamycin treatment does not result in phenotypes typically associated with TOR inhibition (*see Chapter 1 Section 1.3*) (B. Menand et al., 2002). Therefore, we proceeded to use alternative TOR inhibitors for our experiments, namely AZD8055 (AZD) and TORIN1.

AZD8055 is an ATP-competitive inhibitor of the TOR kinase. The mode of action functions by directly binding to the ATP-binding site of TOR and subsequently inhibiting its kinase activity (Chresta et al., 2010). Upon AZD8055 treatment, it was shown to reduced cell proliferation and growth and therefore considered as a powerful tool when studying the TOR signalling pathway (Dong et al., 2015). TORIN1 is also an ATP-competitive inhibitor of the TOR kinase. The key difference between the two inhibitors is the target specificity and potency of the chemical. AZD8055 is considered to be more potent than TORIN1. Moreover, TORIN1 has the ability to effectively inhibit both *m*TORC1 and *m*TORC2 in mammals while AZD8055 seems to only be specific to *m*TORC1 (Amin et al., 2021). Both inhibitors have been used in several *Arabidopsis* studies which provided novel insights into TOR's regulation of growth and development, particularly under nutrient-scarce and light conditions (L. Li et al., 2015; Song et al., 2017).

<u>5.3.1 *At*NOT4s display differential sensitivity to TOR inhibitors (AZD8055 and TORIN1)</u>

5.3.1.1. *Atnot4a* and *Atnot4c* are sensitive to AZD8055

To test the response of wildtype and *Atnot4* mutants to AZD8055, a transient treatment was performed as continuous growth on ½ MS medium supplemented with AZD8055 was too potent, resulting in the death of all seedlings regardless of the concentration used (*data not shown*). Instead, seedlings were germinated and grown on ½ MS for 6 days, and then transferred to ½ MS supplemented with different concentrations of AZD8055 (0 μM, 1 μM, 2 μM, and 5 μM) and left for a further 6 days (**Figure 43a**). To account for the overall smaller seedlings observed in *Atnot4a* and its associated higher-order mutants (*see Chapter 3 Section 3.3*), the analysis was adjusted to consider the growth rate relative to the initial seedling size prior to transplanting onto ½ MS AZD plates. Under control conditions, all genotypes displayed comparable baseline growth levels. This indicates there are no inherent differences in growth rate among the genotypes when growth is assessed relative to their initial size.

At 1 μM AZD8055 treatment, all genotypes displayed growth inhibition with *Atnot4a* and *Atnot4c* mutants displaying a stronger response to *At*TOR inhibition as the seedlings were slightly smaller (**Figure 43b**). This difference becomes more pronounced at 2 μM AZD8055 as the seedlings show greater sensitivity (**Figure 43b**). Perhaps, the plants' ability to maintain sufficient *At*TOR signalling activity is compromised in the absence of *At*NOT4A or *At*NOT4C. Interestingly, the data indicates a non-additive effect as *Atnot4ac* did not have greater sensitivity to AZD8055 compared to the single mutants. Finally at 5 μM AZD8055 treatment, the level of sensitivity across all *Atnot4a* and *Atnot4c* was equal which indicates *At*TOR signalling activity is fully compromised and eliminating any potential differential sensitivity observed at lower concentrations.

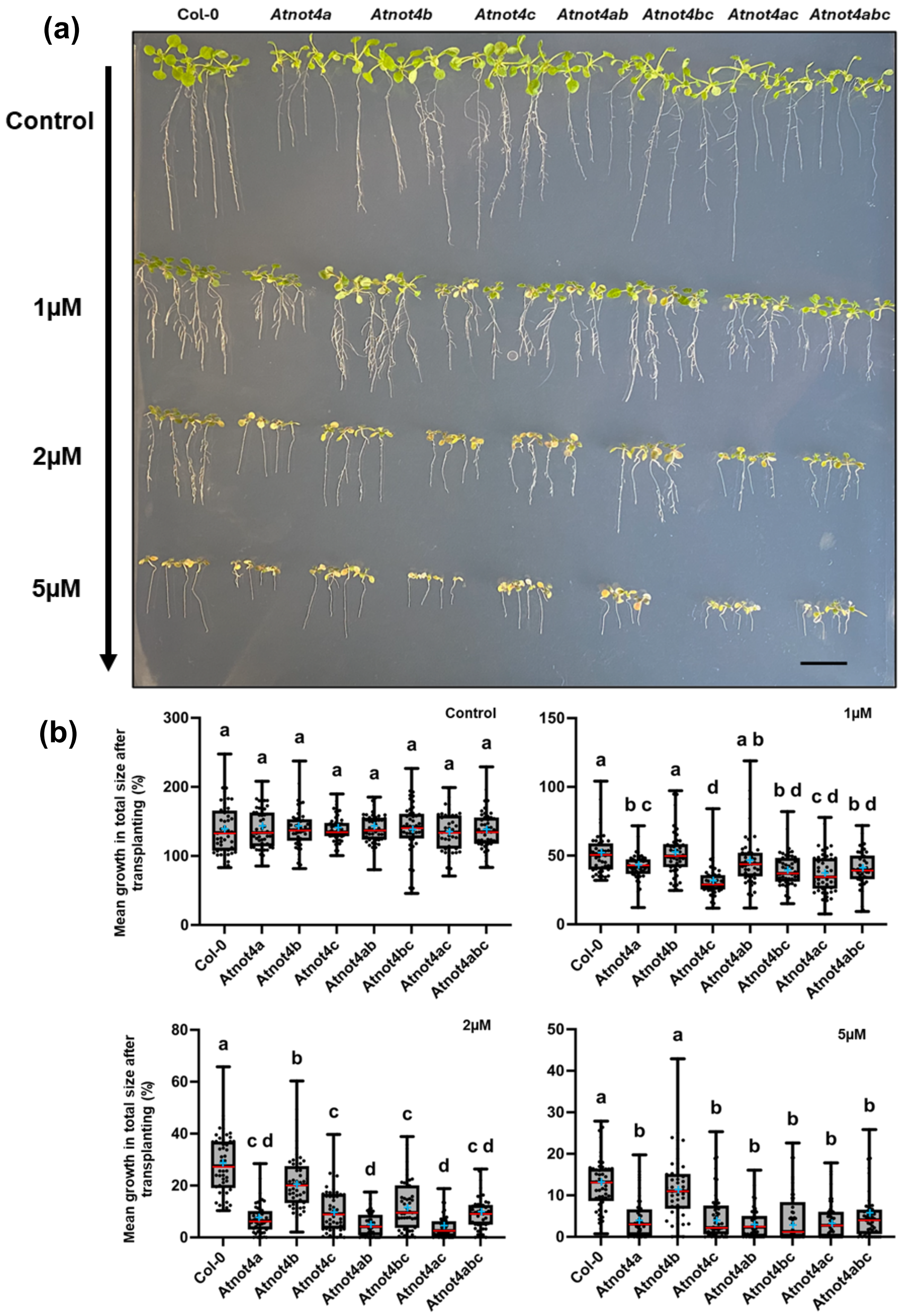

Figure 43 - Sensitivity of *Atnot4* Mutants to TOR Inhibitor AZD8055. (a) Representative images of transiently treated 12-day old *Arabidopsis* seedlings from different genotypes. Seedlings were grown first on ½ MS medium for 5 days and subsequently transplanted onto ½ MS treated plates for an additional 5 days. Image represents 3 biological replicates of similar results. Scale bar = 1 cm. **(b)** Quantification of seedling growth relative to the initial size before transplantation onto AZD plates. The data shows growth for each genotype at different AZD8055 concentrations, emphasizing the heightened sensitivity of *Atnot4a* and *Atnot4c* mutants. Box and whiskers plots show max and min, 25–75th percentiles (box), median (red line) and mean (blue 'x') of three biological replicates, each consisting of ~12 seedlings. Different letters indicate differences in ANOVA tests (Brown-Forsythe test, p-value < 0.05).

5.3.1.2 *Atnot4a* and *Atnot4c* are also sensitive to TORIN1

The transient treatment assay was repeated using TORIN1 to ensure the observed phenotype was indeed due to *At*TOR inhibition and not an off-target effect. Due to the timeline of generating the higher-order mutants, only single mutants were included in this particular analysis. Since the *Atnot4a* and *Atnot4c* single mutants showed clear phenotypes on AZD8055 this was still considered appropriate. Relative growth rates of *Atnot4* mutants were compared to wild type in response to varying concentrations of TORIN1. TORIN1 is less potent than AZD8055, therefore higher concentrations had to be used. These concentrations include 10μM, 15 μM, and 20 μM in order to exhibit were differential effects on growth. Seedlings were initially grown on ½ MS medium for 6 days before being transplanted onto ½ MS plates containing TORIN1 at the specified concentrations for another 6 days. Indeed, pronounced sensitivity to TORIN1 at all concentrations was observed in *Atnot4a* and *Atnot4c* when compared to Col-0 and *Atnot4b* (**Figure 44b**). This aligns with the AZD8500 transient treatment results, confirming that the sensitivity to *At*TOR inhibition is specific to *Atnot4a* and *Atnot4c*.

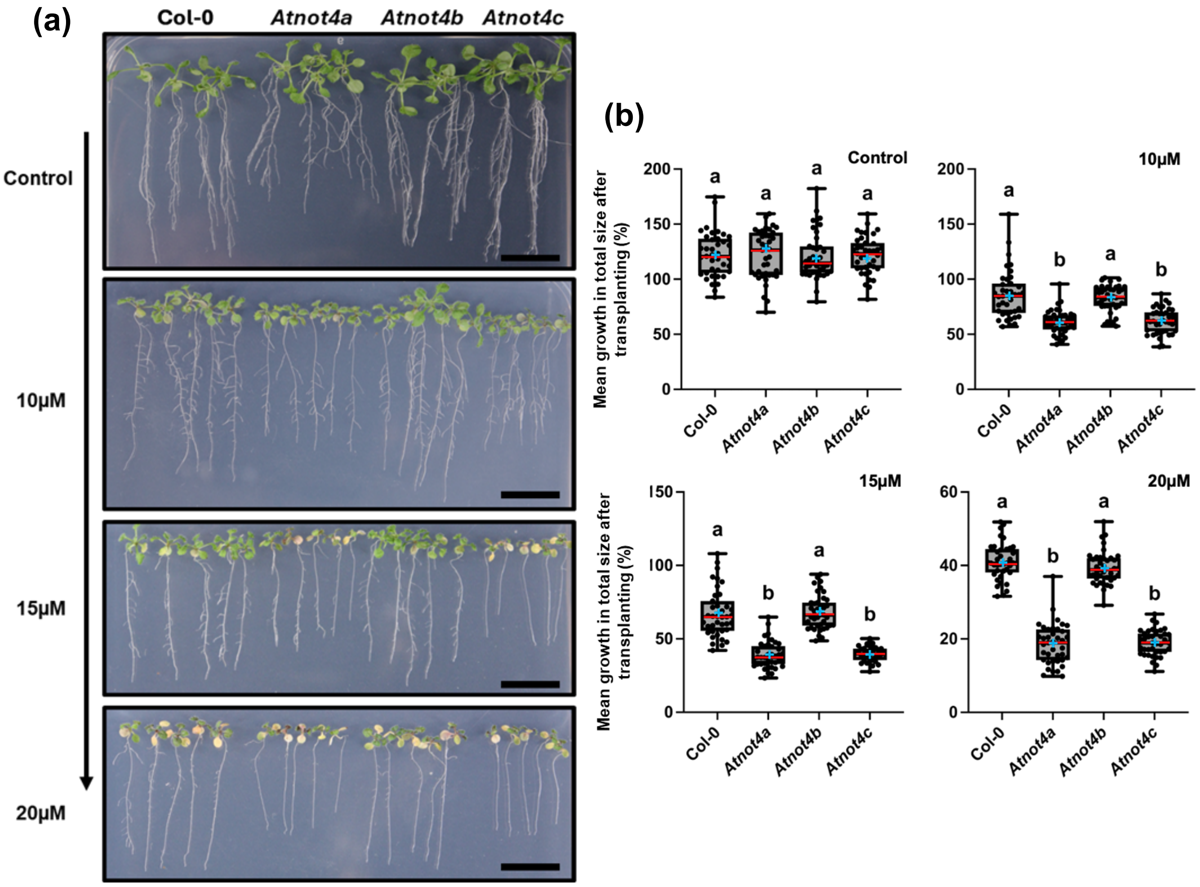

Figure 44 - Sensitivity of *At*not4 Mutants to TOR Inhibitor TORIN1. (a) Representative images of transiently treated 12-day old *Arabidopsis* seedlings from different genotypes. Seedlings were grown first on ½ MS medium for 6 days and subsequently transplanted onto ½ MS treated plates for an additional 6 days. Image represents 3 biological replicates of similar results. Scale bar = 1 cm. **(b)** Quantification of seedling growth relative to the initial size before transplantation onto TORIN1 plates. The data shows growth for each genotype at different TORIN1 concentrations, emphasizing the heightened sensitivity of *Atnot4a* and *Atnot4b*. Box and whiskers plots show max and min, 25–75th percentiles (box), median (red line) and mean (blue 'x') of three biological replicates, each consisting of ~13 seedlings. Different letters indicate differences in ANOVA tests (Brown-Forsythe test, p-value < 0.05).

<u>5.3.2 *Atnot4b* shows hypersensitivity to the S6K1/2 inhibitor Pf4708761</u>

To broaden our understanding and further investigate the potential link to *At*TOR signalling, an alternative inhibitor of the TOR signalling pathway known as Pf4708761 (Pearce et al., 2010) that targets S6K1/2 for inhibition **(see Figure 38**). Due to time constraints, this assay was only conducted on single mutants with just one biological replicate. Unlike the transient treatment described in *Sections 4.3.1.1 and 4.3.1.2*, seeds were directly sown on plates containing the inhibitor, resulting in a continuous exposure. Differential sensitivities in *Atnot4* single mutants was observed upon *At*S6K1/2 inhibition (**Figure 45 a/b**). Interestingly (and in contrast to the assays conducted with AZD8500 and TORIN1), it was only *Atnot4b* that showed a higher degree of sensitivity to *At*S6K1/2 inhibition, whilst *Atnot4a* and *Atnot4c* appeared to be less sensitive. Although the assay requires further biological repeats, the results are promising. Speculatively, *Atnot4b*'s sensitivity to the S6K1/2 kinase inhibitor Pf4708761 suggests that *At*NOT4B might be directly involved in pathways specifically linked to the *At*S6K1/2 branch of *At*TOR signalling. This perhaps aligns with *At*NOT4B being a direct interactor with *At*LST8-1 (Van Leene et al., 2019); a component essential for *At*TOR complex assembly and function.

*At*TOR activity can be measured through the phosphorylation status of *At*RPS6A as this is a well-established downstream substrate of *At*TOR-activated *At*S6K (*to be further described in Section 5.4*). In this regard, *Atnot4b* had lower *At*TOR signalling activity compared to the other single mutants *Atnot4a* and *Atnot4c* (*to be shown in the next section*). *At*NOT4Bs interaction with *At*LST8-1 may be necessary for the stability and assembly of *At*TORC in relation to *At*TOR-*At*S6K1-AtRPS6A signalling cascade. Furthermore, the absence of *At*NOT4B causes inefficient phosphorylation of *At*S6K1/2, ultimately leading to diminished capabilities of *At*TORC to fully engage with its substrates.

Despite their hypersensitivity to direct *At*TOR inhibition (**Figures 43 and 44**), *Atnot4a* and *Atnot4c* mutants were relatively insensitive to Pf4708761 as compared to *Atnot4b* (**Figure 45**). This suggests that *At*NOT4A and *At*NOT4C might be involved in broader *At*TOR functions extending beyond the *At*S6K1/2 pathway. Their sensitivity to TOR inhibitors could therefore indicate a disruption in these fundamental processes, independent of *At*S6K1/2 but still under *At*TOR's control. Conclusively, the differential responses of the *Atnot4* mutants to the *At*TOR inhibitors AZD8500 and TORIN1, and to the *At*S6K1/2 inhibitor Pf4708761 suggest that all three *At*NOT4s likely fulfil functions associated with *At*TOR signalling. Though, they also possess distinct subspecialisations within the pathway. *At*NOT4A and *At*NOT4C might be directly associated more with the general regulatory activities of *At*TOR and hence affect a broader array of *At*TOR-dependent processes. In contrast, *At*NOT4B appears more narrowly targeted toward processes dependent on AtS6K1/2, reflecting its interaction with *At*LST8-1.

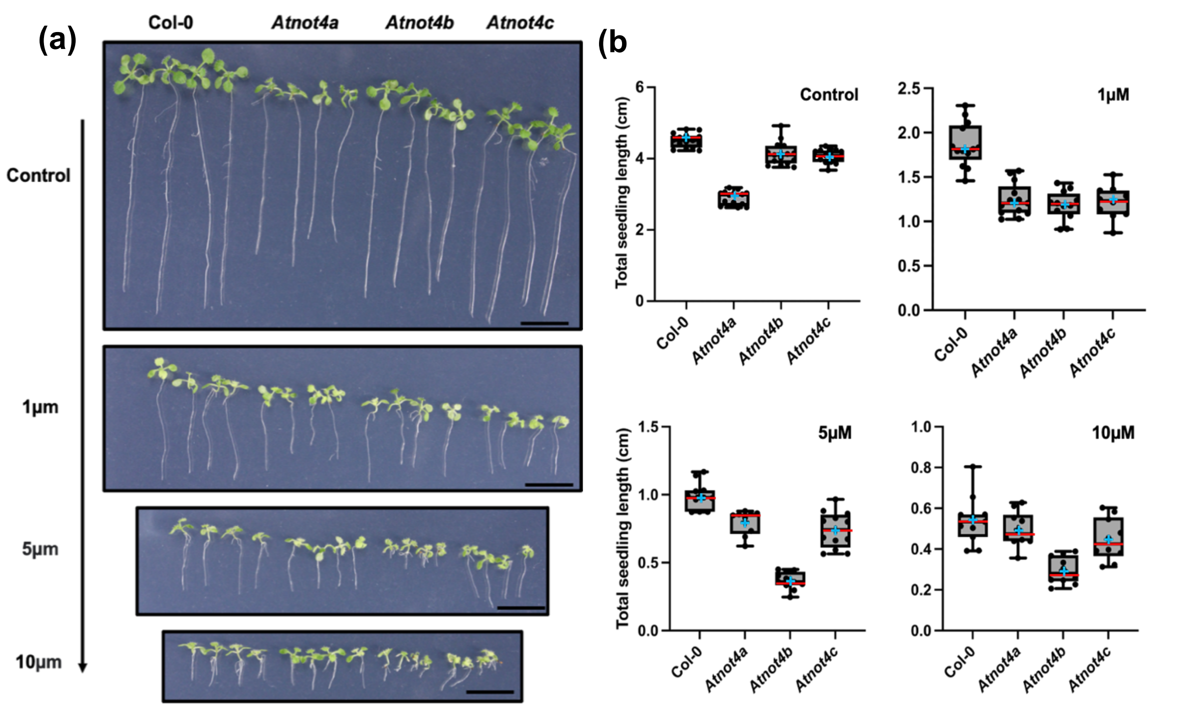

Figure 45 – S6K inhibitor direct treatment on Col-0 and *At*NOT4 single mutants. (**a**) Representative images of Col-0 (wild type), *Atnot4a*, *Atnot4b*, and *Atnot4c* grown for 10 days under normal conditions and with S6K inhibitor treatment (Pf4708761) at 1, 5, and 10μM concentration. (**b**) Quantification of seedling size (measured as total seedling length) in response to varying concentrations of Pf4708761. Box and whiskers plots show max and min, 25–75th percentiles (box), median (red line) and mean (blue ‘x’). No statistical analyses were conducted due to the limited sample size and the use of a single biological replicate. Scale bar = 1 cm.

5.4 Comparative analysis of *At*TOR activity in *At*NOT4s

A molecular assessment of *At*TOR activity was conducted to further explore the differential sensitivities of *Atnot4* mutants to *At*TOR inhibition. *m*TOR can regulate translation in animals by phosphorylating mammalian S6 kinase (*m*S6K), which in turn targets *m*RPS6 for phosphorylation. *m*RPS6 is known to have a role in facilitating cap-dependent translation (Holz et al., 2005; Magnuson et al., 2012; Schepetilnikov et al., 2013). There are two homologs of *At*RPS6 (*At*RPS6A and *At*RPS6B) present in *Arabidopsis* (Chen et al., 2018; Creff et al., 2010; Obomighie et al., 2021). Since *At*TOR activity in plants has been widely monitored by the phosphorylation status of *At*RPS6A, we concentrated on this protein for our investigation. Furthermore, the phosphorylation status of *At*RPS6A serves as a reliable readout of *At*TOR activity because *At*S6K1/2s are the only known kinases to phosphorylate *At*RPS6A/B in plants (Dinkova et al., 2007; Reyes de la Cruz et al., 2004). In maize, the increase in phosphorylated *At*RPSA/B resulted in an increase in overall growth as well as translational activity (Dinkova et al., 2007). As mentioned in *Section 1.7.5*, *At*RPS6A is involved in photomorphogenesis (Chen et al., 2018; Schepetilnikov et al., 2017; Schepetilnikov & Ryabova, 2018) and is stimulated upon exposure to light. Therefore, we opted to use light exposure to validate the performance of the antibodies, ensuring they function as expected. In the presence of light, *At*TOR becomes more active which leads to the increase phosphorylation of *At*RPS6A/B. In contrast, *At*RPS6A/B phosphorylation is either lacking or highly reduced in the absence of light (**Appendix 4**).

We therefore hypothesised that *Atnot4* mutants may have differential *At*TOR signalling activity based on the sensitivity of *Atnot4a* and *Atnot4c* to AZD8055 and TORIN1, their increased translation rates (as shown by puromycin incorporation assays *see Section 4.2*), and the GO term enrichment of upregulated DEGs associated with ribosome biogenesis and translation. Thus, novel insights on how *At*NOT4s affect *At*TOR signalling and its subsequent consequences on translation can be made by comparing *Atnot4* mutants to wild-type and measuring the ratio of phosphorylated to non-phosphorylated *At*RPS6A.

<u>5.4.1. *At*TOR activity is differentially affected in *Atnot4* mutants</u>

Using commercially available antibodies for both total and phosphorylated *At*RPS6A (*see Chapter 2 Methods, Section 2.3*), Western blot analysis was used to measure the ratio of phosphorylated ribosomal protein S6A (P-*At*RPS6A) to total *At*RPS6A in wild type and *Atnot4* mutant lines (**Figure 46a**). Image J was used to quantify the relative band intensities across multiple replicates (**Figure 46b**). A non-parametric test similar to One-way ANOVA known as the Kruskal-Wallis test was used to account for variations in biological replicates (Ostertagova et al., 2014). The results showed a statistically significant difference among the genotypes ($p < 0.001$, Kruskal-Wallis). Significantly higher P-*At*RPS6A/Total *At*RPS6A ratios was observed in *Atnot4a* and *Atnot4c* compared to wild-type (**Figure 46b**). The higher ratio indicates increased basal *At*TOR activity in these mutants. In contrast, the ratio of P-*At*RPS6/Total *At*RPS6 in *Atnot4b* was similar to Col-0, indicating no difference in *At*TOR activity (**Figure 46b**). This corroborates with the earlier observation where *Atnot4b* lacks the direct *At*TOR inhibitor hypersensitivity (**Figures 43 and 44**) as seen in *Atnot4a* and *Atnot4c*.

Interestingly, *At*NOT4C was not identified as a target or interactor of *At*TORC in the study by Van Leene et al. (2019). However, the increased *At*TOR activity observed in *Atnot4c* (**Figure 46b**), coupled with the heightened sensitivity of to *At*TOR inhibition (**Figures 43 and 44**), does indicate an important role for this paralog in *At*TOR signalling. *At*NOT4C may be part of other signalling pathways which likely intersect with *At*TOR signalling. Additionally, coverage and sensitivity issues related to the phosphorproteomic study by Van Leene et al. (2019) could have overlooked possible *At*NOT4C interactions within the dynamic *At*TOR signalling landscape. The increase in *At*TOR signalling activity in *Atnot4a* and *Atnot4c* mutants correlates with their heightened sensitivity to *At*TOR inhibitors. Though, this may be somewhat counter-intuitive as one might expect more *At*TOR activity (compared to wild-type) would lead to greater resistance to *At*TOR inhibition. However, the faster rates of inhibition upon AZD8055 treatment (*to be discussed in Section 5.4.3*) highlights the correlation between increased sensitivity to AZD8055 further. This sensitivity suggests that these *At*NOT4 paralogs are modulators of *At*TOR signalling.

The increase in global translation rates as well as the upregulation of translation and ribosome biogenesis genes seen in *Atnot4abc* vs Col-0 (*see Chapter 4, Section 4.2*) could be explained by the heightened *At*TOR activity.

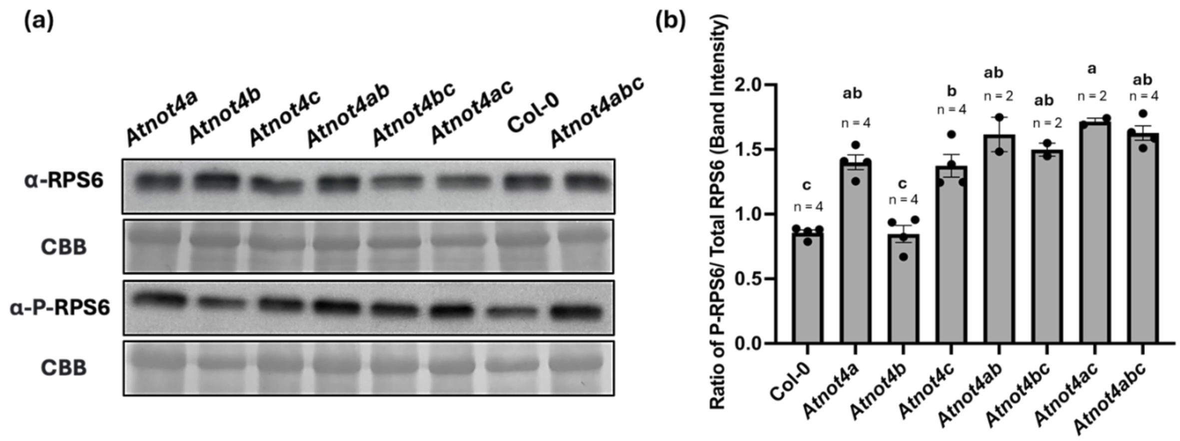

Figure 46 – Steady state levels of Total *At*RPS6 and Phosphorylated *At*RPS6 (P-*At*RPS6) in *At*NOT4 mutants. (a) Representative Western blot probing for anti-RPS6 and anti-P-RPS6 for all *At*NOT4 mutants. CBB, Coomassie Brilliant Blue loading control **(b)** Bar graph showing the average band intensity ratio between P-RPS6/Total RPS6 in all *At*NOT4 mutants and Col-0 calculated from multiple independent biological repeats of Western blots conducted as in (**a**). Statistical significance was determined by Kruskal-Wallis test (p-value < 0.0001, f-value = 49.60) and significant differences are indicated by letters. Exact number of biological replicates (n) is shown in above each bar. *Please note the different order of genotypes in (**a**) vs (**b**).*

5.4.2 No Increase in *At*TOR Protein Abundance Across *Atnot4* Mutants and Wild Type

Transcriptomic analysis of the *At*TORC-AtS6K-*At*RPS6 pathway was conducted to follow-up on the findings of the previous section. Indeed, there was no significant difference in the expression levels *AtTOR*, *AtS6K1/2*, and *AtRPS6A/B* in *Atnot4abc* relative to Col-0 (**Figure 47**). Collectively, these findings imply that the observed phenotypic differences in *At*TOR signalling in *Atnot4* mutants are not due to changes in the transcription or translation of *At*TOR components, but rather due to post-translational modifications that likely also change the interaction dynamics. This shows the complexity of *At*TOR regulation, where alterations in signalling can occur independently of gene expression changes, emphasizing the importance of post-translational mechanisms in regulating *At*TOR activity.

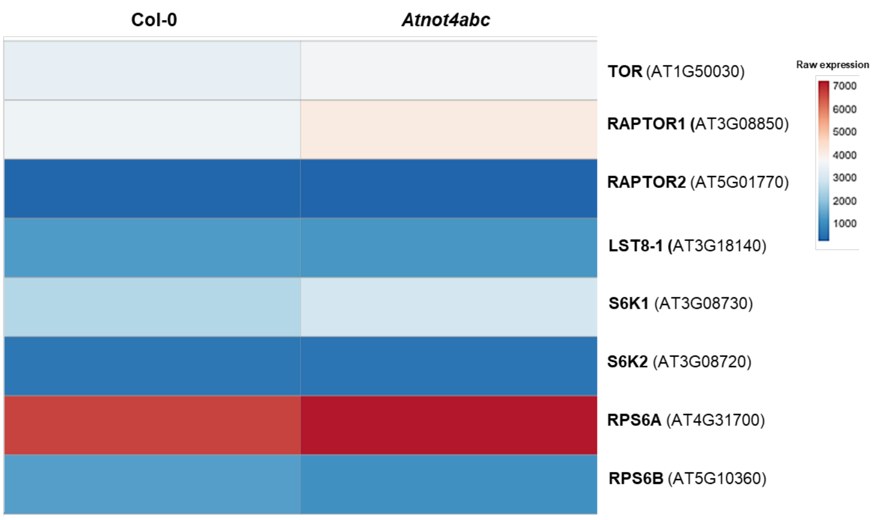

Figure 47 - Heatmap of Mean Expression Levels in Col-0 and *Atnot4abc*. Heatmap of the relative raw mean expression levels of the *At*TORC-*At*S6K-*At*RPS6 related genes in Col-0 (wild type) and *Atnot4abc* (ns, Wald test). Expression intensities are presented according to a colour scale that ranges from light blue (1000 units) to dark red (7000 units).

Increased *At*TOR activity in *Atnot4a* and *Atnot4c* mutants may be due to an increase of *At*TOR proteins. Western blotting analysis was done using a commercially available *At*TOR antibody to quantify total *At*TOR proteins in the *Atnot4* single mutants relative to wildtype. Interestingly, there was no increase in *At*TOR protein abundance across *Atnot4* single mutants when compared to wild-type (**Figure 48**). Therefore, the heightened *At*TOR signalling activity is not due to an increase of *At*TOR proteins. Perhaps, changes in the regulatory environment that *At*TOR experiences when *At*NOT4A and *At*NOT4C are absent enhances its signalling activity. As a direct *At*TOR phosphotarget, *At*NOT4A might paradoxically lead to an increase in *At*TOR activity as a compensatory response by the cell. This may be the cells attempt to phosphorylate the absent *At*NOT4A proteins in order to activate them, and therefore unintentionally increasing *At*TOR activity in the process. Therefore, the observed increase in *At*TOR signalling activity in *Atnot4a* could be a direct consequence of abolished AtNOT4A-mediated processes.

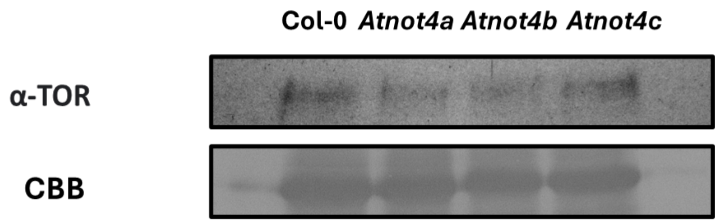

Figure 48 - Western Blot Analysis of *At*TOR Protein Levels in *At*NOT4 single mutants and wild-type. Western blot analysis was performed to determine *At*TOR protein levels in *Atnot4a*, *Atnot4b*, *Atnot4c*, and Col-0 using an α-TOR antibody. The upper panel displays the detected *At*TOR protein, while the lower panel shows the corresponding loading control to ensure equal protein loading across samples (100ug loaded). No increases in *At*TOR steady state levels were observed in the *Atnot4* mutants vs wild type. Western blot was performed twice with similar results.

5.4.3 Rapid Dephosphorylation of *At*RPS6A in *At*NOT4 Mutants in Response to *At*TOR Inhibition

A further investigation was done into the molecular effects of AZD8055 on *At*TOR activity in *Atnot4* mutants. Similar to the approach in *Section 5.4.1*, Western blot analysis was used to measure the ratio of phosphorylated ribosomal protein S6A (P-*At*RPS6A) to total *At*RPS6A in wild type and *Atnot4* mutants following a time course treatment of 1µM with the TOR inhibitor AZD8055. Both total *At*RPS6A and P-*At*RPS6A were assessed at 0, 2, and 4 hours post-AZD8055 treatment across different *Atnot4* mutants. The way AZD8055 affects the phosphorylation of *At*RPS6A is by disrupting the *At*TOR-*At*S6K-*At*RPS6 signalling cascade (*refer to Chapter 1, Section 1.7.3 **Figure 7***). Wild-type had a gradual reduction in P-*At*RPS6 levels, consistent with the expected inhibition of *At*TOR activity over time (**Figure 49a-f**). Across all *Atnot4* single and higher order mutants, faster dephosphorylation of *At*RPS6*A* was observed. A closer examination in the single mutants revealed a similar trend in response (**Figure 49a-i**). A significant decrease in P-*At*RPS6A is observed immediately by 2 hours when compared to Col-0 with a further decline by 4 hours. This confirms the hypersensitivity of *Atnot4a* and *Atnot4c* to TOR inhibition, aligning with the phenotypic sensitivity to AZD8055 (*see Section 5.3*).

Interestingly, *Atnot4b* also shows a rapid dephosphorylation of *At*RPS6A upon AZD8055 treatment despite having equivalent basal *At*TOR activity to wildtype as well as no obvious stunt in growth was observed in the AZD8055 seedling transient treatment assay. The consistency between *Atnot4a* and *Atnot4c* implies that these two paralogs may have somewhat overlapping functions in the context of *At*TOR signalling dynamics. Although all three E3 ligases show similar rates of *At*RPS6A dephosphorylation, this alone may not be enough to dictate the phenotypic response observed in *Atnot4a* and *At*not4c when treated with *At*TOR inhibitors. The phenotypic differences observed across *Atnot4* single mutants may stem from temporal or specific factors that are simply not captured by *At*RPS6A dephosphorylation alone.

Atnot4ab shows a pattern of P-*At*RPS6A reduction similar to the single *Atnot4a* and *Atnot4c* (**Figure 50 a/d/g**) which suggest that the combined loss of *Atnot4a* and *Atnot4b* does not additively affect *At*TOR activity but rather reflects the predominant role of *Atnot4a*. The *Atnot4bc* mutant, while showing a faster dephosphorylation than Col-0 (**Figure 50 b/e/h**), does not appear to deviate significantly from the trends observed in the single mutants. In line with the previous results, this might indicate that *Atnot4b* plays a more subtle or specific role in this signalling cascade process. *Atnot4ac* also follows the trend, where P-*At*RPS6A levels drop rapidly upon by 2- and 4-hours post-treatment (**Figure 50 c/f/i**). The lack of an even greater reduction in the *Atnot4ac* mutant compared to the single mutants could also suggest that there is a threshold effect, beyond which additional *At*NOT4s disruption cannot further intensify the response. Lastly, *Atnot4abc* shows a similar effect to the *Atnot4* single and double mutants (**Figure 51a**), a steep decline in *At*RPS6A dephosphorylation, particularly between the 0 to 2-hour mark, followed by a further reduction relative to WT by 4 hours (**Figure 51b/c**).

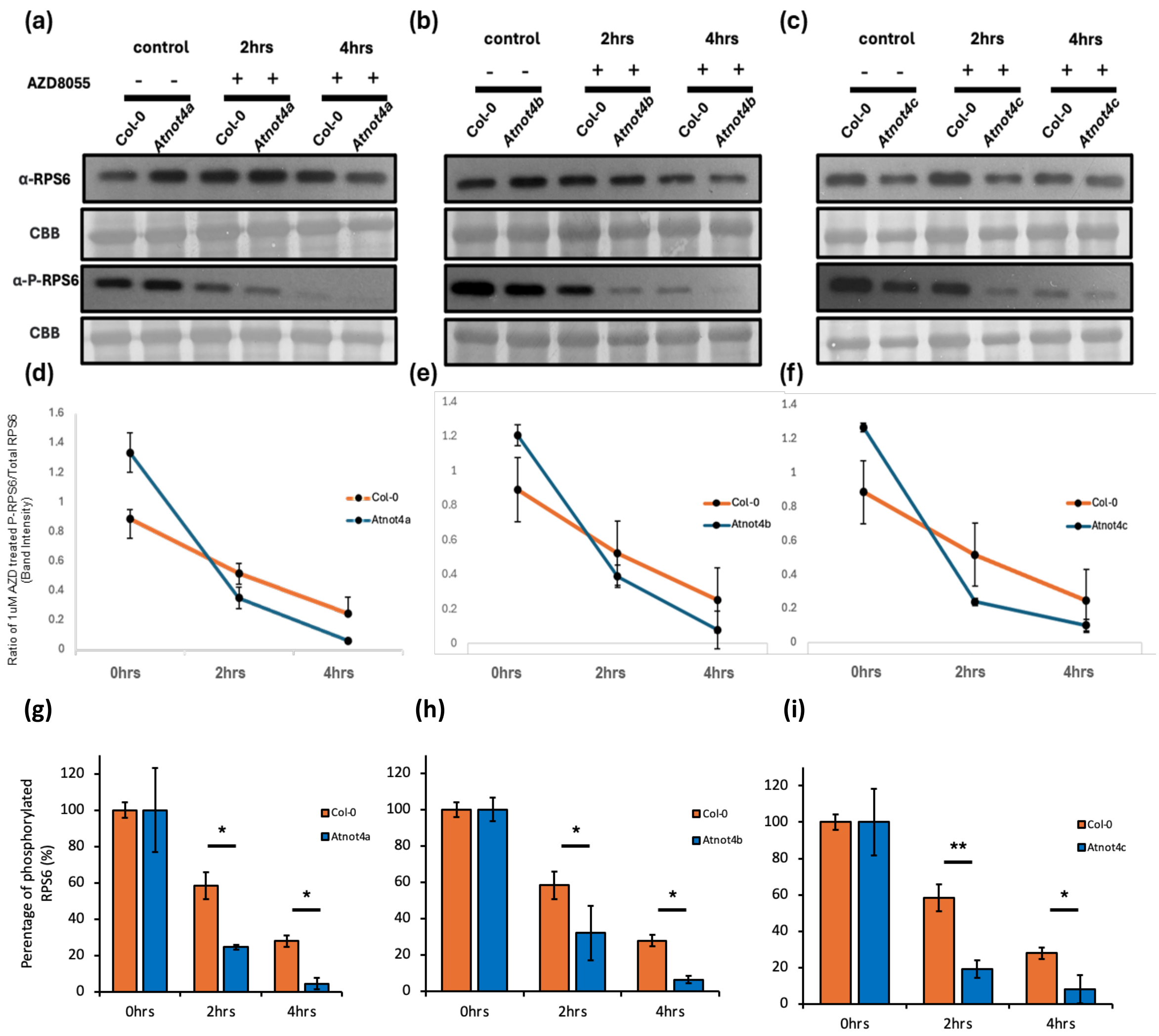

Figure 49 – Effect of 1μM AZD8055 Time Course Treatment on Total *At*RPS6A and Phosphorylated *At*RPS6 (P-*At*RPS6) Levels in *At*NOT4 single mutants. (**a-b**) Western blot analysis probing for a-RPS6 and a-P-RPS6 for *Atnot4a*, *Atnot4b*, and *Atnot4c*. The Western blot was repeated at least 3 times for each genotype in which similar results were produced. (**d-f**) Graphs show the average band intensity ratio between P-*At*RPS6A/Total *At*RPS6A in WT vs the corresponding mutant in response to 0h, 2h or 4h AZD8500 treatment, calculated from multiple independent biological repeats of Western blots conducted as in (a-c). Error bars indicate +/- SEM. (**g-i**) Bar graphs depicting mean temporal depletion of phosphorylated *At*RPS6A in Col-0 compared to the *Atnot4* single mutants. Within each genotype, the level of phosphorylation at the 0-hr time point was normalized to 100%, and further percentage changes at 2 hrs and 4 hrs were calculated with reference to this baseline. The overlay graphs in each panel provide a visual representation of the rate of decrease in phosphorylation, which shows a quicker attenuation in the single mutants as compared to the wild type. Error bars represent +/- SEM. Pair-wise Wilcoxon t-test was performed for statistical analyses (Asterisks indicate level of significance: *p < 0.05, **p < 0.01)

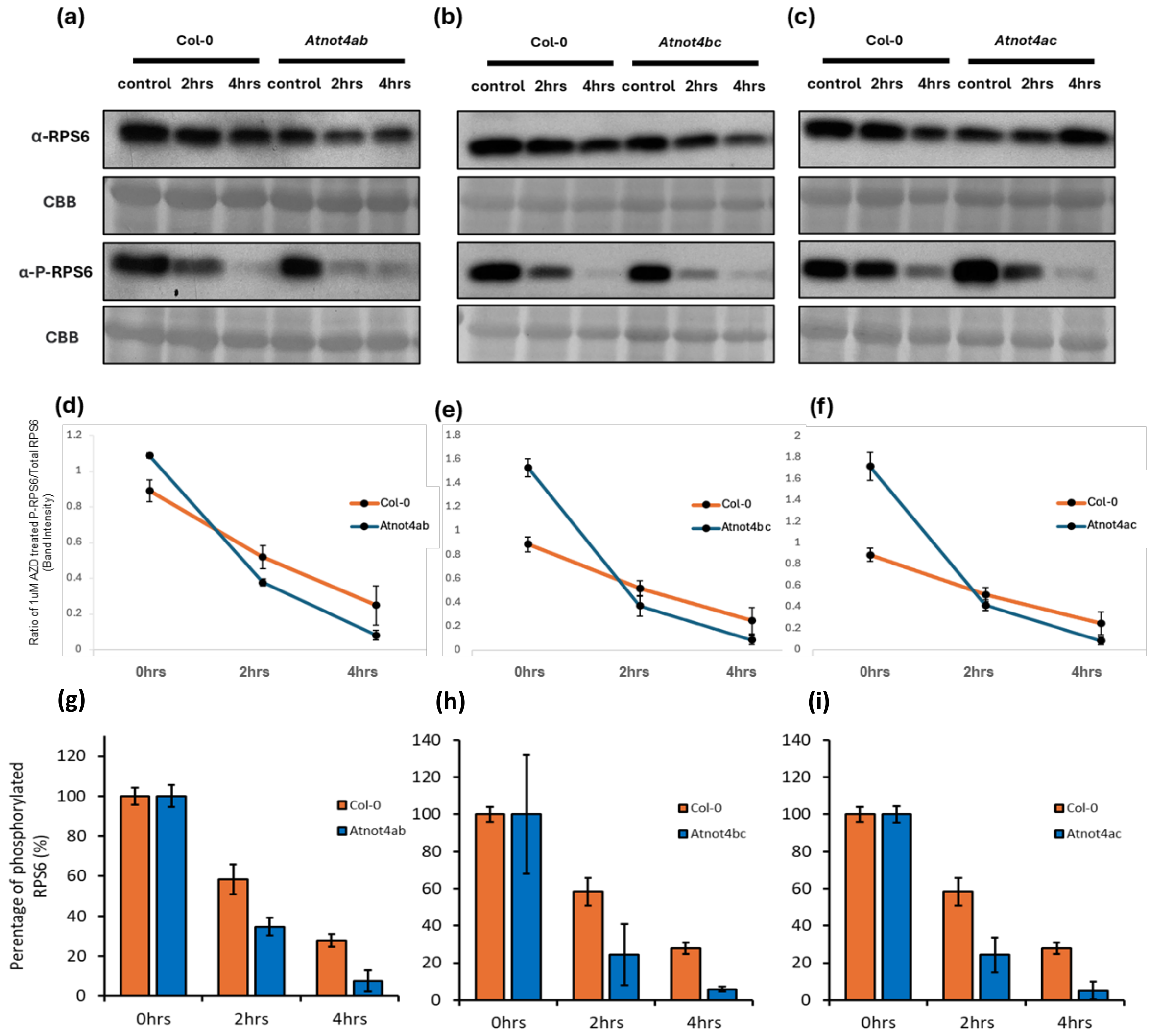

Figure 50 – Effect of 1μM AZD8055 Time Course Treatment on Total *At*RPS6A and Phosphorylated *At*RPS6A (P-*At*RPS6A) Levels in *At*NOT4 double mutants. (**a-b**) Western blot analysis probing for a-RPS6A and a-P-RPS6A for *Atnot4ab*, *Atnot4bc*, and *Atnot4ac*. The Western blot was repeated twice for each genotype in which similar results were produced. (**d-f**) Graphs show the average band intensity ratio between P-*At*RPS6A/Total *At*RPS6A in WT vs the corresponding mutant in response to 0h, 2h or 4h AZD8500 treatment, calculated from multiple independent biological repeats of Western blots conducted as in (a-c). Error bars indicate +/- SEM. (**g-i**) Bar graphs depicting mean temporal depletion of phosphorylated AtRPS6A in Col-0 compared to the *At*not4 double mutants. Within each genotype, the level of phosphorylation at the 0-hr time point was normalized to 100%, and further percentage changes at 2 hrs and 4 hrs were calculated with reference to this baseline. The overlay graphs in each panel provide a visual representation of the rate of decrease in phosphorylation, which shows a quicker attenuation in the single mutants as compared to the wild type. Error bars represent +/- SEM. No statistical significance could be tested as only two replicates were available.

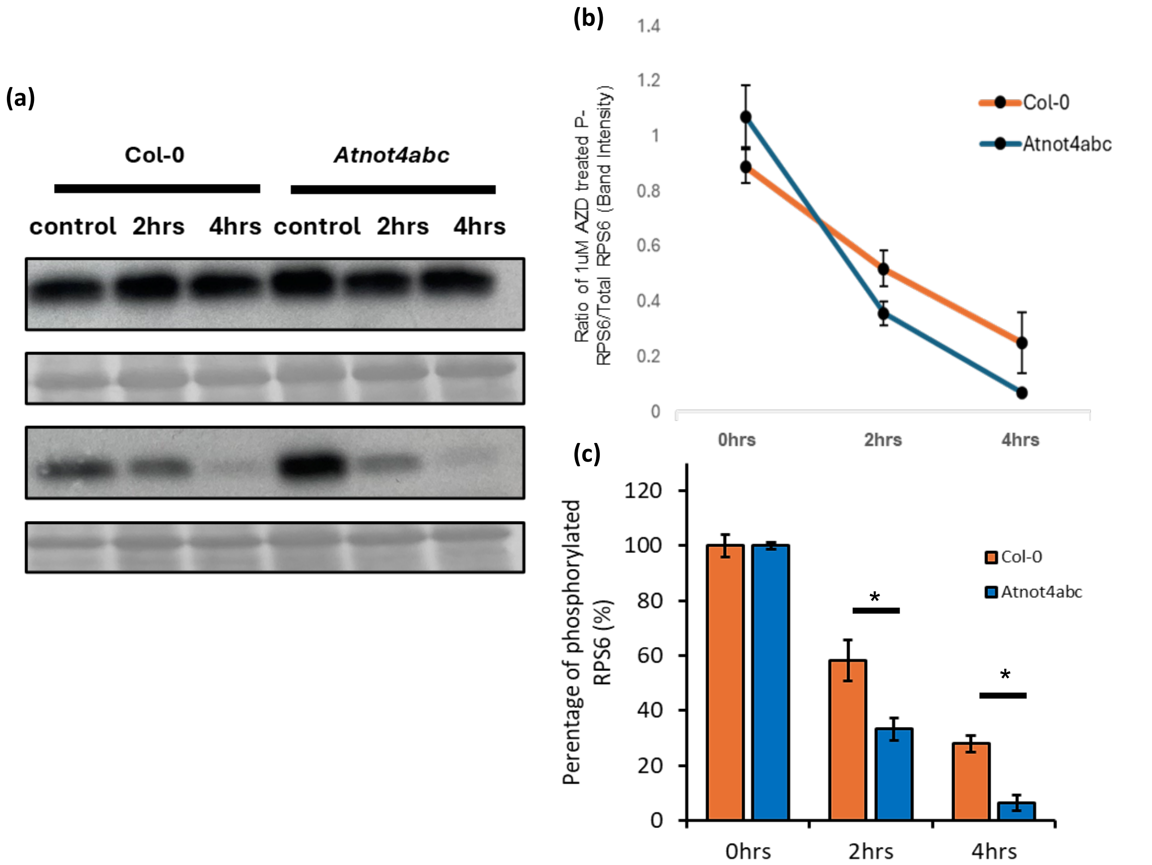

Figure 51 – Effect of 1µM AZD8055 Time Course Treatment on Total *At*RPS6A and Phosphorylated *At*RPS6A (P-*At*RPS6) Levels in *Atnot4abc*. (**a**) Western blot analysis probing for a-RPS6 and a-P-RPS6 for *Atnot4abc*. The Western blot was repeated at least 3 times for each genotype in which similar results were produced (**b**) Graphs show the average band intensity ratio between P-*At*RPS6A/Total *At*RPS6A in WT vs the corresponding mutant in response to 0h, 2h or 4h AZD8500 treatment, calculated from multiple independent biological repeats of Western blots conducted as in (a). Error bars indicate +/- SEM. (c) Bar graphs depicting mean temporal depletion of phosphorylated *At*RPS6A in Col-0 compared to the *Atnot4*abc mutant. Within each genotype, the level of phosphorylation at the 0-hr time point was normalized to 100%, and further percentage changes at 2 hrs and 4 hrs were calculated with reference to this baseline. The overlay graphs in each panel provide a visual representation of the rate of decrease in phosphorylation, which shows a quicker attenuation in the single mutants as compared to the wild type. Error bars represent +/- SEM. Pair-wise Wilcoxon t-test was performed for statistical analyses (Asterisks indicate level of significance: *p < 0.05, **p < 0.01)

5.5 Sucrose Treatment Does Not Differentially affect *At*TOR activity in *Atnot4a* relative to Wild type

*At*TOR signalling activity can be enhanced in the presence of sucrose (Dobrenel, Mancera-Martinez, et al., 2016; Xiong et al., 2013; Xiong & Sheen, 2012). The rescue of growth phenotype in *Atnot4a* upon sucrose supplementation aligns with the emerging link between *At*NOT4s, *At*TOR and energy utilisation. This prompted a further investigation into *At*TOR activity in relation to exogenous sucrose application. Western blotting was conducted, specifically probing for the *At*RPS6A and P-*At*RPS6A in order to monitor *At*TOR activity (**Figure 52**). Only *Atnot4a* was examined as the other paralogs did not display the same obvious growth phenotype. Wild-type and *Atnot4a* seedlings were treated with 1% sucrose (v/v) for 2, 4 and 24 hours. Interestingly, comparable amount of *At*RPS6A across all time points was observed in both genotypes. Thus, even in the presence of excess energy availability, the phosphorylation of *At*RPS6A remains relatively stable when compared to wild-type.

Moreover, a distinct phosphorylation pattern is observed across the time points in both wild-type and *Atnot4a*. Both genotypes displayed a comparable pattern of sucrose-triggered phosphorylation, with P-*At*RPS6A levels peaking at 4 hours and declining by 24 hours. Even with elevated basal *At*TOR activity in *Atnot4a*, the increase at both 2 and 4 hours is still comparable to Col-0. Another interesting finding is that at 24 hours, *Atnot4a* exhibits a drastic decline in P-*At*RPS6A levels, even below the basal levels compared to the control time point. This could indicate a specific characteristic of the *At*TOR signalling dynamics in the absence of *At*NOT4A. Possibly, such rapid deactivation is part of the response when challenged by prolonged external energy supply. Although *Atnot4a* mutants showed changed *At*TOR signalling activity under conditions of *At*TOR inhibition, no clear difference in response was observed in conditions of *At*TOR activation.

Furthermore, the difference between the 2- and 4-hour timepoints is minimal across both genotypes, thus suggesting that *At*TOR activation has reached maximal phosphorylation of *At*RPS6A. It's likely that 100% of *At*TOR proteins have already been induced at the 4-hour point and therefore reached their potential activity. Even in a mutant background like *Atnot4a* that experiences hyperactivated *At*TOR signalling, further enhancement of *At*TOR phosphorylation capacity is limited.

The recovery of growth in *Atnot4a* mutants by sucrose supplementation and the higher basal levels of *At*TOR activity underlines a complex interplay between the *At*TOR signalling, energy metabolism, and growth control via *At*NOT4A. It is plausible that *At*TOR signalling may not be solely responsible for the growth retardation observed in *Atnot4a* mutants. A broader range of metabolic pathways could be affected and therefore causing many deficiencies that lead to ineffective support of growth and developmental processes. Therefore, sucrose could be one of many different factors that can compensate for these metabolic deficiencies and enhance protein translation crucial for growth. Ultimately, this compensation enables *Atnot4a* mutants to bypass certain disrupted processes that limit their growth which aligns their growth rate to that of wild-type. Thus, these growth restrictions that occur in the absent of *At*NOT4A may stem from an impaired ability to expend endogenous energy reserves efficiently rather than inadequate *At*TOR activity.

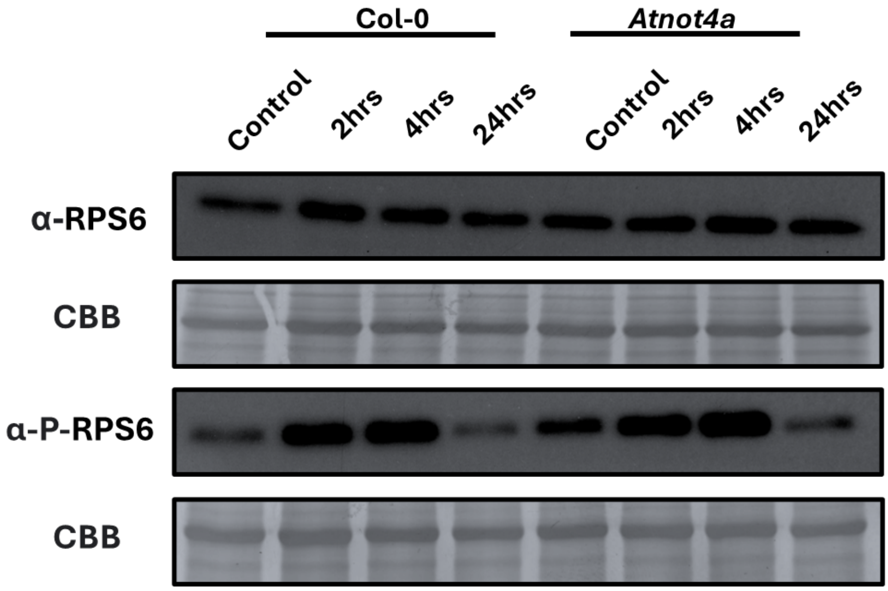

Figure 52 – Western blot analysis of total *At*RPS6A and phosphorylated *At*RPS6 (P-RPS6) in Col-0 and *Atnot4a* following sucrose supplementation. Steady-state levels of total *At*RPS6 and its phosphorylated form (P-*At*RPS6A) in both Col-0 and *Atnot4a* seedlings under control conditions and at various time points (2 hrs, 4 hrs, and 24 hrs) following sucrose treatment. Coomassie Brilliant Blue (CBB) staining was used as a loading control to ensure equal protein loading across the samples. *It must be noted that this blot was only conducted once.*

5.6 Impact of *At*TOR inhibition on *Atnot4abc* transcriptome

5.6.1 Overview of RNAseq approach

RNA-seq was performed on the following four sample groups: untreated Col-0, Col-0 treated with 1 µM AZD8500 for 2 hrs, untreated *Atnot4abc* and *Atnot4abc* treated with 1 µM AZD8500 for 2 hrs (**Appendix 5**). The aim of this RNA-seq experiment is to gain further insights into the molecular mechanisms responsible for the observed sensitivity to *At*TOR inhibitors, increased *At*TOR activity, and the accelerated dephosphorylation of *At*RPS6A upon *At*TOR inhibition in the *Atnot4* mutants. The goal of the RNA-seq experiment is to identify DEGs upon *At*TOR inhibition and to compare transcriptomic changes between wild-type and *Atnot4abc*. More precisely, this experiment was designed to:

1. Identify genes and biological pathways that are differentially expressed upon *At*TOR inhibition in Col-0 and in *Atnot4abc* plants.

2. To assess whether the Col-0 transcriptomic response to *At*TOR inhibition mimics or contrasts with the intrinsic transcriptomic profile of the *Atnot4abc* mutant.

3. Determine plausible molecular mechanisms that may explain the increased sensitivity of *Atnot4abc* to *At*TOR inhibitors, including changes in expression of genes associated with: ribosome biogenesis, translation, stress responses, and metabolic regulation.

5.6.2 Transcriptomic Changes in Col-0 upon AZD8500 Treatment

5.6.2.1 Differentially Expressed Genes (DEGs) in untreated Col-0 vs 1µM AZD8055 treated Col-0

The global transcriptome of untreated and 1 µM AZD8055 treated Col-0 to was analysed in hope to identify genes that are differentially expressed upon *At*TOR inhibition. The resulting data is presented in the form of a volcano plot, which provides a visual summary of the DEGs observed between the two conditions within the same genotype (**Figure 53**). For this analysis, the fold change was set at 2 and therefore the threshold values were set at Log_2 fold change > 1 for upregulation (red) and < -1 for downregulation (blue). Alongside this criterion, the significance threshold was set at a p-value < 0.05 (horizontal dashed line). In accordance with these parameters, a total of 356 differentially expressed genes were identified of which 171 were significantly downregulated and 185 genes were significantly upregulated.

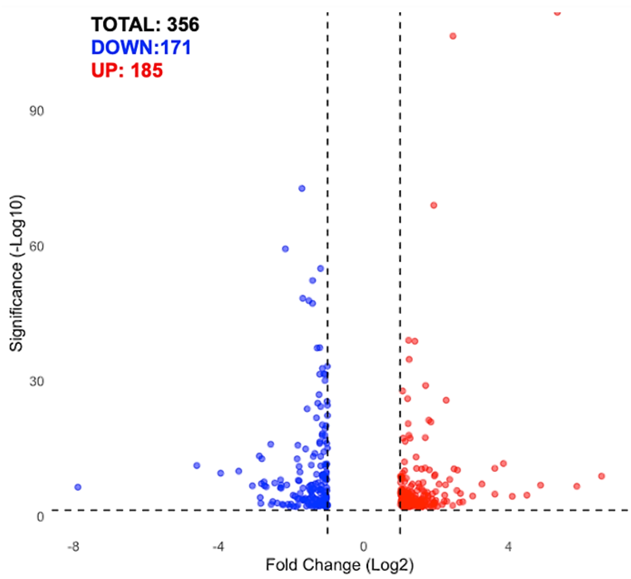

Figure 53 – Differential Expressed Genes comparing untreated Col-0 to 1µM AZD8055 treated Col-0. Volcano plot displays DEGs, showing the fold change ($Log_2(2)$) on the x-axis and the significance ($-Log_{10}$(p-value)) on the y-axis. A total of 356 genes were differentially expressed of which 171 were downregulated (blue) and 185 upregulated (red).

5.6.2.2 GO Term Enrichment Analysis for Upregulated Genes in 1 µM AZD8055 treated Col-0

GO term enrichment analysis for upregulated genes in Col-0 following treatment with 1 µM AZD8055 was performed (**Figure 54**). “Hydrolase activity, acting on glycosyl bonds" (11 DEGS, p-value = 3.554×10^{-4}, Fischer’s Exact Test) was the most enriched GO term. This suggests that transcripts involved in catalysing glycosidic bonds were upregulated. The increase in hydrolase activity may indicate the need for redistribution of stored carbohydrates as well as recycling of cellular components to meet energy depends in order to maintain essential cellular function that are disrupted due to *At*TOR inhibition. "Intracellular signal transduction" was another GO term significantly enriched (8 DEGs, p-value = 4.62x10-3, Fischer's Exact Test). This suggests that multiple signalling pathways are being upregulated in response to the suppression of AtTOR. Loss of *At*TOR kinase activity may cause the cells to rely more heavily on alternate signalling mechanisms as a compensatory mechanism for the loss of such an important regulator.

Furthermore, "response to drug" had a total of 8 DEGs (p-value = 9.76×10^{-3}, Fischer’s Exact Test). It may be triggering stress response genes involved in detoxification pathways in order to mitigate the presence of AZD8055 and repair any damaged caused by it. This also highlights the dynamic response mechanism of *Arabidopsis* to exogenous chemical stressors in light of when an essential signalling pathway such as *At*TOR signalling is affected. In addition, transcription-related GO terms were enriched, namely “RNA polymerase II transcription factor activity” (6 DEGs, p-value = 7.64×10^{-3} and "positive regulation of transcription" (6 DEGs, p-value = 4.97×10^{-2}, Fischer’s Exact Test). It seems like there is a coordinated effort of cells to increase the transcription and processing of RNA, perhaps as a means to maintain the expression of genes critical for survival under stress conditions.

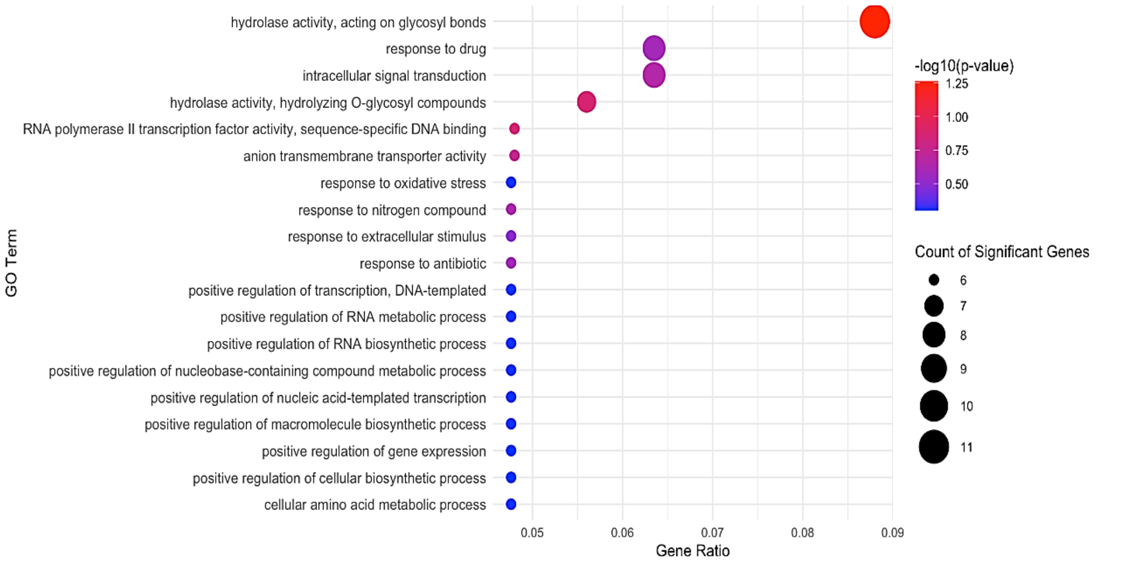

Figure 54 – Gene Ontology (GO) term enrichment analysis of upregulated genes in Col-0 upon treatment with 1 µM AZD8055 compared to untreated Col-0. The dot plot represents highly enriched GO terms corresponding to up-regulated DEGs. The x-axis shows the gene ratio, while on the y-axis GO terms are listed. Colour intensities of the dots correspond to statistical significance -log10(p-value), the higher the colour intensity the higher the significance. Dot size corresponds to the number of significant genes assigned to a particular GO term.

5.6.2.3 GO Term Enrichment Analysis for Downregulated Genes in 1 µM AZD8055 treated Col-0

Highly enriched GO terms in significantly downregulated genes were associated to cell wall organisation and biogenesis (**Figure 55**) This includes "external encapsulating structure organization" (16 DEGs, p-value = $6.4x10^{-10}$, Fischer's Exact Test), "cell wall organization" (16 DEGs, p-value = $7.9x10^{-11}$, Fischer's Exact Test), and "plant-type cell wall organization or biogenesis" (15 DEGs, p-value = $2.37x10^{-9}$, Fischer's Exact Test). All these GO terms collectively highlight the impact of *At*TOR inhibition has in the regulation, synthesis and stability of cell walls.

Furthermore, GO terms "response to oxidative stress" (15 DEGs, p-value = $7.2x10^{-7}$, Fischer's Exact Test) and "antioxidant activity" (6 DEGs, p-value = $6.04x10^{-5}$, Fischer's Exact Test) were also downregulated upon *At*TOR inhibition in Col-0. This infers that the plants ability to alleviate oxidative damage is compromised. *At*TOR can transcriptionally induce superoxide dismutase and catalase which are enzymes known for reactive oxygen species (ROS) detoxification (Tsang et al., 2018). Therefore, the observed downregulation due to supressed *At*TOR activity aligns well the role of *At*TOR and redox homeostasis. "Vacuolar membrane" (6 DEGs, p-value = $6.52x10^{-3}$, Fischer's Exact Test) and "vacuolar part" (6 DEGs, p-value = $7.21x10^{-3}$, Fischer's Exact Test) were also GO terms that were significantly underrepresented. Intracellular compartmentalisation and storage functions may be altered upon AZD8055 treatment.

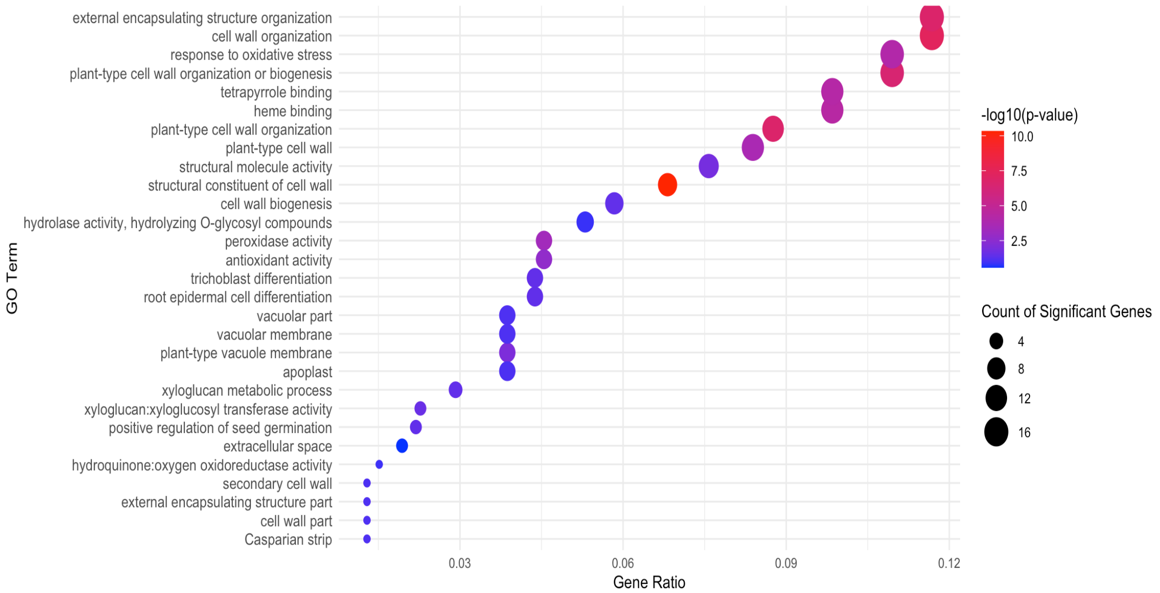

Figure 55 – Gene Ontology (GO) term enrichment analysis of downregulated genes in Col-0 upon treatment with 1µM AZD compared to untreated Col-0. The dot plot illustrates significantly enriched GO terms related to the downregulated DEGs. The x-axis represents the gene ratio, while the y-axis lists the GO terms. The colour intensity of the dots corresponds to the statistical significance (-log10(p-value)), with more intense colours indicating higher significance. The size of the dots reflects the count of significant genes associated with each GO term.

5.6.3 Transcriptomic Changes in *Atnot4abc* upon AZD Treatment

5.6.3.1 Differentially Expressed Genes (DEGs) in *Atnot4abc* vs 1µM AZD treated *Atnot4abc*

Having established a foundation of the biological mechanisms affected by *At*TOR inhibition in wild-type, it was important to analyse the disruptions of these mechanisms in *Atnot4abc*. The comparison of transcriptomic profiles between Col-0 and *Atnot4abc* can lead to the identification of shared or specific biological processes that are affected upon *At*TOR inhibition.

Transcriptomic analysis of *Atnot4abc* mutants treated with 1 µM AZD8055 showed differential gene expression (2-fold, $p < 0.05$), represented by a total of 464 differentially expressed genes (**Figure 56**). *Atnot4abc* therefore has 108 more unique DEGs compared to Col-0, highlighting pronounced changes in gene expression which likely reflects the altered signalling pathways and stress responses of the mutant under conditions of diminished *At*TOR activity. This may also form the molecular basis for the observed phenotypic differences upon *At*TOR inhibition (*to be further analysed in the following sections)*. Moreover, a total of 183 genes were downregulated, whereas 281 genes were upregulated in response to *At*TOR inhibition. These are displayed on the volcano plot (**Figure 55**) where the distribution of DEGs across the transcriptome of *Atnot4abc* differs from Col-0.

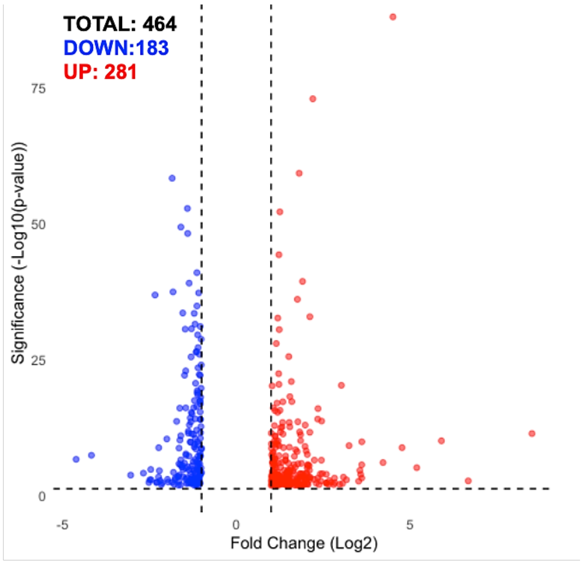

Figure 56 – Differential Expressed Genes comparing *Atnot4abc* to 1 μM AZD treated *Atnot4abc*. Volcano plot displays DEGs, showing the fold change ($Log_2(2)$) on the x-axis and the significance ($-Log_{10}$(p-value)) on the y-axis. A total of 464 genes were differentially expressed of which 183 were downregulated (blue) and 281 upregulated (red).

5.6.3.2 GO Term Enrichment Analysis for Upregulated Genes in 1 µM AZD8055 treated *Atnot4abc*

Interestingly, the same GO terms that were shown as significantly downregulated genes in Col-0 were in fact upregulated in *Atnot4abc* (**Figure 57**). These upregulated genes were associated to GO terms like "external encapsulating structure organization" (7 DEGs, p-value = 3.65×10^{-2}, Fischer's Exact Test) and "plant-type cell wall organization or biogenesis" (4 DEGs, p-value = 2.35×10^{-3}, Fischer's Exact Test). A possible explanation of these genes being downregulated in Col-0 is *At*TOR role in modulating growth and development. When *At*TOR signalling is supressed, a reduction of growth-related processes is observed. However, the upregulation of the same GO terms in *Atnot4abc* may suggest a compensatory mechanism, where the loss of *At*NOT4s induces robust cellular pathways to ensure the maintenance and reinforcement of the cell wall integrity and structure.

A further shared GO term that was downregulated in Col-0 but upregulated in *Atnot4abc* are genes linked to oxidative stress, specifically "response to oxidative stress" (3 DEGs, p-value = 3.97×10^{-3}, Fischer's Exact Test). *At*TOR signalling activity is highly linked to maintaining redox homeostasis (Tsang et al., 2018) which is disrupted upon inhibition. However, the inhibition of *At*TOR in *Atnot4abc* seems to have the opposite effect as it increases redox response-genes to relieve oxidative stress. This could be due to the build-up of ROS when *At*TOR signalling activity is dysfunctional, as a consequence of both the presence of AZD8055 and absence of *At*NOT4s. Thus, *Atnot4abc* may be attempting to restore balance as a protective measure when *At*TOR signalling is suppressed.

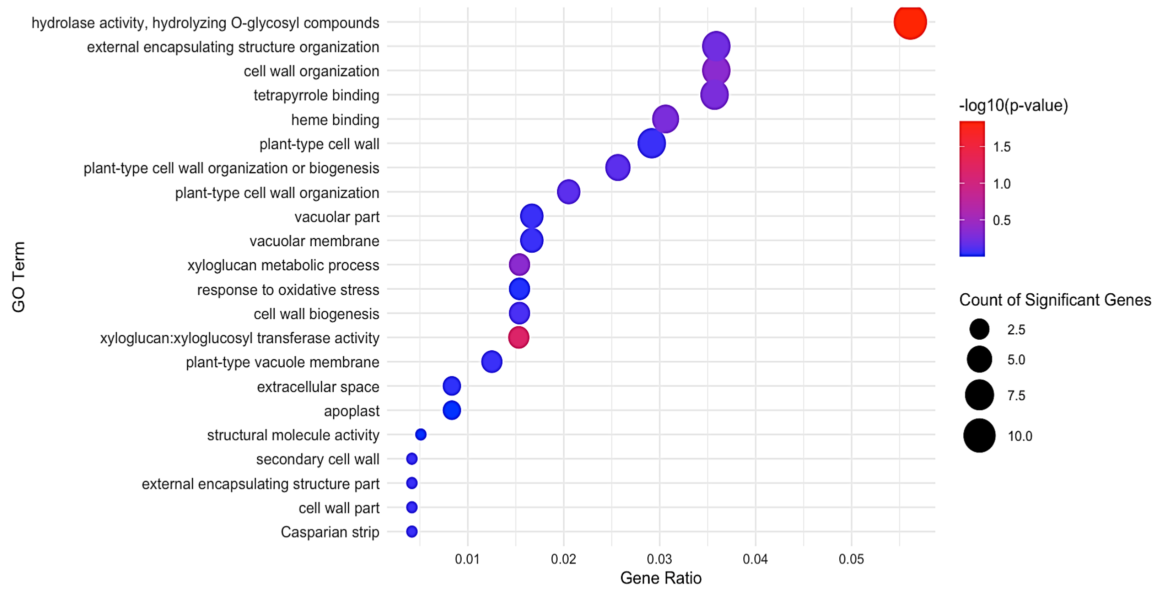

Figure 57 - GO Term enrichment of upregulated genes in *Atnot4abc* treated with 1 µM AZD versus untreated *Atnot4abc*. Dot plot shows significant enriched GO terms among the up-regulated DEGs. The x-axis represents the gene ratio, and the y-axis represents the GO terms. Colour intensity of the dots is based on statistical significance (-log10(p-value)) where the darker the colour, the more statistically significant. Dot size represents the number of significant genes for each GO term.

5.6.3.3 GO Term Enrichment Analysis for Downregulated Genes in 1 µM AZD treated *Atnot4abc*

GO term enrichment of downregulated genes in *Atnot4abc* treated with 1 µM AZD8055 reveals a dramatically changed transcriptomic profile compared to their untreated state (**Figure 58**). Indeed, several key biological processes related to translation, and ribosome biogenesis that were previously upregulated in untreated *Atnot4abc*, are now significantly downregulated upon AtTOR inhibition. This includes "ribosome" (5 DEGs, p-value = 8.78x10-3, Fischer's Exact Test), "cytosolic ribosome" (11 DEGs, p-value = 2.09x10-5, Fischer's Exact Test), and "structural constituent of ribosome" (8 DEGs, p-value = 1.15x10-3, Fischer's Exact Test). This suggest that *At*TOR inhibition leads to the repression in ribosomal functions and biogenesis in *Atnot4abc*.

Notably, these processes were previously upregulated in the untreated *Atnot4abc* which suggests a reversal in their transcriptional regulation upon exposure to the *At*TOR inhibitor. This suppression of ribosome-related processes may be directly linked to the fact that AZD8055 causes a much faster 'shutdown' of *At*TOR activity in *Atnot4abc* compared to WT (*see 5.4.3*). The increased sensitivity to AZD8055 likely leads to an accelerated and more extensive inhibition of *At*TOR signalling, thus rapidly supressing translation and ribosome biogenesis. In wild-type, this effect is more gradual since the reduction in *At*TOR activity is slower, allowing a better control in necessary adjustments for translation-related processes. This infers that the downregulation of ribosome-related genes in the *Atnot4abc* cannot buffer the *At*TOR inhibition, leading to faster and more severe impairment of translation machinery. *Atnot4abc* is already predisposed to dysfunctional translation as evident of the increased global translation rates (*see Chapter 4 Section 4.2*) and upregulation of translation and ribosome biogenesis gene in untreated *Atno4abc* (*see Chapter 3 Section 3.4.2*). However, hindering *At*TOR signalling activity offsets this predisposition and causes the suppression of genes linked to ribosome biogenesis and protein synthesis. This is further supported by the rapid dephosphorylation of P-*At*RPS6A levels (*see 5.4.3*, **Figure 51**) which indicate a critical role of *At*TOR in maintaining translational homeostasis, especially in *Atnot4abc* which is known to have pre-existing translation-related vulnerabilities. An interesting follow-up experiment would be to compare puromycin incorporation in Col-0 and *Atnot4abc* - with and without AZD treatment - to directly assess the impact of TOR inhibition on global translation rates. Nevertheless, these findings indicate a dependency that *Atnot4abc* has on *At*TOR activity to maintain translational homeostasis.

Another interesting is GO terms that were enriched in both up- and downregulated genes. *Atnot4abc* treated with AZD8055 showed significant enrichment for cell wall-related processes and oxidative stress responses. GO terms such as "cell wall organization", "cell wall biogenesis", and "response to oxidative stress", were represented both in the up-and downregulated GO term enrichment lists. In response *At*TOR inhibition, some genes involved in cell wall remodelling or modification might be upregulated to maintain cellular integrity during such stress. Simultaneously, genes directly involved with the synthesis or reinforcement of the cell wall would be downregulated for conservation of energy and resources by the cell, ultimately reducing the growth-related activities and prioritising survival. Similarly, the oxidative stress response genes may be induced for minimizing immediate damage, while other components in the same pathway are also reduced as part of a general stress adaptation strategy. The regulation of both cell wall processes and oxidative stress responses in *Atnot4abc* under *At*TOR inhibition is rather complex, with both induction and repression of various components in the same biological pathways occur to adapt to the changed environmental conditions.

Lastly, jasmonic acid (JA) is one of the main phytohormones involved in the regulation of plant responses against herbivore attacks, pathogen infection, and mechanical wounding (Song et al., 2017). Decrease in genes associated with "jasmonic acid biosynthetic process" (4 DEGs, p-value = 9.72x10-5, Fischer’s Exact Test) was also observed which implies a reduced capacity for plant defence and hormone signalling. The biosynthesis and signalling pathways of JA are important regulators in the activation of defence mechanisms which produce secondary metabolites and defensive proteins (Song et al., 2017). Consequently, downregulation of genes in this pathway in *Atnot4abc* under *At*TOR inhibition reflects the inability to sustain such defence responses and ultimately leading to higher vulnerability and susceptibility.

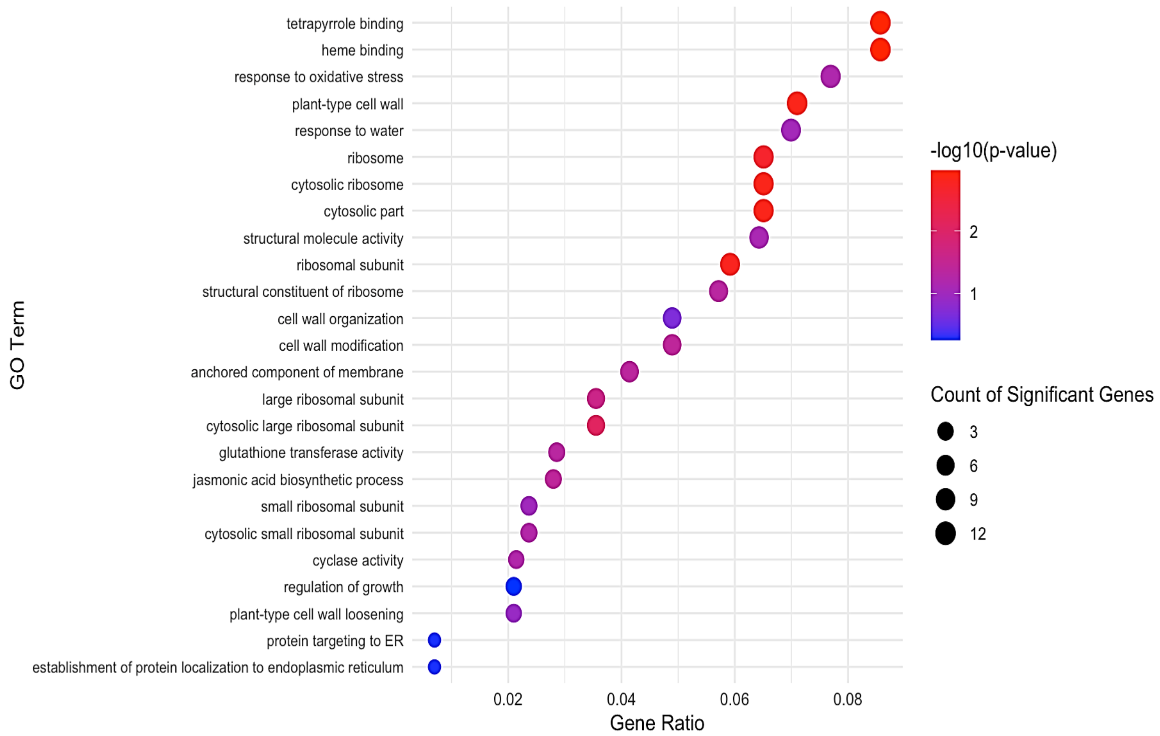

Figure 58 – Gene Ontology (GO) term enrichment analysis of downregulated genes in *Atnot4abc* upon treatment with 1µM AZD compared to untreated *Atnot4abc*. The dot plot illustrates significantly enriched GO terms related to the downregulated DEGs. The x-axis represents the gene ratio, while the y-axis lists the GO terms. The colour intensity of the dots corresponds to the statistical significance (-log10(p-value)), with more intense colours indicating higher significance. The size of the dots reflects the count of significant genes associated with each GO term.

5.6.4 Comparative Analysis: (untreated Col-0 vs 1 µM AZD8055 treated Col-0AZD) vs (*Atnot4abc* vs 1 µM AZD treated *Atnot4abc*)

The UpSet plot depicts the intersection of DEGs between two main comparisons: Col-0 (WT_azd) treated with 1 µM AZD8055 versus untreated Col-0 (WT), and *Atnot4abc* treated with 1 µM AZD8055 versus untreated *Atnot4abc* (**Figure 59**).

The comparison between control *Atnot4abc* and *Atnot4abc* 1 µM AZD8055 treated contained the largest intersection size, comprising a total of 323 unique DEGs that are specifically induced or repressed under *At*TOR inhibition. These extensive DEGs reflect the biological processes, molecular functions and cellular components that are affected when *At*TOR is dysfunctional in addition to *At*NOT4s absence. A smaller intersection size of 215 DEGs was observed when comparing Col-0 and treated Col-0 with 1 µM AZD8055 which highlights specific DEGs of the wild-type background under TOR inhibition.

The smaller set of 141 DEGs is the intersection which is shared between the two comparisons and genotypes. This shared set of DEGs suggests a conserved core response to *At*TOR inhibition, regardless of the genetic background, and reflects the fundamental processes that are universally affected by *At*TOR signalling. This includes GO terms such as “response to stimulus” (47 DEGs, p-value = 1.9x10-5, Fischer’s Exact Test), “response to stress” (27 DEGs, p-value = 2.18x10-3, Fischer’s Exact Test), “response to chemical (22 DEGs, p-value = 5.4x10-3, Fischer’s Exact Test) which are all indicative of the cell recognising and attempting to cope with the presence of AZD8055.

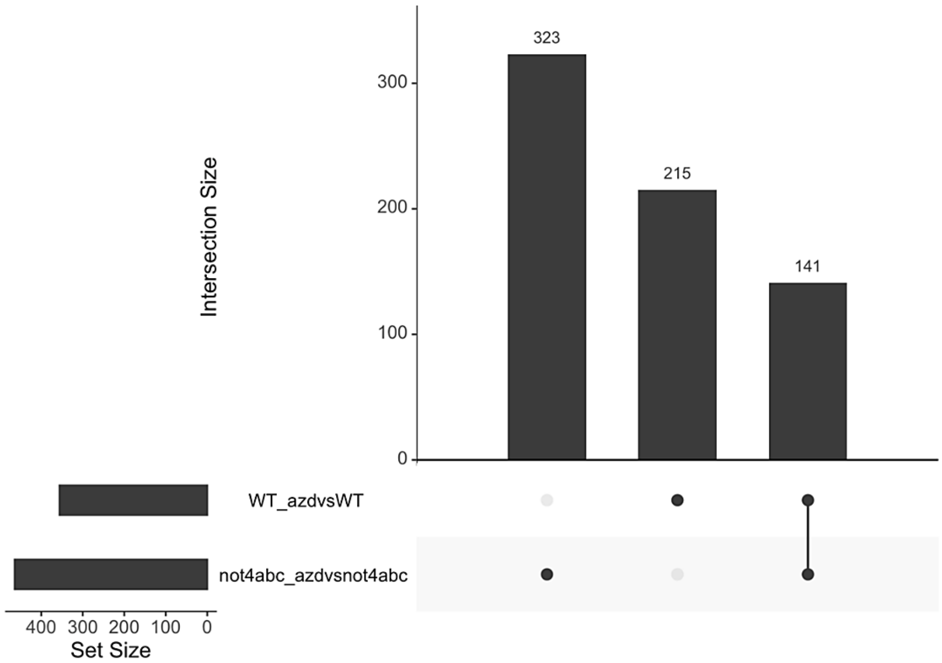

Figure 59 - UpSet Plot of Differentially Expressed Genes (DEGs) in WT and *Atnot4abc* Mutants Treated with AZD8055. UpSet plot visualizes the intersection of differentially expressed genes between two conditions, namely 1 µM AZD8055 treated Col-0 vs. untreated Col-0 (WT_azdvsWT) and 1 µM AZD8055 treated Atnot4abc vs. untreated Atnot4abc (not4abc_azdvsnot4abc). The bar chart on the right gives the total number of DEGs in each condition. the dot chart below depicts the intersection for each overlap combination.

5.6.4.1 Differentially Expressed Genes (DEGs) unique to AZD8500-treated vs untreated *Atnot4abc*

GO analysis of the UpSet plot, specifically into the intersection of the 323 unique DEGs in *Atnot4abc* untreated vs *Anot4abc* 1 μM AZD8055 treated relative to Col-0 untreated vs Col-0 1 μM AZD8055 treated was performed (**Figure 60**). A strong enrichment of the GO term was “posttranslational protein targeting to membranes” (2 DEGs, p-value = 4.82×10^{-3} , Fischer’s Exact Test). Even in the absence of external stressors, *Atnot4abc* experiences heightened protein folding stress which is likely due to compromised co-translational quality control mechanisms (*see Chapter 4 Section 4.4*). The added stress from *At*TOR inhibition on an already overwhelmed quality control system may likely escalate disruptions in proteostasis and contribute to the observed *Atnot4abc* growth phenotype. Another interesting GO term among the list was 'regulation of organ growth' (2 DEGs, p-value = 8.18×10^{-3}, Fischer’s Exact Test). When *At*TOR is inhibited, these already compromised pathways are likely experiencing excessive stress, which *Atnot4* mutants are unable to compensate for, leading to heightened sensitivity and further suppression of growth. This transcriptional change in response to *At*TOR inhibition likely reflects an attempt by the cells to adapt to the reduced *At*TOR signalling. However, in the context of *Atnot4a* and its higher order mutants, these adaptations may be insufficient to support normal growth, resulting in the observed phenotypic differences.

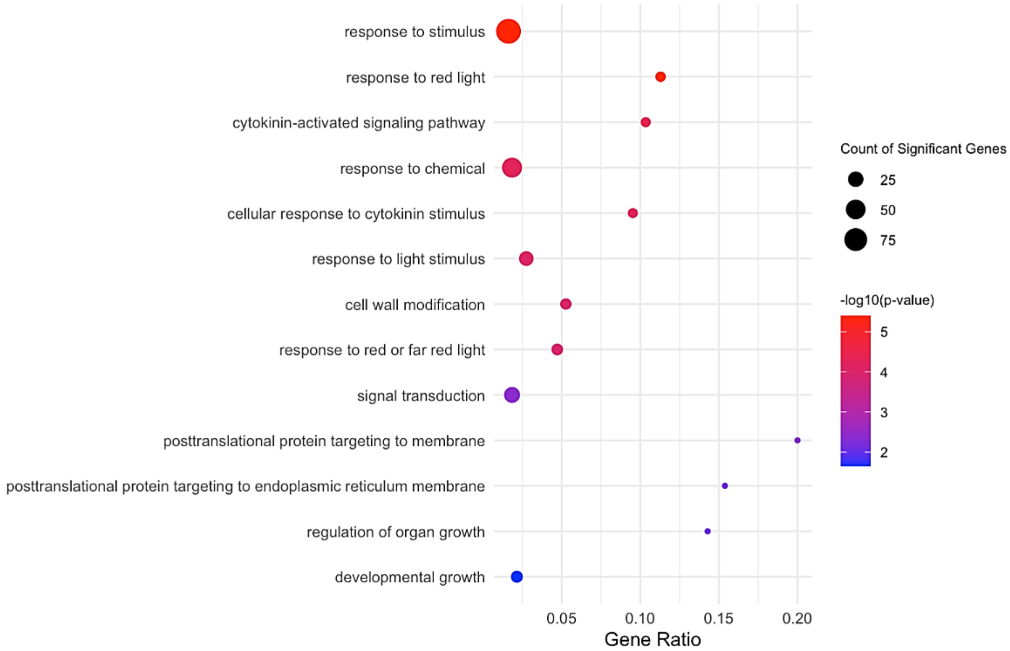

Figure 60 – Go term Enrichment Analysis of All Differentially Expressed Genes (DEGs) in *Atnot4abc* Treated with 1 µM AZD8055 vs untreated *Atnot4abc* compared to untreated Col-0 vs 1 µM AZD8055 treated Col-0. The x-axis represents the gene ratio, while the y-axis lists the GO terms. The colour intensity of the dots corresponds to the statistical significance (-log10(p-value)), with more intense colours indicating higher significance. The size of the dots reflects the count of significant genes associated with each GO term.

5.6.4.2 GO Term Downregulation in Untreated *Atnot4abc* Mimics 1 µM AZD8055 Treated Col-0

Remarkably, the transcriptomic analysis revealed that several GO terms associated with downregulated genes in AZD8055-treated Col-0 (vs untreated Col-0) are similar to those downregulated in untreated *Atnot4abc* (vs untreated Col-0) (**Figure 61-62**). This overlap suggests that *Atnot4abc* may inherently possess a transcriptomic profile that mimics, at least in part, the effects observed upon *At*TOR inhibition in wild-type plants. Specifically, GO terms such as "cell wall organization", "external encapsulating structure organization", and "antioxidant activity" which are typically downregulated in response to *At*TOR inhibition, appear to be similarly repressed in *Atnot4abc* in the absence of AZD treatment. This convergence in transcriptional responses implies that the absence of *At*NOT4s may precipitate a baseline cellular state that is akin to *At*TOR suppression. This is to a certain extent paradoxical, since *Atnot4abc* has increased *At*TOR activity (*see 5.4.1*). As discussed further below, this suggests that the compensatory increase in *At*TOR activity is still not sufficient to compensate for the impact that the loss of *At*NOT4s has on *At*TOR pathway function and may explain heightened sensitivity of *Atnot4abc* to TOR inhibitors (*see 5.3.1*).

Moreover, the observed GO term enrichments underscore a pivotal role of *At*NOT4s in supporting *At*TOR-mediated cellular processes. The significant downregulation of genes involved in “cell wall organization” in *Atnot4abc* (28 DEGs, p-value = 2.26×10^{-15}, Fischer’s Exact Test) and AZD8055 treated Col-0 (16 DEGs, p-value = 4.60×10^{-8}, Fischer’s Exact Test) share a total of 12 genes (**Figure 63a**), and are all similarly expressed (**Figure 63b**). Additionally, the significant downregulation of genes involved in “antioxidant activity” in *Atnot4abc* (8 DEGs, p-value = 6.11×10^{-5}, Fischer’s Exact Test) and AZD8055 treated Col-0 (6 DEGs, p-value = 6.04×10^{-5}, Fischer’s Exact Test) share 4 genes in total (**Figure 64a**) and are also similarly expressed (**Figure 64b**). This indicates that Anot4abc may be operating under a condition of partial *At*TOR disruption even without external AZD8055 treatment. This inherent similarity to the *At*TOR-inhibited state of AZD8055-treated Col-0 could provide a molecular basis for the pronounced phenotypic defects observed in

Atnot4abc. Their ability to compensate for *At*TOR pathway disruption appears fundamentally impaired, despite an upregulation in basal *At*TOR activity. Therefore, this suggests a complex dynamic interplay between *At*TOR signalling and *At*NOT4s functions. For instance, increased *At*TOR activity in *Atnot4abc*, as indicated by higher levels of phosphorylated *At*RPS6A, suggests that *At*TOR is active, but it does not necessarily mean that *At*TOR signalling is fully functional. The loss of *At*NOT4 might disrupt other aspects of *At*TOR signalling that are crucial for normal cellular function. This disruption could lead to a transcriptomic profile that appears similar to *At*TOR inhibited Col-0, even though *At*TOR kinase itself is more active. This implies that *At*NOT4s are needed for the correct interpretation and execution of *At*TOR signals within the cell. Additionally, the absence of *At*NOT4s creates a state of pre-existing stress in cellular functions. This stress might prime the cells to maintain a transcriptional state similar to that induced by *At*TOR inhibition. The elevated *At*TOR activity might then be a response to this stress, attempting to maintain growth and survival, but not sufficiently altering the transcriptome to match that of a healthy, unstressed wild-type plant. Lastly, loss of *At*NOT4s could be interfering with growth-related signalling pathways dependent on *At*TOR. Even with heightened *At*TOR activity observed in *Atnot4* mutants, it is possible that these pathways are no longer fully functional and leading to a transcriptomic profile that resembles inhibited *At*TOR signalling activity. In essence, *At*TOR is "on," but its signals are not being correctly processed or executed, resulting in a phenotype and transcriptome that resemble *At*TOR inhibition. Notably, while the downregulated DEGs in *Atnot4abc* and AZD-treated Col-0 show significant overlap, the upregulated DEGs in these comparisons do not exhibit a similar pattern of convergence

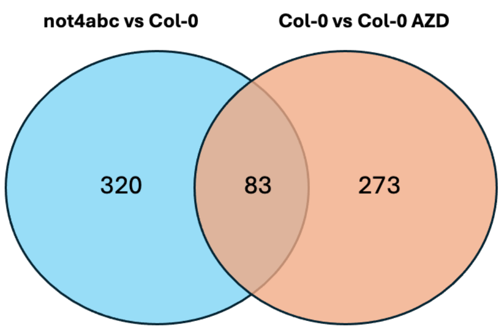

Figure 61 – Venn diagram comparing DEGs of untreated not4abc vs AZD treated Col-0. The figure highlights the differentially expressed genes shared and unique to untreated not4abc and AZD-treated Col-0.

Figure 62: Comparison of GO Terms between untreated *Atnot4abc* and Col-0 Treated with 1 µM AZD8055. The figure highlights the GO terms shared across the two genotypes and experimental conditions. The gene ratio is depicted on the x-axis while the y-axis lists the GO term. The size of the dot corresponds to the number of significant genes while the colour determines statistical significance (-log10(p-value).

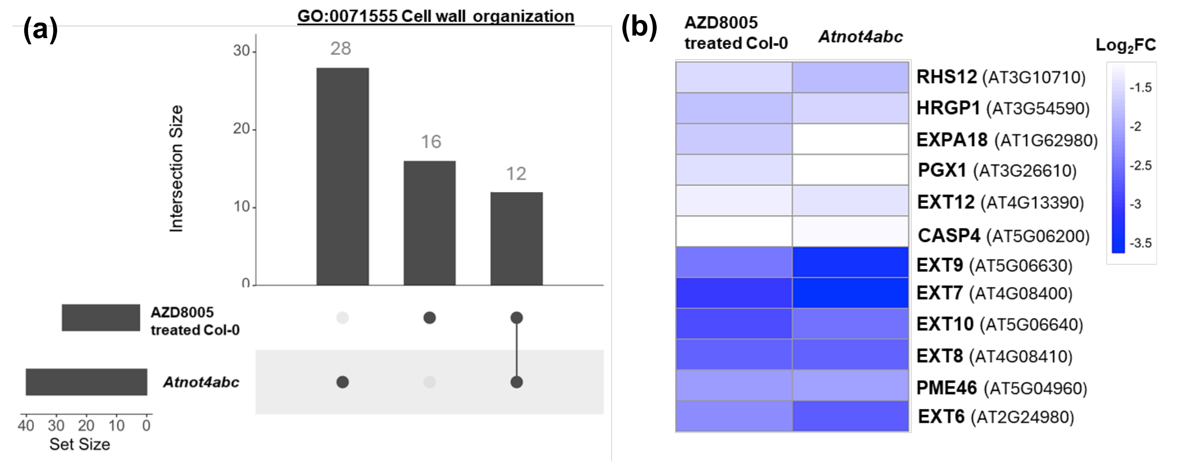

Figure 63 - GO term: Cell wall organisation analysis between AZD8055 Treated Col-0 and *Atnot4abc*. (a) UpSet plot illustrates the overlap of downregulated expressed genes associated to GO term: "Cell wall organisation" between 1 µM AZD8005 treated Col-0 and *Atnot4abc*. The bar chart on the left shows the total number of DEGs in each condition. Dot chart on the right shows the intersection for each overlap combination. **(b)** Heatmap displaying log_2foldchange (Log_2FC) mean values of shared genes related to in GO term "Cell wall organisation". The darker the blue colour, the smaller the Log_2FC value of the associated gene.

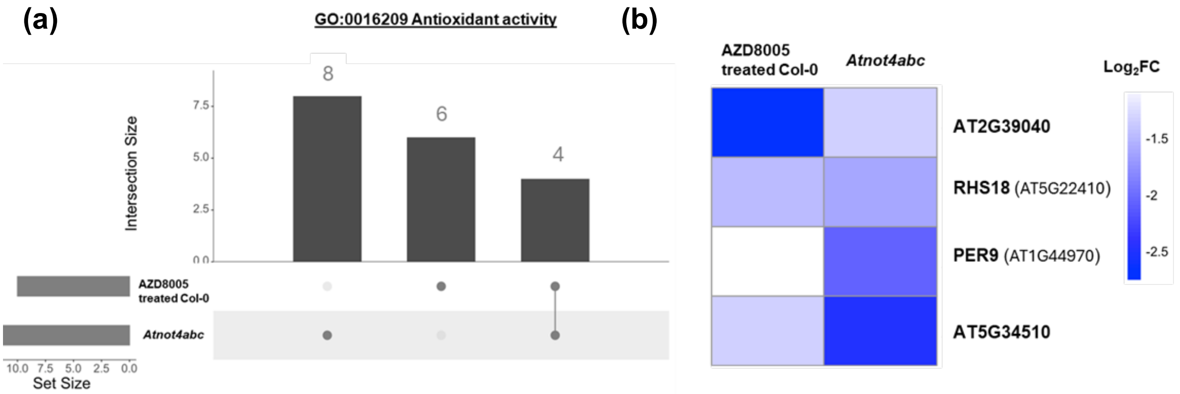

Figure 64 - GO term: Antioxidant activity gene analysis between AZD8055 Treated Col-0 and *Atnot4abc*. (a) UpSet plot illustrates the overlap of downregulated expressed genes (DEGs) between associated to GO term: Antioxidant activity between 1 µM AZD8055 treated Col-0 and *Atnot4abc*. The bar chart on the left shows the total number of DEGs in each condition. Dot chart on the right shows the intersection for each overlap combination. **(b)** Heatmap displaying log_2foldchange (Log_2FC) mean values of shared genes related to in GO term "Antioxidant activity". The darker the blue colour, the smaller the Log_2FC value of the associated gene.

5.7 Discussion

This chapter presented evidence of *At*NOT4s involvement in *At*TOR signalling. Specifically, *Atnot4a* and *Atnot4c* have increased basal *At*TOR activity which suggests a predisposition towards maintaining higher levels of protein synthesis and growth-related processes, driven by *At*TOR signalling. *At*TOR signalling activity is known to directly correlate to the enhancement of mRNA translation, specifically inducing ribosomal proteins and components required for protein synthesis. Despite such upregulation, *Atnot4a* mutants are known for its smaller seedling size compared to Col-0 under normal growth conditions (*see Chapter 3 Section 3.3*), which would seem to contradict the expected outcomes from enhanced *At*TOR activity. This paradoxical observation is likely to be a consequence of dysregulation in *At*TOR-dependent or *At*TOR-independent pathways. While *At*TOR signalling is hyperactivated, its downstream translational machinery or some other important growth-related processes may be defective. This could arise as a consequence of faults in co-translational quality control, a function attributed to *At*NOT4s. The imbalances in other signalling networks that influence growth could also contribute to this phenotype, whereby the hyperactivated *At*TOR pathway does not necessarily translate into effective growth promotion.

The phosphorylation landscape of the *At*NOT4 proteins, and more precisely the confirmed *At*TOR-dependent phosphorylation at S888 on *At*NOT4A, underlines their role as a putative regulator within the *At*TOR signalling network. The post translation modification analysis of *At*NOT4 proteins emphasised various modifications with predominance of phosphorylation sites. This suggests that *At*NOT4s are highly regulated through multiple signalling inputs. The extensive phosphorylation may reflect a mechanism by which *At*TOR exerts a degree of control over co-translational quality control and other cellular processes governed by *At*NOT4s. Though, *At*NOT4B has not been confirmed to be phosphorylated by *At*TOR, it does interact directly with *At*TORC which emphasises a unique role for *At*NOT4B. Sustaining overall proteostasis and ensuring proper translation may depend on *At*TOR's phosphorylation of *At*NOT4A due to the increased basal *At*TOR signalling activity in *Atnot4a*. On the other hand, *At*NOT4B may operate more as a facilitator than a direct effector in *At*TOR activity due to its direct interaction, and equal basal *At*TOR activity to Col-0. Therefore, the lack of elevated *At*TOR activity in *Atnot4b* mutants may be a direct result attributed to the absence of its direct phosphorylation by *At*TOR as seen with *At*NOT4A. The role of *At*NOT4C in the dynamic AtTOR signalling network remains questionable. The comparable *At*TOR molecular profile in terms of sensitivity to *At*TOR inhibition and altered *At*TOR signalling activity, infers a role of *At*NOT4C that functions similarly to *At*NOT4A. Thus, the specific roles of the *At*NOT4s within the *At*TOR signalling pathways seem partly determined by their phosphorylation status.

The addition of sucrose negated the growth phenotype in *Atnot4a* mutants (*see Chapter 3 Section 3.3*). The supplementation of an external energy source seems to compensate for some of the underlying defects in *Atnot4a*-related mutants. Besides being an energy source, sucrose also acts as a signalling molecule that stimulates *At*TOR activity (*see Chapter 1 Section 1.6.3.3*). Though, the phenotypic rescue by sucrose might not be attributed solely to further *At*TOR activation, given that the steady-state *At*TOR activity is already elevated. In fact, sucrose may influence other downstream or parallel pathways which are required for growth. The phenotype of *Atnot4a* mutants under normal conditions may reflect a critical energy-dependent regulation of growth. The supplementation of sucrose likely provides the energy or metabolic intermediates necessary for components in the *At*TOR signalling network to work more efficiently again, and bypassing the repression created by loss of function in *At*NOT4A. Sucrose addition appears to enable *Atnot4a* mutants to overcome limitations imposed under normal conditions which stunts their growth.

The unique sensitivity of *Atnot4b* to the S6K kinase inhibitor Pf4708761 and its lack of elevated basal *At*TOR activity, contrasted with *Atnot4a* and *Atnot4c*. This suggests that *At*NOT4B plays a specialized role within the *At*TOR signalling pathways, potentially in relation to *At*S6K1/2-mediated processes. This observation raises several questions concerning specific functions and interactions of *At*NOT4B. The physical interaction of *At*NOT4B with *At*LST8-1, a central member of the *At*TORC, implies that *At*NOT4B might be necessary for efficient phosphorylation and activation of*At*S6K1/2. It is possible that *At*NOT4B's role in the *At*TOR pathway is more closely tied to maintaining the structural integrity or functional specificity of the *At*TORC. *At*NOT4B may act as a scaffold or chaperone in the proper assembly or spatial orientation of the *At*TOR complex, and specifically when it comes to the activation of *At*S6K1/2. Such functions have been described for other E3 ligases such as *At*RNF8 central role in DNA damage response (Mailand et al. 2009). Beyond its ubiquitin ligase activity, *At*RNF8 facilitates the assembly of DNA repair complexes at sites of DNA double-strand breaks (DSBs). Upon DNA damage, *At*RNF8 is rapidly recruited to DSB sites through its interaction with *At*MDC1, which is phosphorylated by *At*ATM kinase. The *At*RNF8 acts therefore as scaffold, promoting the retention and assembly of key repair proteins such as *At*53BP1 and *At*BRCA1 at damage sites. The scaffolding serves to keep the repair machinery in the correct spatial orientation so that DNA repair can occur in an efficient and error-free manner. This can be directly related to *At*NOT4Bs interaction with *At*LST8-1 in stabilising and organising the assembly of *At*TORC. *At*NOT4B may also recruit other auxiliary proteins to facilitate this process, similar to the way *At*RNF8 recruits the repair proteins to ensure the integrity of the DNA repair process.

A deeper insight into the molecular basis underlying the sensitivity of *Atnot4abc* to TOR inhibitors was revealed through transcriptomic analysis of both Col-0 and *Atnot4abc* mutants under *At*TOR inhibition. The transcriptomic profile of untreated *Atnot4abc* resembles that of a 1 μM AZD8055 treated wild-type. Even though *Atnot4abc* has hyperactive *At*TOR signalling activity, this paradoxical result suggests that many downstream processes of the *At*TOR signalling network may not be fully operational in the absence of *At*NOT4 proteins, leading to an ineffective translation of *At*TOR's growth-promoting signals. For example, the strong downregulation of the cell wall organization, oxidative response, and ribosome biogenesis-related genes in *Atnot4abc* mutants after AZD treatment is among the most notable findings within the RNA-seq data. These processes are generally important to maintain cellular growth and integrity, and their suppression is coherent with the stunted growth phenotype.

DEGs associated to ribosome biogenesis and translation are upregulated in untreated *Atnot4abc*. Despite this upregulation, *Atnot4abc* still functions in a compromised cellular state because of other dysregulations in critical pathways. The overactivation of ribosome biogenesis and translation genes could be the reason why *Atnot4abc* is highly sensitive to further disturbance, specifically in the context of *At*TOR inhibition. The inhibition of such an influential kinase might exacerbate an imbalance in cellular homeostasis, resulting in a rapid and severe suppression of growth-related processes and an explanation of their heightened sensitivity to *At*TOR inhibitors. Further supporting this is that these GO terms were significantly downregulated upon 1 μM AZD8055 treated *Atnot4abc*.

It is likely from the presented data that *At*NOT4s operate in conjunction with *At*TOR in co-translational quality control to regulate growth and stress responses. *At*NOT4s are hypothesised to act as surveillance units during co-translational quality control to ensure mRNA and translational fidelity by removing aberrant proteins when they emerge from the ribosome. Not only is proteostasis compromised in the absence of *At*NOT4s but it also seems to destabilize broader *At*TOR-dependent pathways critical for cellular growth and stress response. These findings provide a better understanding of the complex regulatory networks that govern plant growth and stress responses, emphasizing the crucial balance between signalling inputs, translation quality, and their proper execution in maintaining cellular homeostasis, proteostasis, and development.

Chapter 6 – General Discussion

6.1 Introduction

The research undertaken in this doctorate study was intended to extend our knowledge on the NOT4 E3 ligases in *Arabidopsis* with regards to their function in co-translational quality control and their functional relation to *At*TOR kinase.

The evolutionary conservation between *At*NOT4s and their yeast counterpart *Sc*NOT4, with analysis of their expression patterns (*see Section 3.3.2.1*) and specific attention to the growth phenotypes of single and combination mutants (*see Section 3.3*), were highlighted in Chapter 3. Here, an RNA seq analysis revealed a significant upregulation of genes linked to GO terms such as ‘translation’ and ‘ribosome biogenesis’ in *Atnot4abc* mutants (*see Section 3.4*), suggesting a role for *At*NOT4s in translational regulation. These findings were further expanded on in Chapter 4, which revealed that *Atnot4abc* has increased global translation rates (*see Section 4.2*), an aggregation of polyubiquitinated conjugates (*see Section 4.3*), and is hypersensitive to tunicamycin (*see Section 4.4*). Together, these results suggest an important role for *At*NOT4s in co-translational quality control, ensuring that nascent proteins are properly folded and degraded when defective. The experiments also suggested that *At*NOT4s influence the unfolded protein response (UPR) under stress conditions (*see Section 4.5*). The final results Chapter 5 focused on the functional interplay between *At*NOT4s and *At*TOR signalling, following evidence of *At*NOT4A and *At*NOT4B being direct targets of *At*TOR-dependent phosphorylation and interaction, respectively. Here, it was revealed that *Atnot4* mutants have elevated basal TOR activity, and that they are differentially sensitive to TOR inhibition when considering kinase activity, transcriptional changes, and plant growth (*see Section 5.6*). Thus, identifying them as important and new regulatory components in the *At*TOR signalling cascade.

A broader discussion on the role of *At*NOT4s in translation, likely as part of a co-translational quality control mechanism, and their extended function in plant growth and stress adaptation via the *At*TOR-signalling pathway are outlined in the following sections.

6.2 Overview of *Arabidopsis* NOT4s and their Evolutionary Context

The single copy *Sc*NOT4 full-length sequence from yeast was utilized in reciprocal BLASTs to identify three putative homologs in *Arabidopsis*, namely *At*NOT4A, *At*NOT4B and *At*NOT4C (Collart & Struhl, 1994; Preissler et al., 2015). The three paralogs share high identity with *Sc*NOT4, specifically across the RING and RRM domains. The presence of three *At*NOT4 paralogs in *Arabidopsis* compared to the single copy in yeast and humans (Dai et al., 2021) raises intriguing evolutionary questions. Perhaps the genetic expansion was a critical evolutionary innovation that allowed plants to more accurately and flexibly control mRNA and protein quality in various cellular and environment contexts. Moreover, each paralog might have come to perform divergent functions to handle specific aspects of basal and stress-responsive translation. The observation that there is strong feedback to upregulate *At*NOT4s when one or more is mutated implies some degree of redundancy, since it indicates, the cells are attempting to compensate for loss of function of one paralog by upregulating the expression of others. This supports the hypothesis that *At*NOT4s have some shared roles, but also likely evolved paralog-specific functions, especially during developmental stages or under abiotic or biotic stress. When analysing *At*NOT4 translational-GUS fusions, *At*NOT4A was primarily localized to the vascular tissues and emerging leaves in young seedlings (7 days old), which are areas of high protein turnover due to their rapid development (*see Section 3.3.2*). On the other hand, *AtNOT4B* and *AtNOT4C* were expressed more broadly in the cotyledons. These slight variations in protein expression patterns also indicate potential divergence of function across tissue types.

Phenotypic analysis of *Atnot4a* and higher order mutants showed reduced seedling and rosette size and delayed flowering under normal long day growth conditions (*see Section 3.3*), though the number of leaves during bolting remained the same as in Col-0 (*see Section 3.3*). This suggests that that the phenotype is not a developmental one *per se*, but instead is linked to slow growth, possibly as a result of reduced energy availability or metabolic capacity. The fact that sucrose supplementation restored growth similar to Col-0 (*see Section 3.3*) further supports this hypothesis. It may be of interest to repeat the flowering time experiment with the addition of sucrose. This could provide more insights by helping to understand whether the delayed flowering is a secondary effect of energy deprivation and/or utilisation. In contrast, *Atnot4b* and *Atnot4c* mutants did not show any obvious growth phenotype under normal conditions, which further supports the concept of paralog-specific functions.

The next point of discussion is *At*NOT4's role in regulating global translation. Due to supporting evidence of genetic redundancy among *At*NOT4 paralogs, it was essential to proceed with the triple mutant for such studies in order to fully investigate the impact on translation when all three AtNOT4s being absent.

6.3 *At*NOT4s Influence on Global Translation Rates

The observed upregulation of translation-associated genes in *Atnot4abc* (*see Section 3.4.2*) suggests that the loss of A*t*NOT4s disrupts normal translation processes, mirroring the known role of *Sc*NOT4 in mRNA decay and translation regulation in yeast (Collart, 2013a; Preissler et al., 2015). *Sc*NOT4 represses the expression of several ribosome-related proteins as well as translation initiation factors (Panasenko & Collart, 2012). This likely has extended to *At*NOT4s in *Arabidopsis* as evident by the upregulation of translation-associated genes in *Atnot4abc*, in particular the three initiation factors eIF1-5, eIF3 and eIF4B and other genes associated to 'ribosome biogenesis'. In yeast, the repression of these genes via *Sc*NOT4 function is responsible for reducing translation capacity in order for the cell to adapt appropriately to environmental stresses. This is done to conserve energy and allocate resources more effectively under nutrient-limited conditions (Azzouz, Panasenko, Deluen, et al., 2009; Collart, 2013a). This is interesting to consider within the context of *AtNOT4A*, as the phenotypic rescue of *Atnot4a's* slow growth upon sucrose supplementation may be indicative of an energy-regulation role. Thus, *At*NOT4A may function similarly to *Sc*NOT4 in that regard by modulating translation rates based on energy availability. This modulation may be affected when *At*NOT4s are disrupted leading to an increase of translation and ribosome biogenesis related genes. In support of this, the puromycin incorporation assay revealed faster global translation rates in *Atnot4abc* (*see Section 4.2*), which is likely a consequence of the increases in the translational machinery. In

Atnot4abc, the lack of this coordination likely results in excessive protein synthesis which can be partially alleviated by external energy supplementation. Further investigation of the *Atnot4abc* transcriptome and translation rates in response to sucrose supplementation may help to resolve this further.

Thus, the data presented indicate that *At*NOT4s may modulate protein synthesis according to metabolic cues. This is likely to be in tandem with other key regulators of cellular metabolism, such as the *At*TOR pathway, which is known to integrate nutrient availability and energy demand to regulate growth through protein synthesis (Schepetilnikov & Ryabova, 2018).

6.4 *At*NOT4s and *At*TOR Signalling

*At*NOT4A and *At*NOT4B were identified in a large scale phosphoproteomics study to be phosphorylated by *At*TOR and to directly interact with *At*TORC, respectively (Van Leene et al., 2019). Moreover, all three *At*NOT4s are reported to be highly phosphorylated at multiple serines (Willems et al., 2024). Based on this and given the links to protein translation and plant growth, it was important to consider the functional relationship between *At*NOT4s and the *At*TOR signalling pathway. Notably, this has not previously been explored in yeast and mammals.

A simple method of assessing *At*TOR signalling activity and its direct relation to ribosome biogenesis (and ultimately translation) is through monitoring the phosphorylation status of *At*RPS6A via the *At*TOR-*At*S6K-*At*RPS6 cascade. Increased levels of phosphorylated *At*RPS6A, which is indicative of elevated *At*TOR activity, were observed in *Atnot4a*, *Atnot4c* and higher order mutants, but not in the *Atnot4b* single mutant (*see Section 5.4*). This heightened activity correlates with the increased rates of translation observed in these mutants and may indicate a compensatory response to help maintain proper *At*TOR signalling in the absence of *At*NOT4 function. Considering the slow growth phenotype in *Atnot4a* within the context of elevated *At*TOR signalling – that normally would promote growth - it is possible that hyperactive *At*TOR activity is still unable to compensate for loss of NOT4 function, despite enhancing translation rates. This may be due to the fact that *At*NOT4s are themselves *At*TOR targets, and therefore suggests that they are required for normal TOR signalling. In support of this, *Atnot4a* and *Atnot4c* mutants displayed hypersensitivty to both AZD8055 and TORIN1 which further indicates a role of these *At*NOT4s in modulating proper *At*TOR signalling dynamics (*see Section 5.3.1*). The rapid dephosphorylation of *At*RPS6A upon *At*TOR inhibition (*see Section 5.4.3*) further emphasizes impaired *At*TOR regulation and signalling in the absence of *At*NOT4s. *Atnot4b*, on the other hand, responded similary to Col-0 upon direct TOR inhibitor treatment, but in contrast was relatively hypersensitive to more specific inhibition of the S6K branch of TOR signalling. This indicates that different *At*NOT4 paralogs may have different roles in the *At*TOR signalling network, which should be explored further.

Interestingly, a comparison of the downregulated genes in untreated *Atnot4abc* and *At*TOR-inhibited Col-0 plants revealed a significant overlap in transcriptomic profiles (*see Section 5.6.4.2*), suggesting that plants lacking *At*NOT4s have reduced *At*TOR signalling capacity relative to wild type. This was unexpected, since *Atnot4abc* mutants have increased basal *At*TOR activity and translation rates. This paradoxical finding may suggest that the cells are not able to sufficiently compensate for the loss of the *At*NOT4s, further supporting the hypothesis that *At*NOT4 activity is needed for fully functional *At*TOR signalling, and possibly providing another explanation for the mutant's increased sensitivity to TOR inhibitors and impaired growth despite having increased basal rates of *At*TOR activity.

The data presented in this thesis indicate that *At*NOT4s and *At*TOR may be working in tandem to regulate cellular energy management and metabolism. *At*NOT4s may be coordinating translation and driving growth dependent energy availability through their interaction with *At*TOR. This idea is supported by the fact that *At*TOR is a major cellular sensor and transducer of energy status. This hypothesis is further supported by the rescue of the slow growth phenotype upon sucrose supplementation. Interestingly however, the phosphorylation status of *At*RPS6A upon sucrose supplementation was similar in both *Atnot4a* and Col-0 (*see Section 3.3*) indicating that the capacity for *At*TOR activation in response to energy supply is not compromised in *Atnot4a*. This may be due to the maximal phosphorylation of *At*RPS6A being reached, beyond which no further increase can be elicited even in a mutant background like *Atnot4a*. Alternatively, it might be that phosphorylation of other TOR targets is affected, and this should be explored in the future.

It is important to consider that the growth retardation of *Atnot4* mutants may not be a direct result of the dysregulated *At*TOR signalling but could instead be due to wider metabolic inefficiencies. This is potentially supported by the presence of significantly down-regulated GO terms linked to carbohydrate, isoprenoid, terpenoid and phenylpropanoid signalling/metabolism in the *Atnot4abc* RNAseq (see Section 3.4.3). Interestingly, isoprenoids represent precursors for several plant hormones that include ABA, Gibberellin, brassinosteroids, and cytokinins. In its turn, terpenoids carry out a variety of basic functions in growth and development (Câmara et al., 2024). The application of external energy sources (e.g., sucrose) could potentially bypass these limitations. Another correlation can be made between the overexpression of translation-related genes in *Atnot4abc* and the known functions of the *At*TOR. Specifically, *At*TOR has been reported promoting ribosome biogenesis and translation (Chen et al., 2018; Schepetilnikov & Ryabova, 2018; Shahbazian, 2008). The increase in *At*TOR activity in *Atnot4abc* directly correlates with the increase in global translation rates, as evident by the puromycin incorporation assay (*see Chapter 4 Section 4.2*). Furthermore, a specific initiation factor (eIF4B) that was significantly upregulated in *Atnot4abc* is known to be transcriptionally induced and phosphorylated by *At*TOR (Dong et al., 2023).

Though it was verified that *At*NOT4B directly interacts with *At*LST8-1, a component of *At*TORC, its role in the *At*TOR signalling pathway remains in question. However, the sensitivity to the S6K inhibitor (*see Section 5.3.2*) hints towards a function in this specific pathway but further investigation needs to be conducted. While *At*NOT4A and *At*NOT4B were identified in the study by Van Leene et. al (2019), a direct link between *At*NOT4C and *At*TOR is yet to be established. However, since the *Atnot4c* single mutants have increased *At*TOR activity and hypersensitivity to TOR inhibition, the data presented in this thesis do indicate a functional role for this paralog in the *At*TOR signalling pathway, potentially similar to that of *At*NOT4A.

To further explore the mechanistic connections between *At*NOT4s and *At*TOR signalling and its influence on global translation, future experiments should aim to assess translation rates in *Atnot4* mutants under *At*TOR inhibition. Polysome profiling as well as a puromycin incorporation assay with seedlings treated with TOR inhibitors can provide more insights on the interplay between *At*NOT4s and *At*TOR on translation dynamics and efficiency. Additionally, generating phospho-dead or phosphor-mimic serine 888 variants, the confirmed site of *At*TOR-mediated phosphorylation in *At*NOT4A, would help further define whether the phenotypes observed are directly linked to *At*TOR signalling through *At*NOT4 . This would further our understanding of the significance of TOR-dependent phosphorylation in regulating roles of *At*NOT4s in energy utilization, translation and overall growth. Alternatively, taking advantage of TOR RNAi lines in combination *Atnot4* mutants would also provide a better understanding of the functional link between *At*NOT4s and *At*TOR.

It is also important to consider the (still putative) E3 ubiquitin ligase activity aspect of *At*NOT4s within the context *At*TOR signalling. The observed increase of phosphorylated *At*RPS6A in *Atnot4a* and *Atnot4c* mutants may suggest unregulated *At*RPS6A activity, thus raising the possibility that it may be a direct target for *At*NOT4-mediated ubiquitination. Though the total amount of *At*RPS6A in *Atnot4* mutants was comparable to Col-0, suggesting it is not a degradation target, *At*NOT4s may modulate its activation state rather than its total abundance. One hypothesis is that *At*NOT4-mediated ubiquitination could influence the interaction between *At*RPS6 and other components of the ribosome and translation machinery, ultimately impacting protein translation. *At*RPS6A contains a total of 10 ubiquitination sites (Willems et al., 2024). These are all possible target sites for *At*NOT4A and *At*NOT4C-mediated ubiquitination. It could be that when *At*NOT4A and *At*NOT4C are absent, this regulation is disrupted causing an accumulation of phosphorylated *At*RPS6A. This example is one of many proteins that may be affected due the functional absence of *At*NOT4-mediated ubiquitination.

6.5 *At*NOT4s in Co-translational Quality Control and Protein Ubiquitination

Similar to *Sc*NOT4, *At*NOT4s are hypothesised to play a role in co-translational quality control by either ensuring that proteins are folded correctly and/or that aberrant ones are degraded efficiently, thus preventing the accumulation of defective proteins. *At*NOT4s can tag such proteins with ubiquitin, which then signals their degradation through the 26S proteasome. Paradoxically, however, the disruption of all three *At*NOT4s led to an increase in total polyubiquitinated conjugates (*see Section 4.3*). This overaccumulation of polyubiquitinated conjugates was also reported in yeast studies where the deletion of *Sc*NOT4 led to an increase in ubiquitinated nascent chains (Duttler et al., 2013). This is rather counterintuitive as the loss of a ubiquitin ligase is expected to lead to a reduction in target ubiquitination. Instead, the increase in ubiquitinated nascent chains could be explained due to reduced translational quality control in the absence of *At*NOT4s, leading to the production of aberrant/misfolded nascent chains that are subsequently ubiquitinated by other downstream E3 ligases. Indeed this was previously shown for *Sc*NOT4, where other translation associated E3 ligases such as LTN1 were shown to account for increased nascent chain polyubiquitination when *Sc*NOT4 was knocked out (Duttler et al., 2013). With its RRM domain, it is tempting to speculate *At*NOT4s could serve dual functions during co-translation quality control by monitoring both mRNA and polypeptide chains, acting as part of an early surveillance module to clear defective mRNAs limit aberrant protein synthesis. The RRM could alternatively play an important role in anchoring *At*NOT4s to the ribosome to help it fulfil this co-translational function.

Another explanation for the accumulation of total polyubiquitinated conjugates and impaired overall proteostasis in *Atnot4abc* is linked to the increased translation rates. Removing the 'surveillance' activity of *At*NOT4s during translation may also lead to increased incorporation of errors into nascent chains. Furthermore, *Sc*NOT4 was shown to promote efficient proteasome assembly and maturation (Panasenko & Collart, 2011). Whilst this is yet to be explored in *Arabidopsis*, perhaps a similar proteasomal defect is present in *Atnot4abc,* and this could lead to increased levels of polyubiquitinated proteins. To resolve this, proteasome composition and activity should be monitored in *Atnot4* mutants.

Further supporting a role for *At*NOT4s in co-translational quality control for limiting aberrant protein production is the observed hypersensitivity of *Atnot4* mutants to protein misfolding elicitors and increased induction of the unfolded protein response. It was shown in yeast that *Sc*NOT4 deletion led to its hypersensitivity to misfolding agents such as AZC (Halter et al., 2014). This was mirrored using the alternative misfolding agent Tunicamycin in *Atnot4abc* mutants, where extreme growth inhibition and chlorosis was observed (*see Section 4.4*). Hypersensitivity to Tm and increased induction of UPR genes upon Tm stress is indicative of overall defects in proteostasis, likely due to an over accumulation of aberrant proteins stemming from decreased quality control. It can be rationalised that this hypersensitivity arises from already high levels of misfolded proteins in *Atnot4* mutants, and that the cells become overwhelmed upon further elicitation of protein misfolding.

To summarise, it is proposed that the combination of reduced mRNA translational fidelity, increased rates of translation, and potentially impaired proteasome assembly could all contribute to the accumulation of total polyubiquitinated conjugates.

6.6 Future Directions

The work in this thesis represents the first detailed investigation of NOT4 protein function in the plant kingdom, and opens many avenues for further exploration, particularly with respect to how plant NOT4s impact and regulate basal and stress-responsive translation. Several key findings were described, with *At*NOT4s having clear roles in regulating translational quality control, maintaining proteostasis, and modulating plant growth and development in accordance with energy availability, most likely through *At*TOR signalling. Indeed, the novel link to TOR signalling presented is of particular interest since this has not yet been described in any kingdom and provides a significant advance in our broader understanding of how NOT4s intersect with translational regulation.

The *At*NOT4s were mainly studied as individual units, however in yeast and mammals they are part of the CCR4-NOT complex, and this association remains unexplored in plants. While studies in yeast have shown that *Sc*NOT4 associated with the *Sc*NOT1 backbone of this complex (Schwenk et al., 2021), in humans it is known to form interactions with the CAF40 subunit, and can also act independently through monomeric functions (Preissler et al., 2015). Therefore, it will be important to investigate whether *At*NOT4s associate with putative *Arabidopsis* CCR4-NOT components, and whether this is constitutive or dynamic. Moreover, diverse ubiquitination targets for *Sc*NOT4 in yeast and CNOT4 in humans have been characterised (Mersman et al., 2009; Mulder et al., 2007; Panasenko & Collart, 2012), and their ubiquitination has been linked to proteasomal targeting and other regulatory roles. Whether these targets are conserved in the plant kingdom is currently unknown, but a concerted effort to identify *At*NOT4 targets would help to determine this and provide further insight into the functional parallels across kingdoms. Besides the identification of conserved targets, investigation into components of translational machinery as potential targets may be of interest, considering the fact that genes of ribosome biogenesis and translation are highly upregulated. Several initiation factors, elongation factors and ribosomal components could be substrate targets of *At*NOT4s. Therefore, determining whether *At*NOT4s ubiquitinate specific ribosomal or translation factors can further our understanding on how *At*NOT4s modulate translation. In addition to its RING domain, the presence of the RRM in *At*NOT4s suggests potential functional conservation of mRNA decay processes with *Sc*NOT4 (De Vleesschauwer et al., 2018). Future studies should include investigating *At*NOT4s direct role in degrading non-optimal mRNAs under normal and stress conditions. Co-translational decay of stalled mRNAs presents an important mechanism in which *At*NOT4s may regulate global mRNA turnover to ensure mRNA quality control and translation fidelity.

An exciting hypothesis is that *At*NOT4s may act as components of stress-responsive “translasomes”. The main purpose of these translasomes could be to integrate protein synthesis and degradation at the level of polypeptide synthesis. The co-localisation of ribosomes and proteasomes during translation may be essential for ensuring error-free protein synthesis, and it is tempting to speculate that *At*NOT4s could be part of such a complex, acting as functional bridges between the translation and degradation machineries that could be adaptive to stress. Whilst such translasomes remain hypothetical in plants, it is speculated that, like *Sc*NOT4, *At*NOT4s will physically associate with ribosomes, and this should be tested through polysome enrichment. Moreover, unpublished data from the Gibbs lab has shown that *At*NOT4A and *At*NOTC can both interact with a regulatory component of the proteasome in a yeast two hybrid assay, indicating that exploration of *in vivo* associations between *At*NOT4s and the proteasome should also be explored, and adding further credence to the concept of NOT4-containing translasomes.

Though there is some evidence of functional redundancy across the three *At*NOT4 paralogs, specific roles have also been hinted at. The paralog-specific roles may become more obvious under specific stress condition or developmental stages. Therefore, a deeper understanding of the particular and shared function of each paralog will further clarify whether *At*NOT4s have evolved for specialised functions that allow plants to adapt to varying environmental conditions. Ultimately, such studies can provide a molecular framework for future investigation in the manipulation of these co-translational quality control mechanisms, potentially impacting traits of agronomic significance.

Reference List

Akutsu, M., Dikic, I., & Bremm, A. (2016). Ubiquitin chain diversity at a glance. *Journal of cell science*, *129*(5), 875-880.

Al-Saharin, R., Hellmann, H., & Mooney, S. (2022). Plant E3 ligases and their role in abiotic stress response. *Cells*, *11*(5), 890.

Alarcon, C. M., Heitman, J., & Cardenas, M. E. (1999). Protein kinase activity and identification of a toxic effector domain of the target of rapamycin TOR proteins in yeast. *Molecular biology of the cell*, *10*(8), 2531-2546.

Albert, T. K., Hanzawa, H., Legtenberg, Y. I., de Ruwe, M. J., van den Heuvel, F. A., Collart, M. A., Boelens, R., & Timmers, H. T. M. (2002). Identification of a ubiquitin–protein ligase subunit within the CCR4–NOT transcription repressor complex. *The EMBO journal*, *21*(3), 355-364.

Alexa, A., & Rahnenfuhrer, J. (2010). topGO: enrichment analysis for gene ontology. *R package version*, *2*(0), 2010.

Amin, A. G., Jeong, S. W., Gillick, J. L., Sursal, T., Murali, R., Gandhi, C. D., & Jhanwar-Uniyal, M. (2021). Targeting the mTOR pathway using novel ATP-competitive inhibitors, Torin1, Torin2 and XL388, in the treatment of glioblastoma. *International journal of oncology*, *59*(4), 83.

Anderson, G. H., Veit, B., & Hanson, M. R. (2005). The Arabidopsis AtRaptor genes are essential for post-embryonic plant growth. *BMC biology*, *3*, 1-11.

Arae, T., Morita, K., Imahori, R., Suzuki, Y., Yasuda, S., Sato, T., Yamaguchi, J., & Chiba, Y. (2019). Identification of Arabidopsis CCR4-NOT complexes with pumilio RNA-binding proteins, APUM5 and APUM2. *Plant and Cell Physiology*, *60*(9), 2015-2025.

Aravind, L., & Koonin, E. V. (2000). The U box is a modified RING finger—a common domain in ubiquitination. *Current Biology*, *10*(4), R132-R134.

Assenholt, J., Mouaikel, J., Saguez, C., Rougemaille, M., Libri, D., & Jensen, T. H. (2011). Implication of Ccr4-Not complex function in mRNA quality control in Saccharomyces cerevisiae. *Rna*, *17*(10), 1788-1794.

Aviner, R. (2020). The science of puromycin: From studies of ribosome function to applications in biotechnology. *Computational and Structural Biotechnology Journal*, *18*, 1074-1083.

Azzouz, N., Panasenko, O. O., Colau, G., & Collart, M. A. (2009). The CCR4-NOT complex physically and functionally interacts with TRAMP and the nuclear exosome. *PLoS One*, *4*(8), e6760.

Azzouz, N., Panasenko, O. O., Deluen, C., Hsieh, J., Theiler, G., & Collart, M. A. (2009). Specific roles for the Ccr4-Not complex subunits in expression of the genome. *Rna*, *15*(3), 377-383.

Baena-González, E., & Sheen, J. (2008). Convergent energy and stress signaling. *Trends in plant science*, *13*(9), 474-482.

Baldwin, T. O. (1999). Protein folding in vivo: the importance of ribosomes. *Nature Cell Biology*, *1*(6), E154-E155.

Baliga, B., Cohen, S., & Munro, H. (1970). Effect of cycloheximide on the reaction of puromycin with polysome-bound peptidyl-tRNA. *FEBS letters*, *8*(5), 249-252.

Barrada, A., Djendli, M., Desnos, T., Mercier, R., Robaglia, C., Montané, M.-H., & Menand, B. (2019). A TOR-YAK1 signaling axis controls cell cycle, meristem activity and plant growth in Arabidopsis. *Development*, *146*(3), dev171298.

Basquin, J., Roudko, V. V., Rode, M., Basquin, C., Séraphin, B., & Conti, E. (2012). Architecture of the nuclease module of the yeast Ccr4-not complex: the Not1-Caf1-Ccr4 interaction. *Molecular cell*, *48*(2), 207-218.
Bassham, D. C., Laporte, M., Marty, F., Moriyasu, Y., Ohsumi, Y., Olsen, L. J., & Yoshimoto, K. (2006). Autophagy in development and stress responses of plants. *Autophagy*, *2*(1), 2-11.
Bengtson, M. H., & Joazeiro, C. A. (2010). Role of a ribosome-associated E3 ubiquitin ligase in protein quality control. *Nature*, *467*(7314), 470-473.
Benjamini, Y., & Hochberg, Y. (1995). Controlling the false discovery rate: a practical and powerful approach to multiple testing. *Journal of the Royal statistical society: series B (Methodological)*, *57*(1), 289-300.
Beretta, L., Gingras, A. C., Svitkin, Y. V., Hall, M. N., & Sonenberg, N. (1996). Rapamycin blocks the phosphorylation of 4E-BP1 and inhibits cap-dependent initiation of translation. *The EMBO journal*, *15*(3), 658-664.
Berndsen, C. E., & Wolberger, C. (2014). New insights into ubiquitin E3 ligase mechanism. *Nature structural & molecular biology*, *21*(4), 301-307.
Biratsi, A., Athanasopoulos, A., Kouvelis, V. N., Gournas, C., & Sophianopoulou, V. (2021). A highly conserved mechanism for the detoxification and assimilation of the toxic phytoproduct L-azetidine-2-carboxylic acid in Aspergillus nidulans. *Scientific Reports*, *11*(1), 7391.
Borden, K. L., & Freemont, P. S. (1996). The RING finger domain: a recent example of a sequence—structure family. *Current opinion in structural biology*, *6*(3), 395-401.
Boutilier, J. A. (1992). METEI: A Canadian medical expedition to Easter Island, 1964-65. *Rapa Nui Journal*, *6*(2), 21-44.
Brown, E. J., Albers, M. W., Bum Shin, T., Ichikawa, K., Keith, C. T., Lane, W. S., & Schreiber, S. L. (1994). A mammalian protein targeted by G1-arresting rapamycin–receptor complex. *Nature*, *369*(6483), 756-758.
Browning, K. S., & Bailey-Serres, J. (2015). Mechanism of cytoplasmic mRNA translation. *The Arabidopsis book/American Society of Plant Biologists*, *13*.
Brunkard, J. O. (2020). Exaptive evolution of target of rapamycin signaling in multicellular eukaryotes. *Developmental Cell*, *54*(2), 142-155.
Busche, M., Scarpin, M. R., Hnasko, R., & Brunkard, J. O. (2021). TOR coordinates nucleotide availability with ribosome biogenesis in plants. *The plant cell*, *33*(5), 1615-1632.
Cade, R. M., & Errede, B. (1994). MOT2 encodes a negative regulator of gene expression that affects basal expression of pheromone-responsive genes in Saccharomyces cerevisiae. *Molecular and cellular biology*, *14*(5), 3139-3149.
Cadwell, K., & Coscoy, L. (2005). Ubiquitination on nonlysine residues by a viral E3 ubiquitin ligase. *Science*, *309*(5731), 127-130.
Caldana, C., Li, Y., Leisse, A., Zhang, Y., Bartholomaeus, L., Fernie, A. R., Willmitzer, L., & Giavalisco, P. (2013). Systemic analysis of inducible target of rapamycin mutants reveal a general metabolic switch controlling growth in Arabidopsis thaliana. *Plant J*, *73*(6), 897-909. https://doi.org/10.1111/tpj.12080
Callis, J. (1995). Regulation of protein degradation. *The plant cell*, *7*(7), 845.
Callis, J. (2014). The ubiquitination machinery of the ubiquitin system. *The Arabidopsis book/American Society of Plant Biologists*, *12*.
Cao, P., Kim, S.-J., Xing, A., Schenck, C. A., Liu, L., Jiang, N., Wang, J., Last, R. L., & Brandizzi, F. (2019). Homeostasis of branched-chain amino acids is critical for the activity of TOR signaling in Arabidopsis. *Elife*, *8*, e50747.

Carter, C., & Houlihan, D. (2001). Protein synthesis. *Fish physiology*, *20*, 31-75.
Chapat, C., & Corbo, L. (2014). Novel roles of the CCR4–NOT complex. *Wiley Interdisciplinary Reviews: RNA*, *5*(6), 883-901.
Chauvin, C., Koka, V., Nouschi, A., Mieulet, V., Hoareau-Aveilla, C., Dreazen, A., Cagnard, N., Carpentier, W., Kiss, T., & Meyuhas, O. (2014). Ribosomal protein S6 kinase activity controls the ribosome biogenesis transcriptional program. *Oncogene*, *33*(4), 474-483.
Chen, G.-H., Liu, M.-J., Xiong, Y., Sheen, J., & Wu, S.-H. (2018). TOR and RPS6 transmit light signals to enhance protein translation in deetiolating Arabidopsis seedlings. *Proceedings of the National Academy of Sciences*, *115*(50), 12823-12828.
Chen, L., & Hellmann, H. (2013). Plant E3 ligases: flexible enzymes in a sessile world. *Molecular plant*, *6*(5), 1388-1404.
Cheng, C., Wang, Z., Ren, Z., Zhi, L., Yao, B., Su, C., Liu, L., & Li, X. (2017). SCFAtPP2-B11 modulates ABA signaling by facilitating SnRK2. 3 degradation in Arabidopsis thaliana. *PLoS Genetics*, *13*(8), e1006947.
Cheng, M.-C., Hsieh, E.-J., Chen, J.-H., Chen, H.-Y., & Lin, T.-P. (2012). Arabidopsis RGLG2, functioning as a RING E3 ligase, interacts with AtERF53 and negatively regulates the plant drought stress response. *Plant physiology*, *158*(1), 363-375.
Chiu, M. I., Katz, H., & Berlin, V. (1994). RAPT1, a mammalian homolog of yeast Tor, interacts with the FKBP12/rapamycin complex. *Proceedings of the National Academy of Sciences*, *91*(26), 12574-12578.
Cho, H., Banf, M., Shahzad, Z., Van Leene, J., Bossi, F., Ruffel, S., Bouain, N., Cao, P., Krouk, G., & De Jaeger, G. (2023). ARSK1 activates TORC1 signaling to adjust growth to phosphate availability in Arabidopsis. *Current Biology*, *33*(9), 1778-1786. e1775.
Chresta, C. M., Davies, B. R., Hickson, I., Harding, T., Cosulich, S., Critchlow, S. E., Vincent, J. P., Ellston, R., Jones, D., & Sini, P. (2010). AZD8055 is a potent, selective, and orally bioavailable ATP-competitive mammalian target of rapamycin kinase inhibitor with in vitro and in vivo antitumor activity. *Cancer research*, *70*(1), 288-298.
Ciechanover, A. (1994). The ubiquitin-proteasome proteolytic pathway. *Cell*, *79*(1), 13-21.
Ciechanover, A. (1998). The ubiquitin–proteasome pathway: on protein death and cell life. *The EMBO journal*.
Clague, M. J., & Urbé, S. (2010). Ubiquitin: same molecule, different degradation pathways. *Cell*, *143*(5), 682-685.
Clough, S. J., & Bent, A. F. (1998). Floral dip: a simplified method for Agrobacterium-mediated transformation of Arabidopsis thaliana. *The Plant Journal*, *16*(6), 735-743.
Collart, M. A. (2013a). The NOT4 RING E3 ligase: a relevant player in cotranslational quality control. *International Scholarly Research Notices*, *2013*.
Collart, M. A. (2013b). The NOT4 RING E3 ligase: a relevant player in cotranslational quality control. *International Scholarly Research Notices*, *2013*(1), 548359.
Collart, M. A., & Panasenko, O. O. (2012). The Ccr4–not complex. *Gene*, *492*(1), 42-53.
Collart, M. A., & Struhl, K. (1994). NOT1 (CDC39), NOT2 (CDC36), NOT3, and NOT4 encode a global-negative regulator of transcription that differentially affects TATA-element utilization. *Genes & development*, *8*(5), 525-537.

Couso, I., Pérez-Pérez, M. E., Ford, M. M., Martínez-Force, E., Hicks, L. M., Umen, J. G., & Crespo, J. L. (2020). Phosphorus availability regulates TORC1 signaling via LST8 in Chlamydomonas. *The plant cell*, *32*(1), 69-80.

Creff, A., Sormani, R., & Desnos, T. (2010). The two Arabidopsis RPS6 genes, encoding for cytoplasmic ribosomal proteins S6, are functionally equivalent. *Plant molecular biology*, *73*, 533-546.

Crespo, J. L., Díaz-Troya, S., & Florencio, F. J. (2005). Inhibition of target of rapamycin signaling by rapamycin in the unicellular green alga Chlamydomonas reinhardtii. *Plant physiology*, *139*(4), 1736-1749.

Cruz, M. C., Cavallo, L. M., Görlach, J. M., Cox, G., Perfect, J. R., Cardenas, M. E., & Heitman, J. (1999). Rapamycin antifungal action is mediated via conserved complexes with FKBP12 and TOR kinase homologs in Cryptococcus neoformans. *Molecular and cellular biology*, *19*(6), 4101-4112.

Curtis, M. J., Belcram, K., Bollmann, S. R., Tominey, C. M., Hoffman, P. D., Mercier, R., & Hays, J. B. (2009). Reciprocal chromosome translocation associated with TDNA-insertion mutation in Arabidopsis: genetic and cytological analyses of consequences for gametophyte development and for construction of doubly mutant lines. *Planta*, *229*, 731-745.

Dai, X. X., Jiang, Y., Gu, J. H., Jiang, Z. Y., Wu, Y. W., Yu, C., Yin, H., Zhang, J., Shi, Q. H., & Shen, L. (2021). The CNOT4 subunit of the CCR4-NOT complex is involved in mRNA degradation, efficient DNA damage repair, and XY chromosome crossover during male germ cell meiosis. *Advanced Science*, *8*(10), 2003636.

Davarinejad, H. (2015). Quantifications of western blots with ImageJ. *University of York*.

De Vleesschauwer, D., Filipe, O., Hoffman, G., Seifi, H. S., Haeck, A., Canlas, P., Van Bockhaven, J., De Waele, E., Demeestere, K., & Ronald, P. (2018). Target of rapamycin signaling orchestrates growth–defense trade-offs in plants. *New Phytologist*, *217*(1), 305-319.

Deprost, D., Truong, H. N., Robaglia, C., & Meyer, C. (2005). An Arabidopsis homolog of RAPTOR/KOG1 is essential for early embryo development. *Biochem Biophys Res Commun*, *326*(4), 844-850. https://doi.org/10.1016/j.bbrc.2004.11.117

Dezfulian, M. H., Jalili, E., Roberto, D. K. A., Moss, B. L., Khoo, K., Nemhauser, J. L., & Crosby, W. L. (2016). Oligomerization of SCFTIR1 is essential for Aux/IAA degradation and auxin signaling in Arabidopsis. *PLoS Genetics*, *12*(9), e1006301.

Díaz-Troya, S., Florencio, F. J., & Crespo, J. L. (2008). Target of rapamycin and LST8 proteins associate with membranes from the endoplasmic reticulum in the unicellular green alga Chlamydomonas reinhardtii. *Eukaryotic Cell*, *7*(2), 212-222.

Dice, J. F. (2007). Chaperone-mediated autophagy. *Autophagy*, *3*(4), 295-299.

Diehl, J. A., Zindy, F., & Sherr, C. J. (1997). Inhibition of cyclin D1 phosphorylation on threonine-286 prevents its rapid degradation via the ubiquitin-proteasome pathway. *Genes & development*, *11*(8), 957-972.

Dikic, I., & Schulman, B. A. (2023). An expanded lexicon for the ubiquitin code. *Nature reviews Molecular cell biology*, *24*(4), 273-287.

Dimitrova, L. N., Kuroha, K., Tatematsu, T., & Inada, T. (2009). Nascent peptide-dependent translation arrest leads to Not4p-mediated protein degradation by the proteasome. *Journal of Biological Chemistry*, *284*(16), 10343-10352.

Dinkova, T. D., De La Cruz, H. R., García-Flores, C., Aguilar, R., Jiménez-García, L. F., & De Jiménez, E. S. (2007). Dissecting the TOR–S6K signal transduction pathway in maize seedlings: relevance on cell growth regulation. *Physiologia Plantarum*, *130*(1), 1-10.
Dobrenel, T., Caldana, C., Hanson, J., Robaglia, C., Vincentz, M., Veit, B., & Meyer, C. (2016). TOR signaling and nutrient sensing. *Annual review of plant biology*, *67*, 261-285.
Dobrenel, T., Kushwah, S., Mubeen, U., Jansen, W., Delhomme, N., Caldana, C., & Hanson, J. (2021). The phosphate starvation response recruits the TOR pathway to regulate growth in Arabidopsis cell cultures. *bioRxiv*, 2021.2003. 2026.437164.
Dobrenel, T., Mancera-Martinez, E., Forzani, C., Azzopardi, M., Davanture, M., Moreau, M., Schepetilnikov, M., Chicher, J., Langella, O., & Zivy, M. (2016). The Arabidopsis TOR kinase specifically regulates the expression of nuclear genes coding for plastidic ribosomal proteins and the phosphorylation of the cytosolic ribosomal protein S6. *Frontiers in plant science*, *7*, 1611.
Dong, P., Xiong, F., Que, Y., Wang, K., Yu, L., Li, Z., & Ren, M. (2015). Expression profiling and functional analysis reveals that TOR is a key player in regulating photosynthesis and phytohormone signaling pathways in Arabidopsis. *Frontiers in plant science*, *6*, 677.
Dong, Y., Aref, R., Forieri, I., Schiel, D., Leemhuis, W., Meyer, C., Hell, R., & Wirtz, M. (2022). The plant TOR kinase tunes autophagy and meristem activity for nutrient stress-induced developmental plasticity. *The plant cell*, *34*(10), 3814-3829.
Dong, Y., Srour, O., Lukhovitskaya, N., Makarian, J., Baumberger, N., Galzitskaya, O., Elser, D., Schepetilnikov, M., & Ryabova, L. A. (2023). Functional analogs of mammalian 4E-BPs reveal a role for TOR in global plant translation. *Cell Reports*, *42*(8).
Downes, B. P., Stupar, R. M., Gingerich, D. J., & Vierstra, R. D. (2003). The HECT ubiquitin-protein ligase (UPL) family in Arabidopsis: UPL3 has a specific role in trichome development. *The Plant Journal*, *35*(6), 729-742.
Duttler, S., Pechmann, S., & Frydman, J. (2013). Principles of cotranslational ubiquitination and quality control at the ribosome. *Molecular cell*, *50*(3), 379-393.
Düvel, K., Yecies, J. L., Menon, S., Raman, P., Lipovsky, A. I., Souza, A. L., Triantafellow, E., Ma, Q., Gorski, R., & Cleaver, S. (2010). Activation of a metabolic gene regulatory network downstream of mTOR complex 1. *Molecular cell*, *39*(2), 171-183.
Eisenhaber, B., Chumak, N., Eisenhaber, F., & Hauser, M.-T. (2007). The ring between ring fingers (RBR) protein family. *Genome biology*, *8*, 1-10.
Engelman, J. A., Luo, J., & Cantley, L. C. (2006). The evolution of phosphatidylinositol 3-kinases as regulators of growth and metabolism. *Nature Reviews Genetics*, *7*(8), 606-619.
Etherington, R. D. (2022). *Functional analysis of Arabidopsis DOA10-like E3 ligases* University of Birmingham].
Etherington, R. D., Bailey, M., Boyer, J.-B., Armbruster, L., Cao, X., Coates, J. C., Meinnel, T., Wirtz, M., Giglione, C., & Gibbs, D. J. (2023). Nt-acetylation-independent turnover of SQUALENE EPOXIDASE 1 by Arabidopsis DOA10-like E3 ligases. *Plant physiology*, *193*(3), 2086-2104.

Feng, Y., He, D., Yao, Z., & Klionsky, D. J. (2014). The machinery of macroautophagy. *Cell research*, *24*(1), 24-41.
Figura, K. v., & Hasilik, A. (1986). Lysosomal enzymes and their receptors.
Frias, M. A., Thoreen, C. C., Jaffe, J. D., Schroder, W., Sculley, T., Carr, S. A., & Sabatini, D. M. (2006). mSin1 is necessary for Akt/PKB phosphorylation, and its isoforms define three distinct mTORC2s. *Current Biology*, *16*(18), 1865-1870.
Fu, L., Wang, P., & Xiong, Y. (2020). Target of rapamycin signaling in plant stress responses. *Plant physiology*, *182*(4), 1613-1623.
Furniss, J. J., Grey, H., Wang, Z., Nomoto, M., Jackson, L., Tada, Y., & Spoel, S. H. (2018). Proteasome-associated HECT-type ubiquitin ligase activity is required for plant immunity. *PLoS pathogens*, *14*(11), e1007447.
Gallie, D. R., & Browning, K. S. (2001). eIF4G functionally differs from eIFiso4G in promoting internal initiation, cap-independent translation, and translation of structured mRNAs. *Journal of Biological Chemistry*, *276*(40), 36951-36960.
Garzón, M., Eifler, K., Faust, A., Scheel, H., Hofmann, K., Koncz, C., Yephremov, A., & Bachmair, A. (2007). PRT6/At5g02310 encodes an Arabidopsis ubiquitin ligase of the N-end rule pathway with arginine specificity and is not the CER3 locus. *FEBS letters*, *581*(17), 3189-3196.
Gibbs, D. J., Bacardit, J., Bachmair, A., & Holdsworth, M. J. (2014). The eukaryotic N-end rule pathway: conserved mechanisms and diverse functions. *Trends in Cell Biology*, *24*(10), 603-611.
Glickman, M. H., & Ciechanover, A. (2002). The ubiquitin-proteasome proteolytic pathway: destruction for the sake of construction. *Physiological reviews*.
Grau-Bove, X., Sebé-Pedrós, A., & Ruiz-Trillo, I. (2013). A genomic survey of HECT ubiquitin ligases in eukaryotes reveals independent expansions of the HECT system in several lineages. *Genome biology and evolution*, *5*(5), 833-847.
Gulshan, K., Thommandru, B., & Moye-Rowley, W. S. (2012). Proteolytic degradation of the Yap1 transcription factor is regulated by subcellular localization and the E3 ubiquitin ligase Not4. *Journal of Biological Chemistry*, *287*(32), 26796-26805.
Halter, D., Collart, M. A., & Panasenko, O. O. (2014). The Not4 E3 ligase and CCR4 deadenylase play distinct roles in protein quality control. *PLoS One*, *9*(1), e86218.
Hanzawa, H., de Ruwe, M. J., Albert, T. K., van der Vliet, P. C., Timmers, H. M., & Boelens, R. (2001). The Structure of the C4C4RING finger of human NOT4 reveals features distinct from those of C3HC4 RING fingers. *Journal of Biological Chemistry*, *276*(13), 10185-10190.
Haq, S. I. U., Shang, J., Xie, H., & Qiu, Q.-S. (2022). Roles of TOR signaling in nutrient deprivation and abiotic stress. *Journal of Plant Physiology*, *274*, 153716.
Heitman, J., Movva, N. R., & Hall, M. N. (1991). Targets for cell cycle arrest by the immunosuppressant rapamycin in yeast. *Science*, *253*(5022), 905-909.
Herath, V., Gayral, M., Adhikari, N., Miller, R., & Verchot, J. (2020). Genome-wide identification and characterization of Solanum tuberosum BiP genes reveal the role of the promoter architecture in BiP gene diversity. *Scientific Reports*, *10*(1), 11327.
Hershko, A., & Ciechanover, A. (1998). The ubiquitin system. *Annual review of biochemistry*, *67*(1), 425-479.

Heyninck, K., Kreike, M. M., & Beyaert, R. (2003). Structure–function analysis of the A20-binding inhibitor of NF-κB activation, ABIN-1. *FEBS letters*, *536*(1-3), 135-140.
Hicke, L., Zanolari, B., & Riezman, H. (1998). Cytoplasmic tail phosphorylation of the alpha-factor receptor is required for its ubiquitination and internalization. *J Cell Biol*, *141*(2), 349-358. https://doi.org/10.1083/jcb.141.2.349
Hinnebusch, A. G. (2014). The scanning mechanism of eukaryotic translation initiation. *Annual review of biochemistry*, *83*, 779-812.
Holz, M. K., Ballif, B. A., Gygi, S. P., & Blenis, J. (2005). mTOR and S6K1 mediate assembly of the translation preinitiation complex through dynamic protein interchange and ordered phosphorylation events. *Cell*, *123*(4), 569-580.
Hope, I., & Struhl, K. (1987). GCN4, a eukaryotic transcriptional activator protein, binds as a dimer to target DNA. *The EMBO journal*, *6*(9), 2781-2784.
Horman, S., Browne, G. J., Krause, U., Patel, J. V., Vertommen, D., Bertrand, L., Lavoinne, A., Hue, L., Proud, C. G., & Rider, M. H. (2002). Activation of AMP-activated protein kinase leads to the phosphorylation of elongation factor 2 and an inhibition of protein synthesis. *Current Biology*, *12*(16), 1419-1423.
Hou, Y., Guo, X., Cyprys, P., Zhang, Y., Bleckmann, A., Cai, L., Huang, Q., Luo, Y., Gu, H., & Dresselhaus, T. (2016). Maternal ENODLs are required for pollen tube reception in Arabidopsis. *Current Biology*, *26*(17), 2343-2350.
Houlihan, D., Carter, C., & McCarthy, I. (1995). Protein synthesis in fish. In *Biochemistry and molecular biology of fishes* (Vol. 4, pp. 191-220). Elsevier.
Hüttner, S., Veit, C., Schoberer, J., Grass, J., & Strasser, R. (2012). Unraveling the function of Arabidopsis thaliana OS9 in the endoplasmic reticulum-associated degradation of glycoproteins. *Plant molecular biology*, *79*, 21-33.
Iadevaia, V., Liu, R., & Proud, C. G. (2014). mTORC1 signaling controls multiple steps in ribosome biogenesis. Seminars in cell & developmental biology,
Ingargiola, C., Jehanno, I., Forzani, C., Marmagne, A., Broutin, J., Clement, G., Leprince, A. S., & Meyer, C. (2023). The Arabidopsis Target of Rapamycin kinase regulates ammonium assimilation and glutamine metabolism. *Plant Physiol*, *192*(4), 2943-2957. https://doi.org/10.1093/plphys/kiad216
Ingargiola, C., Turqueto Duarte, G., Robaglia, C., Leprince, A.-S., & Meyer, C. (2020). The plant target of rapamycin: a conduc TOR of nutrition and metabolism in photosynthetic organisms. *Genes*, *11*(11), 1285.
Jacinto, E., Loewith, R., Schmidt, A., Lin, S., Rüegg, M. A., Hall, A., & Hall, M. N. (2004). Mammalian TOR complex 2 controls the actin cytoskeleton and is rapamycin insensitive. *Nature Cell Biology*, *6*(11), 1122-1128.
Jackson, R. J., Hellen, C. U., & Pestova, T. V. (2010). The mechanism of eukaryotic translation initiation and principles of its regulation. *Nature reviews Molecular cell biology*, *11*(2), 113-127.
Jia, J.-J., Lahr, R. M., Solgaard, M. T., Moraes, B. J., Pointet, R., Yang, A.-D., Celucci, G., Graber, T. E., Hoang, H.-D., & Niklaus, M. R. (2021). mTORC1 promotes TOP mRNA translation through site-specific phosphorylation of LARP1. *Nucleic acids research*, *49*(6), 3461-3489.
Jiang, X., Feng, S., Chen, Y., Feng, Y., & Deng, H. (2016). Proteomic analysis of mTOR inhibition-mediated phosphorylation changes in ribosomal proteins and eukaryotic translation initiation factors. *Protein & Cell*, *7*(7), 533-537.
Jung, C. H., Jun, C. B., Ro, S.-H., Kim, Y.-M., Otto, N. M., Cao, J., Kundu, M., & Kim, D.-H. (2009). ULK-Atg13-FIP200 complexes mediate mTOR signaling to the autophagy machinery. *Molecular biology of the cell*, *20*(7), 1992-2003.

Jyothishwaran, G., Kotresha, D., Selvaraj, T., Srideshikan, S., Rajvanshi, P., & Jayabaskaran, C. (2007). A modified freeze–thaw method for efficient transformation of Agrobacterium tumefaciens. *Current science*, *93*(6), 770-772.
Kanehisa, M., & Goto, S. (2012). KEGG: Kyoto encyclopedia of genes and genomes. *Kanehisa laboratories*.
Kapp, L. D., & Lorsch, J. R. (2004). The molecular mechanics of eukaryotic translation. *Annual review of biochemistry*, *73*(1), 657-704.
Kelley, D. R. (2018). E3 ubiquitin ligases: key regulators of hormone signaling in plants. *Molecular & Cellular Proteomics*, *17*(6), 1047-1054.
Kelsall, I. R., Zhang, J., Knebel, A., Arthur, J. S. C., & Cohen, P. (2019). The E3 ligase HOIL-1 catalyses ester bond formation between ubiquitin and components of the Myddosome in mammalian cells. *Proceedings of the National Academy of Sciences*, *116*(27), 13293-13298.
Kim, J., & Guan, K.-L. (2019). mTOR as a central hub of nutrient signalling and cell growth. *Nature Cell Biology*, *21*(1), 63-71.
Kim, L. C., Cook, R. S., & Chen, J. (2017). mTORC1 and mTORC2 in cancer and the tumor microenvironment. *Oncogene*, *36*(16), 2191-2201.
Kim, S. T., Kim, S. G., Agrawal, G. K., Kikuchi, S., & Rakwal, R. (2014). Rice proteomics: a model system for crop improvement and food security. *Proteomics*, *14*(4-5), 593-610.
Klein, A. M., de Queiroz, R. M., Venkatesh, D., & Prives, C. (2021). The roles and regulation of MDM2 and MDMX: it is not just about p53. *Genes & development*, *35*(9-10), 575-601.
Komander, D., & Rape, M. (2012). The ubiquitin code. *Annual review of biochemistry*, *81*, 203-229.
Konigsberg, W. (1972). [13] Reduction of disulfide bonds in proteins with dithiothreitol. In *Methods in enzymology* (Vol. 25, pp. 185-188). Elsevier.
Kornitzer, D., Raboy, B., Kulka, R., & Fink, G. (1994). Regulated degradation of the transcription factor Gcn4. *The EMBO journal*, *13*(24), 6021-6030.
Kraft, E., Stone, S. L., Ma, L., Su, N., Gao, Y., Lau, O.-S., Deng, X.-W., & Callis, J. (2005). Genome analysis and functional characterization of the E2 and RING-type E3 ligase ubiquitination enzymes of Arabidopsis. *Plant physiology*, *139*(4), 1597-1611.
Kruk, J. A., Dutta, A., Fu, J., Gilmour, D. S., & Reese, J. C. (2011). The multifunctional Ccr4–Not complex directly promotes transcription elongation. *Genes & development*, *25*(6), 581-593.
Labbadia, J., & Morimoto, R. I. (2015). The biology of proteostasis in aging and disease. *Annual review of biochemistry*, *84*, 435-464.
Lahr, R. M., Fonseca, B. D., Ciotti, G. E., Al-Ashtal, H. A., Jia, J.-J., Niklaus, M. R., Blagden, S. P., Alain, T., & Berman, A. J. (2017). La-related protein 1 (LARP1) binds the mRNA cap, blocking eIF4F assembly on TOP mRNAs. *Elife*, *6*, e24146.
Laloum, D., Magen, S., Soroka, Y., & Avin-Wittenberg, T. (2022). Exploring the contribution of autophagy to the excess-sucrose response in Arabidopsis thaliana. *International Journal of Molecular Sciences*, *23*(7), 3891.
Laribee, R. N., Shibata, Y., Mersman, D. P., Collins, S. R., Kemmeren, P., Roguev, A., Weissman, J. S., Briggs, S. D., Krogan, N. J., & Strahl, B. D. (2007). CCR4/NOT complex associates with the proteasome and regulates histone methylation. *Proceedings of the National Academy of Sciences*, *104*(14), 5836-5841.

Leberer, E., Dignard, D., Harcus, D., Whiteway, M., & Thomas, D. (1994). Molecular characterization of SIG1, a Saccharomyces cerevisiae gene involved in negative regulation of G-protein-mediated signal transduction. *The EMBO journal*, *13*(13), 3050-3064.

Lee, D. Y., & Fiehn, O. (2013). Metabolomic response of Chlamydomonas reinhardtii to the inhibition of target of rapamycin (TOR) by rapamycin. *Journal of microbiology and biotechnology*, *23*(7), 923-931.

Lehmann, A., Niewienda, A., Jechow, K., Janek, K., & Enenkel, C. (2010). Ecm29 fulfils quality control functions in proteasome assembly. *Molecular cell*, *38*(6), 879-888.

Leppek, K., Das, R., & Barna, M. (2018). Functional 5′ UTR mRNA structures in eukaryotic translation regulation and how to find them. *Nature reviews Molecular cell biology*, *19*(3), 158-174.

Letunic, I., & Bork, P. (2018). 20 years of the SMART protein domain annotation resource. *Nucleic acids research*, *46*(D1), D493-D496.

Li, F., Fan, G., Lu, C., Xiao, G., Zou, C., Kohel, R. J., Ma, Z., Shang, H., Ma, X., & Wu, J. (2015). Genome sequence of cultivated Upland cotton (Gossypium hirsutum TM-1) provides insights into genome evolution. *Nature biotechnology*, *33*(5), 524-530.

Li, L., Song, Y., Wang, K., Dong, P., Zhang, X., Li, F., Li, Z., & Ren, M. (2015). TOR-inhibitor insensitive-1 (TRIN1) regulates cotyledons greening in Arabidopsis. *Frontiers in plant science*, *6*, 861.

Li, W.-w., Li, J., & Bao, J.-k. (2012). Microautophagy: lesser-known self-eating. *Cellular and molecular life sciences*, *69*, 1125-1136.

Liao, Y., Smyth, G. K., & Shi, W. (2014). featureCounts: an efficient general purpose program for assigning sequence reads to genomic features. *Bioinformatics*, *30*(7), 923-930.

Liebl, M. P., & Hoppe, T. (2016). It's all about talking: two-way communication between proteasomal and lysosomal degradation pathways via ubiquitin. *American Journal of Physiology-Cell Physiology*, *311*(2), C166-C178.

Lin, L., Zhang, C., Chen, Y., Wang, Y., Wang, D., Liu, X., Wang, M., Mao, J., Zhang, J., & Xing, W. (2019). PAWH1 and PAWH2 are plant-specific components of an Arabidopsis endoplasmic reticulum-associated degradation complex. *Nature Communications*, *10*(1), 3492.

Liu, H. Y., Badarinarayana, V., Audino, D. C., Rappsilber, J., Mann, M., & Denis, C. L. (1998). The NOT proteins are part of the CCR4 transcriptional complex and affect gene expression both positively and negatively. *The EMBO journal*.

Liu, J. X., & Howell, S. H. (2016). Managing the protein folding demands in the endoplasmic reticulum of plants. *New Phytologist*, *211*(2), 418-428.

Liu, Q., Ren, T., Fresques, T., Oppliger, W., Niles, B. J., Hur, W., Sabatini, D. M., Hall, M. N., Powers, T., & Gray, N. S. (2012). Selective ATP-competitive inhibitors of TOR suppress rapamycin-insensitive function of TORC2 in Saccharomyces cerevisiae. *ACS Chem Biol*, *7*(6), 982-987. https://doi.org/10.1021/cb300058v

Liu, Y., Duan, X., Zhao, X., Ding, W., Wang, Y., & Xiong, Y. (2021). Diverse nitrogen signals activate convergent ROP2-TOR signaling in Arabidopsis. *Developmental Cell*, *56*(9), 1283-1295. e1285.

Liu, Y., & Li, J. (2014). Endoplasmic reticulum-mediated protein quality control in Arabidopsis. *Frontiers in plant science*, *5*, 162.

Love, M. I., Huber, W., & Anders, S. (2014). Moderated estimation of fold change and dispersion for RNA-seq data with DESeq2. *Genome biology*, *15*, 1-21.

Lu, K., Wei, L., Li, X., Wang, Y., Wu, J., Liu, M., Zhang, C., Chen, Z., Xiao, Z., & Jian, H. (2019). Whole-genome resequencing reveals Brassica napus origin and genetic loci involved in its improvement. *Nature Communications*, *10*(1), 1154.
Luo, C., Cai, X.-T., Du, J., Zhao, T.-L., Wang, P.-F., Zhao, P.-X., Liu, R., Xie, Q., Cao, X.-F., & Xiang, C.-B. (2016). PARAQUAT TOLERANCE3 is an E3 ligase that switches off activated oxidative response by targeting histone-modifying PROTEIN METHYLTRANSFERASE4b. *PLoS Genetics*, *12*(9), e1006332.
Maekawa, S., Sato, T., Asada, Y., Yasuda, S., Yoshida, M., Chiba, Y., & Yamaguchi, J. (2012). The Arabidopsis ubiquitin ligases ATL31 and ATL6 control the defense response as well as the carbon/nitrogen response. *Plant molecular biology*, *79*, 217-227.
Magnuson, B., Ekim, B., & Fingar, D. C. (2012). Regulation and function of ribosomal protein S6 kinase (S6K) within mTOR signalling networks. *Biochemical Journal*, *441*(1), 1-21.
Maillet, L., & Collart, M. A. (2002). Interaction between Not1p, a component of the Ccr4-not complex, a global regulator of transcription, and Dhh1p, a putative RNA helicase. *Journal of Biological Chemistry*, *277*(4), 2835-2842.
Maillet, L., Tu, C., Hong, Y. K., Shuster, E. O., & Collart, M. A. (2000). The essential function of Not1 lies within the Ccr4-Not complex. *Journal of molecular biology*, *303*(2), 131-143.
Mallén-Ponce, M. J., Pérez-Pérez, M. E., & Crespo, J. L. (2022). Analyzing the impact of autotrophic and heterotrophic metabolism on the nutrient regulation of TOR. *New Phytologist*, *236*(4), 1261-1266.
Maris, C., Dominguez, C., & Allain, F. H. T. (2005). The RNA recognition motif, a plastic RNA-binding platform to regulate post-transcriptional gene expression. *The FEBS journal*, *272*(9), 2118-2131.
Mbow, C., Rosenzweig, C. E., Barioni, L. G., Benton, T. G., Herrero, M., Krishnapillai, M., Ruane, A. C., Liwenga, E., Pradhan, P., & Rivera-Ferre, M. G. (2020). *Food security*.
McCready, K., Spencer, V., & Kim, M. (2020). The importance of TOR kinase in plant development. *Frontiers in plant science*, *11*, 506669.
Mehrtash, A. B., & Hochstrasser, M. (2022). Elements of the ERAD ubiquitin ligase Doa10 regulating sequential poly-ubiquitylation of its targets. *Iscience*, *25*(11).
Meinke, D. W. (1995). Molecular genetics of plant embryogenesis.
Menand, B., Desnos, T., Nussaume, L., Berger, F., Bouchez, D., Meyer, C., & Robaglia, C. (2002). Expression and disruption of the Arabidopsis TOR (target of rapamycin) gene. *Proceedings of the National Academy of Sciences*, *99*(9), 6422-6427.
Menand, B., Desnos, T., Nussaume, L., Berger, F., Bouchez, D., Meyer, C., & Robaglia, C. (2002). Expression and disruption of the Arabidopsis TOR (target of rapamycin) gene. *Proc Natl Acad Sci U S A*, *99*(9), 6422-6427. https://doi.org/10.1073/pnas.092141899
Mergner, J., Frejno, M., List, M., Papacek, M., Chen, X., Chaudhary, A., Samaras, P., Richter, S., Shikata, H., & Messerer, M. (2020). Mass-spectrometry-based draft of the Arabidopsis proteome. *Nature*, *579*(7799), 409-414.
Mersman, D. P., Du, H.-N., Fingerman, I. M., South, P. F., & Briggs, S. D. (2009). Polyubiquitination of the demethylase Jhd2 controls histone methylation and gene expression. *Genes & development*, *23*(8), 951-962.
Meyuhas, O. (2008). Physiological roles of ribosomal protein S6: one of its kind. *International review of cell and molecular biology*, *268*, 1-37.

Miflin, B. J., & Lea, P. J. (1976). The pathway of nitrogen assimilation in plants. *Phytochemistry*, *15*(6), 873-885.

Mizushima, N., & Komatsu, M. (2011). Autophagy: renovation of cells and tissues. *Cell*, *147*(4), 728-741.

Montane, M. H., & Menand, B. (2013). ATP-competitive mTOR kinase inhibitors delay plant growth by triggering early differentiation of meristematic cells but no developmental patterning change. *J Exp Bot*, *64*(14), 4361-4374. https://doi.org/10.1093/jxb/ert242

Moreau, M., Azzopardi, M., Clément, G., Dobrenel, T., Marchive, C., Renne, C., Martin-Magniette, M.-L., Taconnat, L., Renou, J.-P., & Robaglia, C. (2012). Mutations in the Arabidopsis homolog of LST8/GβL, a partner of the target of rapamycin kinase, impair plant growth, flowering, and metabolic adaptation to long days. *The plant cell*, *24*(2), 463-481.

Moreno, A. A., Mukhtar, M. S., Blanco, F., Boatwright, J. L., Moreno, I., Jordan, M. R., Chen, Y., Brandizzi, F., Dong, X., & Orellana, A. (2012). IRE1/bZIP60-mediated unfolded protein response plays distinct roles in plant immunity and abiotic stress responses. *PLoS One*, *7*(2), e31944.

Morgan, M., Kabayama, Y., Much, C., Ivanova, I., Di Giacomo, M., Auchynnikava, T., Monahan, J. M., Vitsios, D. M., Vasiliauskaitė, L., & Comazzetto, S. (2019). A programmed wave of uridylation-primed mRNA degradation is essential for meiotic progression and mammalian spermatogenesis. *Cell research*, *29*(3), 221-232.

Morreale, F. E., & Walden, H. (2016). Types of ubiquitin ligases. *Cell*, *165*(1), 248-248. e241.

Mortazavi, A., Williams, B. A., McCue, K., Schaeffer, L., & Wold, B. (2008). Mapping and quantifying mammalian transcriptomes by RNA-Seq. *Nature methods*, *5*(7), 621-628.

Motomura, K., Arae, T., Araki-Uramoto, H., Suzuki, Y., Takeuchi, H., Suzuki, T., Ichihashi, Y., Shibata, A., Shirasu, K., & Takeda, A. (2020). AtNOT1 is a novel regulator of gene expression during pollen development. *Plant and Cell Physiology*, *61*(4), 712-721.

Mubeen, U., Jüppner, J., Alpers, J., Hincha, D. K., & Giavalisco, P. (2018). Target of rapamycin inhibition in Chlamydomonas reinhardtii triggers de novo amino acid synthesis by enhancing nitrogen assimilation. *The plant cell*, *30*(10), 2240-2254.

Mulder, K. W., Inagaki, A., Cameroni, E., Mousson, F., Winkler, G. S., De Virgilio, C., Collart, M. A., & Timmers, H. T. M. (2007). Modulation of Ubc4p/Ubc5p-mediated stress responses by the RING-finger-dependent ubiquitin-protein ligase Not4p in Saccharomyces cerevisiae. *Genetics*, *176*(1), 181-192.

Nacry, P., Camilleri, C., Courtial, B., Caboche, M., & Bouchez, D. (1998). Major chromosomal rearrangements induced by T-DNA transformation in Arabidopsis. *Genetics*, *149*(2), 641-650.

Nelson, C. J., & Millar, A. H. (2015). Protein turnover in plant biology. *Nature Plants*, *1*(3), 1-7.

Nishizawa, M., Kawasumi, M., Fujino, M., & Toh-e, A. (1998). Phosphorylation of sic1, a cyclin-dependent kinase (Cdk) inhibitor, by Cdk including Pho85 kinase is required for its prompt degradation. *Molecular biology of the cell*, *9*(9), 2393-2405.

O'Leary, B. M., Oh, G. G. K., Lee, C. P., & Millar, A. H. (2020). Metabolite regulatory interactions control plant respiratory metabolism via target of rapamycin (TOR) kinase activation. *The plant cell*, *32*(3), 666-682.

Obomighie, I., Lapenas, K., Murphy, B. E., Bowles, A. M., Bechtold, U., & Prischi, F. (2021). The role of ribosomal protein S6 kinases in plant homeostasis. *Frontiers in molecular biosciences*, *8*, 636560.

Ohtake, F., Saeki, Y., Sakamoto, K., Ohtake, K., Nishikawa, H., Tsuchiya, H., Ohta, T., Tanaka, K., & Kanno, J. (2015). Ubiquitin acetylation inhibits polyubiquitin chain elongation. *EMBO reports*, *16*(2), 192-201.

Oldham, S., Montagne, J., Radimerski, T., Thomas, G., & Hafen, E. (2000). Genetic and biochemical characterization of dTOR, the Drosophila homolog of the target of rapamycin. *Genes & development*, *14*(21), 2689-2694.

Ostertagova, E., Ostertag, O., & Kováč, J. (2014). Methodology and application of the Kruskal-Wallis test. *Applied mechanics and materials*, *611*, 115-120.

Otten, E. G., Werner, E., Crespillo-Casado, A., Boyle, K. B., Dharamdasani, V., Pathe, C., Santhanam, B., & Randow, F. (2021). Ubiquitylation of lipopolysaccharide by RNF213 during bacterial infection. *Nature*, *594*(7861), 111-116.

Panasenko, O., Landrieux, E., Feuermann, M., Finka, A., Paquet, N., & Collart, M. A. (2006). The yeast Ccr4-Not complex controls ubiquitination of the nascent-associated polypeptide (NAC-EGD) complex. *Journal of Biological Chemistry*, *281*(42), 31389-31398.

Panasenko, O. O., & Collart, M. A. (2011). Not4 E3 ligase contributes to proteasome assembly and functional integrity in part through Ecm29. *Molecular and cellular biology*, *31*(8), 1610-1623.

Panasenko, O. O., & Collart, M. A. (2012). Presence of Not5 and ubiquitinated Rps7A in polysome fractions depends upon the Not4 E3 ligase. *Molecular microbiology*, *83*(3), 640-653.

Panasenko, O. O., David, F. P., & Collart, M. A. (2009). Ribosome association and stability of the nascent polypeptide-associated complex is dependent upon its own ubiquitination. *Genetics*, *181*(2), 447-460.

Pao, K.-C., Wood, N. T., Knebel, A., Rafie, K., Stanley, M., Mabbitt, P. D., Sundaramoorthy, R., Hofmann, K., van Aalten, D. M., & Virdee, S. (2018). Activity-based E3 ligase profiling uncovers an E3 ligase with esterification activity. *Nature*, *556*(7701), 381-385.

Park, K. C., Woo, S. K., Yoo, Y. J., Wyndham, A. M., Baker, R. T., & Chung, C. H. (1997). Purification and Characterization of UBP6, a New Ubiquitin-Specific Protease inSaccharomyces cerevisiae. *Archives of biochemistry and biophysics*, *347*(1), 78-84.

Parkhomchuk, D., Borodina, T., Amstislavskiy, V., Banaru, M., Hallen, L., Krobitsch, S., Lehrach, H., & Soldatov, A. (2009). Transcriptome analysis by strand-specific sequencing of complementary DNA. *Nucleic acids research*, *37*(18), e123-e123.

Patrick, R. M., Lee, J. C., Teetsel, J. R., Yang, S.-H., Choy, G. S., & Browning, K. S. (2018). Discovery and characterization of conserved binding of eIF4E 1 (CBE1), a eukaryotic translation initiation factor 4E–binding plant protein. *Journal of Biological Chemistry*, *293*(44), 17240-17247.

Pause, A., Belsham, G. J., Gingras, A.-C., Donzé, O., Lin, T.-A., Lawrence Jr, J. C., & Sonenberg, N. (1994). Insulin-dependent stimulation of protein synthesis by phosphorylation of a regulator of 5'-cap function. *Nature*, *371*(6500), 762-767.

Pearce, L. R., Alton, G. R., Richter, D. T., Kath, J. C., Lingardo, L., Chapman, J., Hwang, C., & Alessi, D. R. (2010). Characterization of PF-4708671, a novel and highly specific inhibitor of p70 ribosomal S6 kinase (S6K1). *Biochemical Journal*, *431*(2), 245-255.

Peng, L., Wan, X., Huang, K., Pei, L., Xiong, J., Li, X., & Wang, J. (2019). AtPUB48 E3 ligase plays a crucial role in the thermotolerance of Arabidopsis. *Biochemical and biophysical research communications*, *509*(1), 281-286.

Pertea, M., Pertea, G. M., Antonescu, C. M., Chang, T.-C., Mendell, J. T., & Salzberg, S. L. (2015). StringTie enables improved reconstruction of a transcriptome from RNA-seq reads. *Nature biotechnology*, *33*(3), 290-295.

Philippe, L., van den Elzen, A. M., Watson, M. J., & Thoreen, C. C. (2020). Global analysis of LARP1 translation targets reveals tunable and dynamic features of 5′ TOP motifs. *Proceedings of the National Academy of Sciences*, *117*(10), 5319-5328.

Preissler, S., Reuther, J., Koch, M., Scior, A., Bruderek, M., Frickey, T., & Deuerling, E. (2015). Not4-dependent translational repression is important for cellular protein homeostasis in yeast. *The EMBO journal*, *34*(14), 1905-1924.

Pruneda, J. N., Littlefield, P. J., Soss, S. E., Nordquist, K. A., Chazin, W. J., Brzovic, P. S., & Klevit, R. E. (2012). Structure of an E3: E2∼ Ub complex reveals an allosteric mechanism shared among RING/U-box ligases. *Molecular cell*, *47*(6), 933-942.

Pucker, B., Kleinbölting, N., & Weisshaar, B. (2021). Large scale genomic rearrangements in selected Arabidopsis thaliana T-DNA lines are caused by T-DNA insertion mutagenesis. *BMC genomics*, *22*, 1-21.

Pullen, N., Dennis, P. B., Andjelkovic, M., Dufner, A., Kozma, S. C., Hemmings, B. A., & Thomas, G. (1998). Phosphorylation and activation of p70s6k by PDK1. *Science*, *279*(5351), 707-710.

Qiu, J., Sheedlo, M. J., Yu, K., Tan, Y., Nakayasu, E. S., Das, C., Liu, X., & Luo, Z.-Q. (2016). Ubiquitination independent of E1 and E2 enzymes by bacterial effectors. *Nature*, *533*(7601), 120-124.

Rabeh, K., Oubohssaine, M., & Hnini, M. (2024). TOR in plants: Multidimensional regulators of plant growth and signaling pathways. *Journal of Plant Physiology*, 154186.

Rajyaguru, P., She, M., & Parker, R. (2012). Scd6 targets eIF4G to repress translation: RGG motif proteins as a class of eIF4G-binding proteins. *Molecular cell*, *45*(2), 244-254.

Ralser, M., Kuhl, H., Ralser, M., Werber, M., Lehrach, H., Breitenbach, M., & Timmermann, B. (2012). The Saccharomyces cerevisiae W303-K6001 cross-platform genome sequence: insights into ancestry and physiology of a laboratory mutt. *Open biology*, *2*(8), 120093.

Randles, L., & Walters, K. J. (2012). Ubiquitin and its binding domains. *Frontiers in bioscience (Landmark edition)*, *17*, 2140.

Raught, B., Gingras, A. C., Gygi, S. P., Imataka, H., Morino, S., Gradi, A., Aebersold, R., & Sonenberg, N. (2000). Serum-stimulated, rapamycin-sensitive phosphorylation sites in the eukaryotic translation initiation factor 4GI. *The EMBO journal*.

Ravid, T., & Hochstrasser, M. (2008). Diversity of degradation signals in the ubiquitin–proteasome system. *Nature reviews Molecular cell biology*, *9*(9), 679-689.

Read, A., & Schröder, M. (2021). The unfolded protein response: an overview. *Biology*, *10*(5), 384.

Rexin, D., Meyer, C., Robaglia, C., & Veit, B. (2015). TOR signalling in plants. *Biochemical Journal*, *470*(1), 1-14.
Reyes de la Cruz, H., Aguilar, R., & Sánchez de Jiménez, E. (2004). Functional characterization of a maize ribosomal S6 protein kinase (ZmS6K), a plant ortholog of metazoan p70S6K. *Biochemistry*, *43*(2), 533-539.
Rotin, D., & Kumar, S. (2009). Physiological functions of the HECT family of ubiquitin ligases. *Nature reviews Molecular cell biology*, *10*(6), 398-409.
Ruvinsky, I., Sharon, N., Lerer, T., Cohen, H., Stolovich-Rain, M., Nir, T., Dor, Y., Zisman, P., & Meyuhas, O. (2005). Ribosomal protein S6 phosphorylation is a determinant of cell size and glucose homeostasis. *Genes & development*, *19*(18), 2199-2211.
Sabatini, D. M., Erdjument-Bromage, H., Lui, M., Tempst, P., & Snyder, S. H. (1994). RAFT1: a mammalian protein that binds to FKBP12 in a rapamycin-dependent fashion and is homologous to yeast TORs. *Cell*, *78*(1), 35-43.
Sarbassov, D. D., Guertin, D. A., Ali, S. M., & Sabatini, D. M. (2005). Phosphorylation and regulation of Akt/PKB by the rictor-mTOR complex. *Science*, *307*(5712), 1098-1101.
Scarpin, M. R., Leiboff, S., & Brunkard, J. O. (2020). Parallel global profiling of plant TOR dynamics reveals a conserved role for LARP1 in translation. *Elife*, *9*, e58795.
Scarpin, M. R., Simmons, C. H., & Brunkard, J. O. (2022). Translating across kingdoms: target of rapamycin promotes protein synthesis through conserved and divergent pathways in plants. *Journal of experimental botany*, *73*(20), 7016-7025.
Scheffner, M., Huibregtse, J. M., Vierstra, R. D., & Howley, P. M. (1993). The HPV-16 E6 and E6-AP complex functions as a ubiquitin-protein ligase in the ubiquitination of p53. *Cell*, *75*(3), 495-505.
Scheffner, M., Nuber, U., & Huibregtse, J. M. (1995). Protein ubiquitination involving an E1–E2–E3 enzyme ubiquitin thioester cascade. *Nature*, *373*(6509), 81-83.
Schepetilnikov, M., Dimitrova, M., Mancera-Martínez, E., Geldreich, A., Keller, M., & Ryabova, L. A. (2013). TOR and S6K1 promote translation reinitiation of uORF-containing mRNAs via phosphorylation of eIF3h. *The EMBO journal*, *32*(8), 1087-1102.
Schepetilnikov, M., Makarian, J., Srour, O., Geldreich, A., Yang, Z., Chicher, J., Hammann, P., & Ryabova, L. A. (2017). GTPase ROP2 binds and promotes activation of target of rapamycin, TOR, in response to auxin. *EMBO J*, *36*(7), 886-903. https://doi.org/10.15252/embj.201694816
Schepetilnikov, M., & Ryabova, L. A. (2018). Recent Discoveries on the Role of TOR (Target of Rapamycin) Signaling in Translation in Plants. *Plant Physiol*, *176*(2), 1095-1105. https://doi.org/10.1104/pp.17.01243
Schmelzle, T., Helliwell, S. B., & Hall, M. N. (2002). Yeast protein kinases and the RHO1 exchange factor TUS1 are novel components of the cell integrity pathway in yeast. *Molecular and cellular biology*, *22*(5), 1329-1339.
Schneider, B. L., Patton, E. E., Lanker, S., Mendenhall, M. D., Wittenberg, C., Futcher, B., & Tyers, M. (1998). Yeast G1 cyclins are unstable in G1 phase. *Nature*, *395*(6697), 86-89.
Schuller, A. P., & Green, R. (2018). Roadblocks and resolutions in eukaryotic translation. *Nature reviews Molecular cell biology*, *19*(8), 526-541.
Schulz, J., Avci, D., Queisser, M. A., Gutschmidt, A., Dreher, L.-S., Fenech, E. J., Volkmar, N., Hayashi, Y., Hoppe, T., & Christianson, J. C. (2017). Conserved

cytoplasmic domains promote Hrd1 ubiquitin ligase complex formation for ER-associated degradation (ERAD). *Journal of cell science*, *130*(19), 3322-3335.

Schwenk, P., Sheerin, D. J., Ponnu, J., Staudt, A.-M., Lesch, K. L., Lichtenberg, E., Medzihradszky, K. F., Hoecker, U., Klement, E., & Viczián, A. (2021). Uncovering a novel function of the CCR4-NOT complex in phytochrome A-mediated light signalling in plants. *Elife*, *10*, e63697.

Semenkov, Y. P., Shapkina, T., & Kirillov, S. (1992). Puromycin reaction of the A-site bound peptidyl-tRNA. *Biochimie*, *74*(5), 411-417.

Sen, N. D., Zhou, F., Harris, M. S., Ingolia, N. T., & Hinnebusch, A. G. (2016). eIF4B stimulates translation of long mRNAs with structured 5′ UTRs and low closed-loop potential but weak dependence on eIF4G. *Proceedings of the National Academy of Sciences*, *113*(38), 10464-10472.

Shadfan, M., Lopez-Pajares, V., & Yuan, Z.-M. (2012). MDM2 and MDMX: Alone and together in regulation of p53. *Translational cancer research*, *1*(2), 88.

Shahbazian, D. (2008). Eukaryotic initiation factor 4B (eIF4B): regulation by signaling pathways and its role in translation.

Shi, L., Wu, Y., & Sheen, J. (2018). TOR signaling in plants: conservation and innovation. *Development*, *145*(13), dev160887.

Shinjo, S., Mizotani, Y., Tashiro, E., & Imoto, M. (2013). Comparative analysis of the expression patterns of UPR-target genes caused by UPR-inducing compounds. *Bioscience, biotechnology, and biochemistry*, *77*(4), 729-735.

Simonetti, F., Candelli, T., Leon, S., Libri, D., & Rougemaille, M. (2017). Ubiquitination-dependent control of sexual differentiation in fission yeast. *Elife*, *6*, e28046.

Smith, E. M., Benbahouche, N. E. H., Morris, K., Wilczynska, A., Gillen, S., Schmidt, T., Meijer, H. A., Jukes-Jones, R., Cain, K., & Jones, C. (2021). The mTOR regulated RNA-binding protein LARP1 requires PABPC1 for guided mRNA interaction. *Nucleic acids research*, *49*(1), 458-478.

Song, L., & Rape, M. (2010). Regulated degradation of spindle assembly factors by the anaphase-promoting complex. *Molecular cell*, *38*(3), 369-382.

Song, Y., Li, L., Yang, Z., Zhao, G., Zhang, X., Wang, L., Zheng, L., Zhuo, F., Yin, H., & Ge, X. (2019). Target of rapamycin (TOR) regulates the expression of lncRNAs in response to abiotic stresses in cotton. *Frontiers in Genetics*, *9*, 690.

Song, Y., Zhao, G., Zhang, X., Li, L., Xiong, F., Zhuo, F., Zhang, C., Yang, Z., Datla, R., & Ren, M. (2017). The crosstalk between Target of Rapamycin (TOR) and Jasmonic Acid (JA) signaling existing in Arabidopsis and cotton. *Scientific Reports*, *7*(1), 45830.

Soni, K., Jagtap, P. K. A., Martínez-Lumbreras, S., Bonnal, S., Geerlof, A., Stehle, R., Simon, B., Valcárcel, J., & Sattler, M. (2023). Structural basis for specific RNA recognition by the alternative splicing factor RBM5. *Nature Communications*, *14*(1), 4233.

Sormani, R., Yao, L., Menand, B., Ennar, N., Lecampion, C., Meyer, C., & Robaglia, C. (2007). Saccharomyces cerevisiae FKBP12 binds Arabidopsis thaliana TOR and its expression in plants leads to rapamycin susceptibility. *BMC plant biology*, *7*, 1-8.

Soto-Burgos, J., & Bassham, D. C. (2017). SnRK1 activates autophagy via the TOR signaling pathway in Arabidopsis thaliana. *PLoS One*, *12*(8), e0182591.

Speiser, A., Silbermann, M., Dong, Y., Haberland, S., Uslu, V. V., Wang, S., Bangash, S. A., Reichelt, M., Meyer, A. J., & Wirtz, M. (2018). Sulfur partitioning between glutathione and protein synthesis determines plant growth. *Plant physiology*, *177*(3), 927-937.

Suzuki, Y., Arae, T., Green, P. J., Yamaguchi, J., & Chiba, Y. (2015). AtCCR4a and AtCCR4b are involved in determining the poly (A) length of granule-bound starch synthase 1 transcript and modulating sucrose and starch metabolism in Arabidopsis thaliana. *Plant and Cell Physiology*, *56*(5), 863-874.

Swaminathan, S., Amerik, A. Y., & Hochstrasser, M. (1999). The Doa4 deubiquitinating enzyme is required for ubiquitin homeostasis in yeast. *Molecular biology of the cell*, *10*(8), 2583-2594.

Swatek, K. N., & Komander, D. (2016). Ubiquitin modifications. *Cell research*, *26*(4), 399-422.

Tanida, I. (2011). Autophagy basics. *Microbiology and immunology*, *55*(1), 1-11.

Tatebe, H., & Shiozaki, K. (2017). Evolutionary conservation of the components in the TOR signaling pathways. *Biomolecules*, *7*(4), 77.

Tax, F. E., & Vernon, D. M. (2001). T-DNA-associated duplication/translocations in Arabidopsis. Implications for mutant analysis and functional genomics. *Plant physiology*, *126*(4), 1527-1538.

Tcherkezian, J., Cargnello, M., Romeo, Y., Huttlin, E. L., Lavoie, G., Gygi, S. P., & Roux, P. P. (2014). Proteomic analysis of cap-dependent translation identifies LARP1 as a key regulator of 5'TOP mRNA translation. *Genes Dev*, *28*(4), 357-371. https://doi.org/10.1101/gad.231407.113

Toribio, R., Muñoz, A., Castro-Sanz, A. B., Merchante, C., & Castellano, M. M. (2019). A novel eIF4E-interacting protein that forms non-canonical translation initiation complexes. *Nature Plants*, *5*(12), 1283-1296.

Tsai, Y. C., Fishman, P. S., Thakor, N. V., & Oyler, G. A. (2003). Parkin facilitates the elimination of expanded polyglutamine proteins and leads to preservation of proteasome function. *Journal of Biological Chemistry*, *278*(24), 22044-22055.

Tsang, C. K., Chen, M., Cheng, X., Qi, Y., Chen, Y., Das, I., Li, X., Vallat, B., Fu, L.-W., & Qian, C.-N. (2018). SOD1 phosphorylation by mTORC1 couples nutrient sensing and redox regulation. *Molecular cell*, *70*(3), 502-515. e508.

Tucker, M., Staples, R. R., Valencia-Sanchez, M. A., Muhlrad, D., & Parker, R. (2002). Ccr4p is the catalytic subunit of a Ccr4p/Pop2p/Notp mRNA deadenylase complex in Saccharomyces cerevisiae. *The EMBO journal*.

Tucker, M., Valencia-Sanchez, M. A., Staples, R. R., Chen, J., Denis, C. L., & Parker, R. (2001). The transcription factor associated Ccr4 and Caf1 proteins are components of the major cytoplasmic mRNA deadenylase in Saccharomyces cerevisiae. *Cell*, *104*(3), 377-386.

Tuskan, G. A., Difazio, S., Jansson, S., Bohlmann, J., Grigoriev, I., Hellsten, U., Putnam, N., Ralph, S., Rombauts, S., & Salamov, A. (2006). The genome of black cottonwood, Populus trichocarpa (Torr. & Gray). *Science*, *313*(5793), 1596-1604.

Um, J.-H., Kim, S., Kim, Y.-K., Song, S.-B., Lee, S.-H., Verma, D. P. S., & Cheon, C.-I. (2013). RNA interference-mediated repression of S6 kinase 1 impairs root nodule development in soybean. *Molecules and cells*, *35*, 243-248.

van Dam, T. J., Zwartkruis, F. J., Bos, J. L., & Snel, B. (2011). Evolution of the TOR pathway. *Journal of Molecular Evolution*, *73*, 209-220.

Van Dingenen, J., Vermeersch, M., De Milde, L., Hulsmans, S., De Winne, N., Van Leene, J., Gonzalez, N., Dhondt, S., De Jaeger, G., & Rolland, F. (2019). The role of HEXOKINASE1 in Arabidopsis leaf growth. *Plant molecular biology*, *99*, 79-93.

Van Leene, J., Han, C., Gadeyne, A., Eeckhout, D., Matthijs, C., Cannoot, B., De Winne, N., Persiau, G., Van De Slijke, E., & Van de Cotte, B. (2019). Capturing the phosphorylation and protein interaction landscape of the plant TOR kinase. *Nature Plants*, *5*(3), 316-327.

Varshavsky, A. (2019). N-degron and C-degron pathways of protein degradation. *Proceedings of the National Academy of Sciences*, *116*(2), 358-366.

Vézina, C., Kudelski, A., & Sehgal, S. (1975). Rapamycin (AY-22, 989), a new antifungal antibiotic I. taxonomy of the producing streptomycete and isolation of the active principle. *The Journal of antibiotics*, *28*(10), 721-726.

Walley, J. W., Kelley, D. R., Savchenko, T., & Dehesh, K. (2010). Investigating the function of CAF1 deadenylases during plant stress responses. *Plant signaling & behavior*, *5*(7), 802-805.

Wang, P., Zhao, Y., Li, Z., Hsu, C.-C., Liu, X., Fu, L., Hou, Y.-J., Du, Y., Xie, S., & Zhang, C. (2018). Reciprocal regulation of the TOR kinase and ABA receptor balances plant growth and stress response. *Molecular cell*, *69*(1), 100-112. e106.

Wang, Y., Sun, S., Zhu, W., Jia, K., Yang, H., & Wang, X. (2013). Strigolactone/MAX2-induced degradation of brassinosteroid transcriptional effector BES1 regulates shoot branching. *Developmental Cell*, *27*(6), 681-688.

Wang, Z., Orosa-Puente, B., Nomoto, M., Grey, H., Potuschak, T., Matsuura, T., Mori, I. C., Tada, Y., Genschik, P., & Spoel, S. H. (2022). Proteasome-associated ubiquitin ligase relays target plant hormone-specific transcriptional activators. *Science Advances*, *8*(42), eabn4466.

Wang, Z., & Spoel, S. H. (2022). HECT ubiquitin ligases as accessory proteins of the plant proteasome. *Essays in biochemistry*, *66*(2), 135-145.

Wauer, T., Swatek, K. N., Wagstaff, J. L., Gladkova, C., Pruneda, J. N., Michel, M. A., Gersch, M., Johnson, C. M., Freund, S. M., & Komander, D. (2015). Ubiquitin Ser65 phosphorylation affects ubiquitin structure, chain assembly and hydrolysis. *The EMBO journal*, *34*(3), 307-325.

Wheeler, T., & Von Braun, J. (2013). Climate change impacts on global food security. *Science*, *341*(6145), 508-513.

Willems, P., Sterck, L., Dard, A., Huang, J., De Smet, I., Gevaert, K., & Van Breusegem, F. (2024). The Plant PTM Viewer 2.0: in-depth exploration of plant protein modification landscapes. *Journal of experimental botany*, erae270.

Wolfson, R. L., & Sabatini, D. M. (2017). The dawn of the age of amino acid sensors for the mTORC1 pathway. *Cell metabolism*, *26*(2), 301-309.

Wu, Z., Wang, Y., Lim, J., Liu, B., Li, Y., Vartak, R., Stankiewicz, T., Montgomery, S., & Lu, B. (2018). Ubiquitination of ABCE1 by NOT4 in response to mitochondrial damage links co-translational quality control to PINK1-directed mitophagy. *Cell metabolism*, *28*(1), 130-144. e137.

Wullschleger, S., Loewith, R., Oppliger, W., & Hall, M. N. (2005). Molecular organization of target of rapamycin complex 2. *Journal of Biological Chemistry*, *280*(35), 30697-30704.

Xiong, Y., McCormack, M., Li, L., Hall, Q., Xiang, C., & Sheen, J. (2013). Glucose–TOR signalling reprograms the transcriptome and activates meristems. *Nature*, *496*(7444), 181-186.

Xiong, Y., & Sheen, J. (2012). Rapamycin and glucose-target of rapamycin (TOR) protein signaling in plants. *Journal of Biological Chemistry*, *287*(4), 2836-2842.

Xiong, Y., & Sheen, J. (2015). Novel links in the plant TOR kinase signaling network. *Current opinion in plant biology*, *28*, 83-91.

Xu, Q., Liang, S., Kudla, J., & Luan, S. (1998). Molecular characterization of a plant FKBP12 that does not mediate action of FK506 and rapamycin. *The Plant Journal*, *15*(4), 511-519.

Yaglom, J., Linskens, M. H., Sadis, S., Rubin, D. M., Futcher, B., & Finley, D. (1995). p34Cdc28-mediated control of Cln3 cyclin degradation. *Molecular and cellular biology*.

Yee, D., & Goring, D. R. (2009). The diversity of plant U-box E3 ubiquitin ligases: from upstream activators to downstream target substrates. *Journal of experimental botany*, *60*(4), 1109-1121.

Young, M. D., Wakefield, M. J., Smyth, G. K., & Oshlack, A. (2010). Gene ontology analysis for RNA-seq: accounting for selection bias. *Genome biology*, *11*, 1-12.

Zhang, J., Wei, B., Yuan, R., Wang, J., Ding, M., Chen, Z., Yu, H., & Qin, G. (2017). The Arabidopsis RING-type E3 ligase TEAR1 controls leaf development by targeting the TIE1 transcriptional repressor for degradation. *The plant cell*, *29*(2), 243-259.

Zhang, Y., Xia, G., & Zhu, Q. (2021). Conserved and unique roles of chaperone-dependent E3 ubiquitin ligase CHIP in plants. *Frontiers in plant science*, *12*, 699756.

Zhang, Z., Zhu, J.-Y., Roh, J., Marchive, C., Kim, S.-K., Meyer, C., Sun, Y., Wang, W., & Wang, Z.-Y. (2016). TOR signaling promotes accumulation of BZR1 to balance growth with carbon availability in Arabidopsis. *Current Biology*, *26*(14), 1854-1860.

Zhao, H., Zhang, H., Cui, P., Ding, F., Wang, G., Li, R., Jenks, M. A., Lü, S., & Xiong, L. (2014). The putative E3 ubiquitin ligase ECERIFERUM9 regulates abscisic acid biosynthesis and response during seed germination and postgermination growth in Arabidopsis. *Plant physiology*, *165*(3), 1255-1268.

Zoghbi, H. Y. (2013). The basics of translation. In (Vol. 339, pp. 250-250): American Association for the Advancement of Science.

Zurita-Martinez, S. A., & Cardenas, M. E. (2005). Tor and cyclic AMP-protein kinase A: two parallel pathways regulating expression of genes required for cell growth. *Eukaryotic Cell*, *4*(1), 63-71. https://www.ncbi.nlm.nih.gov/pmc/articles/PMC544169/pdf/0261-04.pdf

Appendix

Appendix Chapter – Investigating the genetic link between *NOT4A* and *PGR3* mutations in *Arabidopsis*.

Abstract

In *Arabidopsis thaliana*, the NOT4A E3 ubiquitin-ligase was initially hypothesised to positively regulate the expression of *PROTON GRADIENT REGULATION 3* (*PGR3*), a nuclear-encoded factor that is imported into plastids to regulate translation of photosynthetic proteins and ribosome biogenesis. It was shown that a loss-of-function *not4a* T-DNA insertional mutant (specifically, GABI_134E03) had a severe reduction in photosynthetic components (including PetC and NdhH) and plastid 30S ribosome subunits (e.g., RPS1), thus reducing translation rates and photosynthetic capacity leading to a slow growing pale-yellow phenotype. Furthermore, transcriptomic, and proteomic data showed that this *not4a* mutant lacked *PGR3* expression, that its molecular defects resembled those of a *pgr3* mutant, and that ectopic expression of PGR3-YFP in *not4a* restored WT like phenotypes. However, a recent finding showed that the *PGR3* locus and two neighbouring genes were completely absent in the *not4a* GABI_134E03 line and therefore the lack of *PGR3* expression is due to an unexpected deletion in the genome.

Remarkably, homozygous PGR3-deleted plants, which have a pale-yellow phenotype, were found to always also homozygous for *not4a*, despite *PGR3* and *NOT4A* being located on separate chromosomes. Through backcrossing *not4a* to WT and monitoring segregation patterns in derived progeny, we were able to demonstrate that transmission of the *PGR3* deletion is highly dependent on the *not4a* T-DNA insertion occurring in a homozygous state. Gametophytic analysis of the double mutant revealed moderate levels of post-meiotic ovule arrest and pollen abortion suggesting that certain allelic combinations may be affecting gametophyte development. Overall, we observe anomalous segregation which consequently leads to skewed offspring ratios and thus does not follow typical Mendelian inheritance patterns.

Introduction

The publication by Bailey et al. (2021) investigated specifically NOT4A function, and initially hypothesised that NOT4A positively regulates the expression of PROTON-GRADIENT-3 (PGR3), a pentatricopeptide protein required for translating several thylakoid-localised photosynthetic components and ribosome subunits within chloroplasts. It was reported that loss-of-function *not4a* mutants have a severe reduction in photosynthetic components (including PetC and NdhH) and plastid 30S ribosome subunits (e.g., RPS1), thus reducing translation rates and photosynthetic capacity leading to a slow growing pale-yellow phenotype. Quantitative transcriptome and proteome analysis of the *not4a* mutant revealed it lacks *PGR3* expression, and that its molecular defects resemble those of a *pgr3* mutant.

A closer analysis of the RNA-seq data revealed that the *PGR3* locus and 2 neighbouring genes (*ENDOL15* and an uncharacterised transmembrane protein At4g31830 known as *TMP*) were completely absent in the *not4a* line used throughout this research and therefore the lack of *PGR3* mRNA recorded previously actually resulted from a gene deletion. *This was brought to our attention by Dr Hannes Ruwe, Prof Christian Schmitz-Linneweber, Prof Alice Barkan, and Rosalind Williams-Carrier.* Remarkably, the homozygous *PGR3*-deleted plants, which have a pale-yellow phenotype, were found to always be homozygous for *not4a,* which is why this deletion was not initially discovered. This suggests a connection between the two loci that is different to that originally hypothesised. Here I outline the specific experiments that were carried out to understand the biological basis of this phenomenon, to isolate homozygous *not4a* line without the *PGR3* deletion, and to determine the frequency at which this can/does occur.

<u>Details on the *PGR3* broad locus deletion in *not4a*</u>

A series of diagnostic tests on the material used in Bailey et al. (2021) was carried out to investigate this deletion further. This included confirming through PCR that the *not4a* mutant line was homozygous for the T-DNA insertion in the *not4a* locus. Furthermore, it was also confirmed that the endogenous *PGR3* is absent in the *not4a* line used. The alignment of the RNA-sequencing data in *not4a* clearly showed no reads (expression) of not only *PGR3*, but the 2 neighbouring genes as well (*ENODL15* and *TMP1*). By using a combination of flanking primers *(as described in Materials and Methodology*), it became apparent that the *not4a* line was producing smaller bands (~1500bp) than Col-0 (~7000bp) (**Figure 1a**). This smaller amplicon was purified and sequenced which revealed that it was indeed specific to the *PGR3* locus (**Figure 1b**). A further analysis also revealed that this deletion is also accompanied by a 49bp T-DNA fragment (*see Supplementary Data*).

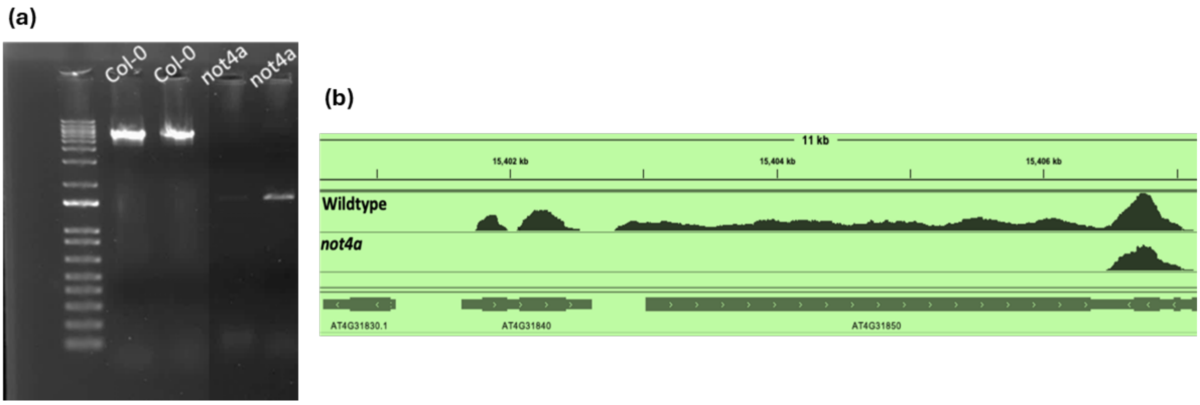

Figure 1 – Evidence of broad locus deletion in the *not4a* line. (**a**) Gel image of PCR amplicon targeting *PGR3* broad locus using 2 independent wildtype and *not4a* lines. *Note: Weak band visible in first not4a lane.* (**b**) RNA-seq reads from *not4a* and Col-0 in the region of PGR3 clearly displaying absent genes (PGR3 - AT4G31850, ENODL15 – AT4G31840 and AT4G31830) in *not4a* (Osborne, unpublished).

<u>Investigating the co-segregation frequency of the *not4a* T-DNA insert and the *PGR3* deletion.</u>

The *not4a* line containing the *PGR3* broad locus deletion was backcrossed to Col-0 to obtain a double heterozygous F_1 progeny. This F_1 progeny was self-fertilised, and the F_2 seeds were used to assess *PGR3* deletion's dependency on *not4a* and to monitor frequency at which this occurs (**Figure 2**, which shows expected inheritance patterns if the two loci are not linked). Following this backcross, the apparent dependency of the deleted *PGR3* region on *NOT4A* also being disrupted could be monitored further by selecting specific F_2 parents, selfing them, and analysing segregation in the F_3 population. As such, two F_2 parents were selected: (1) An individual where *not4a* was in a homozygous mutant state and *PGR3* deletion was heterozygous (Parent A), and (2) An individual where *NOT4A* was in a homozygous wildtype state and the PGR3 deletion was heterozygous (Parent B), and. In both cases, the "status" of *NOT4A* was fixed, allowing for the monitoring of *PGR3* segregation behaviour/frequencies in the F_3 generation, (**Figure 3**). It was speculated that, if the *PGR3* deletion/pale yellow phenotype is dependent on *not4a* being disrupted, then we should see ¼ of plants are pale yellow in the progeny of parent line A, but we should not be able to identify any pale-yellow plants in the progeny of parent line B.

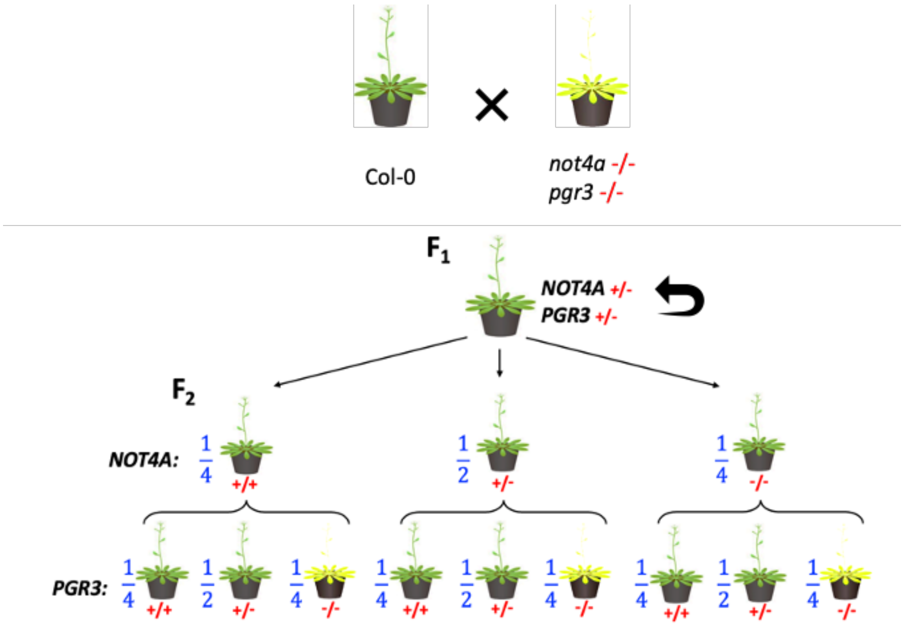

Figure 2 – Schematic of genetic crosses to establish a heterozygous F_1 parent. Depicted in the F_2 generation is the expected inheritance of *NOT4A* and *PGR3* if mendelian inheritance is conserved (as it normally would be for two loci on different chromosomes).

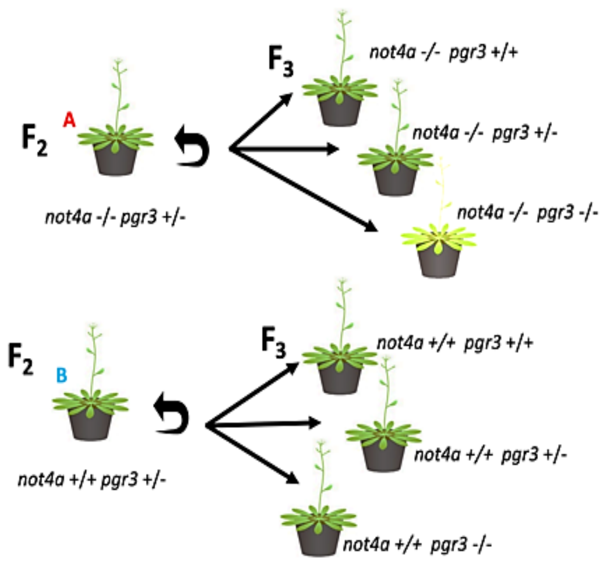

Figure 3 – Diagram of expected Mendelian inheritance of two F_2 generation parents in which *NOT4A* was either fixed in a wild-type or homozygous mutant state.

Results

Anomalous segregation of F_2 and F_3 progeny from selfed NOT4A+/- PGR3+/- heterozygous parents

A quantitative analysis of the distribution of genotypic frequencies among the F_2 progeny from a selfed F_1 double heterozygous (NOT4A+/- PGR3 +/-) parent revealed significant deviations from typical Mendelian inheritance patterns (X^2 (8, n = 174) = 147.4, p <0.0001). A total of 174 progeny from two different generations of selfed double heterozygous parents were analysed (*see Table 1*). Both parent plants used to monitor the segregation ratio were double heterozygous, i.e., NOT4A+/- PGR3+/-. We used a double heterozygous individual from the F_2 generation and took it to the F_3 generation to monitor the segregation again.

As NOT4A is on chromosome V and PGR3 is on chromosome IV, the genes should assort independently. Overall, one genotype was strongly overrepresented, favouring a double heterozygous state (NOT4A+/- PGR3+/-). The moderately overrepresented genotypes include double WT or double homozygous mutants (NOT4A+/+ PGR3+/+, NOT4A-/- PGR3-/-). Furthermore, four genotypes were severely underrepresented (NOT4A-/- PGR3+/+, NOT4A+/+ PGR3-/-, NOT4A+/- PGR3-/-), where these genotypes were simply not observed, while only one was moderately underrepresented (NOT4A-/- PGR3+/-) and considered a rare genotype, as only one progeny was observed (*to be discussed later on and known as Parent C*). Lastly, a single genotype was normally represented (NOT4A+/+ PGR3+/-).

Interestingly, the results suggest that a homozygous PGR3 deletion can only occur if at least one of the NOT4A alleles contains the T-DNA insertion. This is also seen when closely analysing the endogenous PGR3's relation to NOT4A, as there are no +/+ PGR3 genotypes if one of the NOT4A alleles is mutated.

Table 1 - Distribution of genotypic frequencies in F_2 and F_3 progeny from selfed double heterozygous F_1 parent

Pooled Progeny genotype[1]		Observed (freq.)[2]	Expected (freq.)[3]
NOT4A	*PGR3*		
-/-	-/-	26	10.88
+/-	-/-	1	21.75
+/+	-/-	0	10.88
-/-	+/-	11	21.75
+/-	+/-	88	43.5
+/+	+/-	26	21.75
-/-	+/+	0	10.88

[1] Pooled genotype from the analysed F_2 and F_3 progeny

[2] Number of observed samples in respect to their genotype that was confirmed with PCR analysis (as described in Materials and Methods)

[3] Number of expected samples if distribution follows Mendelian inheritance of two independent genes

<u>Transmission of the *PGR3* deletion is highly dependent on the *not4a* T-DNA insertion occurring in a homozygous state</u>

The observation that a homozygous *PGR3* deletion can only occur if at least one allele of *NOT4A is* disrupted was further explored through quantitative analyses of F_3 progenies of three specific parents. Due to the unexpected obtainment of a NOT4A+/- and PGR3-/- genotype (Parent C), which we did not think was possible as we were hypothesizing that PGR3 deletion can only occur if NOT4A is also homozygous for the T-DNA insertion, we took this to another generation to monitor the segregation ratio. Non-Mendelian segregation was observed in the progeny from the parent B (*Not4a +/+ Pgr3 +/-*). The anomalous segregation lies in the fact that no homozygous *PGR3* deletions were observed in the progeny (**Figure 4a**, X^2 (2, n = 36) = 10.49, p <0.025). On the other hand, normal segregation distributions in the progeny that follow Mendelian expectations was observed in the other two parents, A & C (**Figure 4a**, X^2 (2, n = 36) = 0.3297, p = .848 & X^2 (2, n = 29) = 1.366, p = .5052 respectively). The results again indicate that the transmission of the *PGR3* deletion is highly dependent on *not4a* containing a T-DNA insertion in at least one allele.

From this, specifically in parent A, we were able to isolate a *not4a* homozygous mutant with PGR3 restored to its wild-type state. We also further confirmed that the neighbouring genes, *ENODL15* and *TMP*, were also restored via genotyping PCR (**see Figure 4b**).

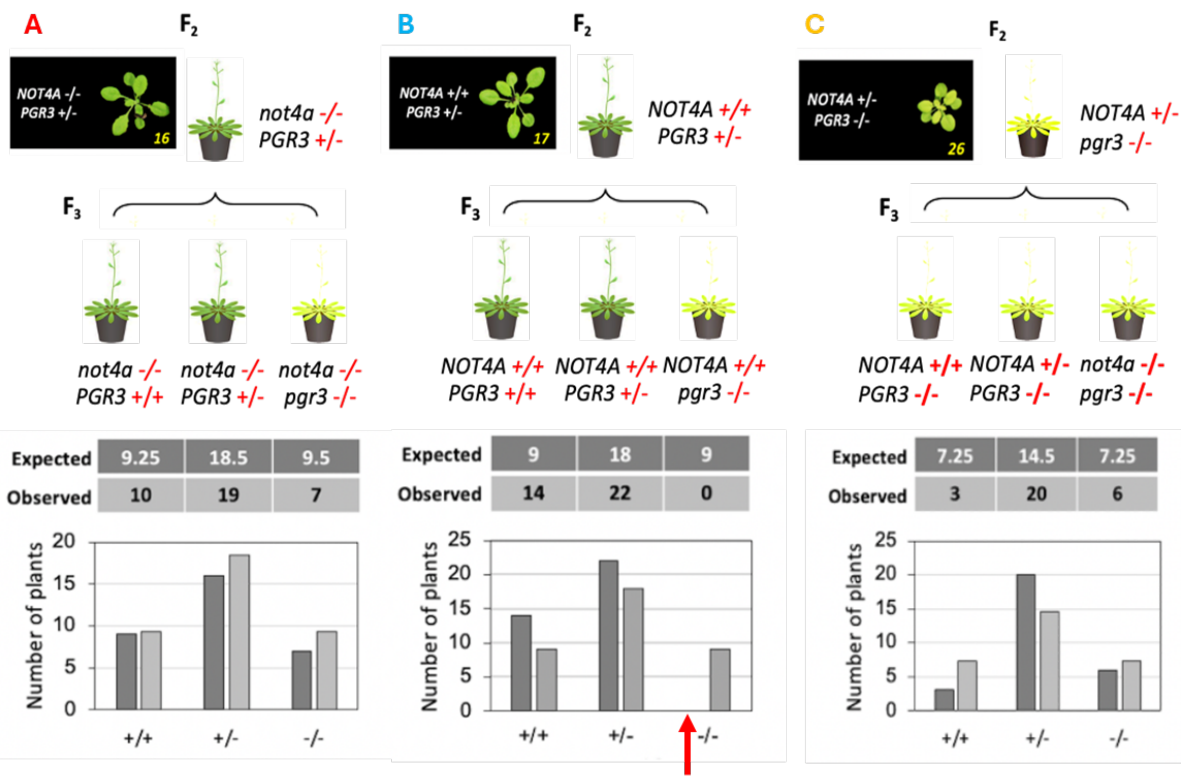

Figure 4a – Schematic of expected Mendelian inheritance of *NOT4A* and *PGR3* in the F_3 generation of differing F_2 Parents. Expected vs Observed number of each genotype in the experimental population. (A) F_2 Parent genotype: *not4a -/- PGR3* +/-, n = 36. (B) F_2 Parent genotype: NOT4A +/+ PGR3 +/-, n = 36. (C) F2 Parent genotype: NOT4A +/- pgr3 -/-, n = 29).

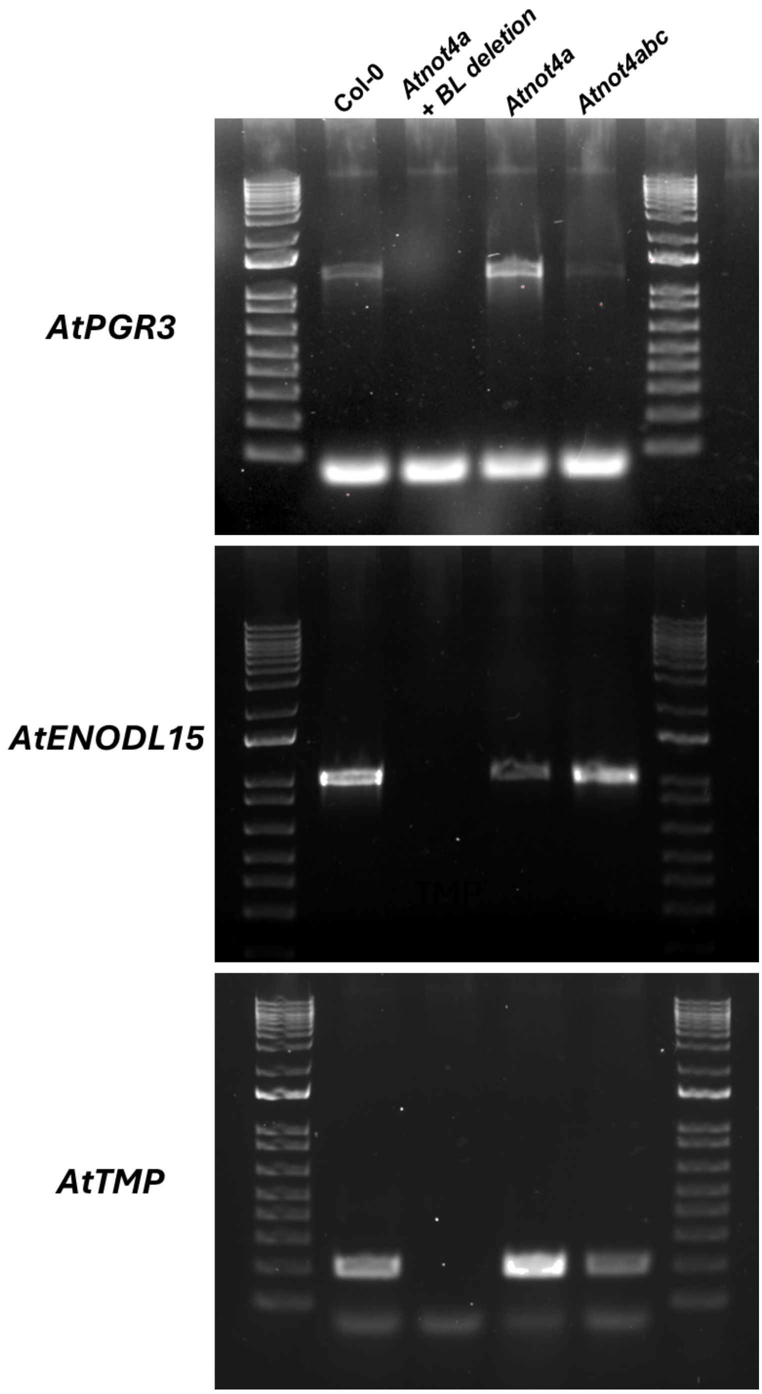

Figure 4b - Gel electrophoresis image of Broad locus (BL) deletion region. Genotyping PCR was conducted to confirm the restoration of the BL region (which includes *At*PGR3, *At*ENODL15 and *At*TMP) in *Atnot4a* and *Atnot4abc. Note: These lines were used throughout the research described in Chapter 4, 5 & 6.*

Moderate levels of post-meiotic ovule arrest observed in *not4a*

The correlation between the lack of specific progeny distribution and a potential defect in gamete transmission was further explored by analysing post-meiotic ovule development, specifically examining silique length, seeds per silique, and total seeds produced. When comparing *not4a* siliques to WT, a significant difference in *not4a* silique length was observed (Student's t-test, $p < 0.0001$). The shortened silique length in the *not4a* mutant also results in fewer seeds per silique, not due to fewer total potential seeds, but rather because of a higher frequency of aborted seeds. This leads to overall fewer viable seeds being produced compared to WT (Mann-Whitney test, $p < 0.0001$, respectively).

On the other hand, this is not observed when comparing a separate null mutant of PGR3 (*pgr3-4)* to its respective WT ecotype Ws-4. Interestingly, *pgr3-4* and Ws-4 do not differ significantly in silique length (Student's t-test, $p = 0.925$), but the total amount of seeds produced differs, with Ws-4 producing more seeds (Mann-Whitney test, $p < 0.05$). This suggests that Ws-4 must contain smaller seeds to fit more in the same size silique compared to *pgr3-4* (i.e., *pgr3-4* must have larger seeds). As the *not4a* mutant also contains a broad locus deletion which includes *PGR3*, we'd expect to see a similar phenotype in the *pgr3-4* mutant. However, they differ significantly in all three aspects (Student's test, $p < 0.0001$; Mann-Whitney test, $p < 0.0001$ & Mann-Whitney test, $p < 0.0001$). In addition, ovule arrest which would lead to aborted seed development was only observed in the *not4a* mutant line (see Figure 5).

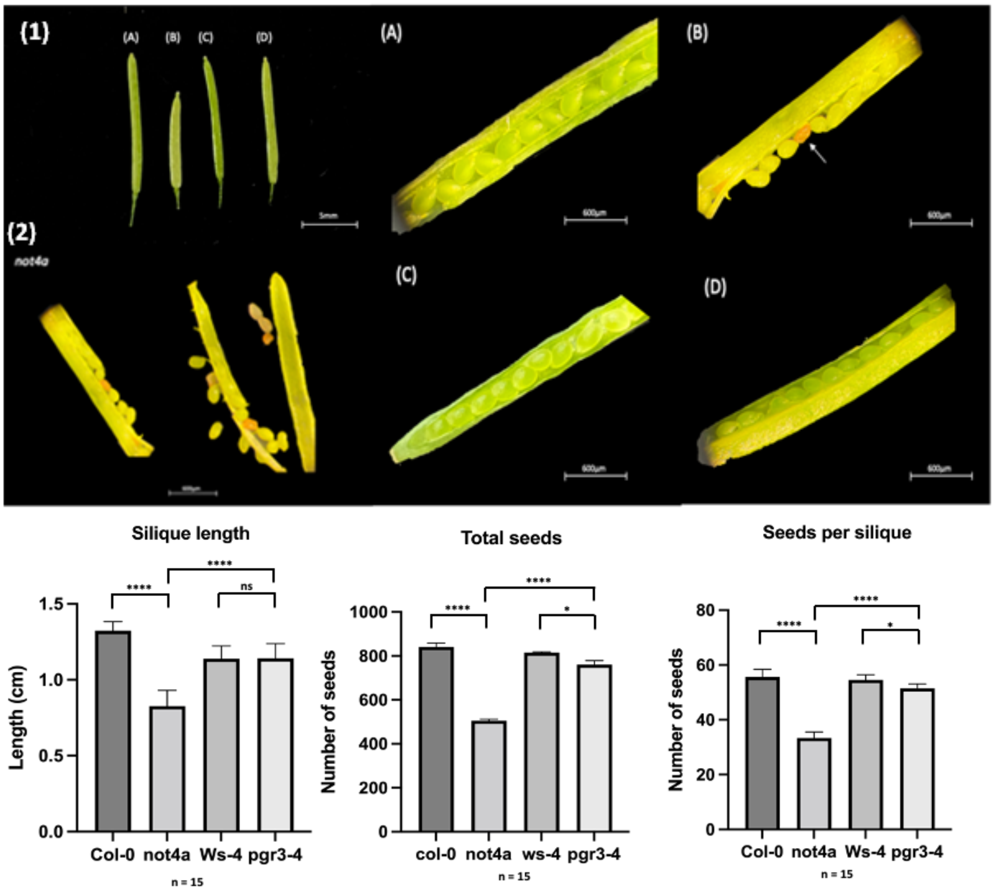

Figure 5 – Silique and ovule analysis. (**1**) Images of siliques and post-meiotic ovule development. (**A**) Col-0. (**B**) *not4a*. (**C**) Ws-4. (**D**) *pgr3-4*. (**2**) Graphical representation of silique length, total seeds, and seed per silique. Student's t-test was performed to analyse silique length analysis and Mann-Whitney test was conducted to analyse total seeds and seeds per silique at a significance level of 0.05, n = 15 (ns = not significant, * <0.05, ** <0.025, *** <0.001, **** <0.0001)

Pollen viability is compromised in *not4a and pgr3-4*

To determine whether the deficiency in reproductive development in *not4a* plants extended to male gametes as well, pollen was stained with Alexander solution and the viability was assessed (as described in Material and Methods, Section XXX see Figure 7). A significant reduction in viable pollen was observed in *not4a* when compared to Col-0 (X^2 (1, n = 3) = 314.7, p <0.0001). In addition, *pgr3-4* also showed a large amount of non-viable pollen compared to Ws-4 (X^2 (1, n = 3) = 43.08, p <0.0001). Though, the numbers of viable pollen differ between *not4a* and *pgr3-4* in which *not4a* produces significantly more non-viable pollen than *pgr3-4* (X^2 (1, n = 3) = 59.21, p <0.0001).

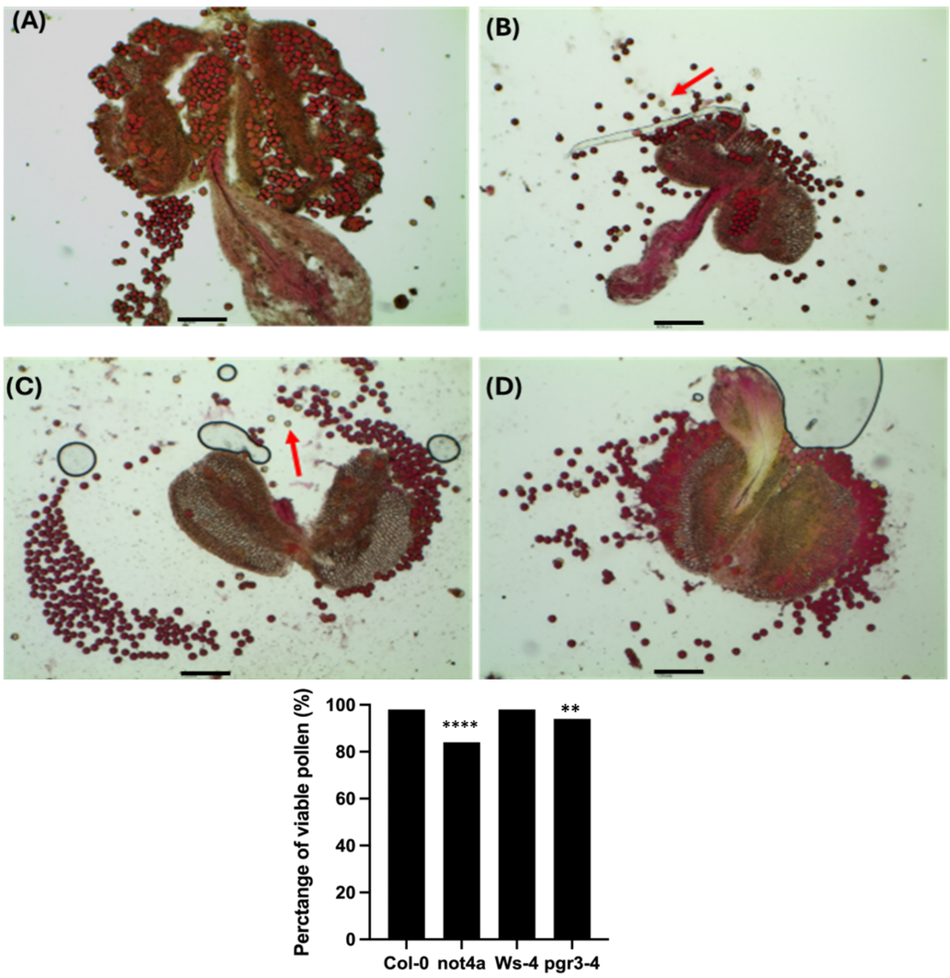

Figure 6 – Images of Alexander-stained pollen in (**A**) Col-0, (**B**) *not4a*, (**C**) *pgr3-4* and (**D**) Ws-4. Red arrows indicate examples of non-viable pollen. Scale bars = 100 µm. (**E**) Graphical representation of the percentage of viable pollen in each genotype. Chi-square test was performed to analysed significant differences each mutant and their respective ecotype.

Discussion

The research described here was conducted in response to the issues linked to the *not4a* T-DNA mutant reported in Bailey et al. (2021). Despite concluding that NOT4A does not directly regulate the expression of *PGR3* and that the reported phenotypes of pale-yellow leaves are due to the *PGR3* locus deletion, various lines of evidence indicate that there still is a connection between *NOT4A* and one, some, or all the genes affected in the *PGR3* broad locus deletion.

Through monitoring the progeny derived from a selfed double heterozygous parent line (i.e. heterozygous for both the *not4a* T-DNA insertion and the *PGR3* broad locus deletion) it was found that the *PGR3* locus was never in a wildtype homozygous state if *NOT4A* contained a T-DNA insertion in either or both alleles. Moreover, the transmission of the *PGR3* deletion was highly dependent on the *not4a* T-DNA insertion occurring in a homozygous state, and it is for this reason that the *PGR3* deletion was not discovered prior to the publication of Bailey et al (2021). One initial hypothesis for this was that the *not4a* mutation could be suppressing a lethal phenotype conferred by the *PGR3* locus deletion. However, the data presented in this chapter indicate that this is not the case, since a single plant in the F2 progeny was found to be heterozygous for *NOT4A* but homozygous for *PGR3 (Parent C, see Figure 4a)*. If the *PGR3* locus deletion caused a lethal phenotype, then it would not be possible to obtain offspring with this homozygous deletion while *NOT4A* remains in its homozygous wild-type state. Therefore, the lethality of the *PGR3* deletion seems to be alleviated when *NOT4A* is disrupted, but it is still unclear why specific allelic combinations are affecting gamete viability. In the subsequent generation, we were able to obtain three individuals with homozygous *PGR3* and a wild-type *NOT4A* state (**Figure 4a**). Nonetheless, the skewed inheritance frequencies still suggest that the transmission of the *PGR3* deletion is somehow dependent on the *not4a* T-DNA insertion.

Our attention was then focused on potential defects in gamete transmission, as specific genotypes were not obtained, and anomalous segregation had occurred. Post-meiotic ovule arrest was observed only in *not4a* while a significant number of aborted pollen grains was observed in both *not4a* and *pgr3-4*, though *not4a* showed a greater amount of non-viable pollen than *pgr3-4*. This suggests that the difference in gametophytic development between the two mutants may not be a result of the *PGR3* deletion but perhaps due to a lack of NOT4A or the other two deleted genes; one of which is known to be involved in co-ordinating pollen tube reception namely *ENODL15* (At4g31840). However, this is quite unlikely as a single null mutation of this gene did not reveal any noticeable phenotype (Hou et al., 2016). Furthermore, quintuple ENODL mutant that consist of T-DNA insertion as well as RNAi knockdown still showed a retention of 30-50% of seed viability (Hou et al., 2016). Overexpression of *ENODL15* did cause disturbed pollen tube guidance and ultimately reduced fertility (Hou et al., 2016). However, this cannot explain our observations, as in the *not4a* line as the *ENODL15* locus is entirely deleted. It is possible that the third gene involved in this broad locus deletion, *TMP1* (At4g31830), could be responsible for the embryo lethality of certain genetic combinations, but this would need to be investigated further. Lastly, it could be a role of NOT4A that is causing the defect in transmission of mutant gametes as this is consistent with the report that loss of NOT1 of the same complex (CCR4-NOT) reduces pollen and egg transmission (Pereira, Boavida, Santos & Becker, 2020).

In addition to exploring possibilities of a functional link or identifying a novel phenotype from one, some or all genes that have been deleted, it could potentially be a result of the T-DNA insertion itself in the *NOT4A* locus that establishes a physical link between *NOT4A* and *PGR3*. Analysis of the F_2 progeny frequencies suggested that *not4a* and *pgr3* were inherited together (i.e. as though they are linked) although they map to separate chromosome (Chromosome V and IV respectively). Therefore these two loci should assort independently from each other; unless a translocation or inversion event had taken place, and the loci are now situated on the same chromosome. Large-scale chromosomal rearrangements due to T-DNA insertions have been extensively reported (B. Menand et al., 2002; Nacry et al., 1998; Pucker et al., 2021; Tax & Vernon, 2001) and typically do not confer obvious phenotypes and hence go unnoticed. Specifically, genetic crosses of mutants that were generated through T-DNA insertion lines that have rearranged chromosomes show perturbed progeny distribution that do not follow Mendelian expectations (Curtis et al., 2009). It is known that inversions reduce recombination within inverted chromosomal regions while translocations alter linkage groups (Curtis et al., 2009). Furthermore, T-DNA insertions are also known to form 'sticky T-DNA' in which tetravalent structures form during meiosis and lead to crossovers between non-homologous chromosomes (Nacry et al., 1998). Interestingly, a secondary T-DNA insertion was reported in the original *not4a* GABI-KAT line used but was crossed out prior further experiments. The process of crossing out the secondary T-DNA may have led to the formation of multivalence and thus explains the remnants 49bp T-DNA fragment located in the deleted region. In most cases, when such multivalent structures form, the cell function collapses and the whole process is aborted which ultimately translates to non-viable pollen or ovules and hence specific genotypes or recombination frequencies are not observed in the progeny (Curtis et al., 2009). On the other hand, it is also possible for the cell to 'correct itself' *per se*, sometimes leading to chromosomal rearrangements (B. Menand et al., 2002; Nacry et al., 1998; Pucker et al., 2021; Tax & Vernon, 2001).

Through the experiments described, we managed to successfully isolate 10 homozygous *not4a* line without the *PGR3* broad locus deletion, which were then used as the not4a mutant line throughout the research presented in Chapters 3, 4, and 5.

Materials and Methods

Identification of genotypes

Genotypes were confirmed by performing PCR analysis of genomic DNA extracted by using tissue from singular leaves. Gene-specific primers for *NOT4A* were 5'-ACTCAAGCCAAATTGCACATC-3' (RP) and 5'-TTTACATTGTTGGGTTGCCTC-3' (LP). To detect TDNA-insertion lines, the RP was used with 5'-GGGCTACACTGAATTGGTAGCTC-3'. Gene-specific primers to detect the broader PGR3 locus is depicted in Figure 8 where the left-flanking primer was 5'-cacatgagtgtttctacctaaca-3' (LociF) and the right-flanking primer was 5'-Ttttctggatgctacagtttcc-3' (LociR). To detect the 45-base T-DNA fragment, 5'-TTGAATATATCCTGGTGGCAAG-3' (InsF) was combined with LociR primer (**Figure 8**).

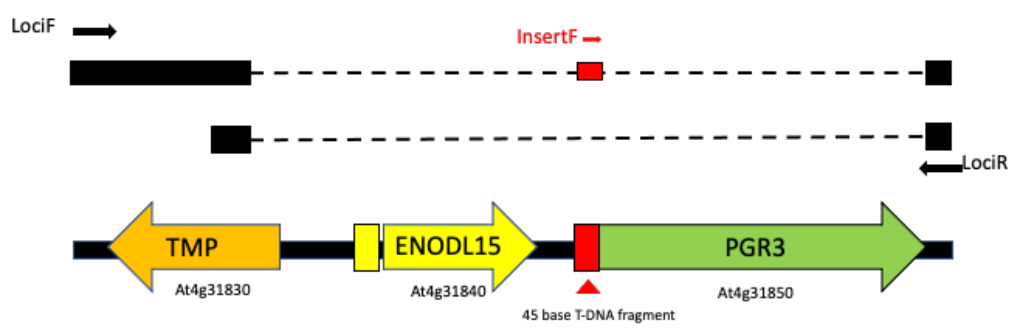

Figure 8 – Schematic of the broad locus region deleted in the *not4a* line. Dotted lines indicate deleted segments. Black bars represent sequences that still map to locus. Primers flanking the region are labelled as LociF and LociR. Primers to detect deletion target 49bp T-DNA fragment**.**

Pollen staining and visualisation

Flowering buds that have not opened completely were removed from the plant and placed in 10% ethanol overnight. The buds were then transferred to a petri-dish and occasionally sprayed with water to avoid it from drying out. The anthers were carefully dissected from the flowering bud and placed on a microscope slide. 5ul of Alexander staining solution was added directly onto the anther and covered with cover slip. The cover slip was gently pressed to tease out the pollen. The slides were then incubated at 50°C for 30mins and then leftover night before visualising and imagine with a light microscope. A total of 3 buds per genotype (6 anthers per bud) was analysed. Pollen that was visibly stained red was considered viable, partly stained in the middle of a pollen grain was considered semi-viable and transparent pollens were considered non-viable (**Figure 9**).

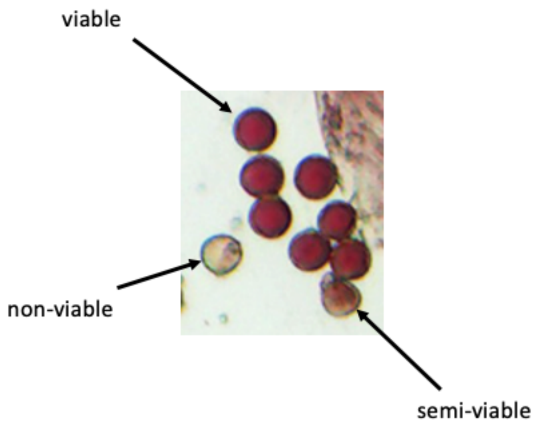

Figure 9 – Alexander-stained pollen grains to highlight examples of viable, semi-viable and non-viable pollen.

Supplementary Data (Appendix Chapter)

Mapping sequence of smaller amplicon produced by *not4a* to PGR3 locus

AGSSCMTAMMMAGCAGTAATGTAGAGGATTCGGTGATCTAAATTATACGCATG
CATTTGCTACACAAGACTACTCTATTCCTCCCATTTTATTCTTCTGCTTGCTCTAG
TAGTTGACATAAGCCATTCTTGGACACGTTATGTTATTTTATTACAAGTAAATAAG
AAGTTCCAACAAGAGCATGAAGCAAGAACAAAATTACAAAAGCAAAAAAAGAAG
AAGAAGATAAACCCTTTAATTCTTCCCTTGAAATTTTACTTTCTTGGATGTGTATC
TTCAGGTTTAGCCGTCCCTGTGGCAGCCTTAGCTACATCAGTGGCAGTGGCTT
CCGGCTTCTTCTTAGCATACATAACAGTGTACATGATGGCCCCCGAGATAGCTA
ATCCGGCTAGAGCCATCGTCGTGTAACTGTATGGCAAGTTACGGCGTTGATGA
AGAACACCACCTGGATTACTTCCTGGCGGGAMATGAAGCCATTTACAATTGAAT
ATATCCTGGTGGCAAGTTACAGTGTAAATGTCTTATTGTTTTGTTTATTTACATGA
TGATATGTTCTTTTAAGGCCAACAACATTTTTACACCAATTATTCCTTTCTACATT
ATGGGAGCTCATGAGACAAAAGTCTGCACACGGAGGAAATGGTGATATACTGA
AATCAACGTCAGGTTGAGATATATAACTGTCTTTCAAAATGATTTACAATCTGAA
CCAAAATACTAGATCTAGAGGGATCTTCCGTGACTCTGAGGATGGGCCTAGTTT
GATGAGCYWC

*Maps to Chr4 WT genome (F)

*TDNA insertion

*Accuracy error from the sequencing

~5532bp was deleted.

CCGKAAYGGCAGATCCTCTAGATCTAGTATTTTGGTTCAGATTGTAAATCATTTT
GAAAGACAGTTATATMTCTCAACCTGACGTTGATTTCAGTATATCACCATTTCCT
CCGTGTGCAGACTTTTGTCTCATGAGCTCCCATAATGTAGAAAGGAATAATTGG
TGTAAAAATGTTGTTGGCCTTAAAAGAACATATCATCATGTAAATAAACAAAACA
ATAAGACATTTACACTGTAACTTGCCACCAGGATATATTCAATTGTAAATGGCTT
CATKTCGCCAGGAAGTAATCCAGGTGGTGTTCTTCATCAACGCCGTAACTTGCC
ATACAGTTACACGACGATGGCTCTAGCCGGATTAGCTATCTCGGGGGCCATCA

TGTACACTGTTATGTATGCTAAGAAGAAGCCGGAAGCCACTGCCACTGATGTAG
CTAAGGCTGCCACAGGGACGGCTAAACCTGAAGATACACATCCAAGAAAGTAA
AATTTCAAGGGAAGAATTAAAGGGTTTATCTTCTTCTTCTTTTTTTGCTTTTGTAA
TTTTGTTCTTGCTTCATGCTCTTGTTGGAACTTCTTATTTACTTGTAATAAAATAA
CATAACGTGTCCAAGAATGGCTTATGTCAACTACTAGAGCAAGCAGAAGAATAA
AATGGGAGGAATAGAGTAGTCTTGTGTAGCAATGCATGCGTATAATTAGATCAC
CGAATCCTCTACATTTCTCTGTGTATGTCGCTTAAAAGTAGGCCATAWTKKKKG
GGSCC

~5430bp was deleted.

*Maps to Chr4 WT genome (R)

*TDNA insertion

*Accuracy error from the sequencing

PGR3 genomic sequence:

GTTTTTTATTATTCTGCTTCGAAAATTCTTTCATCAAAAATCTCCGGTTCACCGAA
TCGACTCCCTCGCGCTCTTTTCAGCCGGTGAACGGAGACGAATCAAAATGCTC
ATAGCTATTCAGCACGTGTTTGTGTTTTGTTAGTTATATCTGCGCCACTTGAAAT
GTGATGAATCATCATCGTTAATCTCTGTTTTCGTTTCAATTTTTGCCGGAGAATT
GAATTGTTTTGCTTGCTTGGCTTATCTCTAGAATGGTCGCGTTCTCTGCTCTGCG
AGTTTGTGTGGTGATATATCAGTTGGTGATGCTTGTCTTGTTAGTAACATCAAAG
CAAAATGTCGCGATAATTTGGTTACTGGAGGATTAAAGTTCCACGCTTTGAAGA
TTGGGTCTCGGAAGAAACACTGGAGAAGGAAGAGTATGAGATGTAGTGTAGTC
TCCATGAAAAGTTCTGACTTTTCGGGTTCTATGATAAGAAAGAGCTCAAAACCTG
ATTTGTCATCGAGTGAAGAAGTAACGAGGGGTTTAAAGTCGTTTCCTGATACTG
ATTCTTCATTTTCGTATTTCAAATCAGTGGCTGGGAATTTGAATTTAGTTCACACT
ACTGAGACTTGTAACTACATGCTTGAAGCTTTGAGGGTTGATGGTAAACTTGAG
GAAATGGCTTATGTGTTTGATTTGATGCAGAAAAGAATCATAAAGAGGGATACTA
ATACTTACTTGACTATCTTCAAGAGTCTTTCTGTGAAAGGTGGATTGAAGCAAGC
ACCTTATGCACTTCGGAAGATGAGAGAATTTGGTTTTGTGTTGAATGCATATTCA
TACAATGGGTTGATTCATCTTCTGCTTAAGTCTAGGTTTTGCACAGAGGCAATG
GAGGTTTATAGAAGAATGATCTTGGAAGGTTTTAGACCTAGTTTGCAGACTTACT
CTTCACTTATGGTAGGTTTGGGGAAAAGAAGGGATATTGATTCTGTGATGGGTT

TACTTAAAGAGATGGAGACTTTGGGGTTAAAGCCGAATGTTTACACCTTTACGA
TATGTATTCGGGTGCTTGGTAGGGCAGGGAAGATTAATGAAGCATATGAAATAC
TGAAGCGGATGGATGATGAAGGATGTGGACCTGATGTAGTTACTTACACTGTTC
TTATTGATGCTCTGTGTACTGCTAGGAAGCTCGATTGTGCGAAGGAGGTTTTCG
AAAAGATGAAAACAGGAAGACACAAACCAGATCGTGTAACTTACATTACTTTGCT
GGACAGGTTTAGTGATAACAGAGATCTGGATTCAGTGAAGCAGTTTTGGAGTGA
AATGGAGAAGGATGGTCATGTACCTGATGTTGTAACCTTTACCATTCTCGTGGA
TGCTCTGTGCAAAGCTGGGAATTTTGGTGAAGCATTTGATACATTGGATGTGAT
GAGGGACCAAGGTATCTTACCGAACCTTCATACATATAACACATTGATTTGCGG
TCTTCTAAGAGTCCACCGGTTGGATGATGCACTTGAACTGTTTGGTAATATGGA
GTCTCTGGGCGTGAAGCCCACTGCCTATACGTACATAGTTTTCATTGATTACTAT
GGAAAGTCTGGAGATTCCGTCAGTGCTCTTGAGACTTTTGAGAAGATGAAAACC
AAAGGAATAGCTCCGAACATTGTAGCCTGTAATGCGTCTCTCTACAGTCTAGCT
AAAGCGGGAAGGGACCGAGAAGCGAAACAAATCTTCTATGGCTTGAAAGACAT
AGGACTGGTCCCTGATTCAGTAACTTATAACATGATGATGAAGTGCTACAGTAA
GGTTGGGGAGATAGATGAAGCCATCAAGCTGCTTTCTGAGATGATGGAGAATG
GTTGTGAACCTGATGTTATTGTTGTTAATTCTTTGATCAATACACTTTACAAAGCT
GATAGAGTAGATGAGGCGTGGAAGATGTTTATGAGAATGAAGGAAATGAAGCT
GAAGCCTACAGTTGTGACTTACAACACATTGCTCGCAGGTCTAGGCAAAAATGG
AAAAATTCAAGAGGCCATTGAGTTGTTCGAGGGGATGGTGCAGAAAGGTTGTC
CACCTAACACAATTACTTTCAACACTCTCTTTGATTGCCTTTGCAAAAATGACGA
GGTGACTCTAGCCTTGAAGATGTTGTTCAAGATGATGGACATGGGTTGTGTCCC
AGATGTTTTTACTTACAATACGATTATCTTTGGTTTGGTGAAGAATGGTCAAGTC
AAAGAGGCAATGTGTTTCTTCCACCAGATGAAGAAACTGGTTTACCCTGATTTT
GTTACACTCTGCACTCTTCTCCCAGGTGTTGTCAAGGCCAGTTTAATCGAAGAT
GCTTACAAAATCATCACCAACTTTCTTTACAATTGTGCAGACCAACCGGCTAATC
TTTTCTGGGAAGACTTGATAGGCTCTATCTTGGCTGAAGCTGGAATAGACAATG
CCGTTTCATTTTCTGAGAGATTGGTAGCTAATGGGATTTGTCGAGATGGTGACT
CTATCCTGGTGCCAATAATCAGATATTCTTGTAAACATAATAACGTCTCAGGTGC
TCGAACTTTATTCGAGAAATTCACAAAAGATCTTGGTGTCCAACCCAAACTCCC
GACTTATAATCTGCTAATCGGCGGGCTTCTTGAAGCTGATATGATTGAAATAGC
ACAGGACGTGTTCCTACAGGTGAAGAGCACTGGTTGCATCCCAGATGTGGCGA
CCTACAACTTCTTGCTTGATGCTTATGGAAAATCAGGAAAAATCGACGAACTGTT
TGAGCTATACAAAGAAATGTCTACCCATGAGTGCGAAGCAAACACAATTACTCA

CAACATTGTCATCTCCGGGCTTGTGAAGGCAGGAAATGTGGACGATGCTCTTG
ATTTATACTACGACCTTATGAGTGATCGGGACTTCTCCCCAACTGCCTGCACGT
ATGGTCCCCTTATCGATGGCCTCTCTAAGTCAGGAAGACTATATGAAGCAAAAC
AACTCTTTGAAGGAATGTTGGACTACGGTTGCAGGCCAAACTGTGCTATCTACA
ACATTCTCATTAACGGGTTTGGAAAAGCAGGTGAGGCTGATGCAGCGTGTGCA
TTGTTCAAAAGGATGGTAAAAGAAGGAGTAAGACCGGATCTCAAGACTTACTCG
GTTCTAGTAGATTGCCTTTGTATGGTCGGAAGAGTTGATGAAGGCTTGCATTAC
TTCAAGGAGCTGAAGGAATCAGGCCTCAATCCCGATGTAGTATGTTACAATCTC
ATAATCAATGGACTTGGGAAATCTCATAGACTTGAAGAAGCTCTTGTGCTTTTCA
ACGAGATGAAGACCAGCAGAGGAATCACCCCTGATCTCTACACTTACAACTCCT
TGATTCTAAACTTGGGTATCGCCGGGATGGTGGAAGAAGCTGGGAAGATTTAC
AATGAGATTCAAAGAGCAGGTCTTGAACCGAATGTTTTTACATTTAACGCTCTGA
TCCGCGGATACAGTTTGTCTGGAAAACCTGAGCACGCTTACGCTGTGTACCAG
ACAATGGTGACCGGTGGTTTTAGCCCCAACACAGGAACATACGAACAGCTCCC
CAATAGAGCTTGACATTTTACGCAGCTAATACAAGTAGAGCTCTACACTAAGTG
AAGCTTTATGTCCATGTGAAGTGTACAAAACATAACGTTGTGTAAATGTCTTATT
GTTTTGTTTATTTACATGATGATATGTTCTTTTAAGGCC

*Deleted

*Present in R strand

<u>ENODL15 genomic sequence:</u>

ACCATTTTTTCCTTTTAATTTTTCGTAATTCCTAAACGGCTAGTTTCCAAGTCCTC
TACCTTTATATAAACCACACAAGATCCACACTCTCTCCATCCTCAACACACTTTA
AAACACATTACACACTCTAATACTTTTAAGGTTTTAGATTCTAATCAATGGCTTCT
TCTTCTCTTTTGGTCACCATCTTCCTCTGCATCTCTGTCTTCTTCTTTTCGTCCGT
GAATGCAAATGAGGTTACCGTCGGTGGAAAATCCGGTGACTGGAAGATCCCTC
CTTCCTCTTCTTTCTCCTTTAACGAATGGGCTCAAAAGGCTCGCTTCAAAGTCG
GCGACTTTATCGGTAAATCCATAATTTTCAACTTTTTTTTTTCAATTAGACATTTT
GTGTGATCTTCAATATACTCTGTTTCTGACATCGTCACATGTTTATTACAGTATTC
AAGTACGAAGCCGGTAAAGACTCGGTTTTGCAAGTGACACGAGAAGCATACGA
GAAATGCAACACCACTAGCCCTAAAGCCAGCTACACCGACGGGAACACAAAGG
TGAAGCTTGACCAAGCTGGTCCGGTCTACTTCGTCAGTGGAACAGAGGGTCAT
TGTCAAAAGGGTCAGAAGCTACGCCTAGTCGTCATCACTCCTCGTAACTCTGCT
TTCTCTCCAGGTCCTTCGCCATCTGAGTTCGACGGTCCAGCCGTAGCTCCTACT

AGTGGTGCCGCTAAGCTCGCCGGCGGATTTAGTGTCGTATTTGGGCTTGTTCTT
GGATTATGGGCCTTCTTCTTTTAAAAGACAATTAGTCTTAATTCTATTTATTAATT
TTGGAATATAAAGTAGAAATCTTTGTTATTTACTACATTAAATTTATTTTAATCTAA
ATTGTTCTTCCTCTTTTTCAATTCTGGATAAATTAGTTGGATCTATCAACAATCAA
CAAAGAAAACAAAACAAAAGTGAATGAGAATTTTGAATTTAGTACCCAAAAAGGT
AAT

*Deleted

<u>TMP genomic sequence</u>:

AAACTCCAACGACACTACGTGTCTTCGTGACTCTTACTATATCCAAAAACCTATA
GCTAAAGCTGAATTTTCCATGATTAGTATAGTCCCAACCAAAAAAATACTGAAGA
AGGCATAAGCATGGCCGGAGAAGAAGACTGGAGAAAAACAGCAGATACGACGA
AGATGAGCTCGGAGGGAGTAAAAGCTGCCGGCGTTGAGTCATCAAAGAGGCC
GCCAGGAAGTAATCCAGGTGGTGTTCTTCATCAACGCCGTAACTTGCCATACAG
TTACACGACGATGGCTCTAGCCGGATTAGCTATCTCGGGGGCCATCATGTACA
CTGTTATGTATGCTAAGAAGAAGCCGGAAGCCACTGCCACTGATGTAGCTAAG
GCTGCCACAGGGACGGCTAAACCTGAAGATACACATCCAAGAAAGTAAAATTTC
AAGGGAAGAATTAAAGGGTTTATCTTCTTCTTCTTTTTTTGCTTTTGTAATTTTGT
TCTTGCTTCATGCTCTTGTTGGAACTTCTTATTTACTTGTAATAAAATAACATAAC
GTGTCCAAGAATGGCTTATGTCAACTACTAGAGCAAGCAGAAGAATAAAATGGG
AGGAATAGAGTAGTCTTGTGTAGCAAA

*Deleted

*Present in both strands

Appendix 1 – Full length alignments of *Sc*NOT4, *At*NOT4A, *At*NOT4B and *At*NOT4C protein

```
ScNOT4   MMNPHVQENLQAIHNALSNFDTSFLSEDEEDYCPLCIEPMDITDKNFFPCPCGYQICQFC      60
AtNOT4C  ------------------------MNEKGEKTCPLCTEEMDLTDQHLKPCKCGYQICVWC      36
AtNOT4A  ------------------------MSDHGEKTCPLCAEEMDLTDQQLKPCKCGYQICVWC      36
AtNOT4B  ------------------------MSDYGEKTCPLCAEEMDLTDQQLKPCKCGYQICVWC      36
                                 :.:  *. **** * **:**:: ** ****** :*

ScNOT4   YNNIRQN---PELNGRCPACRRKYDDENVRYVTLSPEELKMERAKLARKEKERKHREKER      117
AtNOT4C  WHHIIEMAEKDKTEGRCPACRTRYDKEKIVGMTVSCERLVAEFYID------RKKSQKAK      90
AtNOT4A  WHHIVDMAEKDQIEGRCPACRTPYDKEKIVGMTVNCDSLASEGNME------RKKIQKSK      90
AtNOT4B  WHHIMDMAEKDQSEGRCPACRTPYDKEKIVGMTVDQERLASEGNMD------RKKIQKSK      90
         :::* :     : :*******  **.*::  :*:. : *  *          **: :* :

ScNOT4   KENEYTNRKHLSGTRVIQKNLVYVVGINPPVPYEEVAPTLKSEKYFGQYGKINKIVVNRK      177
AtNOT4C  PKPAEGRK-DLTGVRVIQRNLVYVMSLPFDLADED---MFQRREYFGQYGKVVKVAMSRT      146
AtNOT4A  SKSSEGRKQQLTSVRVIQRNLVYIVGLPLNLADED---LLQHKEYFGQYGKVLKVSMSRT      147
AtNOT4B  PKSSDGRK-PLTSVRVVQRNLVYIVGLPLNLADED---LLQRKEYFGQYGKVLKVSMSRT      146
          :    .:  *:..**:*:****::.:   :  *:    :: .:*******: *: :.*.

ScNOT4   TPHSNNTTSEHYHHHSPGYGVYITFGSKDDAARCIAQVDGTYMDGRLIKAAYGTTKYCSS      237
AtNOT4C  AAGAV------QQFPNNTCSVYITYSKEEEAIRCIRSVHGFILDGRNLKACFGTMKYCHA      200
AtNOT4A  ASGVI------QQFPNNTCSVYITYGKEEEAVRCIQAVHGFILDGKPLKACFGTTKYCHA      201
AtNOT4B  ATGLI------QQFPNNTCSVYITYGKEEEAIRCIQSVHGFILDGKALKACFGTTKYCHA      200
         :           :. .   .****:..:::* ***  *.*  :**: :**.:** *** :

ScNOT4   YLRGLPCPNPNCMFLHEPGEEADSFNKRELHNKQ---QAQQQSGGTAFT--RSGIHNNIS      292
AtNOT4C  WLRNMPCSNAECLYLHEIGAQEDSFSKDETISAHMRKMVQDITGWRDHYVRRSGSM--LP      258
AtNOT4A  WLRNVACVNPDCLYLHEVGSQDDSFTKDEIISAYTRSRVQQITGATNILQHHSGNM--LP      259
AtNOT4B  WLRNVACNNQDCLYLHEVGSQEDSFTKDEIISAH--TRVQQITGATNTMQYRSGSM--LP      256
         :**.: * * :*::*** * : ***.* *  .      .*: :*       :**    :

ScNOT4   TSTAGSNTNLLSENFTGTPSPAAMRAQLHHD---SHTNAGTPVLTPAPVPAGSNPWGVTQ      349
AtNOT4C  PP----VDDYVDNESSTRIIPKVVLNNVHSAAKNSPPNDS--NSHSVTLP-AGAMWGMHS      311
AtNOT4A  PP----LDAYCSDSSSAKPIIKVPSTNATSVPRYSPPSGSGSSSRSTALP-AAASWGTH-      313
AtNOT4B  PP----LDAYTSDSSTGNPIAKVPSSTSVSAPKSSPPSGS--SGKSTALP-AAASWGARL      309
                    .:. :      .           *  . .      . :* ..  **
```

```
ScNOT4     SATPVTSINLSKNSSSINLPTLNDSLGHHTTPTTENTIT-STTTTTNTNATSHSHGSKKK    408
AtNOT4C    SVPNTPSS--------------REPLRDK-SAT------VSSAVAINPTQISSRSDELRK    350
AtNOT4A    ---QSLATSVTS----------NGSSDIQRSTSVNGTLPFSAVVANAAHGPVSSNDILKR    360
AtNOT4B    TNQHSLATSALS----------NGSLDNQRSTSENGTLATSTVVTKAANGPVSSSNSLQK    359
                 :               .     : : :       *:..:          .  ::

ScNOT4     QSLAAEEYKDPYDALG-NAVD------FLDAR--LHSLSNYQKRPISIKSNIIDEETYK-    458
AtNOT4C    PALEAA---------GGNVLKPQS---LLDGKTDFPELSSSNKTQISNSRNVVSASVDNS    398
AtNOT4A    PSRKEES-QIVMDKVKPSVLKPLQHNVVVS-G--SERITAPDRDPTSNRLSSSVDSAYGG    416
AtNOT4B    APLKEEI-QSLAEKSKPGVLKPLQQKIVLDPE--SKRTTSPNRDPSSNQISCLVESSYNS    416
                            ..:.      .:.        :  ::   *   .    .

ScNOT4     ---KYPSLFSWDKIEASKKSDNTLA--NKLVE-ILAIKPIDYTASVVQFLQSVNVGVNDN    512
AtNOT4C    RAISEPSDCTD----------------------LPEHTSL--SNGNKMINRRIQNGCSNV    434
AtNOT4A    RDIDQPSAYSGRDIDKPSSTVSSFDAANEAVEDVPTVSNL--LDGVACM--RITMNCR--    470
AtNOT4B    RVIDKPSA-----------VENSLEHTSEIAEDVFDVGKL--SADVAWM--GITTNSR--    459
              . **                          :     :    .   :   :  .

ScNOT4     I-----TITDNTKTPTQPIRLQTVSQQIQPPLNVSTPPPGI----FGPQHKVPIQQQQMG    563
AtNOT4C    VSVDADSVVDGYHGITRSDKSHIDHASIKPTLTEVSQ-DYLQRCVDEPREVQPLQKSGRT    493
AtNOT4A    ---------DERPDITMAIGSQSDQGSIRQPGSEVSKLPDLEQCRIDS----SINTDKKA    517
AtNOT4B    ---------DETPGVPVVIGTHCDLGSITQSDNDV---QNLEQCRKQS----PTNTYAEA    503
                    *           :    .*    .       :             :

ScNOT4     D----------TSSRNSSDLLNQLINGRKIIAGN-------------------------    587
AtNOT4C    N--ANEVGVSREEVNRGTSLMSPLGTGHYLEAEDDISLFYRQRLKDPEVLSCQSNGFLR-    550
AtNOT4A    ISLEDRIPRTRPGWDWISDLQSQMQGSSKLQV-EDISTLDSQRPHPEEDIIHSRLLSNLS    576
AtNOT4B    DISLNGIHGSRPEWDWRSGLQSQIDVKEPLEV-NDFSSFNNNRRGIAEAVSHSTSKFSSS    562
                            :.* . :     : . :

ScNOT4     ------------------------------------------------------------    587
AtNOT4C    ----PSNCMQPCSSQYKAEHDETRTVFGSSYSDSRGSNIAPISNGYTEMPLSEPNQLNGS    606
AtNOT4A    SSSLDTNHMASRSSLP---------------CEVRGSDRLHLPNGFGEKSMS-------S    614
AtNOT4B    ISILDSNHLASRSFQNRETSCGMDS--KTGSSFEIGSDRLHLPNGFSEKAMS-------N    613

ScNOT4     ------------------------------------------------------------    587
AtNOT4C    LNHSILVPDKARDTQPIENCFVDSHESPSEIDDRIIANIMSLDLD---EYLTSPHNYANP    663
AtNOT4A    VEHSLFANE--------------GRNKVNNAEDAILSNILSLDFDPWDESLTSPHNLAEL    660
AtNOT4B    MEHSLFANE--------------GRSNIQNTEDDIISNIL--DFDPWDESLTSQHNFAKL    657
```

```
ScNOT4  ------------------------------------------------------------  587
AtNOT4C FGESDEEARSLKLASSSKVEDNQSRFSFARQEEPKDQAFDSYNA--SNQMSRGNDFYQNS  721
AtNOT4A LGEVDQRSSTLKPSNFLKQHNNQSRFSFARYEESSNQAYDSENYSIYGQLSRDKPIQESA  720
AtNOT4B LGQSDHRASTLESSNLLKQHNDQSRFSFARHEESNSQAYDNRSYSIYGQLSRDQPLQEFG  717

ScNOT4  ------------------------------------------------------------  587
AtNOT4C SERQSPNMGMFGTYNGLSSCYRRGLDYVTESSTLPSSYKPTSVPRCPVSAPPGFSVPTPS  781
AtNOT4A -MSRDIYRNNLGSVNGFASNFAGGLDNFAASPLFSSHKN--PVSRPQVSAPPGFSAP--N  775
AtNOT4B -ANRDMYQDKLGSQNGFASNYSGGYEQFATSPGLSSYKS--PVARTQVSAPPGFSAP--N  772

ScNOT4  ------------------------------------------------------------  587
AtNOT4C RPPPPGFSSNGRDHQMIDGFSGNSRFSDSIAYGNHYQQSLPIEN---VRDVQYMDPAILA  838
AtNOT4A RLPPPGFSSHERVGLSSDTTLGNRFLDST-SLRNAYQVPPPVGNSNGASDIDFVDPAILA  834
AtNOT4B RLPPPGFSSHQRGDLSSDIASGTRLLDSANLLRNAYHVPPPSGNLNAAGDIEFIDPAILA  832

ScNOT4  ------------------------------------------------------------  587
AtNOT4C VGQGF-----ENASLDFRSNFQGNTNMYGSAAKLQQQQQQAVMQ--NPLSMQNPL-SSHQ  890
AtNOT4A VGRGM-----VNADLDMRSGFSSQLNSFENETGLHMLRQQSLSSAQQVNGFHH--DLRNL  887
AtNOT4B VGRGRLHNGMETADFDLRSGFSSQLNSFDNDARLQLLAQRSLA-AQQVNGFHDPRNVNNF  891

ScNOT4  ------------------------------------------------------------  587
AtNOT4C NCRFTDSLGMAPRFIDQSQGNNLL----------TRNMALPNGHWNGLMSN-----EIQT  935
AtNOT4A SPSLNDPYGFSSRLMDQTQGSSLSPFSQLPRQQPSANSILSNGHHWDKWNEGQSVNNIGM  947
AtNOT4B SSSFSDPYGISSRPTDQTQGTGLSPFTQLPRQA-SANPLLSNGHWDNKWNEPQSGNNLGI  950

ScNOT4  ----------------------------------------  587
AtNOT4C RNRLQNERLVGSTN-WIPGYNG-TFRM-------------  960
AtNOT4A AELLRNERLGFNGSLYNNGYEEPKFRIPSPGDVYNRTYGI  987
AtNOT4B TQLLRNERMGFNDNVY-SGFEEPKFRRPGPGDPYNRTYGI  989
```

Appendix 1 - Amino acid sequence alignments of full length *Sc*NOT4, *At*NOT4A, *At*NOT4B, and *At*NOT4C. Asterisks (*) indicate positions where all sequences have the same amino acid, colons (:) denote positions with strongly similar properties, and periods (.) indicate weakly similar properties. Amino acids are color-coded by their chemical properties: red for hydrophobic, blue for acidic, magenta for basic, and green for polar or hydroxyl-containing residues.

Appendix 2 – Chemical list used for high-throughput chemical screening assay

Appendix 2 – Chemical compounds used for the chemical screening assay

Chemical Screen (Syngenta)		
Name	**Target**	**MOA class**
KTRS	tryptophan tRNA synthetase	Eukaryotic protein biosynthesis
Bixlozone	DXS	Non mevalonate pathway
paraquat CL hexahydrate	photosystem I	redox mediator
Oxytriazine 2	dihydrofolate reductase	folate biosynthesis
Fosmidomycin	DXR	non mevalonate pathway IPP synthesis/ carotenoid biosynthesis
FPPS Bisphosphonate	(2E,6E)-farnesyl diphosphate synthase (to be validation in 2016)	isoprenoid biosynthesis
Dinoseb	mitochondrial membrane	uncoupler
Myriocin	serine C-palmitoyltransferase	sphingolipid metabolism
54445	cellulose synthesis inhbitor	
IPMD standard	3-isopropylmalate dehydratase	amino acid biosynthesis - branched chain
Tunicamycin	UDP-N-acetylglucosamine-dolichyl-phosphate N-acetylglucosaminephosphotransferase	glycoprotein synthesis
HOE704	ketol-acid reductoisomerase	amino acid biosynthesis - branched chain
Sterol biosyntesis standard	sterol 14alpha-demethylase	steroid biosynthesis
Asochlorin	quinol-cytochrome-c reductase	mitochondrial electron transport inhibition

Cytochalisin	Actin	cytoskeleton
DMC	homogentisate solanesyltransferase	plastoquinone biosynthesis
Omeprazole	H+/K+-exchanging ATPase	membrane function
Blasticidin S	70S ribosomal subunit (prokaryotes and eukaryotes)	Protein biosynthesis
Alpha-methyl-DL-trptophan	Anthranilate synthase	amino acid biosynthesis - tryptophan
Rapamycin	TOR	TOR signalling pathway
Kyne	unknown	Cell wall biosynthesis
Cantharidin	phosophoprotein phosphatase	signalling - intracellular
5-keto clomazone	1-deoxy-D-xylulose-5-phosphate synthase	non mevalonate pathway
Bialafos	Glutamine synthetase	NH4 + assimilation/photorespir ation
2,4-dithiobiuret	unknown	redox mediator
Pinoxaden	acetyl-CoA carboxylase	fatty acid biosynthesis
Phenoxan	NADH:ubiquinone reductase (H+-translocating)	mitochondrial electron transport inhibition
Eupolauridine	DNA topoisomerase (ATP-hydrolysing)	DNA replication
clethodim	acetyl-CoA carboxylase	Fatty acid biosynthesis
Imazapic	acetolactate synthase	amino acid biosynthesis - branched chain
Amphotericin B	lipid membrane	membrane function - ionophore
IGPD standard	imidazoleglycerol-phosphate dehydratase	amino acid biosynthesis - histidine
Isoxaben	Ces A	cellulose biosynthesis
Fomesafen	protoporphyrinogen oxidase	haem biosynthesis
Chlorsulfuron	acetolactate synthase	amino acid biosynthesis - branched chain

Chloramphenicol	Ribosome large subunit (prokaryotic)	protein biosynthesis
Mefluidide	very-long-chain 3-oxoacyl-CoA synthase	very long chain fatty acid biosynthesis
Diquat	accepts electrons from PS1	photosynthetic electron transport
DNOC	Uncoupler	Uncoupler
Chlorthiamide	cellulose synthesis	Cell wall biosynthesis
Dichlobenil	inhibiton of cellulose synthesis	Cell wall biosynthesis
Cycloheximide	60S ribosomal subunit (euk)	Protein biosynthesis
Naptalam	unknown	signalling - auxin
Triclosan	enoyl-[acyl-carrier-protein] reductase (NADH)	fatty acid biosynthesis
Dicamba	TIR1 F-box protein	signalling - auxin
Propanil	photosystem II	photosynthetic electron transport
Fluridone	Phytoene desaturase	carotenoid biosynthesis
Hydantocidin	Adenylsuccinate synthase	Nucleotide biosynthesis
Isoxaflutole	4-hydroxyphenylpyruvate dioxygenase	plastoquinone biosynthesis
Acetylmethylphosphinate	pyruvate dehydrogenase (acetyl-transferring)	glycolysis / TCA cycle
formycin A	unknown	unknown
Dichlormate	9,9'-dicis-zeta-carotene desaturase	carotenoid biosynthesis
analogue of cinmethlyn	fatty acid biosynthesis	lipid biosynthesis
monic acid	Isoleucine-tRNA ligase (ITRS (plastid), isoleucyltRNA synthetase)	protein biosynthesis
Indaziflam	CWBI and PSII	Cellulose synthesis and photosynthesis
MSMA	unknown MOA	unknown

Appendix 3 – Full list of primers used

Table 12 – List of Primers

#	Name	Sequence	Target	Purpose	Size
1	LociF	CACATGAGTGTTTCTACCTAACA	Pgr3 Broad locus region	PCR (genotyping)	6924 bp
2	LociR	TTTTCTGGATGCTACAGTTTCC			
3	insertF	TTGAATATATCCTGGTGGCAAG	TDNA insertion in PGR3	PCR (genotyping)	1038 bp
4	GABI_134E03_RP	ACTCAAGCCAAATTGCACATC	Targets endogenous NOT4A gene	PCR (genotyping)	1105 bp
5	GABI_134E03_LP	TTTACATTGTTGGGTTGCCTC			
6	MB118_GKLB8760	GGGCTACACTGAATTGGTAGCTC	NOT4A TDNA	PCR (genotyping)	455-755bp
7	qNot4a_F-1	ATAGAAGGGCGTTGTCCAGC	qPCR primers targeting not4a insertion (before and after TDNA)	qPCR expression analysis	~150 bp
8	qNot4a_R-1	GCCTTCAGAAGCCAGACTGT			
9	qNot4a_F-2	GCTTCAAACTTCGCTGGTGG			
10	qNot4a_R-2	ACTTGAGGTCGTGAAACAGGA			
11	qNot4b_F-1	AGTTTGGAGCGAACCGTGAT	qPCR primers targeting not4b insertion (before and		
12	qNot4b_R-1	CTTGAGTCCTCGCCACAGG			
13	qNot4b_F-2	TGCCGCACTCCATATGACAA			
14	qNot4b_R-2	CTTCAGAGGCCAGTCTCTCC			

			after TDNA)		
15	qNot4c_F-1	ACTCCAAAGAGGAGGAAGCG	qPCR primers targeting not4c insertion (after T-DNA insertion for not4c and N59. Before for N65)		
16	qNot4c_R-1	GCATTGGAGCAAGGCATGTT			
17	N59_LP	ATACATCGAATCGCTTCCTCC	Targets TDNA for SALK_099755	PCR (genotyping)	1222 bp
18	N59_RP	AATGTGTGTTTTGGGGTCTTG			
19	LBB	ATTTTGCCGATTTCGGAAC	TDNA border primer	PCR (genotyping)	500-900bp
20	N65_LP	TTTCATGGGAGTCAACGAAAC	Targets TDNA for SALK_152456	PCR (genotyping)	1130 bp
21	N65_RP	TGCAGAATGTACATAGTGCCG			
22	qNot4c_bef_f	AGTCAGCTGTGAAAGGTTGGT	qPCR primers targeting not4c T-DNA insertion (before)	qPCR expression analysis	~150 bp
23	qNot4c_bef_r	GATCTTTCCTTCCCTCCGCA			

24	qNot4c_af_f	TGCAGAATGTACATAGTGCCG	qPCR primers targeting not4c T-DNA insertion (after)		
25	qNot4c_af_r	TTTCATGGGAGTCAACGAAAC			
26	ENODL_LP	GAAACGACTTTAAACCCCTCG	Targets endogenous ENODL 15 gene	PCR (genotyping)	1058 bp
27	ENDOL_RP	AGGGTCAGAAGCTACGCCTAG			
28	TMP_LP	GCCGGAGAAGAAGACTGGAG	Targets endogenous TMP gene	PCR (genotyping)	203bp
29	TMP_RP	ACAGTGTACATGATGGCCCC			
30	NOT4B_LP	TTCCTTGAGAGGTGCTTTCTG	Targets endogenous NOT4B gene	PCR (genotyping)	1207 bp
31	NOT4B_RP	ATATCTGCAGGGCATGTTTTG			
32	NOT4B_LBB	GCCTTTTCAGAAATGGATAAATAGCCTTGCTTCC	NOT4B TDNA		601-901bp
33	NOT4C_LP	GGCAGAACAAAAGGTTTAGCC	Targets endogenous NOT4C gene	PCR (genotyping)	1114 bp
34	NOT4C_RP	AGGCAACAATATAAGGCTGGG			
35	NOT4C_LBB	ATTTTGCCGATTTCGGAAC	NOT4B TDNA		575-875bp
36	qFLZ8_RT1_F	CCAGAATCATCTCCGGCTATTTC	FLZ8 Gene		~150 bp

37	qFLZ8_RT1_R	CGCATGTGTAATCCTCCGATAAC		qPCR expression analysis
38	qTOR_RT_F	TTTGATTGGCTTCGCGTAGA	TOR gene	
39	qTOR_RT_R	AACGGCGGCGAAACG		
40	qS6K1_RT_F	TCTCTCTCCAGGCTGGTGAAC	S6K1 gene	
41	qS6K1_RT_R	CGGGAAAAATCGATACAGAATCA		
42	qLST8-1_RT_F	CGGGATAAAATCGATCGAAAAT	LST8-1 gene	
43	qLST8-1_RT_R	TGTGATCATAGCTAGCCGTAGCAA		
44	qRPS6_F:	GATGACCAGAAACTACGTGCG	RPS6A-gene	
45	qRPS6_R	TGCTTATCGCAACCACCCTT		
46	qRAPTOR1_F	GTCACCTGAACCGCTTGTCT	RAPTOR1-gene	
47	qRAPTOR1_R	AACTGTATGTCACCCGCC TG		
48	MB310_Act7_F	CTGGAATGGTGAAGGCTGGT	ACTIN gene	
49	MB311_ACT7_R	GTGCCTAGGACGACCAACAA		
50	pp2a_F	ACAGTTCAACCACACTAATGGGCTC	Protein phosphatase 2A-2 gene	
51	pp2a_R	TTTGGCGCACTGAACACTGTAACCAC		

Appendix 4 – Validation of *At*RPS6 and *At*RPS6-P antibodies

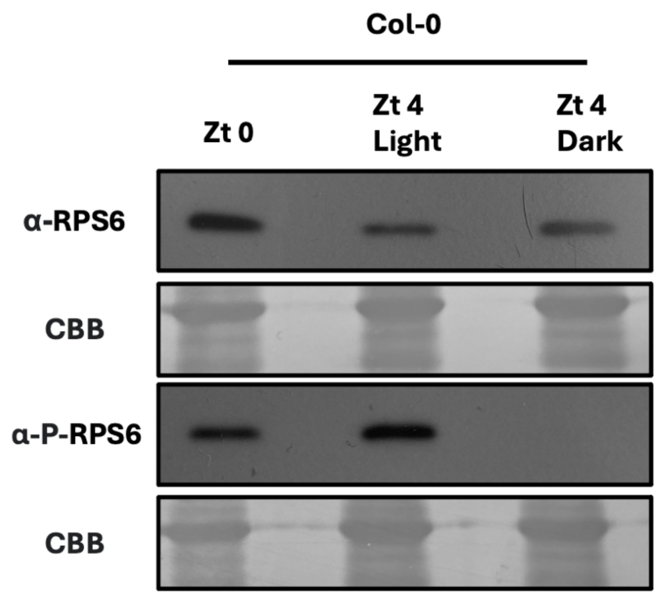

Appendix 2 - Phosphorylation of RPS6 stimulated by light validating α-P-RPS6 function. Western blot analysis probing for total RPS6 (α-RPS6) and phosphorylated RPS6 (α-P-RPS6) in Col-0 after a 4hr light and dark treatment.

Appendix 5 – Confirmation of AZD8055 treatment on samples for RNA-sequencing

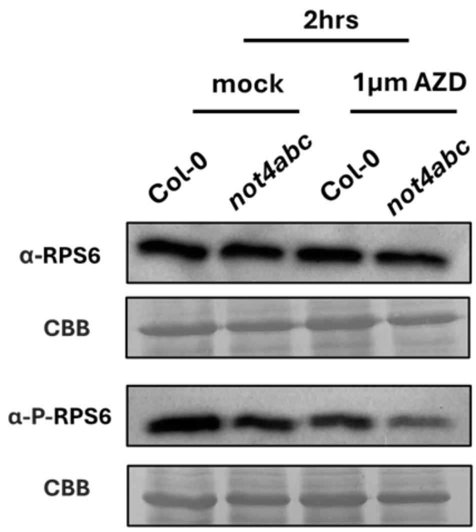

Appendix 3 – Confirming AZD8055 treatment worked for samples sent for RNAseq. Western blot analysis probing for total RPS6 (α-RPS6) and phosphorylated RPS6 (α-P-RPS6) in Col-0 and *Atnot4abc* after a 2hr 1µM AZD8055 treatment.